New methods for Frequency Signal Modelling and Impact Evaluation of New Resources

Francesco Arrigo

* * * * * *

Supervisors
Prof. Ettore Bompard, Supervisor
Prof. Federico Milano. Co-supervisor

I hereby declare that, the contents and organisation of this dissertation constitute my own original work and does not compromise in any way the rights of third parties, including those relating to the security of personal data.

....
Francesco Arrigo
Turin, 2020

Summary

Power systems are increasingly gaining importance. Progressive electrification is happening all over the world in order to enhance energy efficiency and integration of Renewables Energy Sources (RESs). Electricity consumption is growing more than the other energy vectors.

This thesis work deals with the stable operations of electricity systems. Specifically the starting research question is: what is and how can we measure the impact of Battery Energy Storage Systems (BESSs) performing fast frequency control? This question is inserted in the wide area of problems related to the decrease of rotating inertia in the electric grid. Since RESs presence continue to increase, Synchronous Generators (SGs) are being replaced by converters which will change the fundamental dynamics of the power system. Regulating energy from conventional fossil fuels sources will continue to decrease and BESS can provide the fast control needed by power system to remain stable. In chapter 3, the literature about BESS performing frequency control is ordered by proposing a novel categorization of the scientific works. In chapter 4 simulations are performed to quantify the impact of BESSs during a contingency by modelling the power system with a low order model. BESSs fast answer was divided in two services: fast Primary Frequency Control (PFC) and RoCof (Rate of Change of frequency) control which mimics the behaviour of physical inertia. A correct dimensioning of the two services has been assured imitating the behaviour of synchronous generators through the use of an Equivalent Saturation Logic (ESL). Both components of the control are fundamental to stop the frequency decay.

Another part of the Thesis is focused on the impact of BESSs during normal operations of the grid, when frequency is bounded in a strict operating range. In order to address this problem, a closed loop model must be used. In such a model frequency can vary realistically for a long period of time and BESSs can influence the frequency signal. In chapters 5 and 6 are developed two different methodologies to simulate a closed loop system: the first one based on the explicit computation of the load mismatch which creates the frequency deviation, the second one based on the use of the Fourier Transform Theorem (FTT) in order to reproduce the main power disturbances harmonics which are present in the grid. In such a way

It has been possible to quantify the impact of BESSs making use of specific defined indexes. Besides an additional analysis with the low order model is performed in the frequency domain.

Due to the slow nature of the frequency signal in normal operations, RoCof control cannot improve frequency deviations. Even PFC produced by BESSs is not particularly more efficient with respect to Conventional Generation (CG). Secondary frequency control has apparently the most impact on the frequency signal. Moreover, an investigation is conducted on the main effects of PFC on BESS State of Charge (SoC) dynamics: the main result is that the impact of BESS inefficiency is negligible with respect to the effects caused by intra-day and average frequency dynamics. Also, a Variable Droop Strategy (VDS) for PFC is implemented to find out its consequences on the system: the strategy improves the SoC profile without causing frequency unbalances.

Finally, in chapter 7 from utility scale BESS, the focus is moved to the evaluation of the impact of Electric Vehicles (EVs). Due to their expansion, EVs could represent the most part of batteries systems operating in the electric grid, therefore there is a great interest to study their potential for fast frequency control. However, EVs present additional modelling challenges with respect to BESSs for their correct characterization: they are not always attached to the electrical grid and need to recharge after a travel, besides they are connected to the distribution system which is more easily subject to congestion with respect to the transmission system where BESSs are usually installed. A complete framework to study the mentioned problems is detailed in this chapter and first steps are quantitatively developped.

Acknowledgements

acknowledgements will be present in the printed version of this work . . .

Dedication will be present in the printed version of this work . . .

Contents

List of Tables

List of Figures

XIII

xv

List of Abbreviations

ACE	Area Control Error
BESS	Battery Energy Storage System
CG	Conventional Generation
COI	Centre of Inertia
DFT	Discrete Fourier Transform
DSO	Dystribution System Operator
ENTSO-E	European Network of Transmission System Operators for Electricity
ESL	Equivalent Saturation Logic
EV	Electric Vehicle
EU	European Union
FCR	Frequency Containment Reserve
FDS	Fixed droop strategy
FTT	Fast Fourier Transform
ICT	Information and communication technologies
MPC	Model Predictive Control
PDF	Probability Distribution Function
PFC	Primary Frequency Control
PI	Proportional Integral
PID	Proportional Integral Derivative Control
PLL	Phase Locked Loop
PV	Photovoltaic
RES	Renewable Energy Source
RoCof	Rate of Change of frequency
SGAM	Smart Grid Architecture Model
SFC	Secondary Frequency Control
SFRM	System Frequency Response Model
SG	Synchronous Generator
STD	Standard Deviation
VDS	Variable Droop Strategy

Introduction

This Introduction provides a brief description of the content of each chapter. In a parallel way, at the end of the Thesis, the Conclusions gather the main results, lessons learned and suggestions coming from my studies. Few notes are added concerning the scientific works I was involved with, the tools that I have used and the other activities I conducted during my PhD. Besides this introduction, each chapter starts with a small summary and concludes with a brief recap of main results.

Thesis Structure

The work can be divided in three parts:

First part - Background, composed by three chapters. In particular we have:

- **Chapter 1 - Power System Fundamentals.**

  Key data are gathered on the energy transition happening today by using the most recent countries reports. This is a non-technical presentation, but important to contextualize the role of electricity in the energy sector. The electric grid is then presented in its basic structure and components by using SGAM methodology. Finally, are described the stability issues of the grid considering the increase of RESs resources. Part of the content of the chapter was used in the deliverable D1.1 of the European project RESERVE [185] [1]. Besides in order to describe the RESERVE projects use cases [184], I applied SGAM methodology.

- **Chapter 2 - Frequency Dynamics and Control Modelling.**

  A critical description of the grid frequency dynamics is presented along with the main parameters influencing this variable. The classical view of frequency

---

[1]https://www.re-serve.eu/

control is presented in the first part, while a general discussion on the impact of RESs and the potential of new resources for frequency control is presented in the second part.

- **Chapter 3 - Literature Review on Frequency Control.**

  This chapter provides a rigorous and in-depth review on the papers dealing with the impact of BESSs performing fast frequency control. The read works are divided in 3 groups: studies on open loop where the effect of BESS into the grid cannot be evaluated, studies of the impact of BESS after a sudden contingency in the grid, studies of the impact of BESS during normal operations. The papers are sub-divided according to the methods and the main research questions to highlight differences and improvements among them. The chapter (with the addition of chapter 2) works as a basis for a future literature review paper.

Second part - Evaluating the impact of BESSs on frequency dynamics. Also this part is divided into three chapters:

- **Chapter 4 - Impact of BESS fast frequency control after a contingency**.

  The first two studies on BESS impact on frequency control are developed in this chapter. Two channels of control (RoCof and PFC) are simulated using two different grid models considering different analysis and highlighting the most influent parameters. The two studies were published respectively in [183] and [128] in collaboration with other researchers. In [128] I built a basic version of the grid model used in Chapter 5 and the Equivalent Saturation Strategy to dimension frequency Reserves from BESSs. Models are developed in Simulink and the data analysis is performed in Matlab.

- **Chapter 5 - Impact of BESSs in normal grid conditions: a System frequency response model approach**.

  The model of last chapter is expanded and reversed in order to compute the load mismatch which cause the frequency to change during normal conditions of the grid. BESSs are then added to evaluate their impact on the grid. The System Frequency Response Model (SFRM) is studied also in the frequency domain. The results of this part will serve as a basis for a paper to be submitted shortly. Besides another case study (currently submitted for UPEC 2020) making use of the Sardinian system is presented analyzing the impact of BESS over one entire day of frequency oscillations. Secondary and tertiary frequency controls are added as an expansion of the SFRM.

Finally, notes on SoC dynamics, on BESSs modelling and on the frequency signal characteristics are introduced based on the frequency data of the Irish system.

- **Chapter 6 - Impact of BESSs in normal grid conditions: a Fourier Transform approach.**

  The second approach uses FFT to analyze the real frequency signal and its harmonic content. Relevant power disturbances are reproduced in order to recreate frequency deviations in a simulated environment which is compared with the harmonic content of the original frequency data (in this case the Irish signal is used). The study is performed in DOME, a transient power system simulator created by Professor Federico Milano. Beside the classic fixed frequency droop control, VDS is used for BESSs and the impact of this strategy on the grid can be explicitly evaluated. For the data analysis I have used Python programming language. Relevant papers associated with this research are [12, 13].

Third part - This last part is composed just by one chapter and deals with Electric Vehicles.

- **Chapter 7 - Electric Vehicles Studies**.

  This chapter aims to evaluate the impact of EVs performing frequency control when connected to the grid. The final goal is to study the possibility of bottlenecks in the distribution system which can be provoked by frequency control and how Distribution System Operator (DSO) can intervene to secure the grid. In this chapter only two intermediate steps are presented: in particular an agent based modelling framework is built to recreate scenarios with thousand of cars moving in a realistic road network and charging in different points of the electrical grid. The models of this framework were designed and developed in Matlab and presented in [63]. A second part deals with the construction of a sound smart charging strategy for the EVs before performing frequency control. A priority based logic was implemented and proved in a simple case study. The results aare published in [73]. Furthermore a final section is dedicated on how to expand the presented framework in order to fully evaluate EVs impact.

During my PhD I had the opportunity to work on real time simulation [126] developing models in Simulink-Sympowersystems for the RESERVE project. Finally, I am collaborating in a paper currently under revision about the modelling and the simulations of Power to Gas plants in the distribution networks.

In this Thesis when writing about works conducted in collaboration with other researchers, I focus more on my personal contributions.

Chapter 1

Power System Fundamentals

In section 1.1 current and future energy scenarios are presented in order to highlight the important role of electricity to increase the production from renewable sources. European perspective will be explained in detail. Since electric grid is a complex industry, an holistic view on its main features is briefly presented in 1.2 through the description of the SGAM model. In section 1.3 the stability of the grid is explained and the impact of Renewable Energy Sources (RESs) is listed.

1.1 Energy and Electricity Scenarios

1.1.1 World energy transition

Today, energy is at the center of modern society. Several international agencies proposed [191] the use of a set of indicators called Energy Indicators for Sustainable Development. These indicators are 30 and divided in 3 dimensions: social, economic and environmental. Moreover, the importance of energy is highlighted in the Goal 7 of the Millennium Development Goals ratified by United Nations: "Ensure access to affordable, reliable, sustainable and modern energy for all". These goals are a synthesis of the countries' political will and have to be implemented in practical actions in the period 2015-2030 all over the world.

Energy sources and technologies have drastically changed during the years. For example, total final energy consumption (TPES) continues to increase passing from 6101 Mtoe [1] in 1973 to 13972 Mtoe in 2017 [3]). In the current state, the increase of energy consumption comes from development countries, while industrialized nations tends to flatten or even decrease their energy demand. Energy intensity

---

[1]Mtoe stands for Mega tonnes of oil equivalent. A single toe is computed as the energy produced by burning one tonne of crude oil equivalent to 41.868 GJ or 11.63 MWh.

(which is evaluated as energy consumption divided by the value of the Gross Domestic Product) continues to decrease thanks to an improvement in efficiency, technologies and better industrial processes management. New renewable energy sources (mainly solar and wind) are just starting to reach significant amounts in the system, while fossil fuels still cover most of the production. Enormous efforts are still needed to decrease climate change.

In the electricity sector, electricity consumption increases proportionally faster than energy demand. In 2000, electricity accounted for 15% of the total TPES while in 2017 was already 19% and it is still expected to increase. Electricity is in fact a high value energy carrier for several reasons:

- in the presence of a good infrastructure, it is easy to transport in big quantities with low losses;

- electricity eliminates the pollution in the place of consumption. Moreover, power plants using fossil fuels have very efficient filters and pollution abatement systems;

- it helps and sustains the increase of RES such as Wind (Offshore and Onshore) and Photovoltaic power. These naturals sources are usually sparse in the country territory and therefore electric infrastructure is essential to transport the energy produced to consumption centers;

- electricity is a driver for energy efficiency and low environmental impact technologies like heat pumps, electric vehicles and other domestic, commercial and industrial appliances.

For all these reasons, industrialized countries are wired with a strong, meshed electric network. However, still today, a little less of one billion people does not have access to electricity at home. In the last years the Asian and African progress in energy and especially electricity consumption allowed to raise the human standard of living, but, on the other hand, it is a serious cause for environmental concern as green-house gases (GHG) emissions are still rising, overcoming 37.1 Gtonnes in 2018.

China and USA objectives

China is today the biggest energy user and GHG emitter, responsible for the 20.8 % of the total global emissions, still growing at enormous pace. China covers more than 55% of its energy needs by the use of coal. In 2015, with the 13th Five-year Development Plan and in 2017 during the 19th National Congress of the Communist Party, the Chinese government decided to realize an ecological

civilization within 2050 and subscribed the Paris Agreement [37]. By 2050, to reach its goals, electricity, mainly produced by RESs, is expected to represent around 50 % of the final demand. China aspires to overcome Europe and USA becoming the world leader of the renewable energy.

The United States of America is responsible for the 20.1 % of the total global emissions. In recent years it has become a net exporter of oil, oil products and naturals gas thanks to the use of environmental controversial fracking techniques. In 2017, the portion of RESs in total energy demand was just 11 %, a value much lower than Europe. Nevertheless, while at the federal level Trump administration is slowing the pace of reforms, at state level the increase of renewables is being fostered by local government initiatives. However the USA "Reference Energy Scenario towards 2050" [11] projects an energy demand slightly increasing, a big share of gas, still some coal power plants in the power sector and not enough increasing electricity penetration.

1.1.2   The European Perspective

The Europe Objectives

European Union (EU) is a leading force for what concerns the energy transition to a de-carbonized economy. The EU energy reforms aim to strengthen the energy union under five important dimensions [2]:

- **Security, solidarity and trust.** The EU still depends on imported fossil fuels in order to sustain its energy production. Fossil fuels (solid, gas, petroleum, etc.) represented in 2016 the 71% of the total primary energy consumption, 54% of which are imported from abroad (increasing from the 52% of 2005) and represents a high geopolitical risk. RESs are expected to play a key role in decreasing abroad dependence.

- **A fully integrated energy market.** The goals is to foster efficiency by increasing trans-national connections between the countries. The two biggest energy infrastructures, gas and electricity transmission networks, are reaching a more strict technical and economical coupling, summarized in the joint construction and update of the Ten Year Network Development

---

[2]if the reader is interested, more news, documents and data can be found online at the European Commission website in the energy section: https://ec.europa.eu/info/energy-climate-change-environment_en and in the page for statistics data: https://ec.europa.eu/eurostat/data/database

Plan (TYNDP) built by ENTSO-E and ENTSO-G, which are the European agencies gathering the gas and electricity transmission system operators.

- **Energy efficiency.** This is a fundamental driver for energy demand reduction and the increase of high tech jobs and economic growth. The major challenge is the efficiency of house appliances and the reduction of buildings energy needs. The deployment of millions of new smart meters is also considered part of the strategy.

- **Climate action - de-carbonising the economy.** While energy sector produces the most amount of GHG emissions (1,28 billion of tonnes of CO2 equivalent), it accounts for around 25 % of the production. Industry, transport and buildings are notable sectors.

- **Research, innovation and competitiveness.**At the current state, Europe is investing in programmes of research in order to create new patents in various fields from battery storage to bio-energy and smart cities.

The first accountable objectives were established by the **2020 climate & energy package** in 2007. The goals are those of the 20-20-20; 20% decrease of GHG emissions with respect to 1990 levels; 20 % of energy coming from renewable sources (with at least a 10 % share of renewable in the transport sector) and 20% of consumption decrease due to the increase in energy efficiency. Numerous initiatives were taken to ensure these goals:

- ETS (Emission Trading Scheme) for energy and big polluting industries and binding annual targets for other sectors in order to cut GHG emissions;

- national targets for renewable production by considering the starting points and the country potential;

- financial support for the development of low carbon technologies through the NER300 programme for renewable energy technologies and carbon capture & storage and the Horizon 2020 programme for funding research & innovation;

- energy efficiency measures through the Energy efficiency Plan and Directives.

The emissions were cut by 23% between 1990 and 2018, while the economy grew by 63% over the same period. Energy consumption continued to decrease until 2014, but to increase in the years 2014-2017 due to the emissions related to economic growth. So, while energy efficiency is actually increasing at an high rate

(more than 30 % [3]), in 2017 the final energy consumption was 3.3 % above the 2020 target. Finally, renewable sources represent 18.9 % of energy consumed in 2018 and in the transport sector this percentage reached 8.3 % in the same year, in line with 2020 goals.

Europe will continue its efforts in the period 2020-2030 under the 2030 climate & energy framework. The key targets for 2030 are: at least 40% cuts in GHG emissions (compared to 1990 levels). At least 32% share for renewable energy and 32.5% improvement in energy efficiency. In 2018 the European Commission presented its strategic long-term vision for a prosperous, modern, competitive and climate-neutral economy by 2050. This vision is compliant with the Paris Agreement objective to keep the global temperature increase well below 2°C and pursue efforts to keep it within 1.5°C. The detailed plan and the single national efforts are still under discussion.

Electricity sector status and future trends

Various energy scenarios can be formulated to consider the future trends of Europe RES production increase. Energy scenarios are a representation of possible pathways a country will take to fulfill its energy needs. Each scenario is described by a coherent set of assumptions on the current trends or possible different future constraints, like environmental awareness, policy intervention, socio-economic and technological trends. These features are quantitatively linked altogether through the use of key relationships and models mixing several scientific disciplines [131]. Scenarios are not predictions or forecasts of the future, but a way to show all interested people with different backgrounds (policy, technical and research) how the future could unfold as a consequence of certain choices and natural dynamics into society. The task is extremely difficult considering the enormous complexity of today energy systems.

EU Reference Scenarios [31] and the EUCO scenarios [176] are the main studies performed on Europe. EU Reference Scenarios for 2030 and 2050 were built as a benchmark of current policy efforts and market trends, to show the direction of the European energy transition. EUCO are instead built to achieve the 2030-2050 energy objectives. Different EUCO scenarios (such as EUCO3232.5 [156] or EUCO30) were formulated to consider slightly different goals in line with Europe political objectives.

---

[3]https://www.eea.europa.eu/data-and-maps/indicators/progress-on-energy-efficiency-in-europe-3/assessment

In figure 1.1 the historical data about 2000 and 2010 and the projections of electrical generation divided by source in the years 2020, 2030 and 2050 are shown. For 2020 only the EUCO3232.5 values are gathered as they are similar to those of the 2020 EU Reference Scenario. The 2050 is shown only for the Reference Scenario and the EUCO30 as found in [32]. EUCO30 with respect to EUCO3232.5 presents similar assumptions but slightly less ambitious targets.

Table 1.1: Electricity production statistics in Europe. The EUCO scenario 2050 refers to the scenario EUCO30 which is similar to EUCO3232.5

Scenario	-	-	EUCO	EUCO	Ref.	Ref.	EUCO
Year	2000	2010	2020	2030	2030	2050	2050
Generation [TWh]	3005	3332	3378	3498	3527	4063	4300
Fossil fuels [pu]	0.54	0.515	0.42	0.23	0.36	0.27	0.14
Renewable[pu]	0.145	0.21	0.36	0.56	0.42	0.55	0.64
Nuclear [pu]	0.315	0.275	0.22	0.21	0.22	0.18	0.22
El. pen. [pu]	0.15	0.163	0.177	0.217	0.25	0.28	0.381

In all future scenarios, coal (which is the main part of solid fuels) is substantially substituted by gas sources. Gas sources are still needed even in 2050 to add flexibility and back-up capacity to the system although they will operate with a much lower capacity factor. To avoid GHG emission, carbon capture and storage technologies could be utilized or the power plants could burn bio-methane with almost zero impact for the environment. Nuclear sources are expected to decrease until 2020 and then remain substantially stable. Except for hydro (which in Europe already reached an high level of maturity), all other renewable sources will undergo a substantial increase depending on the scenarios. Geothermal production will be limited by its challenging extraction and besides it is more suited for heat production with respect to electricity generation. The slow growth of Biomass sources and their possible decrease in the long run is due to the competition from the biofuels industry which is a more lucrative alternative and besides it is needed to de-carbonize the transport sector. Wind power will be the biggest source pushed by the offshore turbines deployment supported by the construction of the DC super-grid connecting the North Sea. Many assumptions on the diffusion of Power-to-Gas and Power-to-Hydrogen technologies were made that leave space for different future scenarios. As seen in table 1.1, total electricity generation and penetration increase thanks to the diffusion of electrical transport, heat pumps and Power-to-X technologies, even if Reference Scenario is substantially under the EUCO scenarios. EUCO scenarios present more RESs and energy efficiency. Remember that EUCO scenarios are evaluated with the goal of reaching European
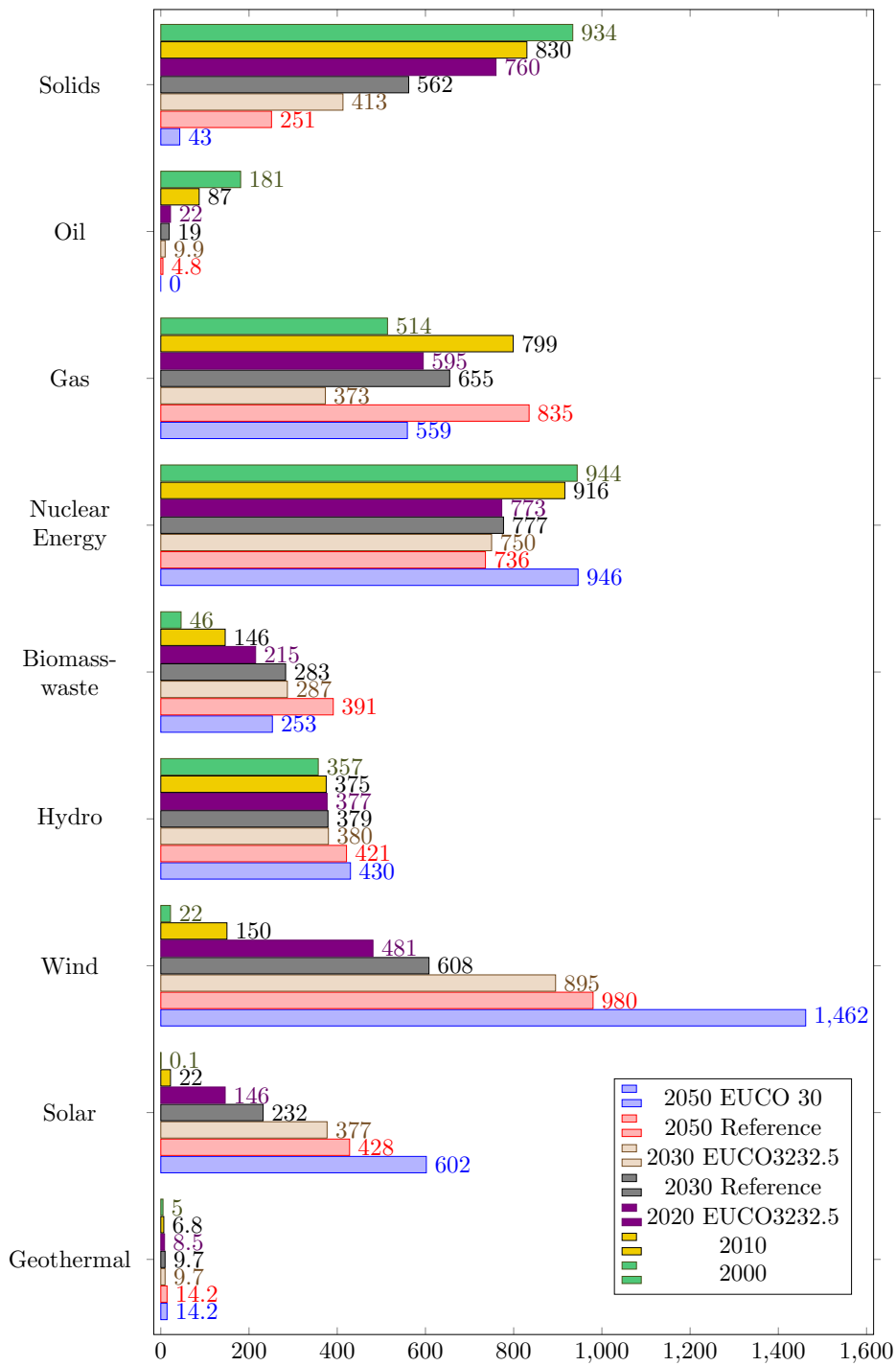
Figure 1.1: yearly electricity production in Europe by source [TWh] in different scenarios.

objectives, while Reference Scenarios are built by trying to intercept the current trends and possible outcome of environmental policies adopted by European countries. Reference scenarios are indeed a pressing remark of the additional effort which is still needed to decarbonize the electricity sector.

1.2 The Electric Grid Structure

1.2.1 A paradigm shift

The electric grid is the biggest industrial system built by humans. It continuously provide energy and for its optimal operation needs to be controlled in all time ranges from milliseconds up to years. Historically, the system has been run in a vertical fashion with power plants connected to the transmission grid optimized to follow the loads at the distribution level. With the liberalization of the power system sector, the system faced numerous changes such as the introduction of thousand of new non dispatchable renewable generators or the most recent possibility for industrial, commercial and private consumer to regulate their loads thanks to the use of storage or advanced managment systems. The active players now include thousands of renewable producers and prosumers (consumers which posses small RES plants and are able to at least partially control their overall consumption profile). In order to make all the new players coordinately interact in a market environment an improvement on the Information and Communication Technologies (ICT) infrastructure of the grid is of fundamental importance.

1.2.2 SGAM approach

In order to systematically describe new architectures or standards to make the grid more efficient and connect all the players, Smart Grid Architecture Model (SGAM) [33] is used. SGAM is very useful especially for use case design in which interoperability of different layers are well represented in a technology neutral manner for both existing and future power systems.

SGAM is a three-dimensional model (see Figure 1.2) that is merging the dimension of 5 interoperability layers including component, communication, information, function and business, with the 2 dimensions of the Smart Grid Plain consisting of zones and domains. Zones represent the hierarchical levels of power system management while domains cover the complete electrical energy conversion chain from bulk generation, transmission, and distribution, to distributed energy resources and customer premises. All classical components and function of the grid and new entries can be introduced and well localized inside the SGAM framework. This
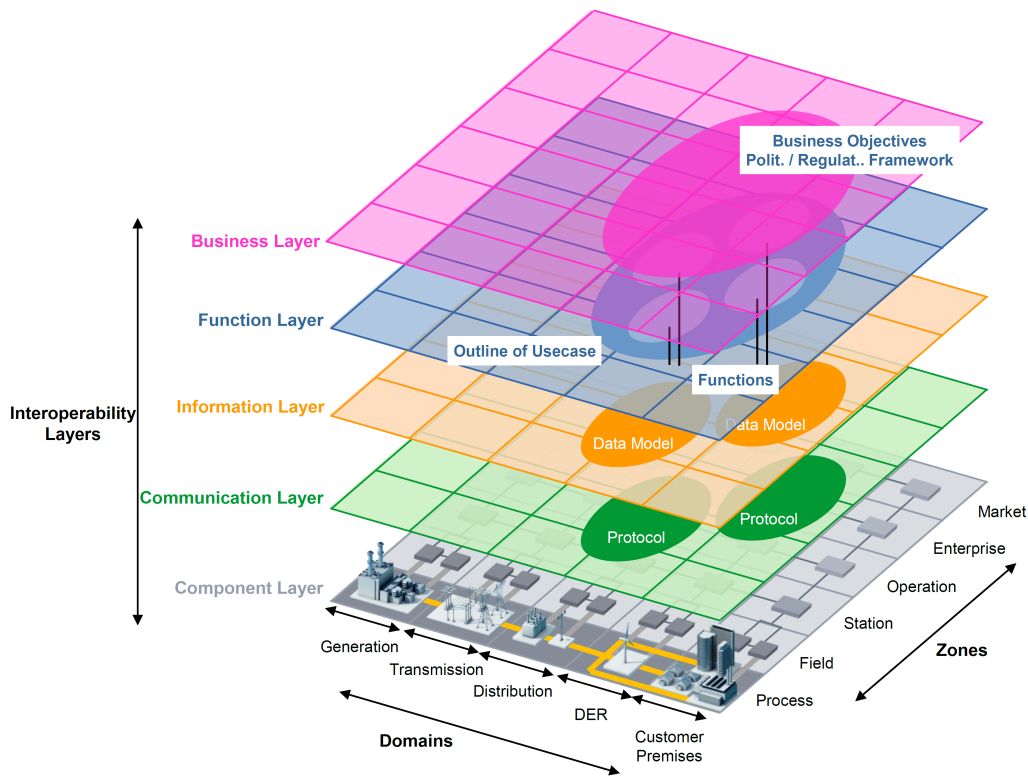
Figure 1.2: Smart Grid Architecture Model (SGAM) - Source: CEN-CENELEC-ETSI Smart Grid Coordination Group

will support gaps identification in Smart Grids standardization, and migration scenarios to improve existing/installed architecture.

SGAM layers

- **Component layer.** The physical distribution of all participating components in the smart grid context, including system actors, applications, power system equipment, protection and tele-control devices, communication network infrastructure and any kind of computers.

- **Communication layer.** In this layer, data exchange procedure, technologies, protocols and standards are described for the specific use case, functions, and information objects.

- **Information layer.** This layer represent messages, measurements, alarms, and in general all data and information which are exchanged between actors of component layer and function layer. It includes information objects

and considered canonical data models which ease communication between different data formats.

- **Function layer.** It includes functions along with their relationships from an architectural viewpoint. The functions are independent from actors and physical implementations in applications, systems and components.

- **Business layer.** The business layer represents the business view on the information exchange related to smart grids. It supports business executives in decision making related to business models and specific business projects (business case) as well as regulators in defining new market models.

SGAM domains

- **Bulk generation.** It includes all types of electricity production in bulk quantities, such as hydro power plants, fossil and nuclear power plants, offshore wind farms, utility scale solar power plant, etc.

- **Transmission.** Infrastructure and organization which are in charge of electricity transportation over long distances.

- **Distribution.** Infrastructure and organization which distributes electricity to customers.

- **Distributed Energy Resources (DER).** DERs are small-scale power generation which are directly connected to the public distribution grid with typical production in the range of 3 kW to 10 MW.

- **Customer Premises.** Hosting prosumers including industrial, commercial, and residential facilities. Prosumers can be either pure consumers or producers such as micro turbines, photovoltaic generation, etc. Electric vehicles storage and batteries are also hosted in this domain.

SGAM hierarchical zones

- **Process.** It covers all types of energy transformations processes and the physical equipment which is directly involved. Equipment examples in the process zone are generators, transformers, transmission lines and cables, circuit breakers, electrical loads, and any kind of sensors and actuators, etc.

- **Field.** Protection, control, and monitoring equipment of the power system process are all considered in the field zone. Any kind of intelligent electronic devices which acquire and use process data from the power system, protection relays, and bay controllers are some examples of the field components.

- **Station.** The area aggregation level for field components falls in the station zone. Station includes substation automation, local SCADA systems, data concentration, plant supervision, etc.

- **Operation.** Systems which are actually hosting power system operation are considered in operation zone. Some examples of operation systems in different domains: Energy Management Systems (EMS) in generation and transmission systems, Distribution Management Systems (DMS), Virtual power plant management systems (aggregating several Distributed Energy Resources), Electric vehicle (EV) charging management systems in customer premises.

- **Enterprise.** Management entities, commercial and organizational processes, services and infrastructures for enterprises (utilities, service providers, energy traders, etc.) are considered in the enterprise zone. Some examples are staff training, customer relation management, asset management, billing and procurement, logistics, etc.

- **Market.** Energy trading and all possible market operations as either mass or retail market are put in the market zone.

1.3   Technical Issues of the Grid

1.3.1   Stability of the grid

The electrical management of the grid is characterized by different physical and market phenomena at various time frames as shown in figure 1.3. In the same figure, are listed the common power system controls which are utilized in order to stabilize and optimize the power system operations. Automatic continuous control or automatic triggered actions maintain stability in the short time frame, while long term actions depend on a technical-economic optimization of the power system generation and reserves.

The definition of stability in a power system is a difficult task in that on one hand it must have a consistent and general mathematical underpinning description but, at the same time, it must have a clear and physical motivated meaning. An attempt was done in 2004 [103]. The proposed definition for the general power system stability is:

> Power System Stability is the ability of an electric system, for a given initial operating condition, to regain a state of operating equilibrium after being subject to a physical disturbance, with most system variables bounded so that practically the entire system remain intact.
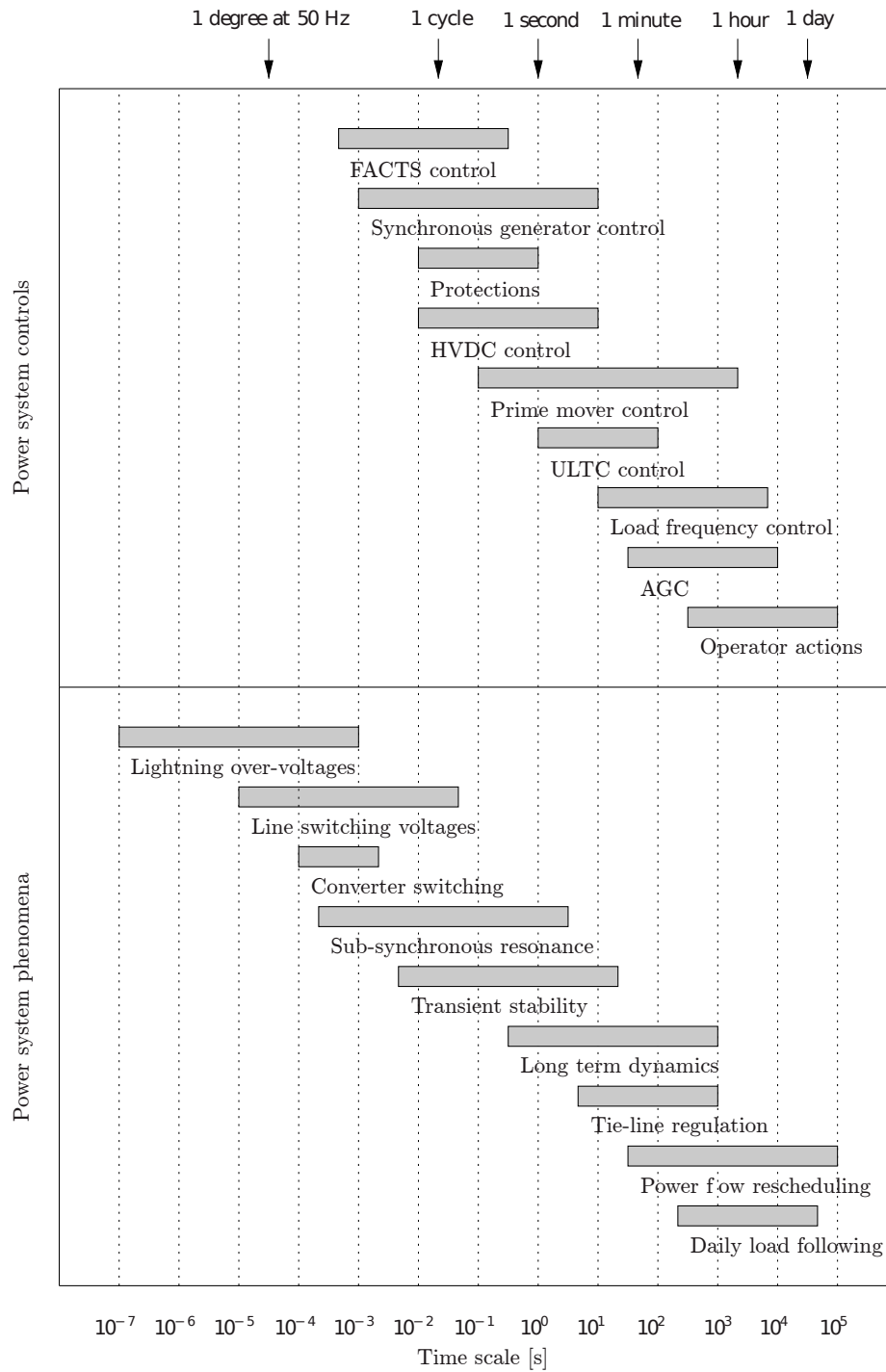
Figure 1.3: time scales of relevant power system dynamics. Figure modified from [123].

The power system, composed by non-linear components, operates under constantly changing disturbances which can be of various nature and intensity, like for instance load stochastic changes, short circuit or big generator trips. To better investigate and improve the system dynamics, simplifying assumptions are made to specify different typologies of grid instability based on: (i) consideration on physical nature of the instabilities and main system variables involved, (ii) size of the disturbance and (iii) relevant time span of the studied instability.

In particular three kinds of stability has been defined in [103] (see figure 1.4):

- **Voltage stability**. Voltage stability refers to the ability of a power system to maintain steady voltages at all buses in the system after being subjected to a disturbance from a given initial operating condition. The main driving force usually resides in the variation of active/reactive power flows from the loads, which cannot be sustained by generators, leading to unstable voltage values at the corresponding buses. Voltage stability is divided in: (i) large disturbance stability, referring to the ability to sustain system faults, loss of generation, circuit contingencies or (ii) small disturbance stability, caused by small perturbations such as incremental load changes. Both kinds can be regarded as short term or long term phenomena, depending on processes and components involved.

- **Rotor angle stability**. Rotor angle stability is the ability of the interconnected synchronous machines, running in the power system, to remain in the state of synchronism. In stable conditions there is an equilibrium between the input mechanical and output electrical torque of each generator. External disturbances affect this balance between the machine torques, which start to oscillate around the nominal angular velocity. Taking into account the non-linear power-angle characteristics of the synchronous generators exchanging power with the electrical grid, continuous and wide acceleration and deceleration could bring the machines to lose their synchronism. Small signal stability refers to the stability of the machines under normal stochastic oscillations due to load noise. Transient stability refers to the ability to withstand synchronism after important grid faults.

- **Frequency stability**. Frequency stability is the ability of a power system to maintain steady frequency following a severe system upset resulting in a significant imbalance between generation and load. Instability can occur in the case of big contingencies leading to fast frequency drop or sustained frequency swings induced by the cascading failure of grid units. Frequency stability may be studied in short time frame, which is linked to the activation of under frequency load shedding and generators protections, or in long time

13

frame focusing on the power response of grid elements such as SGs governors, load and renewables regulators.
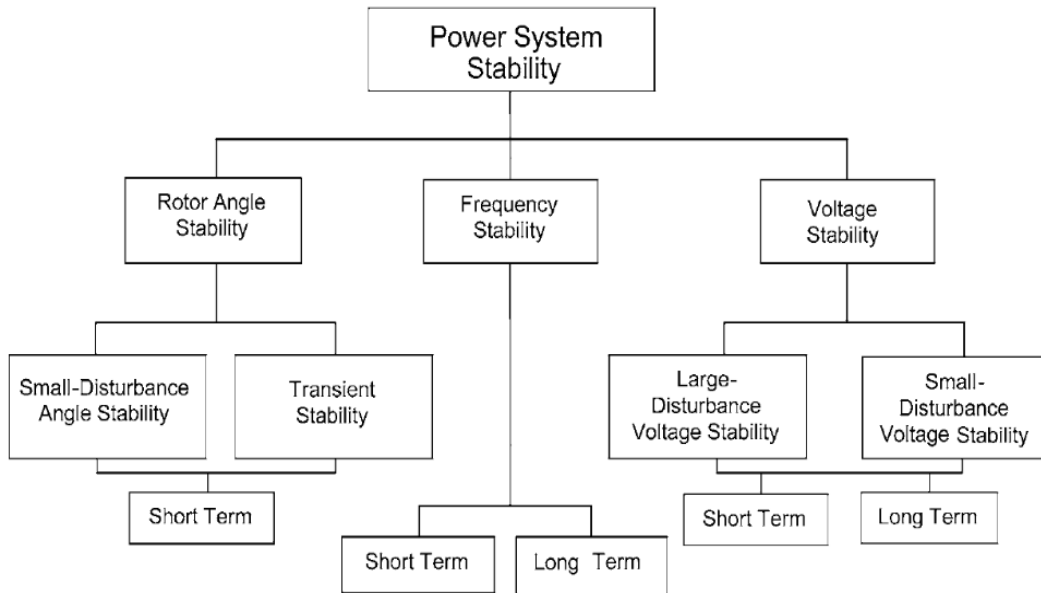
Figure 1.4: classification of power System Stability [103].

1.3.2   Renewable sources issues and solutions

The impacts of RESs is profound and involve the electric grid at all layers and all time ranges. A list of issues and possible solutions is presented below:

- as we will discuss in the next chapter, renewables have a double impact on frequency stability: they lower inertia and increase short and medium term power variability.

- Moreover, RESs variability affects the Net Load profile to be covered by conventional sources in the hour-day time range. Faster and longer ramps will be needed in order to follow the Net Load and avoid the imbalance of the grid. The typical expected scenario is summarized by the "duck curve" (see figure 1.5) which happens in the case of big Photo-voltaic production. At the twilight a sudden decrease in energy production will occur when the requested load is at its peak. The system will need to assure a fast ramp of dispatchable generation in order to avoid an energy imbalance which is expensive and technically difficult for the Transmission System Operator

14
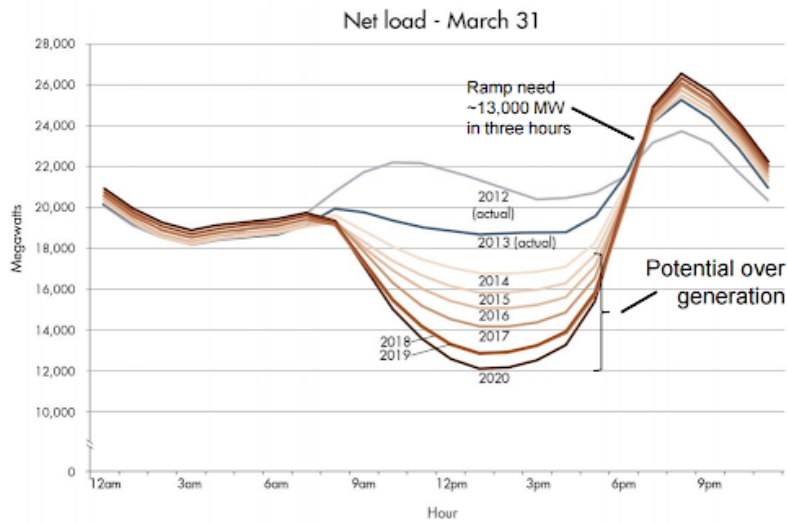
Figure 1.5: duck curve example of the Californian system. Image taken from [87].

(TSO) to obtain. In the case of wind sources, variability in the long term is not forecastable with high precision and could create dangerous situations. Luckily,the big number of RES plants and their geographical dispersion tend to smooth the output variability, however RES plants in the distribution grid are difficult to monitor and therefore their present and future production are typically unknown to the TSO. Major flexibility could be achieved by the use of modern Combined Cycle Gas Turbine plants, more interconnection between countries in order to share power reserves, and finally the intervention of Demand Response which refer to the possibility for the consumers to vary their load profile thanks to the use of ICT technologies coordinated by resource aggregators.

- Weekly and seasonal variability. In the future, there is a serious possibility to have long period of energy production excess or deficit due to RES long term variability like the 2018 July UK wind drought [4] or the big sun radiation differences between summer and winter. In order to overcome this variability, storage facilities (like pump hydro plants or innovative battery energy storage systems) could be used. The possibility of Power-to-X technologies (Power-to-Gas,Hydrogen,Heat) could be exploited to give more flexibility to the electric grid, but it will need a strict coordination between the electrical, natural gas and district heating infrastructure.

---

[4]https://www.newscientist.com/article/2174262-weird-wind-drought-means-britains-turbines-are-at-a-standstill/

- The replacement of synchronous generators with converter-based RES decrease the magnitude of short circuit currents after a fault. This worsens the efficiency of the protection systems and the circuit breakers, jeopardizing the voltage stability of the grid. Converter based RES are often free to disconnect in the case of contingency or in the presence of low voltages, worsening the grid status. However, in the last years new stricter rules demand to RES the Low Voltage Ride Through Capability.

- Converters gates switching give rise to harmonics in the voltage signal and stability problems due to the interaction of a great numbers of units in the distribution networks. Better filtering, procedures and new devices are needed to avoid distribution networks problems.

- The decrease of SGs connected to the grid means loosing fundamental grid regulators being these machines used to provide voltage and frequency reserves, black-start capabilities, inertia and high short circuit currents. Synchronous generators naturally maintain grid synchronization and posses good damping and load sharing capabilities, on the contrary converter based resources do not present these features, however could behave similarly to SGs if properly controlled and in possession of enough back-up storage. [175, 102, 195].

- In the distribution networks, massive number of resources will be installed in the form of Photo-voltaic small plants. Due to the more resistive nature of medium and low voltage lines (especially for underground cables), active power swings of RESs can cause severe voltage oscillations and instabilities. Besides, there is a risk of creating unintentional electrical islands [102] during faults due to the high presence of embedded distributed generation. Another possible problem is [19] the occurrence of reverse power flow when distribution network acts as a net generator of energy into the transmission system. Finally, congestions can happens in specific grid branches due to the high currents injected by RESs.

In order to integrate up to 100 % renewable sources in the grid, no single and easy solution is available. Several changes in technical, commercial and policy regulations must be introduced to lower the costs of having more RESs into the system. A summary and further insights on the problem are reported in [146, 102].

Conclusion

In this chapter, we have introduced the electric power system and its challenges. In section 1.1 we showed that energy demand is going to increase globally while

decreasing in western industrialized countries. Electricity production on the other hand will rise in every country because it is considered to be the best energy vector in order to de-carbonize and increase the efficiency of the whole energy system. Europe, also considering its energy dependency from the external countries, is at the front of the de-carbonizzation challenge, striving for a CO_2 free economy by 2050. However additional efforts are needed to reach this point with respect to the current direction. In section 1.2 the power system industry is presented in a holistic way adopting the SGAM approach: the component layer composed by the physical elements such as electric lines, transformers and generators is only one of the system parts: equal importance have the communication and information layers and also the functional and business layers which provides the architecture, the roles and the responsibilities of the various actors managing the grid. Finally in section 1.3 the definitions of stability in the grid and the impact of RESs are listed: their stochastic nature in time and space will impose a complete shift on how to manage the grid. From power quality issues in the sub-second period to long term yearly equilibrium between generation and demand in the case of exceptional weather conditions, the electric grid will face new problems in all time frames.

17

Chapter 2

Frequency Dynamics and Control Modelling

In this chapter we will focus our attention on the frequency control of the electric grid. First, in section 2.1 we will explain the basics of frequency control and present the main equations and parameters influencing the frequency signal. Three different aspects of the problem are treated: (1) the equation describing the dynamics of the grid frequency, (2) a qualitative analysis of the generators oscillations around COI frequency and (3) the analytical expression of the frequency profile after a contingency. In section 2.2 we describe the current hierarchical control structure commonly used in power systems and the importance of a stable frequency signal is highlighted. Finally, we introduce in section 2.3 new resources that can be used for frequency control.

2.1 Frequency Control Basics

2.1.1 Frequency control modelling basics

(a) Center of inertia frequency computation

Both rotor angle and frequency stability can be explained starting from the swing equation. This equation describes the Synchronous Generator (SG) rotor dynamics which give rise to the electro-mechanical oscillation in power grids. At the SG rotor level we can write [9] (see Figure 2.1):

$$J\frac{d^2\theta_m(t)}{dt^2} = T_m - T_e \tag{2.1}$$

where J is the mechanical rotating inertia of the machine $(Kg \cdot m^2)$ whose value depends on rotor physical structure and materials; θ_m is the mechanical

angle of the rotor in $[rad]$; T_m is the mechanical torque given by the turbine to the electrical machine and T_e is the electrical torque exchanged with electric grid. Making use of the following three equalities [104] $\omega_m = \omega_e/p$, $\theta_e = \omega_e t - \omega_O + \theta_0$ and $H = 0.5 J \omega_{m0}^2/S$, after a few passages, one can write:

$$\frac{2H}{\omega_0} \frac{d^2\theta_e(t)}{dt^2} = P_m - P_e \qquad [p.u.] \qquad (2.2)$$

where p is the number of poles of the electrical machine, S is the MVA rating of the generator, ω_{m0} is the nominal velocity in mechanical radians, ω_0 is the nominal steady state velocity of the rotor in electrical radians and θ_0 is the initial angular position of the rotor; H , expressed in seconds, is called the *inertia constant* and represents half the time for a generator or motor to reach steady state speed at full nominal power.
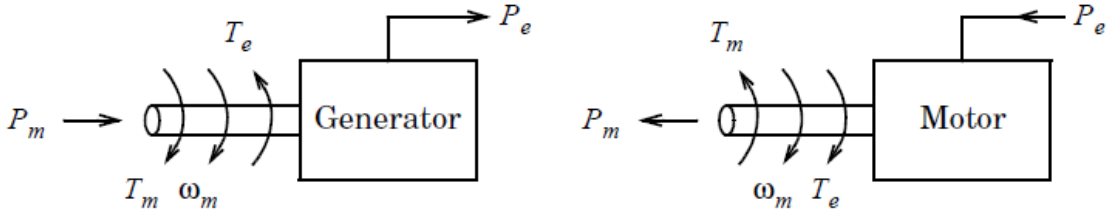
Figure 2.1: rotor dynamic phenomena

The time profiles of P_m and P_e of the single generator give us an idea of the machine rotor angle stability. Under the hypothesis of well damped oscillations and good rotor angle stability, which is often true even in the case of a contingency [145], we can assume all the rotors in the grid to turn almost at the same frequency. Such frequency is called ω_{COI} where COI stands for Center of Inertia and it is computed as the weighted mean of all generators velocities. With this knowledge and normalizing equation 2.2 over a unique power system rating, we can write:

$$\frac{2}{\omega_o} \frac{d^2\omega_{\text{COI}}}{dt^2} = \frac{\sum_{g=1}^{N_g}(P_m)_g - \sum_{l=1}^{N_l}(P_e)_l}{\sum_{g=1}^{N_g} H_g + \sum_{l=1}^{N_l} H_l} \qquad [pu], \qquad (2.3)$$

where N_g is the number of synchronous generators and N_l is the number of electric motors. Whenever there is an imbalance between the electric power requested by the loads and the mechanical power generated by the SGs, after a very brief transients where a small amount of energy can be released or stored by the electric grid lines [124], the frequency of the grid changes according to the equation 2.3. At the same time, the single generators rotate with small negligible oscillations over this frequency.
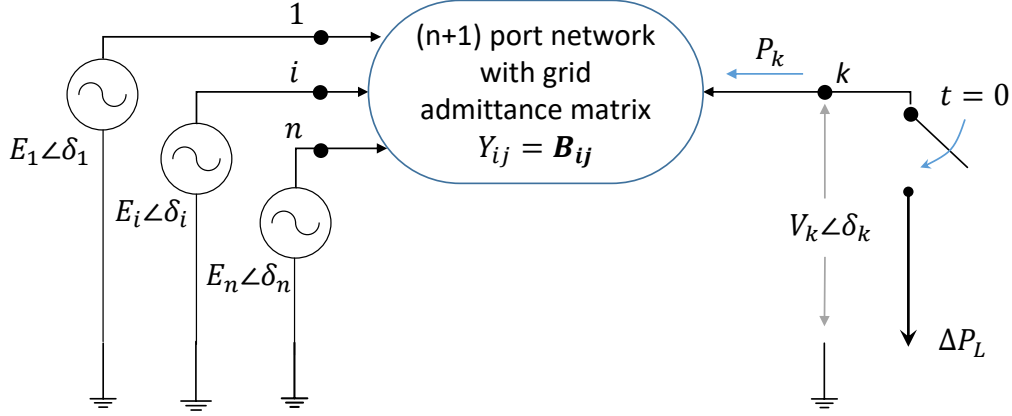
Figure 2.2: network with ΔP_L applied at $t = 0$.

(b) Generators rotors oscillations around COI frequency

The dynamics of the system generators can be qualitatively explained by modelling synchronous machines as constant voltage sources in series with a reactance and the admittance matrix of the grid with negligible resistance values (see [7] for more details). In such a system (see figure 2.2), let us consider the presence of a generic load k which at time $t = 0$ starts consuming a power ΔP_{load}. The transmitted active power in node i and node k can be computed as:

$$P_i = \sum_{\substack{j=1 \\ j \neq i,k}}^{n} E_i E_j B_{\text{ij}} \sin \delta_{\text{ij}} + E_i V_k B_{\text{ij}} \sin \delta_{\text{ik}} \tag{2.4}$$

$$P_k = \sum_{\substack{j=1 \\ j \neq i,k}}^{n} V_k E_j B_{\text{ij}} \sin \delta_{\text{kj}} \tag{2.5}$$

where E and V represent the voltages of the nodes, B_{ij} is the admittance matrix element value and $\delta_{\text{xy}} = \delta_x - \delta_y$ for whatever subscript in use. These expressions can be linearized for small ΔP_{load} values and the synchronizing torques of single generators can be introduced, obtaining:

$$P_{\text{i}\Delta} = \sum_{\substack{j=1 \\ j \neq i,k}}^{n} E_i E_j B_{\text{ij}} \cos\delta_{\text{ij,o}} \delta_{\text{ij},\Delta} + E_i V_k B_{\text{ij}} \cos \delta_{\text{ik,o}} \delta_{\text{ik},\Delta} = \sum_{\substack{j=1 \\ j \neq i,k}}^{n} P_{\text{s,ij}} \delta_{\text{ij},\Delta} + P_{\text{s,ik}} \delta_{\text{ik},\Delta}$$
$$\tag{2.6}$$

$$P_{k,\Delta} = \sum_{j=1}^{n} V_k E_j B_{\text{ij}} \cos \delta_{\text{kj,o}} \delta_{\text{kj},\Delta} = \sum_{j=1}^{n} P_{\text{s,kj}} \delta_{\text{kj},\Delta} \tag{2.7}$$

21

where the symbol Δ represents the variation of the quantity due to the linearization process. A sudden ΔP_{load} in the grid can be modelled in node k by keeping fixed the magnitude of the voltage V_k and changing its phase from $\delta_{k,o}$ to $\delta_{k,o} + \delta_{k,\Delta}$, while SGs cannot instantaneously change the phase due to their inertia. knowing that $\delta_{ij,\Delta} = 0$, $\delta_{ik,\Delta} = \delta_{i,\Delta} - \delta_{k,\Delta} = -\delta_{k,\Delta}$, , we can rewrite equations 2.6 and 2.7 at $t = 0^+$, obtaining:

$$P_{i,\Delta} = -P_{s,ik}\delta_{k,\Delta}(0^+) \tag{2.8}$$

$$P_{k,\Delta} = \sum_{\substack{j=1 \\ j \neq i,k}}^{n} P_{s,kj}\delta_{k,\Delta}(0^+). \tag{2.9}$$

From equation 2.9 it can be noticed that $P_{k,\Delta} = -\sum_{\substack{j=1 \\ j \neq i,k}}^{n} P_{i\Delta}(0^+)$, and knowing (from figure 2.2) that $P_{k,\Delta} = -\Delta P_{\text{load}}$, in view of the equation 2.8, we can write:

$$\delta_{k,\Delta}(0^+) = -\Delta P_{\text{load}} / (\textstyle\sum_{j=1}^{n} P_{s,kj}), \tag{2.10}$$

$$P_{i,\Delta}(0^+) = \left(P_{s,ik} / \textstyle\sum_{j=1}^{n} P_{s,kj} \right) \cdot \Delta P_{\text{load}}. \tag{2.11}$$

Equation 2.11 tells us that in the first instant the delta power to be served to the load is supplied by the energy stored in the magnetic and electric fields of the synchronous generators (and lines). The power load is shared among each generator according to the amount of the synchronizing torque: generators electrically more connected to the load node will initially provide more power regardless of their size. Immediately after, the SGs will start to decelerate/accelerate in case of a positive/negative ΔP_{load}. Starting from equation 2.2, the incremental swing equation governing the frequency dynamics of the SGs can be written as:

$$\frac{2H_i}{\omega_o}\frac{d\omega_{i,\Delta}}{dt} + P_D(\omega_{ij,\Delta}) + P_{i,\Delta}(t_1) = 0 \tag{2.12}$$

where $P_D(\omega_{ij,\Delta})$ is the damping torque of the SG which in a multimachine system depends on the differences between rotors velocities [104, 168]. In the first instants after a ΔP_{load}, generators will start to oscillate depending on their inertia, damping and synchronizing torques. After a certain short time t_1 which is usually lower than the time needed by prime governors of turbines to intervene, oscillations are smoothed and load sharing among SGs can be easily evaluated by using equation 2.12. Summing over each generator i we can write:

$$\frac{d\omega_{i,\Delta}}{dt}\sum_{i}^{n}\frac{2H_i}{\omega_o} + \sum_{i}^{n}P_D(\omega_{ij,\Delta}) + \sum_{i}^{n}P_{i,\Delta}(t) = \frac{2H_{\text{TOT}}}{\omega_o}\frac{d\omega_{COI,\Delta}}{dt} + 0 - \Delta P_{\text{load}}(0^+) = 0, \tag{2.13}$$

$$\Delta P_{mis}(t) \quad \xrightarrow{\quad} \quad \frac{1}{2Hs + D} \quad \xrightarrow{\quad} \quad \Delta f$$

$$\Delta P_m(t) \qquad - \frac{K_m(1+F_H T_R s)}{R(1+T_R s)}$$
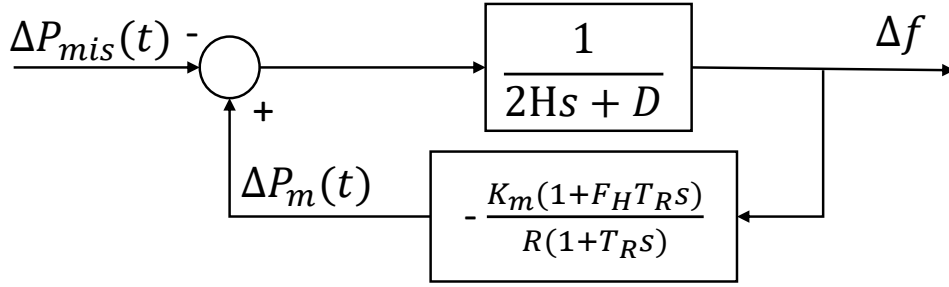
Figure 2.3: low order single system frequency response model example.

where damping torque is negligible as there is no substantial velocity difference among generators and therefore frequency derivatives are all equal to each other. Finally, we substitute the value of the velocity derivative of equation 2.13 into equation 2.12 at time t_1 and we obtain:

$$P_{i,\Delta}(t_1) = \left(H_i / \sum_i^n H_i\right) \Delta P_{\text{load}}(0^+). \tag{2.14}$$

This means that after a brief transient the various machines will swing at the same velocity, sharing the additional load according to their inertia constants.

(c) Analytical expression of frequency after a contingency

After time t_1 the governor response from generators starts to be relevant and makes the frequency to stabilize. To study analytically this equilibrium, we can consider a single machine equivalent system (as presented in [8]) which is based on a linearized version of equation 2.3, where the dynamics of the governor system of the power plant can be modelled as a zero-pole transfer function with the Load characterized by a certain damping coefficient $D[MW/Hz]$ which represents the tendency of loads to increase or decrease their power consumption in the opposite direction of the frequency error. The system is depicted in figure 2.3 where deadband and saturations are neglected to evaluate an exact solution. Now, it is possible to give the analytical formula of the frequency profile considering a step input of magnitude ΔP:

$$\Delta f(t) = \frac{R\Delta P}{DR + 1} \cdot \left(1 + \alpha \exp^{-\zeta \omega_n t} \sin(\omega_r + \phi)\right) \tag{2.15}$$

with:

$$\omega_n^2 = \frac{DR + K_m}{2HRT_R} \qquad\qquad \zeta = \left(\frac{2HR + (DR + K_m F_H)T_R}{2(DR + K_m)}\right) \cdot \omega_n$$

$$\alpha = \sqrt{\frac{1 - 2T_R\zeta\omega_n + T_R^2\omega_n^2}{1 - \zeta^2}} \qquad \omega_r = \omega_n\sqrt{1 - \zeta^2}$$

$$\phi = \phi_1 - \phi_2 = \tan^{-1}\left(\frac{\omega_r T_R}{1 - \zeta\omega_R T_R}\right)$$

(2.16)

where R is the droop of the generators, T_R, K_m and F_H are related to the dynamic description of the turbine-governor systems. Several indicators can help us to evaluate the stability of the system, the most important are: (i) the frequency derivate, especially at the initial time when it has the highest value; (ii) the Δf_{nadir} which is the lowest/highest frequency value (in the case of an under/over-frequency event) and its corresponding time t_{nadir}; (iii) the frequency and its value Δf_{reg} and t_{reg} at the transient end. All these quantities are computed as:

$$\frac{d\Delta f(t)}{dt} = \frac{R\Delta P}{DR + 1} \cdot \alpha\omega_n e^{-\zeta\omega_n t} \sin(\omega_r t + \phi_1) \tag{2.17}$$

$$t_{\text{nadir}} = \frac{1}{\omega_r}\tan^{-1}\left(\frac{\omega_r T_R}{\zeta\omega_n T_R - 1}\right) \tag{2.18}$$

$$\Delta f_{\text{nadir}} = \frac{R\Delta P}{DR + 1} \cdot \left(1 + \sqrt{1 - \zeta^2}\alpha\exp^{-\zeta\omega_n t_{\text{nadir}}}\right) \tag{2.19}$$

$$f_{\text{reg}} = \frac{R\Delta P}{DR + K_m} \tag{2.20}$$

and finally the initial RoCoF at $t = 0$ is simply computed as $\Delta P/2H$ and depends on the grid inertia alone.

To conclude, three figures are presented in order to explain and confirm previous concepts. In the first image (figure 2.4), different machine frequency profiles related to a simulated contingency modelled in [169] are shown. As seen, while the synchronous generators maintain synchronism even after a big contingency, they can potentially continue to oscillate for a long time after the contingency event, well after the Primary Frequency Control (PFC) intervention [1].

---

[1]In this situation a time t_1 (see equation 2.14) cannot be explicitly computed or visualized. Nevertheless, oscillations continue to decrease and equation 2.14 holds in an "averaged" way. It is also important to remember that generators behaviour depends just as first approximation on equation 2.12 and it is influenced by voltage profiles, controls and all other grid interactions
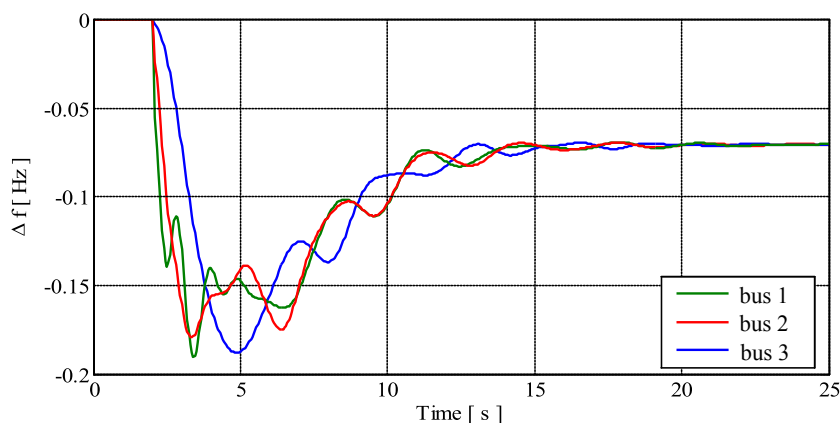
Figure 2.4: contingency simulation results. The figure was slightly modified from figure 14(a) of reference [169].
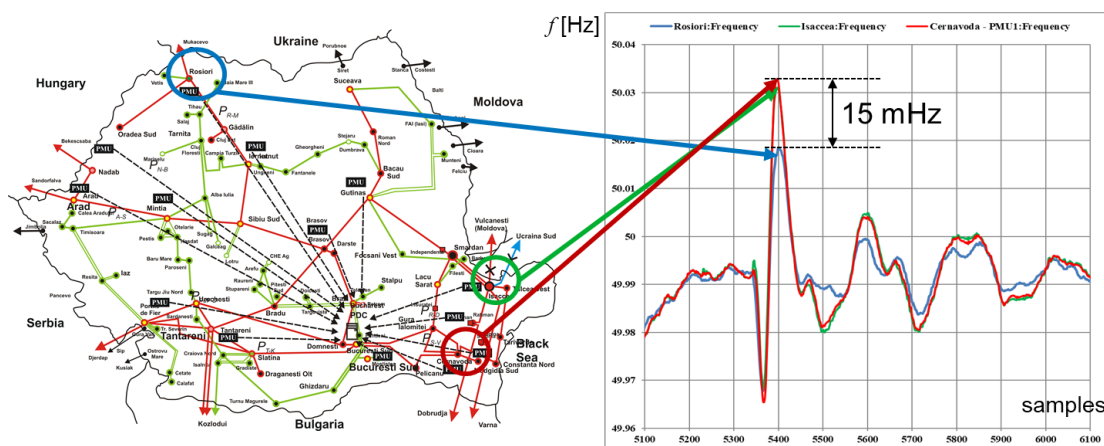
Figure 2.5: PMU measurements in Romanian power system after the disconnection of the Greece-Turkey interconnection line on 23 October 2017.

In the second image (figure. 2.5), real Phasor Measurements Units of the Romanian power system are presented. These devices have different specifics and capabilities based on well known standards [84] which assure the quality of the measurements. The data are recorded after the disconnection of the Greece-Turkey interconnection line on 23 October 2017, which in turn have caused well damped frequency oscillations in the whole European synchronized area.

In the third image (figure 2.6), the frequency signal recorded in Romania and Germany is shown during normal operation of the grid. It is clear how small deviations, which cause second by seconds frequency dynamics, imply no real difference in velocity among generators even for very far buses.
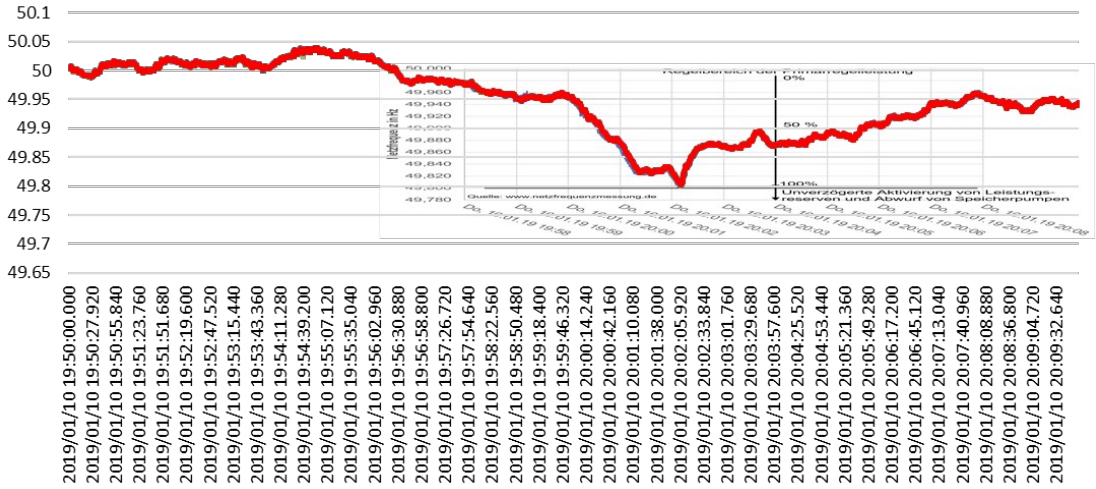
Figure 2.6: overlapping of the frequencies metered in Germany and Romania. Image taken from [45].

2.1.2 Fixed frequency importance and low inertia/reserves challenges

The goal for TSOs is to keep the frequency as constant as possible for several reasons: (i) rotating machines (generator and loads) will work best at nominal velocity; (ii) some electronic loads are very sensible to frequency variations; (iii) a non constant and fleeting frequency is dangerous for the mechanical stress and wear that can cause on the rotors of the generators or on other grid components [199]); (iv) in the case of contingency, if frequency is already unbalanced, less reserves will intervene to counteract the power deviation.

If the initial RoCoF is too high, severe problems can arise [134]. First of all, the synchronous generators could face a series of problem experiencing RoCof values higher than 1 $[Hz/s]$ [188]:

- **Pole slip;** this is directly connected to the rotor instability and the dynamics of the attractive forces between stator and rotor fields of the machine. This dangerous situation is reflected on the pole angle position between the stator and the rotor field. If this value is over 90 degrees there is a danger for the machine to lose its synchronism and become unstable threatening the whole grid. As a consequence it is possible the activation of protection systems for an emergency shut-off of the machine which can potentially lead to a cascading failure of the whole power grid in extreme cases. The outcome dynamics will depend on many factors such as the type of contingency, RoCof levels, inertia values, the power factor and the load of the machine.

26

- **Accidental reverse power flow;** important oscillations of the pole angle can temporarily produce negative output making the generator to behave like a motor. The generator is protected against motor operation by the reverse power protection which, if triggered, it will shutdown the unit. The activation of the control depends on the amount of reverse power flow (usually this should be less than 5 % of the nominal power) and a certain specific time length .

- **Torque swings;** the torque to be sustained after the contingency can be up to 160 % of the nominal value. These values can have an effect on the wear and the stress of the machines, but are well below the requirements of the current Fault Ride-Through capabilities. In fact, during the voltage dips, generators will have to sustain torques up to 300-500 % of the nominal value.

The tripping and/or the instability of a synchronous generator can possibly lead to the cascading failure of the generators in the grid, causing load shedding, system islanding or blackouts [49]. Moreover, SGs can swing and share load against each other causing inter-area oscillations, decreasing the stability and the power quality of the system [143]. Other possible hazards for generators are connected to the particular plant layout and the auxiliary equipment reaction during high RoCof events [52], such as torsional torque on rotor shaft train, flame and combustion control, hydraulic transients in hydro power plants, impacts on auxiliaries components (gas compressors, boilers feed pumps), etc.

It is also worth to remember that in the distributions networks, RESs are equipped with loss-of-mains protection. These protection systems are important to prevent embedded generation supplying an electrical island when a loss of mains event has occurred and are often RoCof activated [50].In such a way, a loss of generation can be triggered without any real islanding event, if the measured RoCof is higher than a certain threshold.

ENTSO-E monitors the European system trying to find out the suitable values for inertia in the grid in order to avoid load shedding or other emergency situations [69]. In the cited study ENTSO-E suggests that every region after a split of the synchronous area should posses a time constant of the network of 12 seconds (nowadays European constant is about 15 seconds, but in continuous decrease) [2]. To cope with this situation, the local TSO will be forced to enlarge the capacity reserves (primary, secondary and spinning reserve), increasing the operative costs (paid by the local community).

---

[2]The time constant of the network is computed as $2 \cdot H$

2.2 Current Frequency Control Structure

2.2.1 Classical frequency control loops

There exist several definitions, technical solutions and market structures to control frequency, all based on three hierarchical levels of control. Definitions, services, rules and operations in Europe are being harmonized by ENTSO-E through the implementations of Network codes: for frequency control, the guidelines were described in the "Load-Frequency Control and Reserves" code [57] merged in 2016 with the "System Operation" code which today has a binding value for all European countries [58]. Frequency control characteristics and its functions can be visualized in figure 2.7. We distinguish:
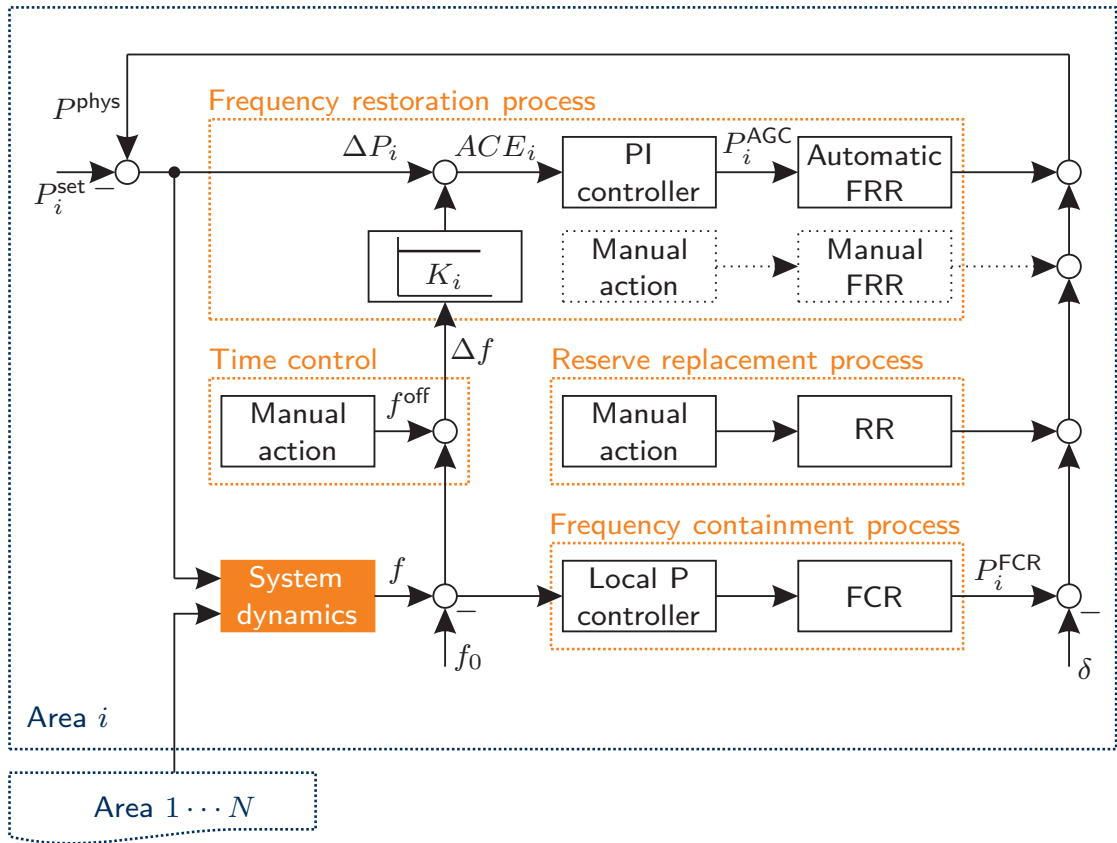
Figure 2.7: four-level hierarchy of frequency control from a TSO perspective. Image taken from [164].

Frequency Containment Reserve. FCR, also called primary frequency control, follows a proportional rule between the frequency deviation and the
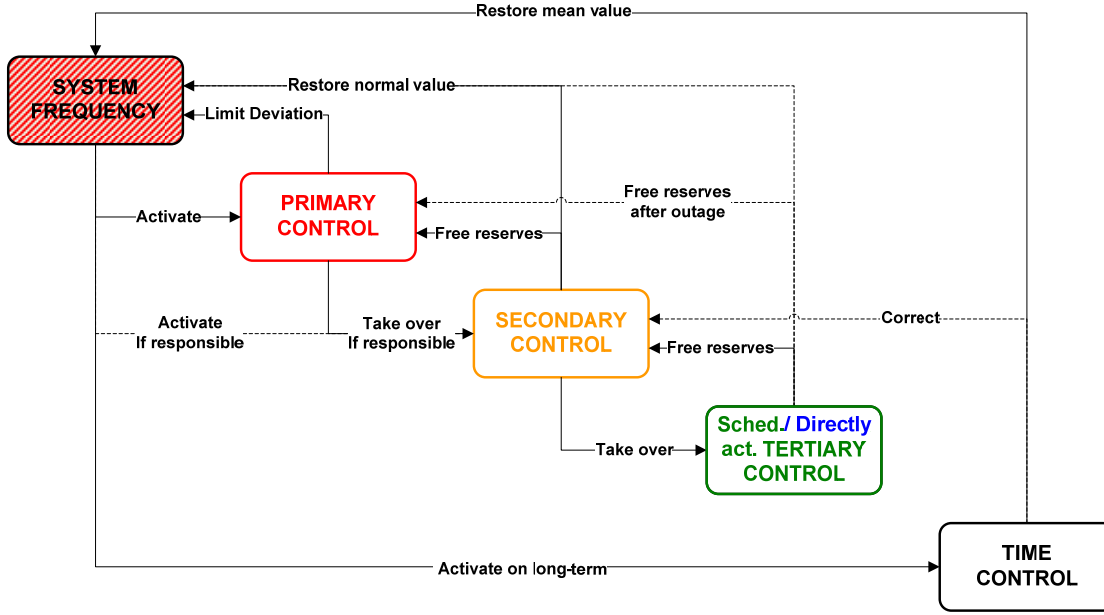
Figure 2.8: frequency controls services relationships and functionalities [187]. The names of these services refer to the names used in the Continental Europe (see appendix B of [59] to map these names to the services of figure 2.7).

power injection in the grid. The aim is not to restore frequency but to balance the power mismatch as soon as possible. Historically, this service is provided by high capacity synchronous generators (according to Italian grid code, all generators with Power rating more than 10 MW should obligatory take part in PFC [177]). Generators measure their rotor velocity, which corresponds to the local frequency, and change immediately their power reference set-point according to their droop defined as:

$$s_g = -\frac{(f_t - f_{nom})/f_{nom}}{P_t - P_{nom}/P_{nom}} \qquad [\%] \tag{2.21}$$

where:

- f_t is the frequency signal measured by the generator;
- f_{nom} is the nominal frequency of the grid: 50 Hertz in Europe;
- P_t is the new instantaneous power-set-point due to primary control in MW;
- P_{nom} is the power set point due to normal market scheduling of the generator.

29
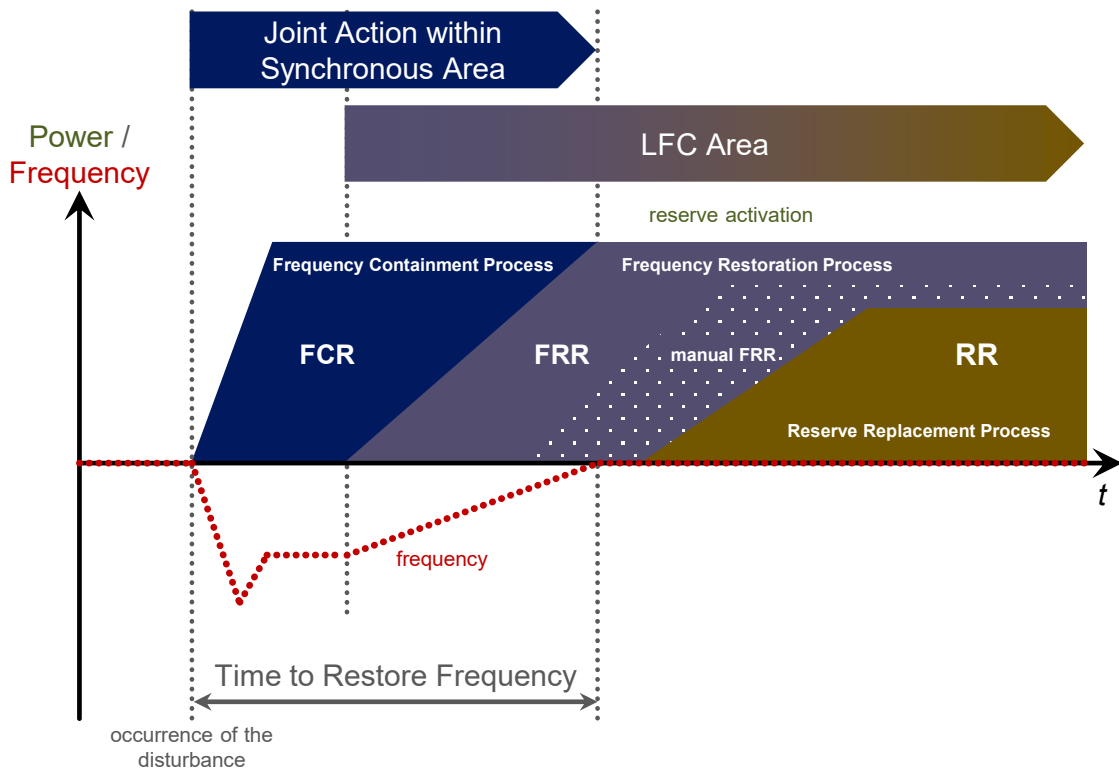
Figure 2.9: dynamic hierarchy of frequency Control processes. Image taken from [59]

Normal values of droop are from 2% to 7 % . Usually, a dead-band is also applied to not over-stress the generator governor mechanisms and to avoid set-point mistakes due to the limitation and error of the measurement system. Every European TSO sets specific values for the PFC in order to guarantee a part of the total amount of the Regulating Energy defined as $\lambda_u = {}^{\Delta P_a}/_{\Delta f}[MW/Hz]$, where ΔP_a is the reference European contingency and Δf is the expected steady-state frequency deviation after the transient (i.e. 200 mHz). The reference incident for the UE grid consists in the tripping of the two biggest nuclear power plants with a combined power loss of 3000 MW. Every area should contribute percentually to the Regulating Energy with a coefficient C_i calculated on the basis of the principle of Joint Action. Dynamic simulations are also performed to assure that transient frequency does not fall lower than 800 mHz in order to avoid automatic load shedding. For these simulations specific assumptions for FCR dynamics and load conditions are made. Every TSO should check that primary reserve is deployed within a certain time (for example: full activation of reserve in Italy by generators is expected in no more than 30 seconds).

Frequency Restoration Process , also called secondary frequency control. After a disturbance has been stabilized by PFC, other generators following the secondary frequency control power signal, restore the nominal frequency. This two-step process (primary + secondary) is required to avoid instability and power sharing conflict among generators governors that would happen in the case an unique control signal is used. The goal of SFC is two-fold:

- restore the nominal frequency of 50 Hz;
- restore the power exchange among European Areas to their reference value.

Secondary control is composed by a proportional-integral controller, computed in such a way that it only activates in the area where the power disturbance has taken place. The secondary controller sends, in real time, a unique control signal to every generator which participate to SFC equal to:

$$L = 50 - \frac{100}{P_D}\beta_1 G_i - \frac{1}{T_r}\int G_i\,dt \qquad [\%], \qquad (2.22)$$

where P_D is the total Secondary Band Reserve in the grid, β_1 is the proportional constant and T_r is the integral constant in seconds and usually quite big (from 100 seconds to 200) to avoid a too fast response and overshooting problems. G_i is the **ACE or Area Control Error** which takes into account the frequency deviation and the power tie-line exchange error. It is calculated as:

$$G_i = P_{meas} - P_{prog} + K_{ri}\Delta f \qquad [MW], \qquad (2.23)$$

where $P_{meas} - P_{prog}$ is the difference between the programmed power exchange among areas and the actual power exchange due to the activation of Primary Reserves or other not scheduled events; K_{ri} is the regulating energy of the area itself. The ACE is 0 for all areas, except for the one in which the disturbance occurs. The signal L goes from 0 to 100 % indicating the power to be produced by the generators for SFC: 50 % corresponds to zero power production, while 0 and 100 % correspond to the production of the total generator secondary band respectively in the downward and upward direction.

Secondary reserves can be computed in different ways depending on the characteristics of the load and the market rules. TSO computes the frequency from a specific stable node and monitors all the tie-lines of its grid, then

gathers all these signals, computes the level L and communicates it to the regulating generators every few seconds (for ex. in Italy, 4 seconds). The time of activation depends on the nature of the generator used: gas, water and coal power plants have different rate constraints and ramp mechanisms. Different quality parameters are used to check the consistency and the intervention of secondary reserve.

Reserve Replacement or Tertiary Control. Tertiary reserves are manually dispatched in order to restore secondary reserves. Least cost dispatching plants are used to fulfil this service.

RoCof control. This new service is still yet to be used. The activated resources will modulate their power depending on the value of the frequency derivate in order to replicate the damping effects of the real rotating inertia. Due to the very fast expected response (ideally less than 10 ms), only machines connected to the grid through fast power electronics could participate to this service.

Time control. It is an index used to measure and control the long term frequency deviation evaluated as the difference between the nominal time and the electrical time, this last being computed as the integration of the second-by-second frequency of the grid. When the grid frequency is fixed to the nominal value, electrical time is equal to the nominal time. Many devices compute the clock time by using the frequency of the system:

- old meters of electrical energy compute the time to distinguish among the different tariff periods;
- power plants control energy systems;
- power quality devices;
- old industry's processes;
- customers in textile industries;
- synchronous motors which drive the value of clocks.

In Europe, time control is adopted since many decades. In practice, the TSOs raise or lower the reference frequency for the SFC by a specific amount for a certain time, so that the electrical clock deviations stay within few seconds.

2.2.2 Renewable impact on frequency stability

As written in subsection 1.1, the major growing renewable sources are Wind and PV technologies respectively connected to the grid through an AC-AC and

a DC-AC converter, both of which hold no rotating part providing no inertia to the system. The converter commonly operates in grid-tied mode reproducing the measured voltage levels and frequency signal at the connection with the grid. Moreover, both technologies are non dispatchable in that they always instantaneously maximize their power production in function of the external conditions: wind gust, Sun and cloud movements are the major phenomena which affect the output of the plants. In order to provide reserves to the grid, the RESs should keep some head to their maximum production. This leads to a waste of primary energy source, and does not guarantee that RES can provide a reliable frequency control. In the case of wind turbines, frequency control is also possible by making use of the kinetic energy stored in the turbine blades [47], but the amount of energy that can be released is limited and needs to be restored immediately after the transient endangering the grid stability.

RESs plants have a double effect on the frequency dynamics as shown in equation 2.3: the numerator will be influenced by the variability of the renewables primary sources (like wind or Sun radiation), while the denominator will decrease as the system has less inertia coming from the SGs. Expected frequency oscillation will be higher and faster. Besides, the RESs reduce the ability to forecast the net Load and increase its ramps, forcing the TSOs to increase the reserve requirements in the case of unbalanced periods.

2.3 New Resources for Frequency Control

In the future, due to RES increase and market integration, the European system can be subject to RoCoF of more than 2 Hz/s, and in case of area splitting power unbalance can reach up to 40% in each area of the total Load [55]. Under normal operation the degradation of the frequency signal can affect the power quality. Various solutions and improvements to manage RESs are detailed in [86]:

Interconnection & market integration. The continental Europe, being a synchronous area, shares already primary reserves among countries. New interconnection lines lower the possibility of bottlenecks among countries facilitating the creation of common power and energy markets: frequency reserves can therefore be dimensioned and operated at the European level increasing in such a way techno-economical performances.

Flexible dispatchable plants. CG, except for Hydro turbines, are generally not very efficient in working outside nominal point and besides can have production ramp constraints. New generation combined cycle gas turbine are

33

designed with much more flexibility and a better dynamic behaviour outside the nominal point.

Demand Side Managment. Different typologies of loads can participate to all frequency markets, thanks to the use of new generation Information and Communication Technologies (ICT). Examples are power-to-gas plants, electric vehicles, RESs (especially in under-production), cooling and refrigeration appliances [20], building systems [193], water heating units, etc.

These resources are commonly aggregated by new entities known as aggregators. When small RES plants are present, load owners become pro-sumers, i.e., at the same time producers and consumers of energy [27]. Different layouts are incentivized and regulated by the various energy regulating authorities [40].

Synchronous compensators. These are essentially synchronous machines running at zero load, which are able to regulate the level of produced reactive energy. Their primary objective is voltage control, but in the same manner of the SGs they provide inertia and high short circuit currents.

Storage. In order to be stored, electricity must be first transformed into another kind of energy (for example potential energy of dams, rotating energy of flywheels, pressure energy of compressed air energy storage systems, etc.) and then, when needed, converted back. Today **the only mature and largely installed technology is pumped hydro**: it is mainly used for energy based services such as peak levelling or energy arbitrage, but the installations of new plants are limited by the presence of suitable physical sites. New technologies storage costs, as known, are very high, but today new technologies have the potential to revolutionize the market and introduce high quantities of storage into the grid, causing an enormous transformation in the grid management [98] [43]. In view of a liberalized and efficient market for the storage, it is important to avoid regulation and economical barriers which could slow the diffusion of new technologies more than the technical problems themselves [174]. Storage can be classified depending on the typology of energy transformation (we usually divide into electrical, electrochemical, mechanical, thermal storage). For a better understanding of the best grid application, it is useful to consider the power and energy typical ranges of the various storage systems: such information is summarized in the Ragone plot (see Fig. 2.10). Other specific-technology characteristics, like geographical limitation or special maintainance needs, are also important to be considered in the storage technology choice (see [152]).

34
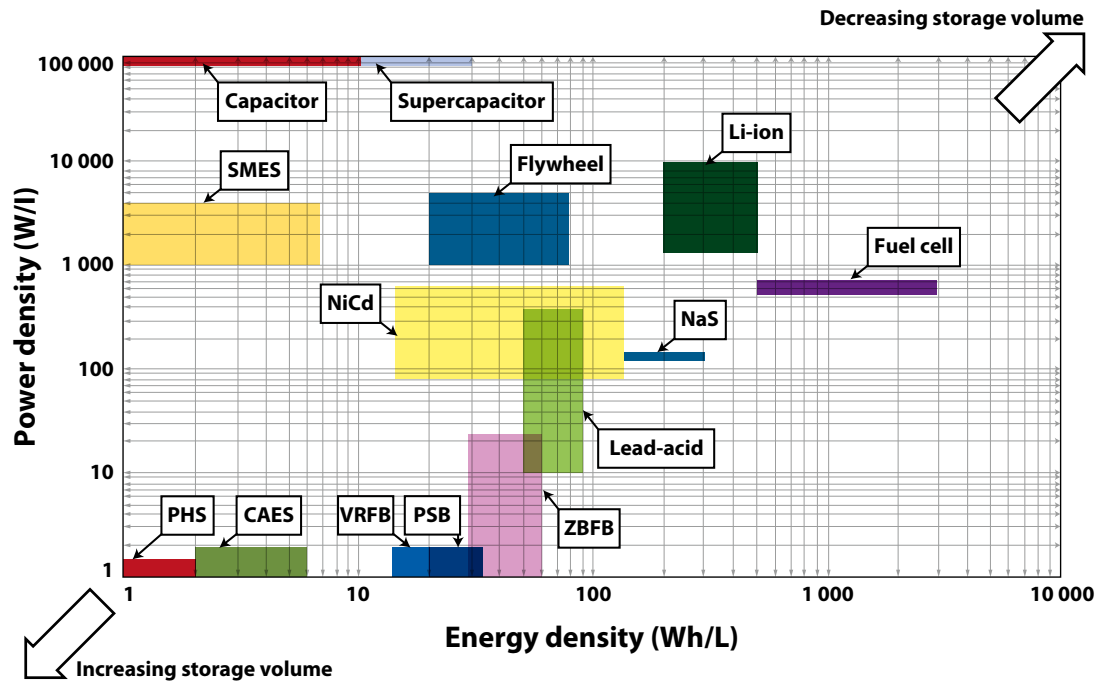
Source: Luo *et al.*, 2015.
Note: SMES = superconducting magnetic energy storage; NiCd = nickel cadmium; NaS = sodium sulphur; PHS = pumped hydro storage; CAES = compressed air energy storage; VRFB = vanadium redox flow battery; PSB= polysulfide bromine flow battery; ZBFB = zinc bromine flow battery.

Figure 2.10: Storage power and energy density characteristics [59].

2.3.1   Battery energy storage systems uses

In the last few years the installations of batteries is gaining a certain momentum and costs are still expected to decrease. BESSs (especially but not exclusively lithium-ion technology), thanks to their velocity and the good power and energy ratings, are already being used in various applications [152]. These systems are easily scalable, packed in different dimensions and not-site dependent like CAES (compressed air energy storage) or PHS (pumped hydro storage). Besides, they are divided between utility grid storages and small home systems installed in combination with PVs systems to increase the self-sufficiency of the owners. [174, 152] investigate the most profitable services BESSs can provide to the grid today and in the near future: these systems will work for the accumulation of electricity produced by home PV systems in order to increase self-consumption (more than half of the use), fast frequency regulation (up to 15 %) and renewable capacity firming (up to 14 %) in order to decrease utility scale RES production variability. The studies clarify that BESSs spread will happen only in the case of a favorable regulating framework for owners. Other possible interesting applications are [95, 10] :

35

Flexible ramping. BESSs, thanks to their high power capability, can lower the stress of the system and decrease the net load variance especially at dawn and twilight, when there is a large presence of PV systems in the grid.

microgrid support. Islanded system needs BESSs at all time ranges: their contribution goes from assuring the daily energy balance to the instantaneous power equilibrium due to load stochasticity. The installation of short and long term storage, characterized respectively by high power and high energy ratings, is needed to optimize the island behaviour. Nowadays, most off-grid systems make use of expensive and polluting diesel generators which nevertheless present a lot of flexibility and management reliability. BESSs can help shifting from diesel based systems to the use of RESs. New generation microgrids are also the first systems where only converter based generation is present, so that different techniques for the parallel connections of converters are tried out in a smaller scale before being deployed in bigger electric systems.

Transmission and distribution congestion relief. Depending on the grid structure, certain particular lines or stations can saturate for a small number of hours due to RESs productions. The use of localized BESSs can help to decongestion the grid without the costly need to upgrade the whole infrastructure.

Energy supply shift. BESSs can be used for energy arbitrage, this means to store energy when the price is low and to resell it when the price is higher at the peak consumption hours. BESSs are suited for 30-minutes to 1-hour time operations and this can be useful for the grid in order to level its peak consumption avoiding the use of expensive gas turbines or the more expensive upgrade of the grid infrastructure.

The installation of new type of storages (except pumped hydro which amount to 198 GW world-wide) have reached more than 3 GW of installed power in 2018 with BESSs, especially lithium ion technology, representing more than 85 % of new installations in 2018. [3]. Around one third of installations comes from South Korea. Other countries in which these systems are quickly developing are Japan, due to PV battery system and to enhance resilience against natural disasters, Germany, United Kingdom, China and USA. In the future, more installations are expected with other technologies such as flow batteries characterized by high energy-ratios. Additionally, manufacturing capacity for lithium-ion batteries is

---

[3]source: https://www.iea.org/tcep/energyintegration/energystorage/

expected to increase threefold by 2022, driven by the booming of the EV market and possible costs decrease. At the end of their useful life, EV batteries can still be utilized in the power sector where space constraints are less strict.

Frequency control regulation is today one of the most lucrative service to be offered by utility scale BESSs systems. With respect to conventional generation, BESSs present inherently advantages[101]: reserve provision from CG limits the maximum output that a power plant can offer to the energy market, decreasing its potential profits. Secondly, when RES production is high, partial closing of renewables plants can be needed to assure that CG can remain connected to the grid. In fact, power plants must run over their minimum production set point in order to provide frequency reserves. On the other end, Batteries provide power control without any need to produce energy decoupling the power and energy market. Besides, they can offer upper and lower regulation with the same nominal capacity, while CG needs to use the double amount of capacity. Fast velocity of response is another element which makes BESSs suitable for frequency control: as a matter of fact, in UK the last tender for "enhanced frequency response" (the fast service provided by BESSs) have being cleared at lower prices with respect to the "firm frequency response" (traditional control performed by slower resources like CG) [4]. Several markets have opened the possibility for BESSs to offer primary control like services. In particular, we can count:

- Australian system. The Australian system operator publishes quaterly report on the market cost and grid dynamics [135]. Starting from the Tesla installation of 100 MW BESS (Hornsdale Power Reserve) in 2017, the frequency control ancillary services (FCAS) costs are reducing thanks to the use of BESSs and demand response services, which accounted respectively for 17 % and 15 % of the whole supply mix in the first quarter of 2019. The Hornsdale Power Reserve has already avoided systems blackout and it is able to intervene in about 100 ms.

- UK market. In UK, a new service called "enhanced frequency response" has been established which requires to provide the full band in less than one second. In the 2016 auction, the TSO contracted 200 MW of reserve capacity for four years: even though the tender was technology neutral, BESSs won the entire offered capacity [10].

- United States. The Order 755 of the Federal Electricity Regulator Commission (FERC) has mandated a separate compensation structure for fast-acting resources, such as batteries with respect to slower acting conventional

---

[4]https://everoze.com/what-7mwhr-for-efr-storage-explain/

resources.

- European Union. Energy directives are moving towards an effective integration and regulation of storage systems. In 2017, System operation guidelines (SOGL) [39] accounted for the possibility of energy storages to provide FCR and in Article 156 point 11, ordered Continental Europe and Nordic Europe TSOs to propose a cost benefit analysis in order to evaluate the best time range for which BESSs must remain available while providing full activation of the FCR. Moreover, in 2019, Electricity Directive [147] states that energy storage facilities should be "market-based and competitive" and explicitly integrated in new market designs. System operators can own storages to assure network security and reliability, but not balancing or congestion management.

- Central Europe. Many TSOs from Central Europe countries (France,Germany, Belgium, Switzerland, Netherlands and Austria) gather FPC reserve in the same competitive market. The tendering period was changed from weekly to daily in 2019 [1] and it is planned to be reduced further to 4 hours in the beginning of 2020. In this market, BESSs are strongly present with more than 100 MW usually assigned causing a decrease in prices in the last years.

- Italy. Our country has implemented a series of pilot projects [179] through its TSO, Terna, and has already installed in 2014 several BESSs in Sardegna and south Italy to test power intensive and energy intensive technologies. Fast services such as primary frequency and RoCof Control were investigated. Today, particular kind of virtual power plants are experimented for the participation in balancing markets: in particular, aggregators of the size of at least 1 MW of RESs, consumption units and storages will be able to offer balancing and tertiary frequency control to the grid (these aggregators are called UVAM or Unità Virtuali Aggregate Miste [180]). Moreover, the Italian TSO Terna [178] has recently started a new ancillary service for storage systems based on the provision of fast droop control expecting to gather at least 200 MW of resources.

Conclusion

In this chapter we analyzed the basics of frequency control and BESS technology. First, in section 2.1 we presented the physics behind frequency signal dynamics of the grid: this value is strictly linked to the rotor velocities of SGs. Real measurement from PMUs have shown that during normal operations frequency is

38

equal in every point of the grid and its dynamics depends on the overall equilibrium between total generation and demand. A constant frequency is therefore a system which maintains its equilibrium. During a contingency the SGs follows a brief transient before returning to rotate at the same exact velocity thanks to the damping torque of the rotors, machine regulators and electric grid characteristics. Currently in Europe a hierarchical control with four levels is implemented to control the frequency value which is described in 2.2: as renewables continue to increase into the grid, new solutions are to be found to control frequency. In section 2.3 we introduce new solutions: among them BESSs seem to represent an optimal techno-economical option since they are able to provide high power and low-medium energy based ancillary services: UK, Australia, Central Europe are starting to make use of BESS in their primary frequency reserve with good technical and economical results.

Chapter 3

Literature Review on Frequency Control

Section 3.1 presents the methodology I followed to organize the literature review. This review critically discusses what is present in literature, categorizing the works in a original way by taking into consideration the scope of the analysis (open loop, closed loop and normal operations) and main relevant areas of research. Papers are critically compared in terms of models, methodologies and results obtained and grouped by similarity. From this chapter, it is possible to grasp the current trends of the existing literature and it serves as a basis for the development of the next chapters. Results and author opinion on the analyzed works are gathered at the Conclusion chapter of the Thesis.

3.1 Methodology

In this chapter I mainly restrict the review to papers concerning the use of BESSs or EVs for fast frequency control services. While it is possible for these storages to participate to other services, I will concentrate on PFC and Rocof control as BESSs are particularly suited and these services are especially remunerative.

Three main typologies of studies have been identified in the literature depending on how the electric grid is modelled and what impact or aspect of the BESSs is analyzed:

Open loop studies. In this group, BESSs contribution to the frequency stability is not evaluated. The grid is not topologically modelled, but it is represented by a series of inputs of the BESS controller and management system (for example, frequency error dynamics, price signal, dispatching orders etc.).
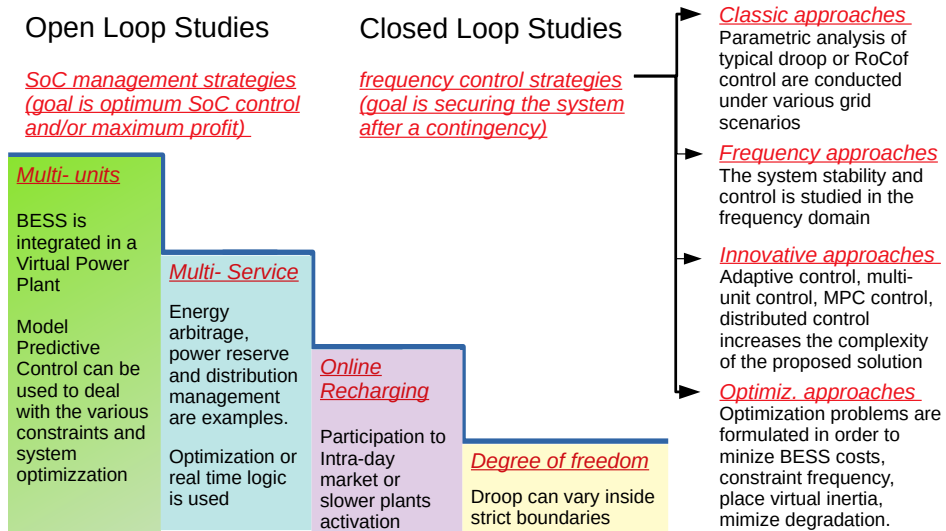
Figure 3.1: Families of strategies and approaches used in the analized works.
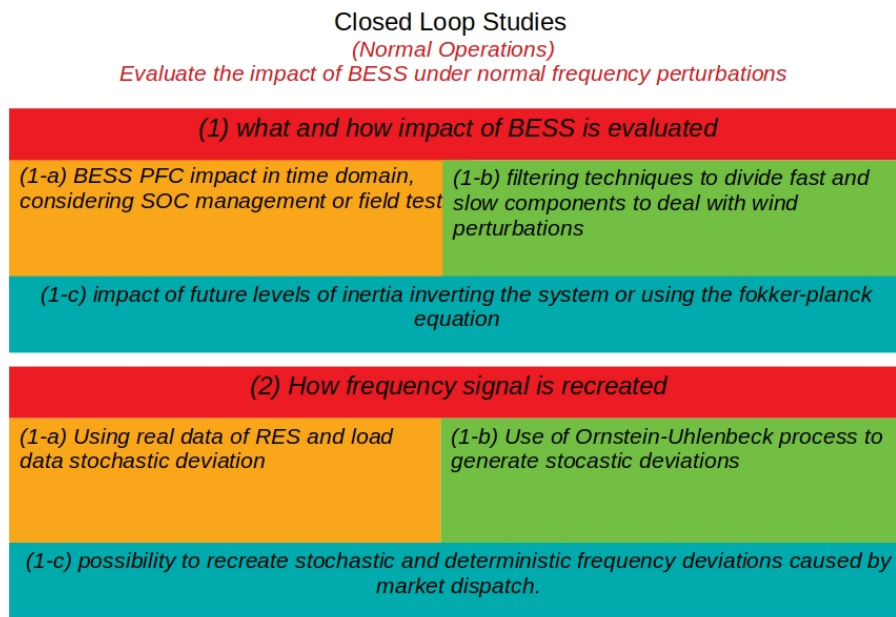
Figure 3.2: research questions of close loop studies.

The major focus is on the the BESS techno-economic operations, multi services provision, degradation of the cell, etc. Usually several days of normal operations frequency profiles are used.

Closed loop studies for Contingency Analysis. The focus of this group is

the simulation of a contingency in the grid. BESSs or other resources are used to assure frequency stability in the system. The goal is to quantify how much BESSs are needed to stabilize the grid, what is the impact of PFC or RoCof control and what is the stress sustained by BESSs.

Close loop studies for Normal Operations In this last group, the main concern is the impact of BESSs on grid frequency signal during normal operations. A difficulty of these studies is to reconstruct a realistic frequency signal. Once this has been done, it is possible to quantify at the same time the BESSs impact on the grid signal and the impact of frequency control on the BESS itself.

The three groups are shown in figure 3.1 and 3.2 where a high level description is presented.

Various choices are possible for the electric grid and the BESSs models. For what concerns the electric grid system I used simplified frequency response dynamic models or complete dynamic models. For BESSs there are several families of dynamic models usually adopted [41] :

Electrochemical Models. These models take into account all the electro-chemical dynamic phenomena happening inside the cells (oxidation-reduction processes of anode-cathode elements of the cells). They are computationally heavy and make use of coupled partial differential equations [92] which describe both macroscopic (voltages and currents) and microscopic quantities like local distribution of charge, materials concentration, current, temperature, etc.

Electrical Models. These models make use of equivalent circuit components to represent the various BESS and cell parts. Usually, voltage sources and passive elements depend on operating conditions and are implemented through look-up tables whose values are obtained by testing batteries cells [14]. Techniques such as impedance spectroscopy tests could also be used [162]. Models are quite accurate (1-5 % range of error), but are valid only for tested conditions. The electric model can be also extended by taking into account SOC runtime computations, degradation and temperature dynamics.

Mathematical Models. These are usually the most computational light models based on analytical or stochastic approach. A physical description of the cell is neglected and BESS parameters like State of Charge (SOC) levels and power production are based on numerical models. Usually current and voltages informations are neglected.

43

Storage units are interfaced to the grid through the use of converters. These units are responsible of converting the DC current produced by the storage device into AC current. The DC current passes through a DC-link capacitance and then is converted by the action of the switching gates. The converter does not naturally interact with the grid but it depends exclusively on the control algorithm [125]. The converter velocity assures the provision of fast services (in the order of few milliseconds) given that no voltage instabilities are created on the DC capacitance. If the storage source behind the DC-link is not sufficiently fast or if strange interactions with fast grid lines dynamics are created, the converter unit is slowed down. [175]

The use of electrochemical models is typically limited to detailed studies of BESSs technologies with little applications to power systems, while electrical and mathematical models have wide applications.

3.2 Papers Groups

3.2.1 Open loop papers

These studies could be categorized starting from three main features of interest:

- the strategy to provide frequency control to the grid and, at the same time, to manage the SOC of the BESS to assure the continuity of the service. PFC is performed in most of the works here analyzed.

- Secondly, the model of the BESS and the possible quantification of BESS degradation due to service provision.

- A third interesting aspect is the use of real input data in order to produce realistic (even if case-specific) results. Economic outputs are often computed to quantify investment viability in BESSs systems by making use of classical indexes such as Return on investement (ROI) and Net Present Value (NPV).

SoC managment. To perform SoC management, the answer of a BESS providing PFC can be divided in two components:

$$P_{\text{BESS}} = P_{\text{PFC}} + P_{\text{SOC}}, \tag{3.1}$$

where P_{PFC} follows a linear droop frequency control with a certain droop $\frac{\sigma = \Delta f / f_n}{\Delta P / P_n}$ usually going from 2 to 5%. This component should be always present in order to better cope with contingency or faults during grid operations. Frequency

control can be considered a zero-mean energy service due to the symmetry of the frequency signal, however the internal BESS losses and the presence of long over or under-frequency periods in the grid, can discharge a BESSs up to 0% or saturate it at the maximum energy content, % unenabling the possibility to perform PFC. For this reason P_{SOC} component is constructed in order to stabilize the SOC. Note that in these works, being the grid not explicitly modelled, it is not possible to quantify the impact of P_{PFC} and P_{SOC} in the grid, and this is clearly a limitation. The various techniques to stabilize the SoC can be grouped in several families:

(a)　　　　　　　　(b)
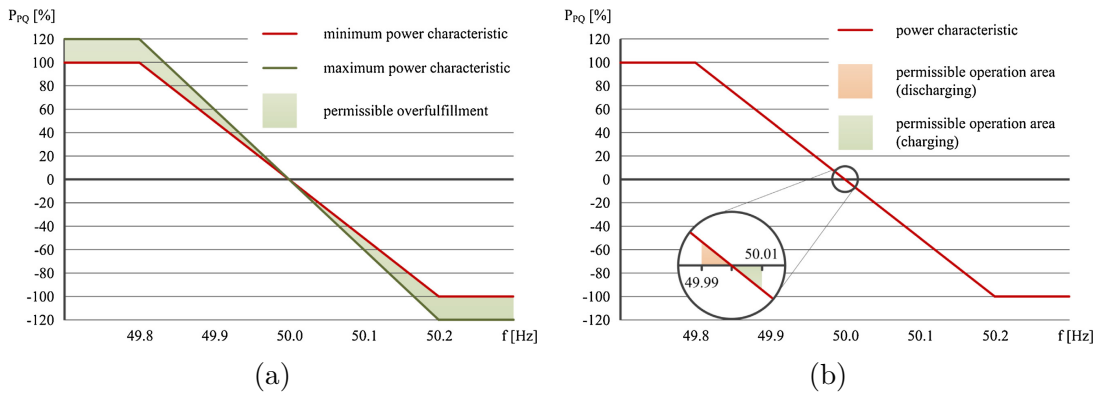
Figure 3.3: Degree of freedom in PFC in Central Europe for BESS [67]
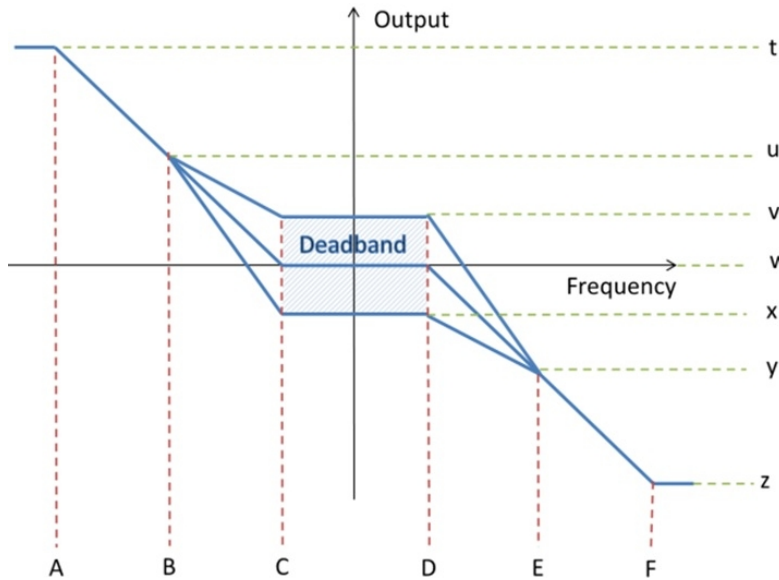
Figure 3.4: UK enahnced frequency response envelope [206].

45

First approaches. Scheduled recharging and dead-band recharging are first simple approaches used in early experimentation or researches. In [105] a pilot project is presented for a battery providing frequency control for the islanded system of West-Berlin. The BESS is recharged during low load hours and clearly in those times cannot provide PFC jeopardizing the grid stability. More recently in [144] and [121] the BESS makes use of the time periods when the frequency error is located inside a narrow window around the nominal value (in continental Europe, ENTSO-E prescribes a value of 10 mHz around 50 Hz). Inside this interval, the BESS will recharge or discharge with a certain rate equal to a small percentage of the nominal power. Although a certain help to SOC control is given, it is possible that the SOC goes to 0 or to 100 % after long over/under frequency periods. Moreover, the massive use of dead-band control can make the grid frequency itself to oscillate more.

Services degree of Freedom. A group of studies are based on the analysis of BESSs operating under the degrees of freedom which are allowed in the Central Europe and UK fast frequency markets. As described in [67] there are three degrees in German market (see figure 3.3): exploitation of the deadband space, over-fulfilment in over or under frequency and scheduled transactions in the intra-day market. In [53] and [68] the same degrees of freedom are exploited with better battery models and optimization techniques. In UK, the BESSs are allowed to operate inside an envelope whose borders depends on the particular market regime (see figure 3.4).

In [88] deadband, constant offset and variable droop strategies based on look up tables are used and results are compared in terms of SOC management. In [114] is treated the problem of optimizing the behaviour of BESS subunits performing PFC in the central Europe market. Since every cell stack possesses its own non linear efficiency curve which depends on the produced power, it is necessary to consider a proper power sharing between the stacks and a corresponding good SOC management to keep all sub-units charged and the BESS working at the highest efficiency possible.

Online Recharging. These strategies fundamentally work like a filter: the BESS responds to dangerous fast frequency error components, while a second much slower component creates an offset in the control used for SOC management. In [118] and [23] this principle is used to find out the optimum energy-to-power ratio for BESS performing primary frequency control. The control technique consists of a P_{SOC} (see equation 3.1) component computed as:

$$P_{\text{SOC}}(t + d) = \frac{\sum_{j=t-a}^{t}(-P_{\text{PFC}} + P_{\text{loss}}(j))}{a},$$ (3.2)

46

where d is the delay period of the control, a is the averaging period and $P_{\mathrm{loss}}(j)$ is the estimated losses of the BESS due to stand-by losses and internal inefficiencies. This power comes from the activation of slower power plants or by buying energy from intra-day market. A faster P_{SOC} component means better SOC management and lower needed BESS capacity but it is more destabilizing for the grid. For this reason in [118] three indexes are computed to quantify how much and often this offset is requested. In [113] and [127] Discrete Fourier Transform (DFT) is used to analyze the frequency signal. Different energy storage technologies were dimensioned to address the different harmonics of the frequency power spectrum. BESSs are very well suited for fast oscillations (with mean zero and low energy content needed), while pumped hydro is more effective in the case of slower oscillations.

MPC and multi-units. Model Predictive Control (MPC) is a technique which can be efficiently used when it is possible to predict inputs data and a reliable dynamic model of the system is available. This performs multiple hours optimizations with a receding horizon of predictions and increases the robustness of the proposed solution under the uncertainty of the real input variables. In our case it is used when there is a need to coordinate a pool of different units. For example in [189] an electric vehicles aggregator and traditional generators provide PFC as a group and MPC optimizes the different resources considering their typical constraints. In [98] combining MPC with short term frequency predictions it is possible to control a BESS performing PFC. Additional multi-units layouts are presented in [171]. In [18] a run of river hydro-electric generator is augmented with a BESS in order to provide PFC, decoupling the provision of this service from the primary source availability. BESS is faster, more precise and always available, but it can lead to economic losses depending on the reserve prices.

Multi-services. To guarantee multiple flows of income, BESSs could provide more services at once. In this case SOC management is even more important as the single services must not limit or conflict with each other. A possibility is to have energy arbitrage in addition to PFC, this enhances BESS profitability and can improve the SoC [35]. A good example is given by [24] where two fuzzy logic controllers are used. The first one utilizes the frequency error and the SoC values in order to perform a variable droop strategy able to contain SOC deviations. The other controller works with SoC and energy price levels in order to buy or sell energy if signal prices are convenient and, at the same time, it avoids SoC mismanagement. In the study these two controllers make SoC management reliable, but gains from

energy arbitrage are not high even when membership function of fuzzy controllers are adjusted. Participation in energy and power markets is studied in [94] and [93] which utilize optimizations techniques and robust approaches to deal with uncertainties and increase BESS profits. Finally, in [132] the BESS performs PFC and distribution grid management. The controller is composed by a day ahead optimization of BESS dispatch followed by a real time strategy in order to assure that SoC and services be fulfilled under different real operating conditions.

BESS models. Various BESS and degradation models were used in the studies. The simplest choice is to model the BESS with a constant charge and discharge efficiency and fix the power and energy values. In [88] and [24] the BESS model, composed of a series of resistance capacitance blocks, is developed starting from experiments and laboratory trials. Each block describes a specific electro-chemical phenomenon happening inside the battery. The SoC is estimated from the voltage of a nonlinear capacitance, taking into account the intercalation of ions into the electrode structure. While this model is more realistic , it is much more computational intensive: as mentioned in [88] simulations can last up to fifty times more than simple models. A good compromise for the BESS models is to utilize empirical models [88, 114] which are based on the presence of a variable efficiency value for the BESS. The efficiency usually depends on the SOC value and it is built starting from empirical studies. In [154] an empirical model is built starting from simple test experiments. A 2 dimensional look-up table is designed to compute the BESS efficiency as a function of the SOC and of the requested power, which also takes into account the auxiliary power coming from the cooling and the power management system. The results show an error with respect to real data of less than 5% in line with the electrical equivalent models, which however are much more computational intensive. A future challenge is to evaluate the degradation of parameters over time without repeating the tests.

Battery degradation. This topic is even more important than the BESS modelling itself for studies which perform techno-economical analysis, in that degradation is an important capital loss for the investment, both in terms of assets life and the performance of the BESSs during its operations. The simplest way to take into account degradation is to evaluate the equivalent number of cycles of energy which is equal to the total energy cycled in the BESS divided by the energy capacity [88]. Another simple method is to compute the average depth of discharge [29] or the C-rate during operations. In [118] is applied a penality factor for battery cycles which goes over 85% or under 15 % SoC. BESS constructors provide a datasheet in which is reported the expected maximum number of

cycles obtained at fixed dept of discharge sustained by the BESS during tests. In the actual operations (especially in the case of FCR provision) cycles are not easily recognizable. Moreover, it is important for every cycle to know the depth of discharge and its average SOC. In [53] and [198] in order to compute the cycles performed, a rainflow counting algorithm is used. Rainflow counting is a technique taken from the study of the mechanical fatigue of materials which are subjected to stochastic load profiles. The degradation process is linked to known chemical processes such as deterioration of electrodes materials, electrolyte film formation, etc.. Experiments connect these phenomena to BESSs operational macro-variables (such as temperature, SOC, DOD of cycles etc.). Degradation can be divided by two main components: calendar ageing and cycle ageing. The first one quantifies the BESS capacity loss over time and is mainly correlated to the long term average SOC and temperature of the BESS during the years. The second component is related to the accumulated losses caused by each operational cycle and it is related to the cycle depth of discharge, temperature and average SOC. Highly non linear expressions considering power and exponential laws and the presence of parametrized corrective factors are employed to capture the complexities of the calendar and cycle aging phenomena with respect to BESS macro-variables. In the case of PFC, it was computed in [53] that calendar aging is actual predominant to cycle ageing due to the shallow nature of BESSs cycles. In [173] different PFC and SoC management strategies are compared in terms of capacity degradation created during BESS operations.

3.2.2   Closed loop contigency papers

Both PFC and RoCof control are evaluated in these studies. The typical (but not exclusive) procedure is to model a contingency (e.g. a loss of a generator) in the grid at various inertia levels and assess the impact of different quantities of BESSs performing fast services on the grid frequency signal.

To present the papers content I will briefly describe the models, methodologies, case studies and results highlighting the most interesting points and differences.

Basic Modelling choices.   Two kinds of grid models can be used to study frequency control. In particular, works like [89, 183, 167, 28] are based on a low-order System Frequency Response Model (SFRM) [8]. The starting point of the model is the Swing equation of the synchronous generators as described in the previous chapter and this approach simplifies the grids dynamics. On the other hand, in [138, 2, 153, 158, 26], algebraic-differential equations are used to describe all relevant components in terms of electrical, mechanical and magnetic phenomena. The models have to be chosen accurately since a big number of equations and non-linearities can increase the

49

computational burden of the time domain simulations. Two objectives are possible [123]: **(a)** assessing the electro-magnetic behaviour of power system devices or, as in our case, **(b)** assessing the electro-mechanical response of the system after a disturbance.

For point (b) there is no need to use electro-magnetic models and solvers in the abc time frame, since fast or non linear phenomena (like switching gates of converters or hysteresis and magnetic flux dynamics of SGs) can be neglected. The description is based on phasor or dynamic phasors models in the dq axis [104, 126] and an appropriate numerical integration method has to be chosen [123]). Typical softwares are Dig-silent, Eurostag, R-scad (used in the field of real time simulation [126]), PSSE and Dome which is a software based on python [122].

The SFRM and complete models are compared in [65] and in [169]. SFRMs are based on certain restrictive hypothesis (rotor angle stability, voltage stability) and assume the power losses to be constant in the grid. These conditions are well respected in the grid even during a contingency [158]. The comparison with complete models shows a pretty good matching between the two simulated frequency dynamics. SFRMs offers a good and fast alternative to the use of complete models in order to study the frequency stability of the system. In all read papers, the system inertia is considered to be one of the most important parameters of the grid [182], especially to limit the Rate of Change of Frequency (RoCoF) value in the first instants.

Objectives and methodologies adopted can be divided in several categories:

Classic/Probabilistic control approaches. In studies like [38] and [136] BESSs are added into the system and their impact evaluated with respect to traditional reserves providing PFC and RoCof control after a contingency. In [75] a probabilistic approach is adopted where relevant grid and BESSs parameters are varied in order to quantify frequency recovery under different conditions. In [100] the equivalent inertia provided by the BESSs H_{BESS} is computed by considering BESSs delays and saturations. In [26] starting from simulations, output surfaces of f_{nadir} and other relevant quantities are built in function of the delay value and of the BESSs installed capacities. In [5] a fleet of Electric Vehicles (EVs) performing PFC is studied: a certain distribution of delays is applied to the population of vehicles to mimic the fleet spatial dispersion and connection to the distribution system. The contingencies are modelled as strong wind changes under a very high penetration of wind sources. In [129] there is a great effort to simulate realistic presence of EVs in the grid by using different categories of vehicles and EV drivers.

Time duration and energy consumption of travels are extracted from specific probability distributions functions. EVs are also charged according to dumb or smart charging strategies and perform PFC with the remnant part of the battery. Another important aspect is investigated in [139] where different typologies of measuring techniques and control strategies are used in order to evaluate the effect of energy storage after a fault in the grid. The local bus frequency measurement, the COI frequency and the bus voltage signal are employed as input of the controller . Several scenarios are constructed based on different strategies, bus locations and fault clearing time. A high number of time domain simulations is performed recording the percentage of unstable simulations.

Frequency domain approaches In addition to explicit time domain simulations, also frequency domain analysis is used to investigate the BESS impact. In [28] and in [167] the asymptotic stability of two slightly different SFRM models is studied by checking the root locus of the system transfer function: instability is rare and is caused by the presence of a negative zero in the governor response of generators. A negative zero is usually present in certain kind of hydro-electric plants. Another source of instability can be the presence of Phase Locked Loop (PLL) devices in combination with RoCof control. Phase Locked loops devices are used to measure the grid frequency. However, the derivative of a signal amplifies noise errors, therefore caution must be used in designing the constants of the PLL loop control.

Innovative control approaches. In [22], the control strategy for BESSs and other resources presented in [23] is evaluated from the point of view of the effect on the grid frequency signal. Frequency control is provided by different storage technologies which are activated optimizing their intervention according to their possible ramp rate and energy content. Every unit participate for a specific part of the control and the frequency signal presents minimal changes with respect to a classical droop approach. In a similar way in [21] the effect of recharge strategies of BESS on the post-fault frequency signal is evaluated. In [203] an adaptive droop control is used for BESSs providing FPC in islanded microgrid. Droop can change depending on the available power margin of the battery and the need for more effective response. This technique guarantee better small signal stability (studied through the root locus) with respect to classical fixed droop control and a better power sharing between BESSs without the need of communications. Other works like [141][138] study the short circuit of a line. In this case BESSs provide local frequency regulation in order to avoid the Synchrnous Generator (SG) loss of synchronism. Proportional Integral or H_{inf} control is used to regulate the converter output. Robust H_{inf} based control is implemented in [97] to

51

manage a microgrid system frequency characterized by renewable and load noises uncertainties. The MPC is present in various studies [190] [189] since it is able to keep into account the different resources energy and power rate constraints when providing frequency control. In [186] the MPC control is improved by inserting a so-called Control Lyapunov Function (CLF) as a terminal cost term which can assure stability. BESSs perform better against the classical approaches but deliver more power with unpredictable profiles. The use of a SFRM let the BESS to achieve optimal control of the system variables being it possible to include the entire grid dynamics in the controller design. Another interesting topic is the study of distributed frequency control as opposed to decentralized PFC and centralized secondary frequency control [110, 137]. For example in [142]) COI frequency signal and the frequency divider formula is used for a coordinated area control rather than the local frequency. Distributed control is a convenient way to gather local demand side resources. Game theory and multi-agent systems are utilized to study such aggregations [46, 109].

Optimization approaches. Some approaches tries to explicitly optimize the system response by controlling the BESSs presence and intervention in the grid. In [116] an optimization problem is formulated in order to minimize the cost of installing BESSs able to assure frequency recovery in the system. A simplified piecewise linear frequency dynamics is used to lighten the complexity of the problem. BESSs installation cost is of quadratic form $C_{\text{inst}}(Pb) = aP_b^2 + bP_b$ where coefficients a and b reflect the real economies of scale [150]. As shown by the results, the linear frequency approximation gives a conservative solution, which is further adjusted by an additional algorithm. In [65] 5 objectives functions are minimized by optimizing the values of droop and inertia provided by energy storage and the PID secondary frequency controllers constants. These objectives functions are based on the frequency signal shape and the value of virtual inertia constant H. An elitist Pareto-based multi-objective evolutionary algorithm finds and ranks the best possible solutions. In [153] an optimization problem is formulated in order to avoid the activation of load shedding after a contingency by using BESSs. The problem is solved through heuristic methods (BAT optimization algorithm) and tries to minimize the participation BESS and its energy content. The BESSs are located in the transmission system buses characterized by the largest transient frequency deviations. The placement of virtual inertia is addressed also in [149] where, considering a linear network reduced power system model, an optimization problem is formulated based on a quadratic performance index measured by the $\mathscr{H}_2$ norm. The solution is non-convex, but it is possible to easily provide a local optimum to particular instances of

the problem. Finally, in [115], an adaptive control optimizes the BESS impact and the SoC levels by changing dynamically the BESS inertia level. A Linear-Quadratic Regulator (LQR)-based optimization technique is utilized considering a linear SFRM model. The proposed controller is then verified through the use of detailed power system simulations.

Models. In these studies particular attention is given to the grid system and to the simulation of numerous scenarios, therefore, BESSs models are kept as simple as possible and typologies are similar to the ones presented in the Open Loop studies (see section 3.2.1). In [26] the delay of the BESS is composed by two parts: a pure delay when BESS does not respond and, a linear ramp to reach the assigned power. In [138] a generalized linear model using ordinary differential equations is presented in order to maintain a realistic approximation of the answer of the BESSs, without the need of modelling a computationally heavy non-linear electrical equivalent system.

Particular attention has been given to the modelling and simulation of the frequency signal and its derivative. As known, the operation of derivative can lead to numerical and physical instability of systems. The first problem is related to the software numerical integration method, the second is related to the actual behaviour of the control in real-world operating scenarios. In the case of RoCoF control, the power variation should theoretically be immediate in order to reproduce the effects of SGs physical inertia. However, the computation of the frequency time derivative is not easy and requires the use of appropriate filtering, computation techniques and temporal windows studied in [157, 141, 158, 26, 48]. A minimum time window of 100 ms or more should be used to avoid excessive measurement noise. Note that today in Ireland and UK a moving window of 500 ms is utilized in the anti-islanding relays [48]. A full power response of RoCof control within at least 300 ms is needed to have a good impact on the frequency which should be reduced to 100 ms to achieve the best control similar to the rotating inertia of Conventional Generations (CGs). In literature, control techniques such as virtual synchronous generators, self synchronizing synchroverters, matching control reproduce RoCof control without requiring the computation of the frequency derivative, on the contrary are affected by specific problems. The interested reader can refer to [125, 157] for further explanations.

Another important aspect to be considered is the frequency measuring device and the converter control mode. Today the most part of converters is operated as grid-following units [175] making use of Phase Locked Loop to measure the frequency. In this mode the converter read and replicates the
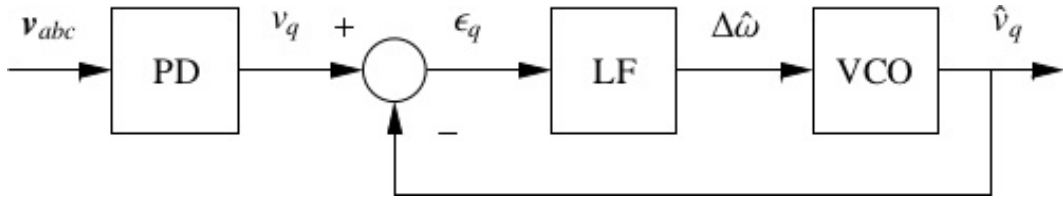
Figure 3.5: PLL basic scheme. Image taken from [125].
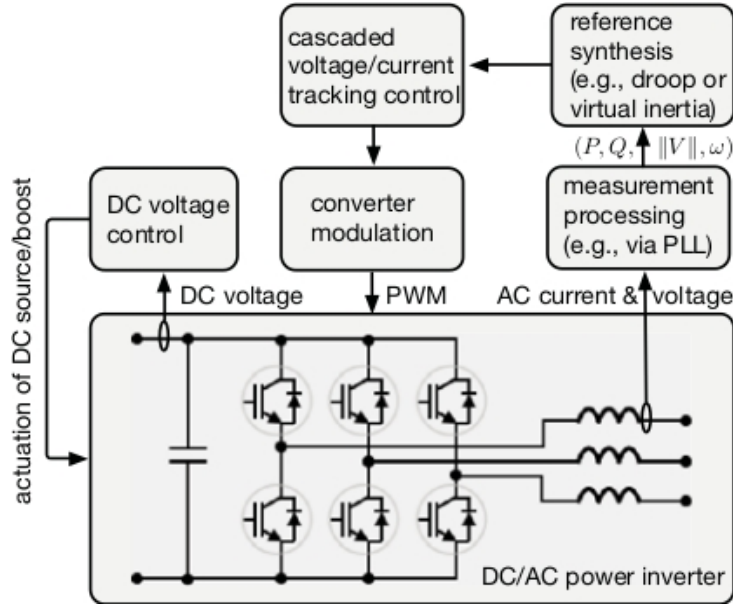
Figure 3.6: converter basic components. Image taken [125].

magnitude, phase and frequency of the voltage phasor imposed by other grid forming units (Synchronous Generators) and as a consequence the device is able to inject the desired level of active and reactive power by regulating the current. A basic scheme and 5 possible implementations of PLLs are presented in [140]. The PLL is composed by three parts (see fig. 3.5): a phase detector to pass from $v_{abc}(t)$ to $v_q(t)$ in the dq reference frame, a loop filter based on tracking controllers which estimate the bus frequency deviation and a voltage-controlled oscillator which provides the estimation of the voltage q-axis component [125]. PLLs can be sensitive to noise, delays and errors under different scenarios [157]. Another problem is the control of the DC-link capacitance voltage which can become unstable if AC-side dynamics are too fast or its value is not correctly designed. Additionally, in order to avoid unstable interaction with grid line dynamics, input power measurements high frequency components can be filtered. On the other hand a converter can

be controlled as a grid forming unit which is able to perform black-start capabilities, load sharing, frequency and voltage regulation. The principle is the opposite of the grid-following unit: the converter imposes and substain the voltage levels of the power systems. For this reason a stiff DC source is needed to adjust the produced active power. The families of possibles controllers in this case are [175]: droop control, virtual synchronous generators [161], matching control [82], virtual oscillator, self-synchronized synchroverters [205] and ICT based techniques. In particular matching control exploits the duality existent between the DC link voltage and the SG rotor angular frequency. Virtual synchronous generators can have both functionalities as grid-forming or grid-following units [16].

The generic scheme of a converter can be viewed in figure 3.6. Another possible simple scheme is to use current and voltage reference controllers in the form of PI controllers to let the unit set a certain power schedule [148] without explicitly modelling the converter phenomena dynamics. More complex approaches can be found in [44]. In [124] converter equations are presented starting from switching gates relations in time domain to reach an averaged dq frame reference model suitable for transient studies.

Indices. Typical variables utilized in the studies to quantify the impact BESS after a contingency are: the initial RoCof of the frequency, the lowest frequency point and the corresponding time f_{nadir} and t_{nadir}, the regime frequency value and time f_{reg} and t_{reg}. In [167] and [65] the frequency integral error and the integral error multiplied by time are computed as:

$$\int_0^t t|\Delta f|dt \quad . \tag{3.3}$$

These last two indexes were introduced to quantify the variability and oscillations of the frequency signal. In [38], SGs are gradually closed in order to favourite RESs. The equivalent BESS inertia is computed as the BESS inertia value which makes the RoCof stable and contained. In the same way, the primary frequency response effective factor is computed by considering the ratio between the classical frequency reserves and the BESS installed capacity needed to obtain the same nadir frequency of the initial case.

Results. All the consulted papers confirm the usefulness of BESSs in providing frequency control. In [26] the optimum delays of BESSs to maximize the impact is equal to 10 ms considering pure delay and ramp components. However, very good results can be reached under 100 ms, a threshold which is already well within today BESSs systems capabilities [15] and also avoid

the presence of too much measurement noise. In [75] the effect of small delays in RoCof control produces in the first instants a small hook transient shape which nevertheless is not dangerous for grid stability.

3.2.3 Closed loop normal operations papers

In this group of studies, the impact of BESS is measured in a day time frame and under normal deviations of the frequency signal caused by the power swings of loads, RES and conventional generation present into the grid. The key questions to construct a realistic study are: (1) how the impact of BESS is quantified ? and (2) how frequency signal is reproduced ?

Impact of BESS resources

For what concern BESS impact quantification, I observe three different families of approaches:

classic primary frequency control impact. A part of the studies deals with secondary frequency control [34, 203, 36] in which BESS impact is compared with CG. Another group deals with PFC. In [172] the impact of a BESS on a small power system is evaluated in field trials by changing the PFC parameters and estimating the change in frequency variation when the BESS is open or close. The decrease in the frequency signal is estimated by looking at the grid frequency deviation. In [91], the frequency signal of the Korean system is reproduced and a specific control algorithm, taking into account droop control and SOC management for the BESS, is implemented. Its effect on the time domain frequency signal is simulated, however no specific index is introduced to quantify its impact. In [120] the effect of BESS providing PFC is assessed on the frequency PDF by considering different controller parameters.

filtering frequency signal techniques. In [30] the effects of wind fluctuations on the grid are simulated. A BESS and a supercapacitor are used to increase frequency stability. The controller is based on fuzzy logic in which the frequency error is filtered into three different ranges and the SoC of the storage are taken into account in order to chose the power to be produced or consumed. Finally, an heuristic differential evolution algorithm is utilized to minimize the cost of installed storages, avoiding large frequency deviations. The approach to divide frequency signal in its harmonic components is also used in [127], where DFT divides the power unbalance in its high and low

frequency components. The energy storages are then dimensioned according to this analysis.

inertia impact. In [107] the BESS performs enhanced frequency control in the UK grid improving the standard deviation of the signal by considering future scenarios with lower inertia. In [192], the Fokker-Planck equation is used to determine the probability density function of the system frequency under a variety of inertia levels, droop characteristics and generators deadbands. In both works it resuts that inertia (and similarly RoCoF control) does not apparently have a big impact on frequency deviations. Note that the utilized UK frequency records have a sampling rate of 1 Hz: this represents a low sampling rate for the RoCoF signal whose dynamics of interest starts well under the second.

Frequency signal reconstruction

In normal grid conditions a correct modelling of the frequency signal is essential for a realistic evaluation of the new frequency services. Different studies investigate the nature of frequency deviations:

- in [159] the area control error (ACE) signal of the American PJM grid operator is analysed using the DFT to highlight the dynamic property of the signal. Distinct peaks in the power spectrum were observed at specific times (5,7.5,10,12,15 and 30 min) due to the market dispatching operations of CG. The analysis was utilized to create a standardized duty-cycle representing fast ancillary services to evaluate the battery system performances of different technologies [160].

- In [61, 54], the nature of frequency perturbations is studied starting from Europe historical records. The liberalization of markets in 2010s has led to a worsening of frequency oscillations especially at hour intervals. Two typologies of deviations exist: (i) stochastic frequency deviations due to the fast variations of loads and renewable sources, (ii) deterministic frequency deviations caused by the ramps of CG following their market scheduling. CG undergoes an hourly or sub-hourly unit commitment: generators are usually allowed to change their set-point as fast as possible, which leads to a mismatch against the continuously slow changing of the net load. Figure 3.7 shows the deviation of frequency from its nominal value at the change of the hour. Moreover, as explained in [54] ACE error measurements can cause the prolonged deviation of the frequency signal during normal operations. Deterministic frequency deviations cause the frequency signal distribution to be not exactly gaussian, presenting heavy tails and possible high kurtosis

57
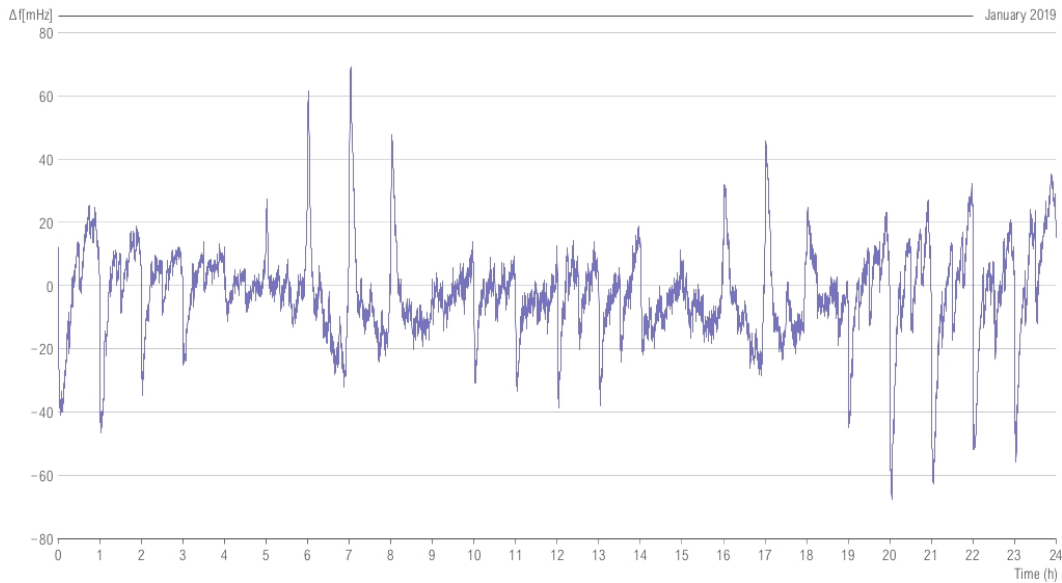
Figure 3.7: monthly average of frequency signal in Europe [54] in January 2019.

values [163]. To minimize these deviations, it was suggested: (a) to decrease to a quarter of hour the time window for all electricity markets (energy and ancillary services), (b) limit the SGs ramp rate, (c) assure redundancy in ACE measurement. The implementation of these actions in the German electricity market led to a lower need of energy and power reserves generating a cost reduction for the management of the power system [155, 197].

In order to reproduce a realistic signal it is necessary to simulate both typologies of frequency deviations and verify the resulting variability of the signal with real-world data. However, usually only stochastic processes are reproduced, for example in [34, 203, 36] recorded load demand and photovoltaic power plant measurements data are utilized, while the power exchanged at the tie lines and frequency reserves are estimated. In [30] wind historical data are used. In [120] and [192] instead of real data, power variations are modelled as a Ornstein-Uhlenbeck stochastic process. In [107] the Swing equation of the system is inverted to compute the power mismatch which causes the frequency deviations. This last approach is promising, but it does not succeed in recognizing power deviations caused by net load dynamics or by CG primary/secondary frequency control responses, producing wrong future scenarios and misleading parameters evaluation. Note that, except for [120], all of these works make use of a SFRM. This model enables the possibility of performing fasts simulations and behaves well in terms of reproducing realistic frequency dynamics because normal grid dynamic conditions are characterized by a series of continuous small disturbances into the grid in which

58

model assumptions are well respected.

The numbers of studies gathered for this third group is lower than the previous two groups in that, according to my opinion this is not due to the lower interest or utility in the proposed objectives, but on the difficulty to model frequency deviations and its root causes.

3.2.4   Notes on zero inertia systems

When SGs are absent in the grid, as in the case of Microgrid or isolated distribution systems, only grid forming converter resources are connected and different possibilities exist for their parallel connection and load sharing management [76]:

Droop based.   This family of techniques works similarly to the typical droop concept in today's frequency and voltage control schemes based on the change of the active and reactive power produced by SGs. On the contrary, in presence of only converters, frequency and voltage are imposed by the converter control as the consequence of the measured ΔP and ΔQ on the local bus. This is enough to implement a correct load power sharing synchronization between all the converters of the system without the need for communication and thus it possesses plug and play features for the converters [170]. Droop can be conventional (P-f, Q-V), inverted (P-V, Q-f) or mixed, depending on the inductive-resistive characteristics of the lines. The presence of a Voltage output virtual impedance is used to improve operations of the microgrid. In top of the described primary control, secondary and tertiary control are needed to assure the proper stability and connection of the island with the main grid. In the secondary control, two additional signals, frequency error $\delta\omega$ and voltage error δE are sent to specific converters (usually the bigger ones) to stabilize the grid. In the case of a connected distribution system, tertiary control will send o the secondary controller the P and Q rated values that the system should exchange with the grid. Moreover, possible synchronization with the main grid must be assured through proper communication and procedures. This flow of signals does not need a very high bandwidth communication and therefore is quite robust (see figure 3.8a and 3.8b). Droop techniques have been the first to appear in the 1990s in order to promote the parallel operation of converters. They represent the first step of the more complete virtual synchronous generators technique and are not subject to numerical instabilities due to the presence of differential equations in the controller.

Communication based techniques In this category, every converter has to be connected to an high bandwidth, fast and reliable communication line which
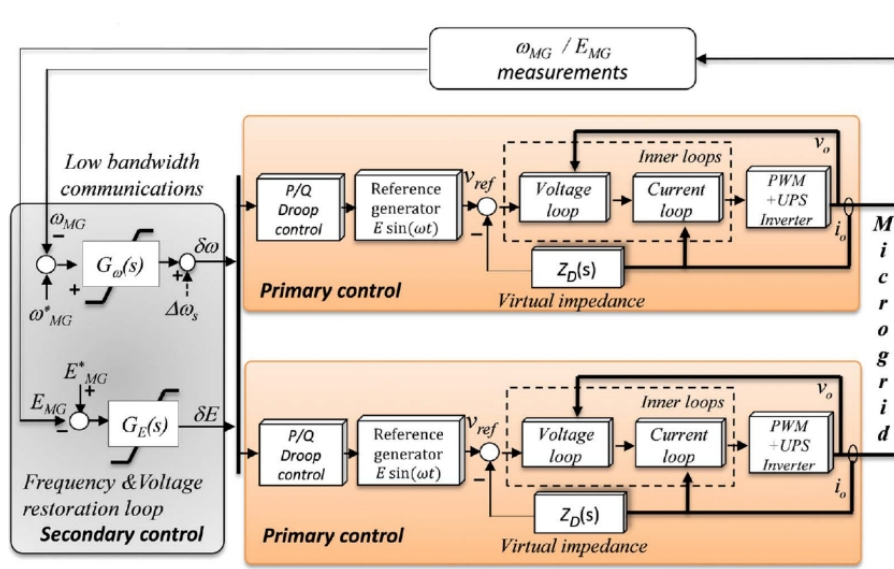
(a) secondary and primary control of inverter-based microgrids [76].
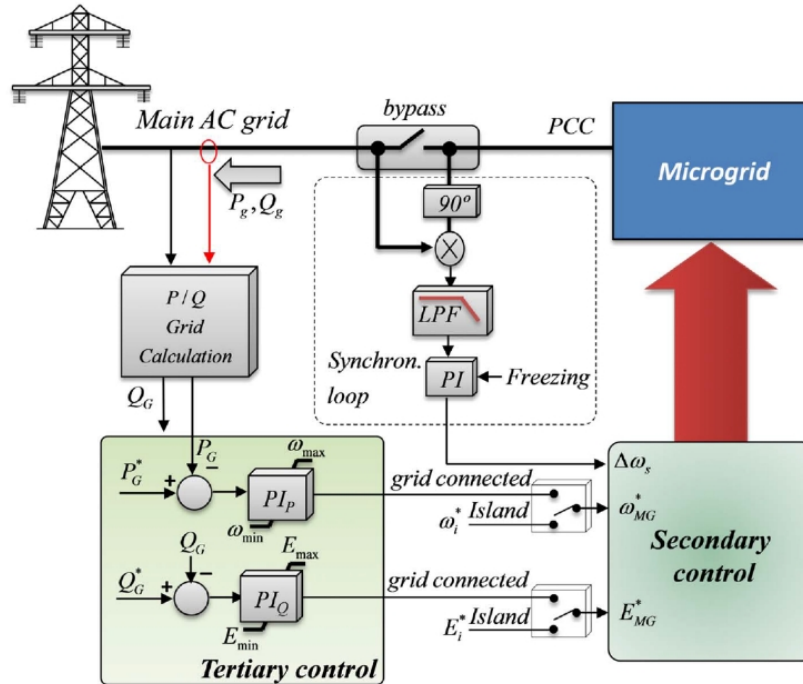
(b) tertiary and grid connection control of microgrid.

Figure 3.8: degree of freedom in PFC in Central Europe for BESS [76]

limits the number of converters utilizable [78] (typical systems making use of communication based techniques are Uninterruptible Power Supply (UPS)

60

systems or ship-systems). Applications on large-scale distribution grids are very difficult and theoretical. Three typologies of control are possible:

- Master/Slave: a master unit will set the voltage level of the principal bus and sends its current to other units; in case of deviations, other slave units will change their output current accordingly. The slaves can also track the voltage of the principal bus to synchronize their voltages. Usually, the Master will be the highest power rated converter to be able to deal with the transient.

- Concentrated control [133]: it is commonly used in the UPS. The total load current is measured and transmitted to a central controller where, according to each unit characteristics, the output current reference set points of each unit are computed and sent back; an outer loop controls simultaneously the voltage of the system also in the case of a grid synchronization. This procedure let a fast mitigation of the transients; however, communication is crucial in this scheme and its failure will lead to a system collapse.

- Distributed control: there is no Master unit and no central control, but it still needs communication lines for sharing current reference and a signal for synchronization. In general it needs less communication bandwidth and moreover it easily permits plug and play of any converter without causing major stability problems.

Direct Current control techniques In absence of SG, can be economically convenient, especially for low and medium voltage systems, to use Direct Current (DC) to power the system in order to save the transformation losses of solar energy and DC loads. For DC grids, applications are referred to small Microgrid and most of the works are still theoretical [85]. A DC grid needs to assure that voltage levels in every bus of the system are kept stable in order to deliver the desired amount of power even in the case of a contingency. The most used scheme is very similar to the hierarchy control used in droop techniques for AC systems, as presented above, and it is based on a droop technique which assure power sharing between the sources. The signal to be communicated is just one (the voltage level) and not two as in the case of AC systems.

Conclusion

This chapter provides a detailed literature review of the works dealing with BESS performing frequency control. Four groups of works were identified according to the way the electric grid is modelled and considered with respect to the BESS impact: in section 3.2.1 the grid is considered as an input-output system where impact of BESS cannot be quantified. The focus is on the BESSs techno-economical performances: studies are going towards the construction of precise but computational light models and multi-services, multi-units layouts in order to increase efficiency and profits for the BESSs. In section 3.2.2 we analyzed the works dealing with the transient after a contingency: literature presents a lot of classic-probabilistic approaches dealing with quantifying the BESSs performance. Innovative techniques and optimization approaches considering at the same time BESS costs and benefits are under development. In section 3.2.3 we noticed how the impact of BESS during normal operations is not adequately investigated for the difficulty of recreating a correct frequency signal composed by its slow and fast components which is needed to correctly quantify BESS impact.

Chapter 4

Impact of BESS Fast Frequency Control after a Contingency

in this chapter, I present two case studies quantifying the impact of fast primary frequency control and rocof control from BESSs. These two case studies are based on the SFRM model of the grid and they are part of the classical approaches papers in the group of closed loop contingency studies as seen from previous chapters. The two case studies are based on different grids and analyze the impact of classical control frequency loops and are presented in [183, 128].

4.1 First Case Study: a 2 Area Frequency Model

4.1.1 System set-up

The first work aims to highlight the impact of BESSs in low inertia power systems, when a proper combination of PFC and RoCof control is used. The study is conducted by considering two-area power system SFRM model (see Figure 4.1. With respect to the one presented in 2 this system consider the presence of two equivalent generators swinging in a coordinated system. The two generators represents two equivalent power system areas transmitting power at the tie lines. In general this power can be expressed as [60]:

$$P_{\text{ik}} = \frac{E_i E_k}{X_L} \sin(\delta_i - \delta_k), \tag{4.1}$$

where E_i and E_k are the voltage magnitudes at the two terminals of the tie-line, X_L is the tie-line reactance, and δ_i and δ_k are the voltage angles at the two terminals. Note that, if ΔP_{ik} (power flowing between areas i and k) is positive for one area, it will be negative for the other area. Linearizing about an initial
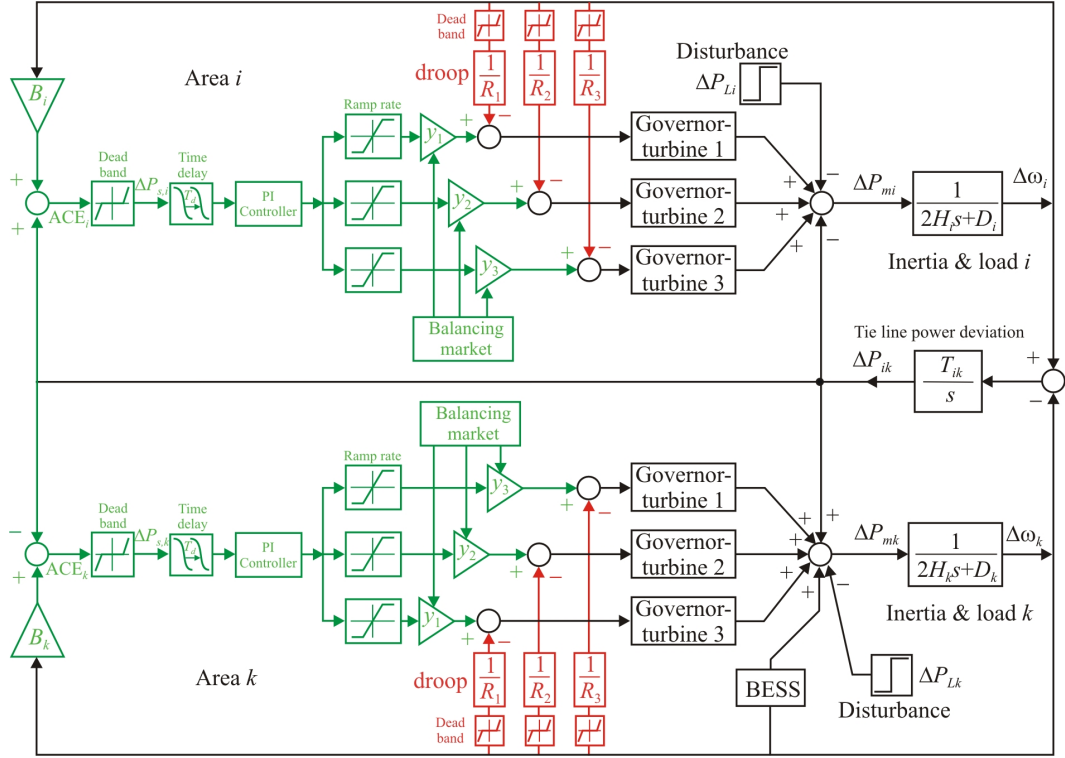
Figure 4.1: Power system model used for the study

operating point represented by $\delta_i = \delta_{i0}$ and $\delta_k = \delta_{k0}$, one can obtain the active power variation on the interconnection line:

$$\Delta P_{ik} = T_{ik}\Delta\delta_{ik}, \tag{4.2}$$

where $\Delta\delta_{ik}$, and T_{ik} is the synchronizing torque coefficient between the two power systems, that is:

$$T_{ik} = \frac{E_i E_k}{X_L}\cos(\delta_{i0} - \delta_{k0}). \tag{4.3}$$

The governors systems model of steam and hydro unit is different depending on the actual primary sources and typical control scheme of power plants (transfer function are of second or third order and are taken from [104]). In figure 4.2 , typical power response of different technologies after a contingency are shown: BESSs are by far the fastest, while hydro power plants usually are characterized by opposite initial response due to the sudden decrease in duct pressure when gate valves moves. Steam power power plant profile usually depends on the presence of reheat units. In fact while steam increase almost immediately its flow in the first high pressure turbine, producing more power, a certain time is needed for the steam to pass though the reheat units and in the second mid-low pressure turbine systems.

64
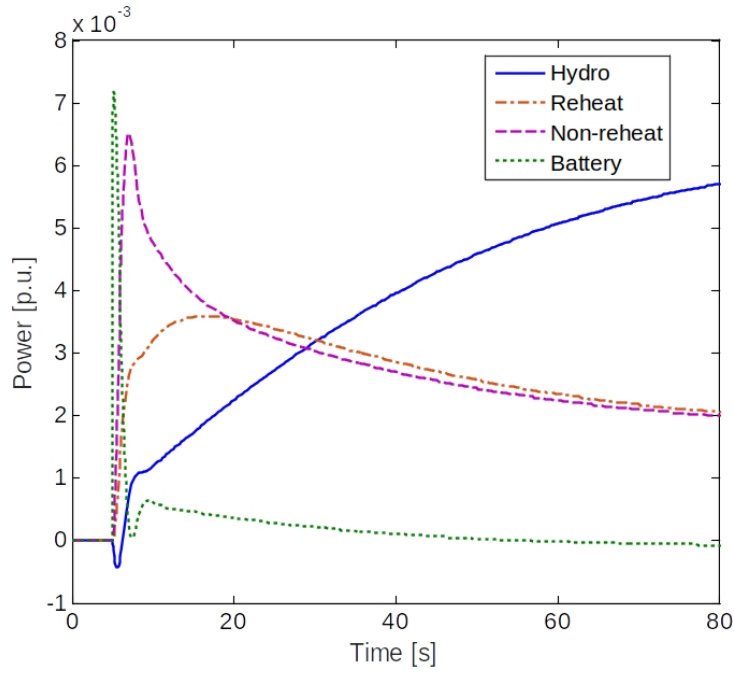
Figure 4.2: power plant response after a contingency.
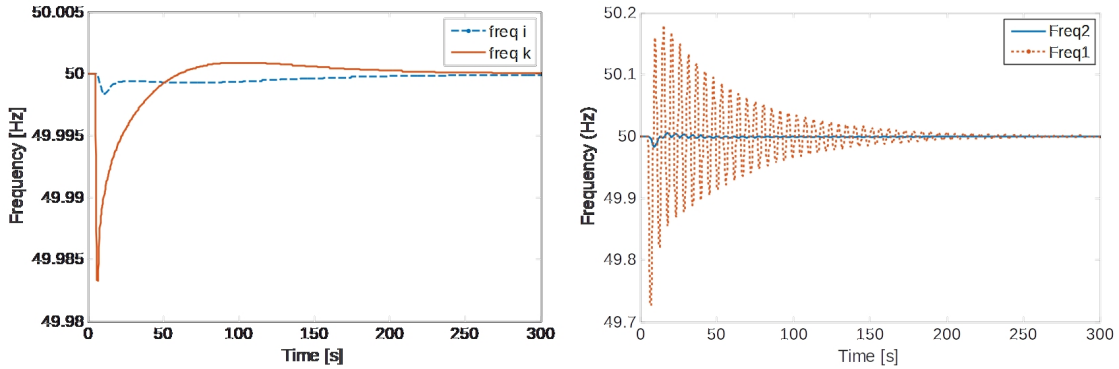
Figure 4.3: frequency response after a contingency. On the left case system behaviour under normal inertia value. On the rigth oscillations behaviour due to low inertia.

Moreover depending on its typology of control (boiler following, turbine following or coordinated control [64]) different dynamics are to be expected (typically an integrated system control is used which guarantee power plant stability and enough response reactivity).

The BESS control is based on a pole constant to model delays and ramp time
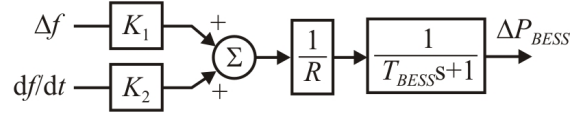
Figure 4.4: BESS model used for simulations.

and two different adjustable coefficients (K_1 and K_2) to simulate different proportions of primary and rocof control (see figure 4.4. In this way we are able to accurately grasp the different impact of primary and rocof control on the grid. PFC follows a typical droop control. Moroever Secondary frequency control is implemented. An Area Control Error (ACE) is calculated for each area, using the following formulas:

$$ACE_i = \Delta P_{\mathrm{ik}} + B_i \Delta \omega_i, \tag{4.4}$$

$$ACE_k = \Delta P_{\mathrm{ki}} + B_k \Delta \omega_k, \tag{4.5}$$

where B is the bias factor and it correspond to the regulating energy of each area. The ACE is followed by a PI controller which forces the area with the disturbance to balance its own power mismatch at steady state, while both areas contributes to frequency control during the the transient condition of the system.

The electric grid is modelled through the Load damping D and the inertia H of the system. In the base case a typical value of $6.5s = 2H$ was chosen; a future scenarios was considered where all synchronous generators excepts hydro power plants are shut off and the inertia is decreased to $2H = 3s$. The system is dimensioned in per unit quantities and the contingency represents 10 % of the model base power power. Without BESSs, in the future scenarios frequency is jeopardized by the lower frequency reserves and by the unstable behaviour of hydric power plants which can enhance power/frequency oscillations through the power tie-lines . As seen in figure 4.3 , the frequency can oscillates a lot in case of low inertia. The contingency is localized in area k, which is also a smaller area and suffers more the frequency oscillations

4.1.2   BESS sensitivity analysis

Three sensitivities are simulated. The first on the value of the weights for PFC and rocof control. The two coefficients range between 0.2 (low weight) to 0.8 (high weight) to initially study the controller response. As further hypothesis, unlimited power is available in the battery for frequency control. Time response $T_{\mathrm{BESS}} = 0.1s$ s was considered and moreover virtual inertia term follows the BESS
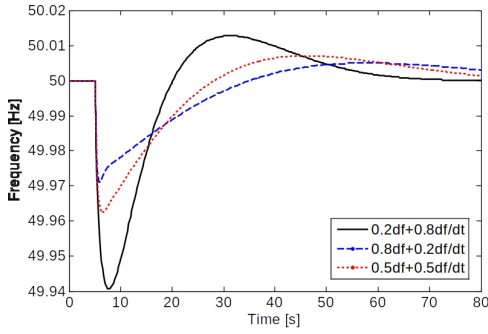
(a) frequency response in low inertia power system by contribution of BESS (the case of unlimited power reserve).
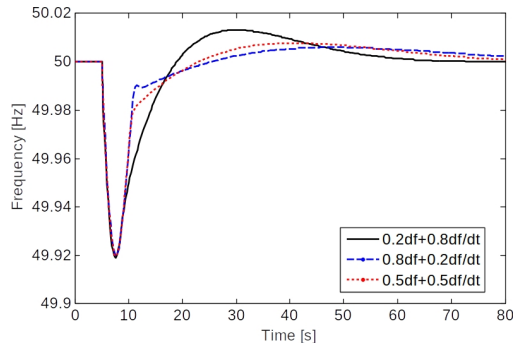
(b) frequency response for battery having reserve limits.
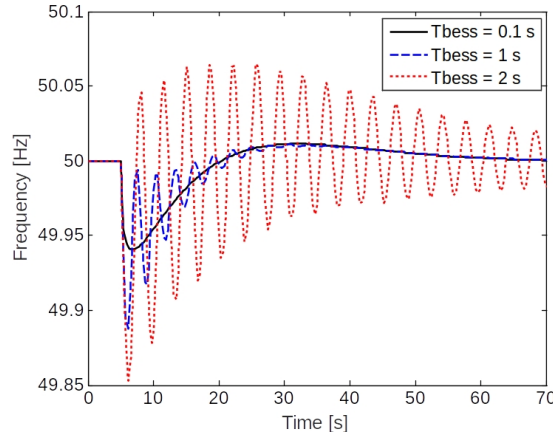
(c) influence of the BESS time response on the frequency stability.

Figure 4.5: BESS parametric sensitivity analysis on the 2 area system.

natural dynamics. Figure 4.5a shows the frequency response when using different weighting factors for the input signals to BESS. The simulations show that a high weighting factor assigned to the frequency variation reduce the frequency sag, whereas a higher weighting factor assigned to the RoCof component provide a smoother behavior in terms of frequency oscillations damping.

in figure 4.5b the same weights are simulated while the reserve available for control was reduced. The BESS control band was set to $P_{max} = 0.005pu$ and $P_{min} = -0.005pu$, values smaller than the unbalance. The frequency signal reach the same f_{nadir} in all the same cases as the BESS reserves are saturated for whatever weights are used. The value it self is much lower with respect to the infinite reserve case. However steady state is reached within a similar time frame. This fact shows

that, even if the size of the deployed reserve is very important to limit the frequency sag, the limited reserve does not affect the frequency stabilization and that rocof control can smooth the frequency signal post-contingency.

Finally last simulation evaluates the effect of different T_{BESS} constants. The input signal of the BESS has been set to $0.2\Delta f + 0.8 df/dt$, and three different time constant for the BESS have been analyzed in figure 4.5c. The figure shows that, in low inertia power systems, for time reactions of the BESS greater than 1 second, the frequency oscillations become unacceptable. The oscillations are caused by the slow intervention of BESS (the figure shows only the frequency of the area k). 0.1 seconds are an acceptable time pole for BESSs to provide fast frequency services.

4.2 Second Case Study: the Sardinian Insular System

In this second case study, the objective was to provide a quantitative analysis and effects of the possible installation of BESS and synchronous compensator in the sardinian insular case. The differences with the previous case study are:

- a single area SFRM model was implemented to model Sardinia which can be considered a synchronous area connected to the mainland through the use of HVDC systems. Also real frequency protection schemes are added. Real presence of conventional SG is modelled and a validation on a real event is performed.

- Reference incident was dimensioned according to historical dispatching of the island, considering the tripping of the biggest plant or off the HVDC lines connecting the island to the mainland.

- An equivalent saturation logic is used to tune in a meaningful way the control parameters of the BESS fast control. In this way Rocof and PFC intervention are dimensioned following the typical layout and capabilities of synchronous generators plants.

4.2.1 Models used

The SFRM model used in this study is depicted in figure 4.6. The various blocks hypothesis are:

- the total inertia of the system is expressed in $MW \cdot s$ and is computed as $E_{\text{k,aya}} = H_{sys} \cdot S_{\text{tot}}$ where $H_{\text{sys}} = \frac{\sum_{i=1}^{N} D_i \cdot H_i}{S-\text{tot}}$ where S_i is the rated power of
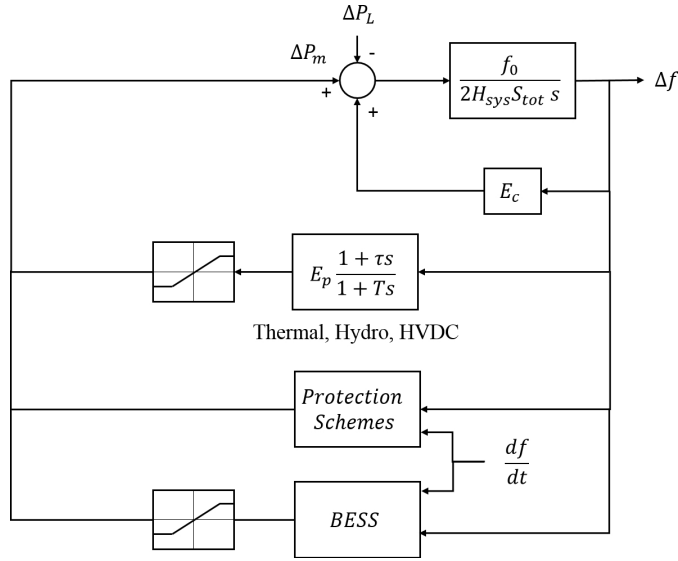
Figure 4.6: one area equivalent model.

the generator i [MW], H_i is the inertia constant of the generator i and N is the number of synchronous generators. $S_{\text{tot}} = \sum_{i=1}^{N} S_i$.

- The load regulating energy $E_c = D_L S_L$ computed as [MW/Hz]. D_L is the damping coefficient of the load and it represents the percentage change load to a frequency deviation.

Table 4.1: dynamic data of resources

Resource	Zero const. τ	Pole const. T	Droop [%]	Band [MW]
Thermal	3	10	5%	$0.1P_n$
Hydro	-1	6	4%	$0.1P_n$
HVDC	3.3	10	5%	$P_{\max}$

- The regulating energy of the single generator is computed as $E_b = \frac{S_i}{f_o \sigma_i}$ where σ_p is the equivalent droop of the generator, f_o is the nominal frequency and S_n is the nominal power of the machine. Thermal , Hydro, HVDC resources are represented by an equivalent transfer block whichs sums together power capacity and droop intervention. Every typology is then characterized by a different pole-zero constants to represent its peculiar plant dynamics. The values are reported in table 4.1. No secondary frequency control is modelled as we are interested in first few seconds after a contingency where secondary

control does not intervene. Moreover secondary scheme in Sardinia operations are typically not automatic, but manually dispatched. HVDC response was modelled following the typical answer of real systems in Sardinia.

- The real protection schemes and thresholds are based on the ones adopted by ENTSO-E [56], with different shedding shares of load and generation depending on frequency values: (a) Wind shedding, starting from 50.6 Hz. (b) Hydro shedding, activated at 51 Hz. (c) Pump shedding, starting from 49.5 Hz. (d) Interruptible load shedding, at 49.3 Hz. (e) Automatic load shedding, for extreme situations from 48.8 Hz.

- model of BESS is a simple fast pole dynamics model like in previous case study (see 4.7). Power saturations are added to the total power output and also to the single control channels. As a matter of fact the two services have two different objectives and in principle TSOs could ask the BESS owner to assure a certain band for pfc and another for rocof control.
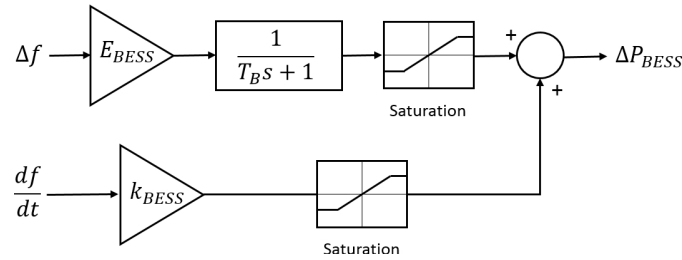
Figure 4.7: BESS model used in the simulations.

4.2.2   Equivalent saturation logic

The services implemented by the BESS are RoCoF control and Primary Frequency Control (PFC). In order to give a reasonable value for the virtual inertia K_{BESS} and regulating energy E_{BESS} we try to mimick the behaviour of CG. For what concern PFC, E_{BESS} is computed such that the saturation of the available power band happens at the same $\Delta f_{\max}$ where the CGs saturate their PFC bands. In general the regulating energy [pu(MW)/pu(Hz)] of a resource is equal to:

$$E_{\text{CG,pu}} = \left| -\frac{f_{\text{nom}}}{\Delta f_{\max}} \cdot \frac{PFC_{\text{band}}^{\text{CG}}}{1} \right| , \qquad (4.6)$$

$$E_{\text{BESS,pu}} = \left| -\frac{f_{\text{nom}}}{\Delta f_{\max}} \cdot \frac{PFC_{\text{band}}^{\text{BESS}}}{1} \right| , \qquad (4.7)$$

where PFC_{band} represents the regulator band in pu. Taking Δf_{max} equal for both resources and dividing equation (4.6) by (4.7), we obtain the relationship which correlates both the regulating energies:

$$E_{\text{BESS,pu}} = E_{\text{CG,pu}} \cdot \frac{PFC_{\text{band}}^{\text{BESS}}}{PFC_{\text{band}}^{\text{CG}}} \ .$$

(4.8)

For each value of the CG regulating energy (which can be evaluated using the droop value used in table 4.1) one obtains a corresponding BESS values which saturates its regulation band at the same frequency deviation of the CG resources. From equation 4.8 E_{BESS} is easily computed as:

$$E_{\text{BESS}} = -E_{\text{BESS,pu}} \cdot \frac{P_{\text{BESS}}}{f_0}.$$

(4.9)

For RoCoF control case, an extreme RoCoF value, df/dt_{max} is set as a limit value which activates all the power band reserved to this service. Grid codes usually fix this maximum admissible value during operations of the system (typical about 1 Hz/s). Starting from this value, it is possible to compute H_{BESS} as:

$$H_{\text{BESS}} = \frac{f_{\text{nom}} \cdot RC_{\text{band}}^{\text{BESS}}}{2 \cdot |\frac{df}{dt}|_{\text{max}}},$$

(4.10)

where $RC_{\text{band}}^{\text{BESS}}$ is the power of the BESS to be used by RoCoF control. From H_{BESS} it is straightforward to compute K_{BESS}. In general the power bands for PFC and RoCoF control go from 0 to 1. In this study their sum is fixed to 1 to avoid the two services sharing part of the power band.

4.2.3 Case study and results

Table 4.2: Calibration Results

	Measured	Simulated
Zenith [Hz]	50.41	50.41
ROCOF [Hz/s]	0.36	0.37
T_{zenith} [s]	2	3.26
f_{reg} [Hz]	50.22	50.23

The Sardinian system has a maximum load of 1500 MW and it is connected to mainland through two HVDC lines (SACOI and SAPEI). The SFRM model

71
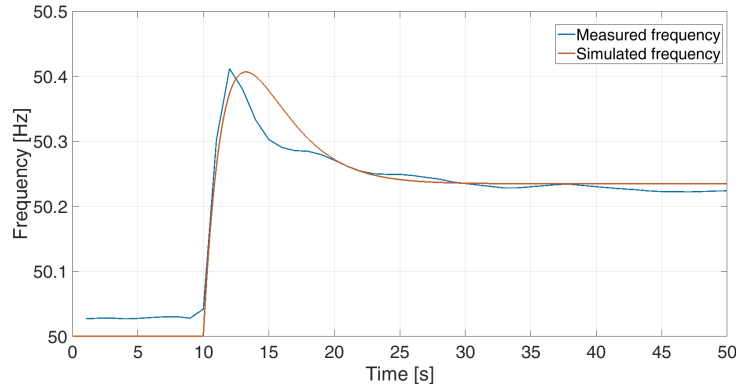
Figure 4.8: comparison of 1 area model with real system
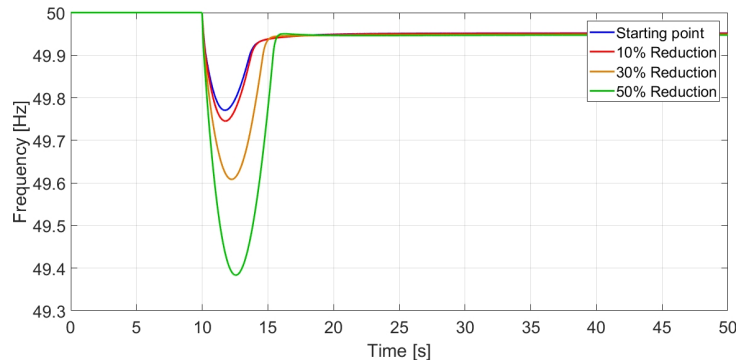
Figure 4.9: Impact of worst under-frequency contingency for the inertia scenarios considered.

is calibrated using a real events during an HVDC failure which lead to an over-frequency event. The two curves are depicted in figure 4.8 and table 4.2 and are pretty similar in terms of main frequency parameters (rocof, f_{zenith} and steady state). Another incidents is compared in the case of an under-frequency event and results are also similare ([128]). Starting from today scenarios, three scenarios were constructed with respectively 10,30 and 50 % of less inertia due to the actual closure of power plants. The chosen contingency represents the biggest thermal unit failure of Sardinia on the winter peak, the 17th january 2018 at hour 10:30 causing a under frequency event, which is also considered very critical because the HVDC SACOI was out of service. Fig 4.9 represents the frequency profile after the contingency at the various inertia levels. Similarly to previous study, BESS and synchrnous compensator are added to improve on the situation.

the table 4.3 present the 9 situations simulated with different amounts and parameters of BESS controls. Also other two additional situations were simulated
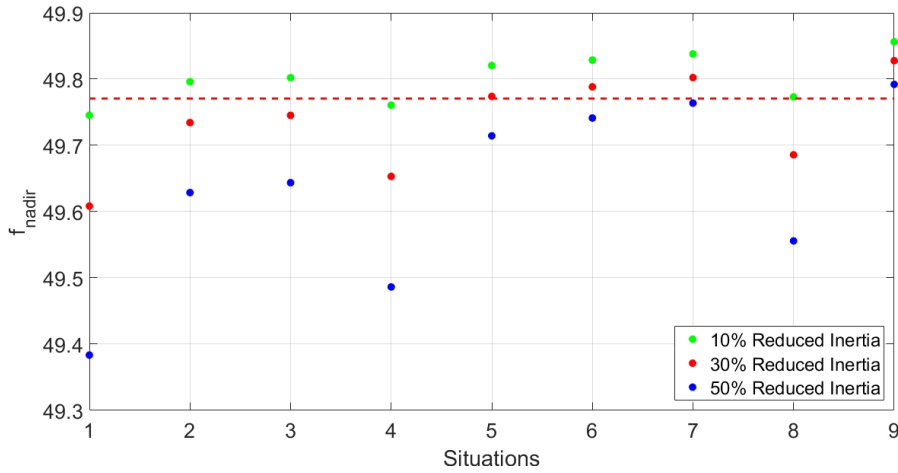
Figure 4.10: BESS impact on f_{nadir}.
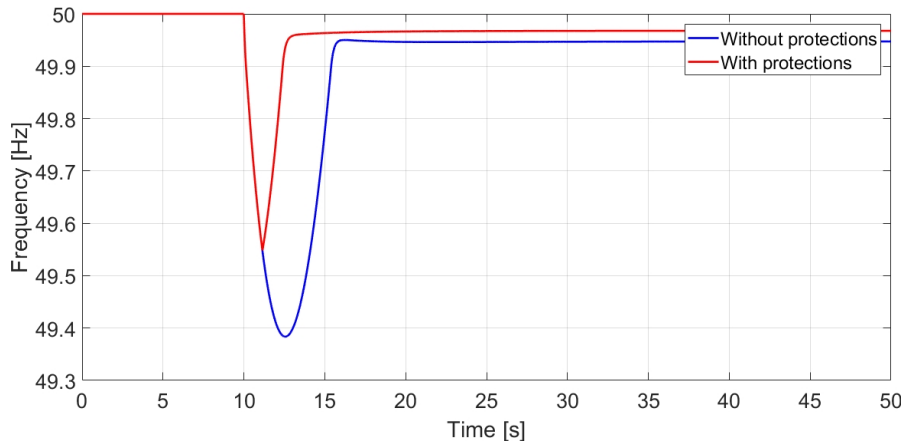
Figure 4.11: Frequency stability due to shedding of wind or load resources.

Table 4.3: BESSs simulated scenarios

n	MW	T_B	$RC_{\text{band}}^{\text{BESS}}$
1	0	0	
2	50	0.3	0.5
3	50	0.1	0.5
4	50	0.3	1
5	50	0.3	0
6	100	0.3	0.5
7	100	0.1	0.5
8	100	0.3	1
9	100	0.3	0

Table 4.4: Results of under-frequency scenario with 50% reduced scenario

n	$f_{\text{nadir}}[Hz]$	RoCof [Hz/s]	$T_{\text{nadir}}[s]$	$T_{\text{reg}}[s]$	f_{reg}
		No BESS addition			
1	49.383	1.066	2.57	5.78	49.947
		Addition of Synchronous Compensator			
6	49.52	0.787	2.57	5.78	49.947
10	49.60	0.623	2.72	6.11	49.947
		Addition of BESS			
2	49.63	0.946	1.85	9.07	49.949
3	49.64	0.946	1.85	9.02	49.949
4	49.49	0.850	2.63	5.90	49.947
5	49.71	1.066	1.11	9.80	49.950
6	49.74	0.850	1.23	9.73	49.950
7	49.76	0.850	1.26	9.66	49.950
8	49.56	0.707	2.68	6.02	49.947
9	49.79	1.066	0.72	9.97	49.952

with 6 and 10 synchronous compensator added. Every set of simulations is re-peated for 3 inertia levels in the grid. The grid contingency is simulated and the relevant results are evaluated. A graph comparing the value of f_{nadir} for the 3 inertia levels scenarios is shown in For brevity, the table 4.4 present the results in the case of 50 % reduction of inertia. This is the most dangerous case and the

rocof value is dangerously over the 1 Hz/s threshold. 50% is also the only scenarios when load or wind shedding is triggered by the severe frequency dynamics (see figure 4.11. When BESS or synchronous compensator are added, shedding is disactivated to properly quantify the BESS impact and be comparable with other scenarios. Synchronous compensator and BESS rocof control avoid to overcome 1 Hz/s while pfc is able to improve the f_{nadir} and t_{nadir} more than rocof. However too much fast t_{nadir} can also be dangerous for SG equilibrium and therefore it is better to keep 50 % rocof and 50 % droop control. A negligible difference is observed when passing from a T_b pole constant of 0.3 to 0.1 seconds. In the case of 50 % inertia reduction it seems clear how at least 50 MW are necessary for Sardinia to overcome a contingency. Also another contingency is considered, i.e. the failure of SAPEI HVDC line. The line is exporting at the time of interest and therefore causes a an over-frequency event. Similar results to the underfrequency-event are reported. For whole set of tables, refer to [128]. Also in simulation
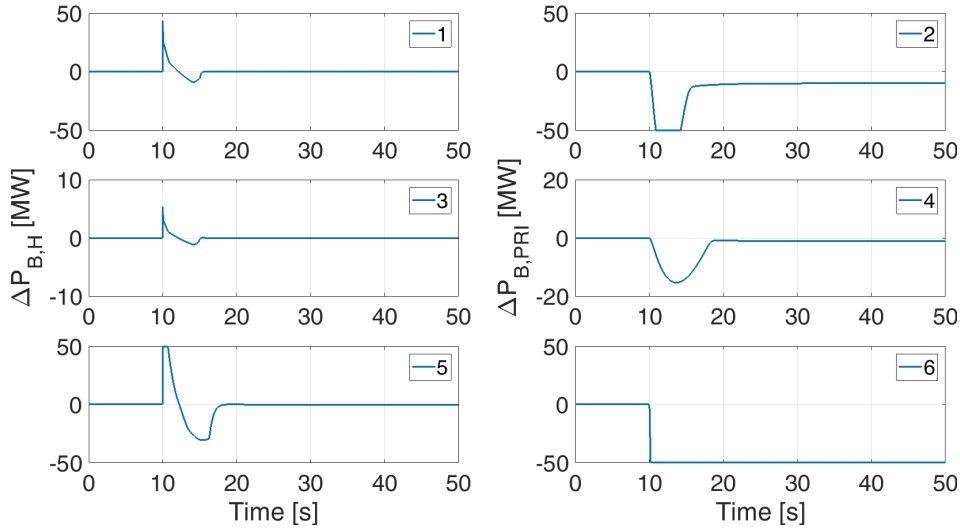
Figure 4.12: comparisons of the inertial and primary BESS delivered with different control parameters.

ESL comparison

ESL is one of the logic that can be used for dimensioning BESS reserves. For example in [4] H_{BESS} varies in the range between 0.01 to 500. To show the effects of different weights a series of simulations were performed with the ten times lower or bigger values for K_{BESS} and H_{BESS}. The over-frequency simulation with BESS situation number 6 was used for this parametric analysis on BESS intervention. Figure 4.12 reports the inertial and primary shares of the BESS delivered power

in the ESL case (1, 2), lower (3, 4) and higher (5, 6) values cases. With lower values, the BESS support is not exploited enough, whereas with higher values the saturation of the BESS is reached with possible concerns for the BESS stress. It is evident that the ESL shows the best compromise in terms of BESS saturation and performance.

Conclusion

This chapter analyzes the impact of BESS after a transient using a classic approach. for both case studies an SFRM model is used in order to shorten the time of computations and offer the possibility of more extensive parametric analysis. In the first case study the impact of quantity, quality and velocity of response of BESSs has been compared considering a two Area system. Oscillations can arise if the BESS is not fast enough. In the second case study, the Sardinian system has been recreated and validated and then BESS are added. The focus was the study of the impact of primary and rocof control. First an ESL to dimension BESS reserve is necessary to make these systems reacts to a frequency change in a similar way of SGs. Both PFC and rocof control have a great importance and a 50 % power band division has been suggested as optimal control solution

Chapter 5

Impact of BESSs in Normal Grid Conditions: a SFRM Approach

In section 5.1 are presented the two parts of the model (FORWARD and RE-VERSE) utilized to reproduce the everyday frequency perturbations. The model quantifies the potential of PFC and RoCof control provided by BESS during normal operations of the grid. In section 5.2 I discuss a case study based on the Irish grid, where an alternative frequency domain approach to evaluate BESS impact is also described. In section 5.3 I introduce the study of the jumps which are present in the Irish frequency signal. Finally in section 5.4 the study of the impact of BESSs on a particular day of the Sardinian System is proposed by reconstructing the frequency signal and using also the secondary and tertiary frequency control. BESS power band is divided between rocof, primary and secondary frequency control

5.1   The Model Construction

The model as described in the previous chapter in section 4.2 was adjusted for normal operations analysis based on the Simulink software. The core of the system remains the Swing equation of the grid generators as expressed in the previous chapter (see figure 4.6:

$$\frac{2H_{\text{sys}}S_{\text{tot}}}{f_0} \cdot \frac{df}{dt} = \Delta P_m - \Delta P_L + \Delta P_{Load}(f), \tag{5.1}$$

First of all, the ΔP_m produced by regulating resources in the grid was augmented by considering the three frequency services which are currently used in the ENTSO-E continental system:

- Frequency Containment Process (also called PFC) based on a linear droop law.

- Frequency Restoration Process (also called SFC) based on the ACE computation as introduced in 4.1.

- Replacement Process (also called Tertiary frequency control or TFC) manually activated by the TSOs in the case SFC Band is saturated to restore the secondary reserves.

During normal operations I use the term ΔP_e to represent ΔP_L of equation 5.1 which in turn represent two different perturbations: the first one caused by the global load swings, the second one caused by the non-dispatchable renewable sources due to the stochastic behaviour of primary sources (like wind velocity and sun radiation). Both phenomena form the stochastic frequency deviations. Moreover, ΔP_e includes the eventual presence of a contingency (for example the trip of a generator producing 500 $[MW]$ will cause a $\Delta P_e = +500$).

As explained in chapter 3, deterministic frequency oscillations are caused by the mismatch between net load and the dispatchable generators which ramps to reach new set points following their market scheduling. In this study this mismatch is included in the ΔP_e term. Finally, a load damping coefficient is applied to consider the frequency dependency of the load. The two terms ΔP_m and ΔP_eì can be written as:

$$\Delta P_m = \Delta P_{PFC} + \Delta P_{Sec} + \Delta P_{ter}, \tag{5.2}$$

$$\Delta P_e = \Delta P_{mis} + \Delta P_{Load}(f) + \Delta P_{contingency}, \tag{5.3}$$

$$\Delta P_{mis} = \Delta P_{Load} - \Delta P_{CG} - \Delta P_{Rene}. \tag{5.4}$$

5.1.1 The FORWARD model

The FORWARD model (see figure 5.1) implements all the components described in equations (5.2)(5.3)(5.4). The model is composed by:

- a unique equivalent power plant for every typology (hydro, steam etc. . . .) composed by the sum of all the respective plants parameters. Specific flags let the user decide what frequency services should be performed by each plant, and how much of the power band is activated as a percentage of each P_{max}.
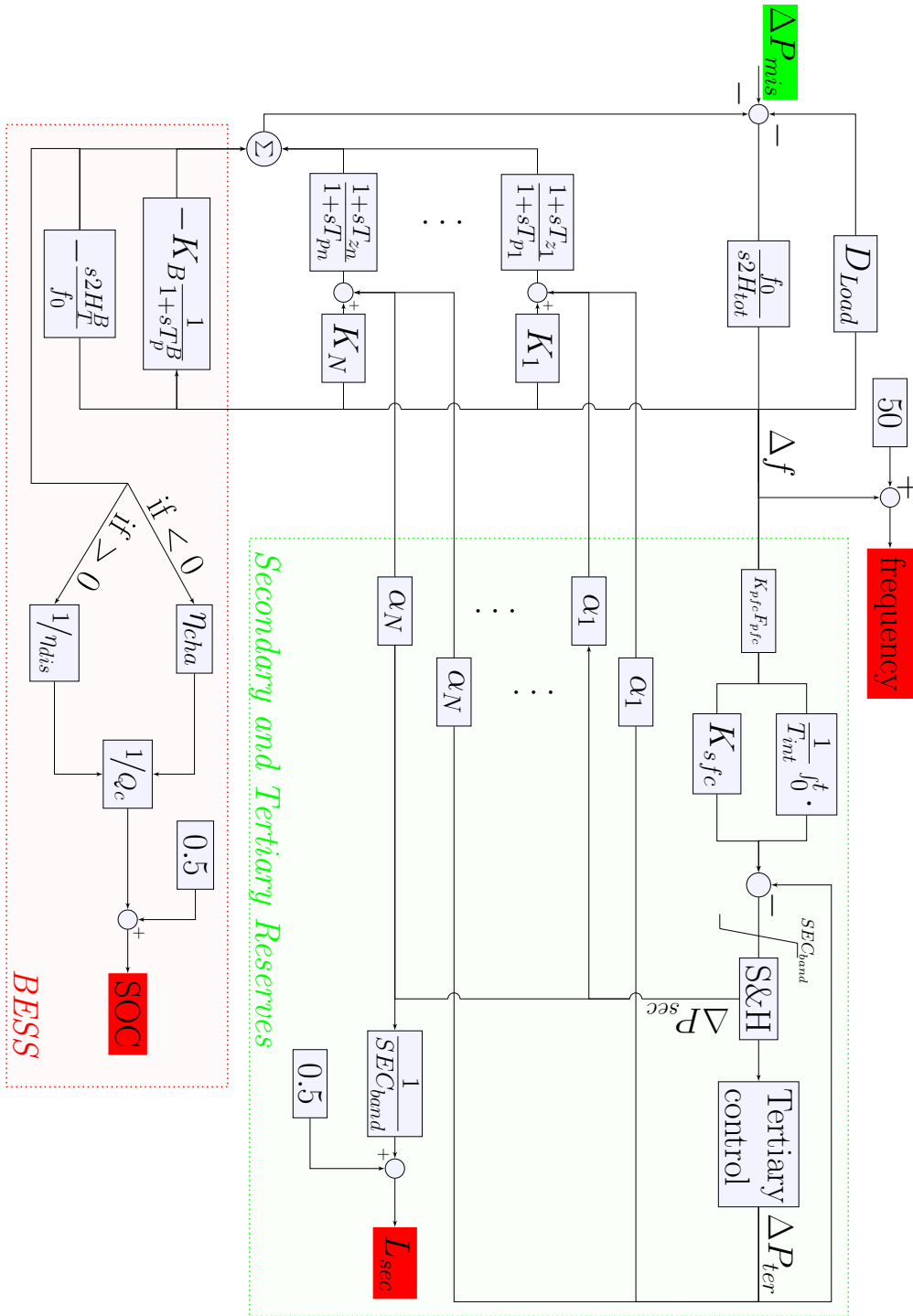
Figure 5.1: the FORWARD model scheme.
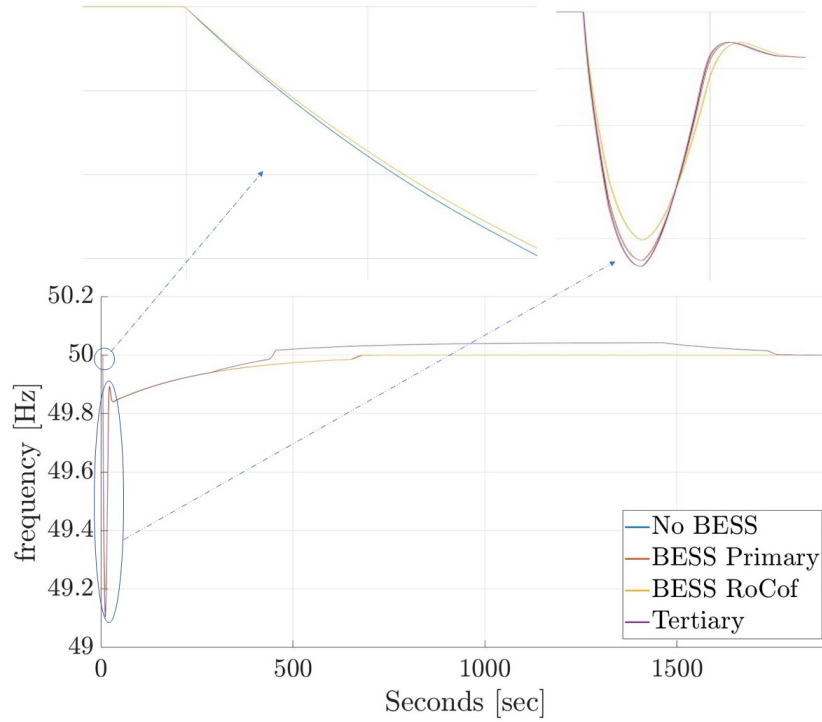
Figure 5.2: simulation of a contingency at time=5*s* in the FORWARD model.

- the PFC response ΔP_{FCR} which considers time changing regulating energy, a dead-band for every plant typology and a zero-pole dynamics of each plant. Even HVDC lines, which connect two asynchronous AC grids, could be considered to provide PFC. Saturation point of PFC can change during the day depending on P_{max}.

- ΔP_{Sec} is computed by evaluating the integral of the frequency error and by considering a certain secondary power band. Firstly, the frequency error is multiplied by the grid regulating energy $(K_{\text{pfc}} F_{\text{pfc}})$. The SFC signal is shared by the equivalent power plants depending on the α coefficient which, in turn, is generally decided by the TSOs and can change during the day. The sum of all α coefficients is equal to 1. In this study, the α value for each equivalent plant is equal to its instantaneous production percentage. $S\&H$ represents the Sample-and-Hold function by which the TSO updates and sends a new value of the secondary level to generators every two to four seconds. The secondary level is computed as:

$$L_{sec} = L_{INI} - \frac{1/T_{SEC} \cdot \int_0^t \Delta f dt}{2 \cdot Band_{SEC}} \qquad [pu(MW)] \qquad (5.5)$$

where L_{INI} in the secondary initial level (usually 0.5), T_{SEC} is the integral constant (usually between 90 and 200), $Band_{SEC}$ is the whole power Band dedicated to secondary control.

- Finally, tertiary frequency control is used to de-saturate the secondary reserves. In real power systems, tertiary reserves are manually dispatched optimizing their costs; however, in this model tertiary reserves are automatically activated when the Secondary level overcome a certain user-defined threshold. As a consequence the amount of activated tertiary reserves will reflect the real needs, but the dynamics of its activation can change depending on real TSO implementation and market design. The de-saturation of secondary reserves can happen in two ways:

  - firstly, as indicated in equation 5.2, a ΔP_{ter} opposite to secondary control comes into play. Tertiary reserves are activated when $|L_{\mathrm{sec}} - L_{\mathrm{sec}}^{\mathrm{rif}}| > L_{\mathrm{threshold}}$ and create a linear power increase which lasts for a certain time (e.g. 30 minutes or 1 hour), or until $L_{\mathrm{sec}} \approx L_{\mathrm{INI}}$. This signal will affect the frequency signal, which, in turn, will balance L_{sec}. in this L_{SEC} can be computed as:

  $$L_{sec} = L_{INI} - \frac{{}^{1}\!/T_{SEC} \cdot \int_0^t \Delta f \, dt}{2 \cdot Band_{SEC}} - \frac{\Delta P_{ter}}{2 \cdot Band_{SEC}} \tag{5.6}$$

  The maximum power ΔP_{ter} depends on the SEC_{band} value to be de-saturated. In such a manner, tertiary reserves operate on the grid stability without the direct coordination with secondary reserves.

  - Another way is to change the ΔP_{sec} signal by ramping CG power plants due to the activation of the tertiary reserves ΔP_{ter} after a certain threshold as in the previous case. This action corresponds to a perfect coordination between secondary and tertiary reserves, so that ΔP_{sec} decrease/increase at exact the same time when ΔP_{ter} changes value, and frequency signal is "virtually" not affected. Such a perfect coordination is difficult to realize but TSOs try to approximate it as much as possible as it does not affect the frequency signal. In this work (as shown in figure 5.1), this solution is implemented because it works flawlessly with the REVERSE model (see next section). Moreover, ΔP_{ter} is shared among the equivalent generators plants with the same α coefficients of ΔP_{sec} in that in our case detailed information on the plants performing TFC is not needed.

- A simple BESS model performing new grid services, such as PFC and RoCof control, which can act almost immediately thanks to the power electronic

interface. Energy constraints are considered using simple efficiency coefficients when charging or discharging. An automatic recharging of the BESS in the case SOC is too low can be implemented. The real charge profile will actually depend on the market prices and regulations.

The FORWARD model simulations will have as input the ΔP_{mis}(see equation (5.4)) and will compute the resulting frequency error by considering the presence of the reserves and the system parameters. As an example, in figure 5.2 is shown the resulting frequency signal coming from an unexpected loss of generation.The contingency is simulated as a step input of value $500MW$ and the grid parameters refers to a specific day of the Irish grid. At first instants, frequency decreases, slowed down by the inertia of the grid. In a brief period of time (under 50 seconds) FCR manages to stabilize the grid. The SFC activates to bring back the frequency to 50 Hz, but it soon saturates and the tertiary control is automatically called. This service activates a certain ΔP_{ter} until L_{SEC} returns around 0.5. Note how BESSs performing PFC is able to increase the frequency nadir while, on the other hand BESS performing rocof control is able to decrease the initial RoCof of the system frequency. The two different approaches for modelling the tertiary reserves are also shown: the first three simulations implement the second method where tertiary intervention does not unbalance the grid, while the last line shows the use of the first method. In this last case the ΔP_{ter} make the frequency rose over 50 Hz for some time which, in turn, lowers secondary level. The fast dynamics around f_n are due to the presence of the dead band of primary controllers.

5.1.2 The REVERSE model

REVERSE model rationale

So far, we used the FORWARD model starting from a ΔP_{mis}, obtaining a certain Δf. The contrary is also possible, and it is what the REVERSE model accomplishes. Rewriting equation (5.2), using equation (5.3) and (5.4) and the definition of ΔP_{mis}we get:

$$\Delta P_{mis} = \Delta P_m(f) + \Delta P_{\text{LOAD}}(f) - \frac{2H_{\text{tot}}}{f_n} \cdot \frac{df}{dt})$$
(5.7)

All the terms on the right depend on the frequency signal and its derivative, therefore by knowing these signals we can compute ΔP_{mis}, which represents the power mismatch which cause the initial frequency oscillation. Frequency data and its computed derivative are the inputs of the REVERSE model to compute the ΔP_{mis}. If we then apply this signal as input to the FORWARD model, we get the same output frequency. At this point, we could change the frequency reserves

parameters (for example reserves quantities, time constants, inertia etc.) and look at its effects on the grid frequency signal and other variables.

Theoretically, there is no strict requirement that grid parameters and real frequency measurements refer to the same grid. Even using "invented" data, the methodology will work as well because the two models are a mathematical abstract representation of the grid balance. However, the more consistency we have between data sources, the more the resulting ΔP_{mis}, L_{SEC} and the other state variables of the system will be realistic. It is important to note that the models parameters can change during the simulation (like production mix, reserves bands and characteristics etc.) as customized by the user.

5.1.3   Methodology validation
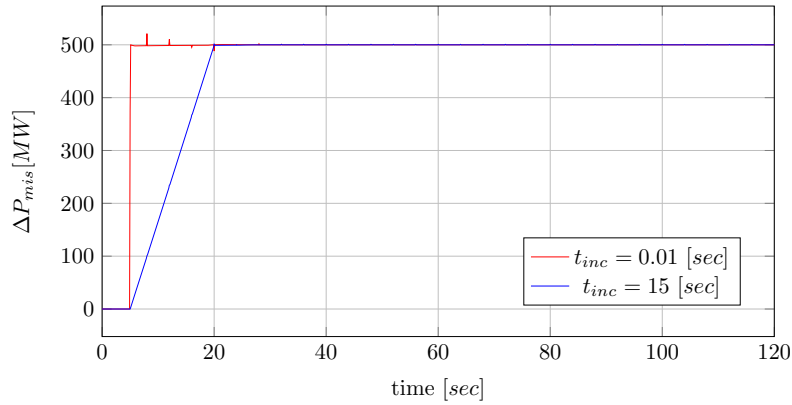
Figure 5.3: ΔP_{mis} signal evaluation by the REVERSE model using the same grid parameters of the FORWARD case.

Step Incident: to validate the model we use the same contingency as applied in the previous paragraph. Starting from the output frequency signal of the simulation without BESS, we try to recover the ΔP_{mis}which gave rise to the unbalance (a step input with a value of $500MW$). First we compute the numeric derivative of the frequency signal and then these two signals are inputted in the REVERSE model. The resulting ΔP_{mis}signal is show in figure 5.3 The $500MW$ step is recovered, except for small "imperfections" due to the difficulty for the Simulink solver to maintain perfect numerical stability when integrating signals with such steep rise (remember that the derivative of the frequency signal was evaluated with a finite step and a simple Euler formula). To prove this, we tried to reconstruct a contingency with a slower ramp time of 15 seconds and, as shown in figure, the
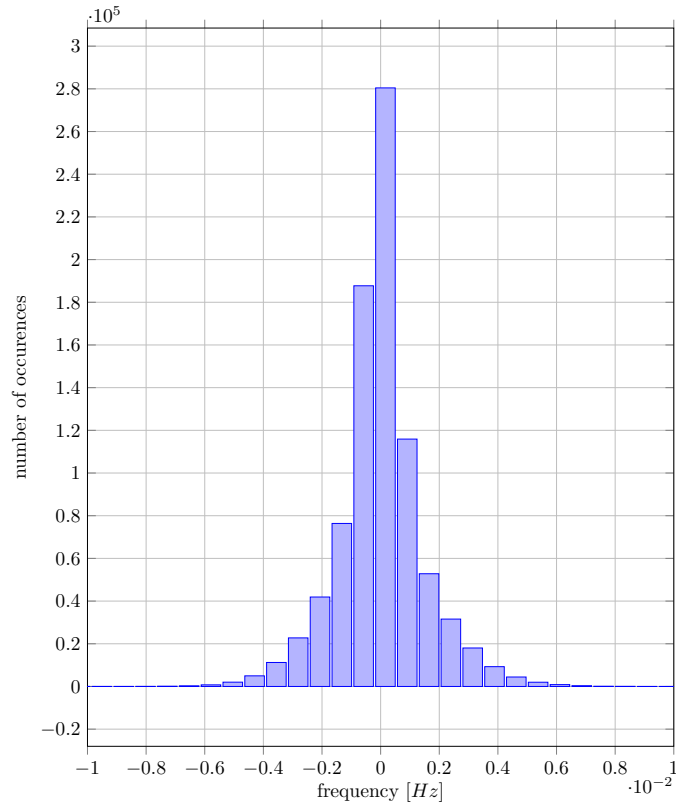
Figure 5.4: the histogram representing the distribution of the error between simulated and real frequency for a day of simulation.

REVERSE model is able to reconstruct the input without errors. Anyway, the differences are negligible and the step incident is well reconstructed in both cases.

Whole day: as a second test case, taking the data of the Irish grid, we have reproduced one real day of frequency variations. The simulated frequency has an error always less than 0.01 $[Hz]$ for every point of the time series (and generally lower 0.001 Hz), as shown in figure 5.4, where the error has been computed as $\Delta f_{sim}(t) - \Delta f_{real}(t)$, with $\Delta f_{real} = f_{real}(t) - f_n$ and $\Delta f_{sim} = f_{sim}(t) - f_n$. 10 Hz data are used, so that the signal is composed by 864000 samples. The errors are much less than the value of the typical governor dead-band, therefore they are negligible with respect to the frequency signal itself. They are related to the numerical methods used by the solver and by the fact that the FORWARD model has one differential equation more than the REVERSE model.

We can now modify the FORWARD model parameters and repeat simulations
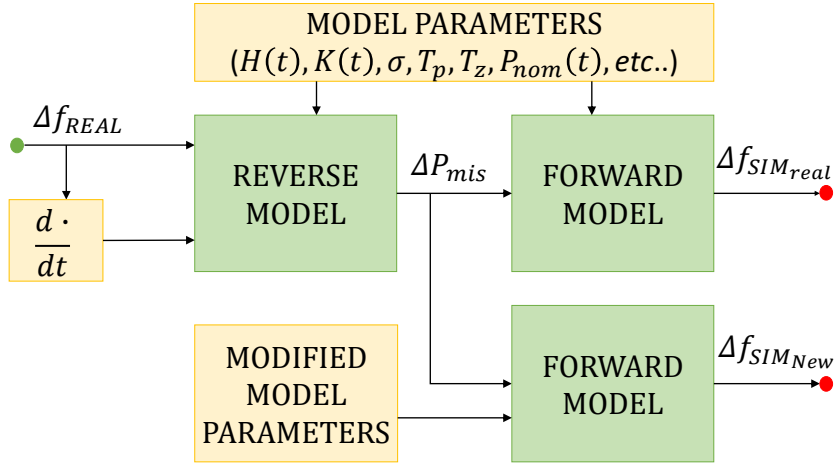
Figure 5.5: time domain approach scheme.

to see the effect on the frequency signal. For example, one could reduce the value of inertia or increase the regulating energy by adding BESS or other new resources (see figure 5.5 with a summary scheme) Reproducing the real frequency signal is fundamental for having realistic results because in today power systems, frequency oscillations are caused both by stochastic phenomena (like wind and load fluctuations) and deterministic ones (due to the hourly energy market). Impact of new regulating resources will strictly depend on the type of frequency signal which characterize the grid: fast or slow frequency dynamics makes a great difference. Our reproduced signal retains those properties and therefore the impact of new resources will be realistic.

5.1.4 BESS model further insights

Until now we have used a simple BESS model based on power, energy and efficiency characterization. This simple model is enough if the main objective is to evaluate grid improvements. In case we need a better appreciation of battery degradation or market strategies It can be interesting to adopt an equivalent electrical model. As known (see for example [88]), running such a model is computationally heavy. In order to fasten the simulation of a closed loop system with an electric equivalent BESS model one can make use of a SFRM model. Moreover, the BESS cell can only consist of the open circuit voltage V_{OC} plus a resistance-capacitance group (characterized by one or more R-C couples [25]). The values for V_{OC} and other circuit elements can be described by using look up tables differentiated between charge and discharge phase and obtained through direct experimentation
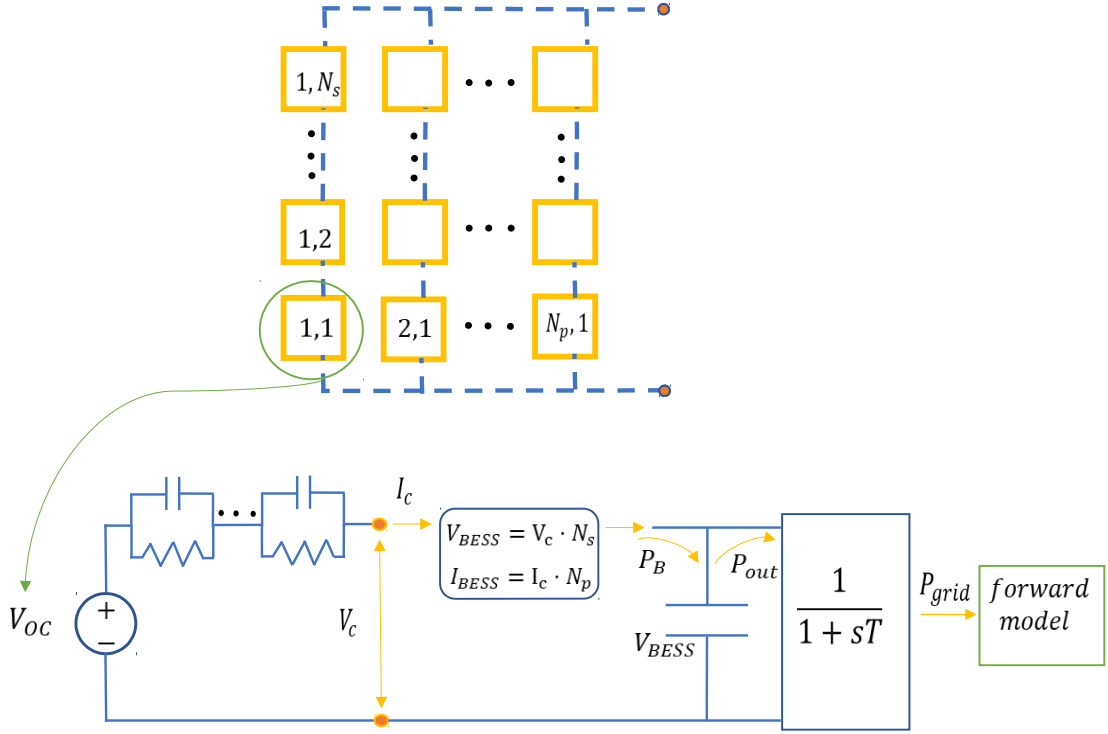
Figure 5.6: BESS model proposed scheme

[83, 71]. The main variables influencing the paramters values are SoC and Temperature.

To connect this circuit to the grid, it is first necessary to multiply the electrical quantities for the number of cells in parallel or in series (under the hypothesis that the cell racks equally share the produced or stored power). Secondly, the converter which connects the battery to the grid can be modelled simply as fast pole dynamics connected to a DC-link capacitance as shown in figure 5.6. In this description, voltage and current quantities are not utilizable in the SFRM, therefore a power balance on the dc link capacitance is solved to connect the power output P_{out} to the power input from the battery cells P_{B}. One can write:

$$P_{\text{out}} = P_B + C \cdot \frac{dV_{\text{BESS}}}{dt} V_{\text{BESS}}. \tag{5.8}$$

DC-link capacitance C can be dimensioned to avoid voltage instabilities considering P_{grid} requests and number of battery cells stacks. P_{grid} is set by the frequency control system and all the other variables are computed applying the fast pole, equation 5.8 and solving the electrical equivalent circuit. The SoC can then computed using a Coulomb counting approach on a single cell considering a symmetric behaviour of all cells:

$$SoC = SoC_0 - \frac{\int_0^t I_c \cdot dt}{Q_c}, \tag{5.9}$$

where Q_c in nominal capacity in [Ah] of the cell and SOC_0 is the initial SoC. With this approach, we can compute detailed cycle and BESS SoC behaviour and at the same time simulate its effect on the grid frequency.

5.2 Irish Case Study

The model presented in the previous section was used to study the impact of pfc and rocof control by BESSs in the Irish power system. Secondary and tertiary reserves are not implemented since they are not present in the Irish grid as automatic frequency services. Irish power system and frequency data used for the REVERSE models are presented in subsection 5.2.2. Beyond a time domain analysis (presented in in subsection 5.2.3) , a preliminary study on the frequency domain is performed by computing the bode plots of the system, the power spectrum of the real power variations and by using the Parseval theorem. While quantitative results will be obtained with the time domain approach, this study helps us to explain why and how primary and RoCoF control impact the frequency stability as presented in subsection 5.2.1. Results for both methodologies are showed in 5.2.4

5.2.1 Frequency domain approach
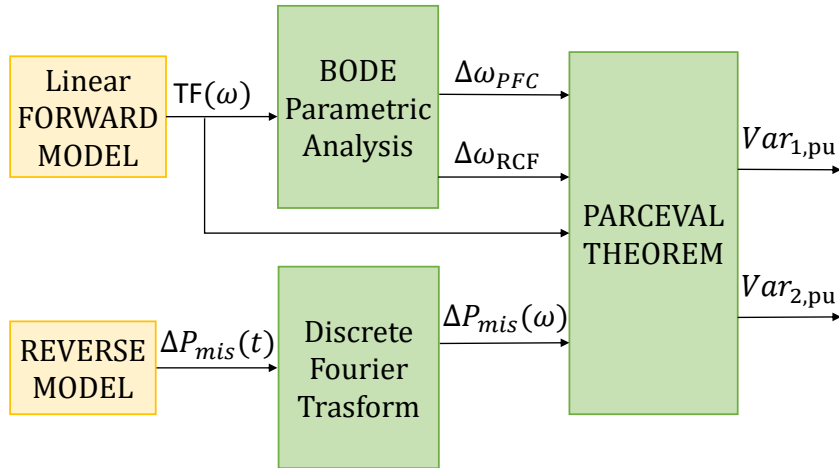
Figure 5.7: frequency domain approach scheme.

87

This approach makes use of a linear version of the Irish SFRM system that does not include deadbands or saturations and considering time invariant parameters. The logic scheme of the approach is presented in figure 5.7. In general, in a linear time invariant FORWARD model with a certain transfer function $TF(\omega)$, input ΔP_{mis} and output Δf, one can write $|\Delta f(\omega)| = |\Delta P_{\text{mis}}(\omega)| \cdot |TF(\omega)|$. From this correlation, applying the Parseval theorem, the $\Delta f(t)$ can be written in function of its power spectrum as:

$$Var(\Delta f(t)) = 2 \cdot \sum_{i=1}^{N/2} |\Delta P_{\text{mis}}(\omega)|^2 \cdot |TF(\omega)|^2 \ , \tag{5.10}$$

where Var is the variance of the signal and N the number of the harmonics. Normalizing equation (5.10) and dividing the sum into two parts at a certain specific harmonic, say N_x, we can write:

$$1 = Var_{1,\text{pu}} + Var_{2,\text{pu}} \text{ with}$$
$$Var_{1,\text{pu}} = \frac{2 \cdot \sum_{i=1}^{N_x} |\Delta P_{\text{mis}}(\omega)|^2 \cdot |TF(\omega)|^2}{Var(\Delta f(t))} \ ,$$
$$Var_{2,\text{pu}} = \frac{2 \cdot \sum_{N_x}^{N/2 - N_x} |\Delta P_{\text{mis}}(\omega)|^2 \cdot |TF(\omega)|^2}{Var(\Delta f(t))} \ . \tag{5.11}$$

A specific N_x can be set by investigating what harmonics are more influenced by RoCoF control or by PFC. In particular, we can qualitatively study the Bode plots resulting from changing the FORWARD model parameters into realistic ranges, and identify two distinct harmonic ranges, say $\Delta \omega_{\text{PRI}}$ and $\Delta \omega_{\text{rocof}}$ and in such a way compute $Var_{1,\text{pu}}$ and $Var_{2,\text{pu}}$ terms as presented in equation (5.11). These two terms are evaluated for each day of real frequency measurements at our disposal giving us a qualitatively weight on the importance of RoCoF control and PFC on the frequency signal.

5.2.2 Irish data and power system parameters

The case study is based on about 300 days of frequency signal measurements made at the University College of Dublin in the years from 2015 to 2016 with a sample of 10 Hz. In order to compute the grid time varying parameters, the data about the consumption and generation of the grid were provided by the Irish TSO Eirgrid divided between wind production and CG generation P_{CG}. The time variant inertia H is computed using equation (5.12):

$$H = \frac{\sum_i H_i \cdot S_i}{\sum_i S_i} \ . \tag{5.12}$$

In this equation, a typical mean inertia value H_{CG} is used for every generator inertia H_i and a certain instantaneous capacity factor c_f equal to $\frac{\sum_i S_i}{P_{CG}} = \frac{S_{CG}}{P_{CG}}$ is set in order to evaluate the nominal power present in the system during the day. The regulating energy K_{CG} is computed as $K_{CG} = K_{CG,pu} \cdot \frac{S_{CG}}{f_{nom}}$. c_f and other important parameters (H_{CG}, generators zero-pole dynamics constant, etc.) are chosen by considering typical values and the Irish grid code (note that the Irish grid has almost no hydro resources, therefore the PFC dynamics shown in figure 5.1 are consistent with a steam generator technology. In such a way the reconstructed inertia levels and regulating energies present realistic changes during the day by considering the real operating conditions of the grid. The parameters which are kept costant in the time domain simulations are shown in table 5.1 and represent realistic mean values. For what concerns the frequency domain, a parametric analysis was performed in order to study the $TF(\omega)$ of the system by changing the parameters related to BESS or to frequency control by CG. The ranges shown in the table 5.2 are obtained multiplying the base value(bv) by the normalized range column elements. In compliance with our frequency data sampling ω goes from 10^-5 to 10 [rad/s]. In general, the delay of the BESS is represented by summing a pure delay part approximated by a Padè polynomial with a ramp part approximated by a fast pole.

Table 5.1: Constant parameters for time domain simulations

H_{BESS}	c_f	$K_{CG,pu}$	D	τ	T_p	T_g	T_c	PFC_{band}^{CG}	T_{BESS}
[MWs]	[pu(MW)]		[%]	[s]	[s]	[s]	[s]	[pu(MW)]	[s]
6	0.7 [1]	20	1	3	10	0.225	0.35	0.10	0.1

Table 5.2: Parameters for frequency domain analysis

Parameter	bv	norm. range	Parameter	bv	range
Inertia $[pu(MWs)]$	6	$0.1 \div 2$	τ $[s]$	2	$0 \div 2$
K_{BESS}	250	$0 \div 4$	T_p $[s]$	8	$0.5 \div 1.5$
δ_{BESS} $[s]$	0	$0 \div 0.1$	τ_{BESS}[s]	0	$0 \div 0.1$
δ_{BESS}^{PFC} $[s]$	0	$0 \div 0.25$	τ_{BESS}^{PFC}[s]	0	$0 \div 0.25$

---

[1]This number was chosen by considering typical values of generators in modern grids in the absence of precise data. In particular using [17] it is possible to reconstruct 15 real capacity factors of the UK grid in different moments. The average is 0.69, a little lower during the night and higher during the day

Table 5.3: BESS parameters simulations

	1	2	3	4	5	6	7
$\sigma_i \ [Hz]$	0.0290	0.0372	0.0455				
$\mu_i \ [Hz]$	50.006	49.995	49.993				
$c_{\text{f,CG}} \ [pu(MW)]$	0.25	0.50	0.75				
$c_{\text{f,BESS}} \ [pu(MW)]$	0	0.35	0.7	1	1.35	1.7	2
$S_{\text{BESS}}^{\text{PFC}} \ [pu(MW)]$	0	0.25	0.50	0.75	1	$1^{\star}$	

5.2.3 Scenarios and indexes

For time domain simulations BESS are added into the system by considering several scenarios. ESL has been considered to dimension PFC (parameter K_B) and RoCof control (parameter H_T^B) with saturations in both control channels. CG presence is progressively decreased in the proposed scenarios, while ΔP_{mis} is kept fixed. The three elements composing ΔP_{mis} (see Equ. 5.4) depend on several factors such as: renewable and load growth, market structure, auto-consumption of renewable energy, renewable source smoothing due to the increased installed capacity, new grid requirements, interconnections and so on. Moreover, it is not easy to model and parameterize the single components of ΔP_{mis} as they represent the global mismatch caused by the power perturbations of hundreds of elements in the grid. In order to avoid unnecessary complications, the ΔP_{mis} time series was left equal in all the scenarios. Instead, CG capacity was decreased reducing the inertia and regulating energy present in the grid, which deeply influence the frequency signal. CG capacity is decreased by a constant amount, which corresponds to a percentage of the mean CG present along the day. At the same time, BESSs are introduced into the grid and their installed capacity is computed as:

$$P_{\text{BESS,i}} = c_{\text{f,BESS}} \cdot (1 - c_{\text{f,CG}}) \cdot \mathbb{E}[P_{\text{nom}}^{CG}(t)_i] \cdot PFC_{\text{band}}^{\text{CG}}, \tag{5.13}$$

where i represents a generic day and $c_{\text{f,CG}}$ defines the percentage of CG to be reduced. The mean CG production $\mathbb{E}[P_{\text{nom}}^{CG}(t)_i]$ is multiplied by the PFC band. In such a way, BESS added capacity results proportionally to the the lost amount of regulating energy in the grid due to the shutting of CG capacity. Three days are simulated representing low, medium and high standard frequency deviation (σ_i) scenarios. For what concerns BESS regulation strategy, we will try out different complementary PFC and RoCoF control bands such that $S_{\text{BESS}}^{\text{PFC}} + S_{\text{BESS}}^{\text{RoCoF}} = 1$. A last strategy considers both $S_{\text{BESS}}^{\text{PFC}}$ and $S_{\text{BESS}}^{\text{RoCoF}}$ equal to 1. In total we consider 3 days σ_i , 3 CG coefficient capacities $c_{\text{f,CG}}$, 7 BESS coefficients $c_{\text{f,BESS}}$ and 6 different sets of values for the BESS band assigned to PFC and RoCoF control

($S_{\text{BESS}}^{\text{PFC}}$ and $S_{\text{BESS}}^{\text{RoCoF}}$), for a total of 378 simulations. All the parameters of the simulations are summarized in table 5.3 ($S_{\text{BESS}}^{\text{RoCoF}}$ is always equal to $1 - S_{\text{BESS}}^{\text{PFC}}$ except in the case when $S_{\text{BESS}}^{\text{PFC}} = 1^\star$, which corresponds to $S_{\text{BESS}}^{\text{RoCoF}} = 1$, so that both services are assigned the full band).

Two simple indexes can help us to investigate the impact of BESSs. The first one is represented by the letter h and provides a measure of the relative improvement to the dynamics response due to the BESSs. It is defined as:

$$h_{\text{BESS}} = 1 - \frac{\sigma_{\text{BESS}}}{\sigma_o} \ , \tag{5.14}$$

where σ_{BESS} is the standard deviation of the frequency of the system with inclusion of BESSs and σ_o is the standard deviation of the frequency for the same scenario without BESSs. The index can therefore go from 0 (no improvement) to 1 (no frequency deviations). Similarly, in the place of σ_o we can use σ_{CG}, the standard deviation of the system which considers the original presence of CG. In this way, it is possible to quantify the amount of BESS reserves needed to substitute the original CG reserves $S_{\text{CG,o}}^{PFC}$. We can evaluate this quantity in the point where $\sigma_{CG} = \sigma_{BESS}$ and define a new index k:

$$k = 1 - \frac{P_{\text{BESS}}}{P_{\text{CG,o}}^{PFC}}. \tag{5.15}$$

This index is < 0 in the case BESSs are less efficient of original reserves in limiting frequency excursions, and tend to 1 in the case of optimal performance.

5.2.4 Results

Frequency domain results

In figure 5.11 is shown the magnitude of the system transfer function obtained by changing the values of the selected parameters. For brevity, only 5 relevant parameters for PFC and 3 for RoCoF control are shown (the delay parameter δ is modelled by using a Padè polynomial approximation of the fifth order) both for BESS and CG resources. The figures suggest that the impact of PFC and RoCoF control can be roughly divided in two areas: PFC has a great influence on slow harmonics up to 1 rad/sec, in the second area inertia and RoCoF control are limited to fast frequency harmonics starting from 0.5 rad/sec. This is expected as RoCoF control mimics physical rotating inertia, which smooth fast power torque changes, while slightly opposing slow ones. Delays of rocof and primary control can worse the system response but only for big values which are already outside the technology capability. Note that for fast PFC CG control dynamics, we have
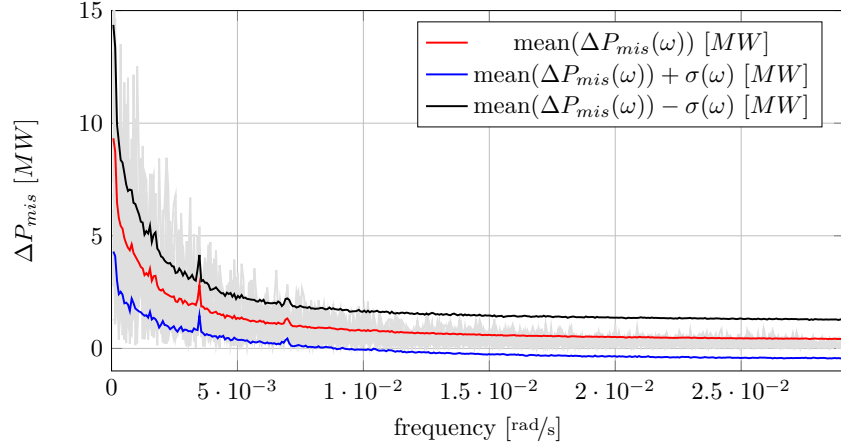
Figure 5.8: ΔP_{mis} Fourier amplitudes.
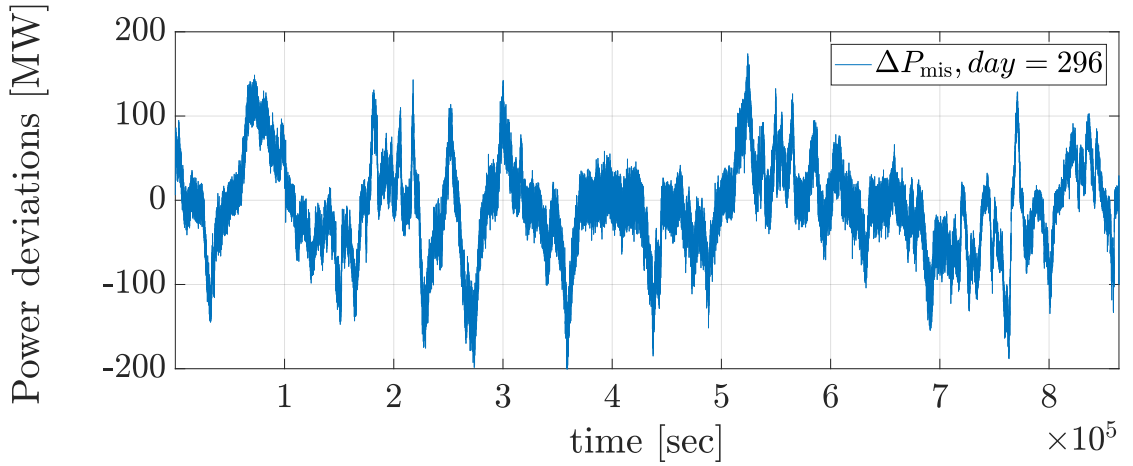
Figure 5.9: ΔP_{mis} profile example for one day.

a lower resonance peak in the transfer function (with τ having more importance than T_p). Finally, it is important to highlight that even without BESS and with lower inertia from CG, high frequency harmonics are usually well damped except for very low values of inertia (less than 10 % with respect to average today values). From the above analysis we have thus identified three possible values for the N_x corresponding to 0.1,0.5,1 rad/sec frequency harmonics.

ΔP_{mis} times series are computed for more than 300 days following the approach proposed in the previous section. In figure 5.9 is shown an example of time profile for one day, while in figure 5.8 the DFT is applied to each day and the first 400 harmonics amplitudes are drawn. In the frequency domain, the days are quite similar to each other and the first harmonics present much higher values than
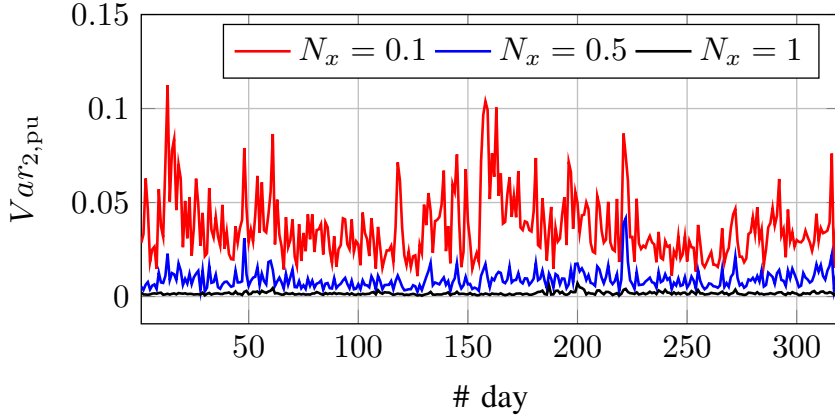
Figure 5.10: $Var_{2,\text{pu}}$ results for all the days considered.
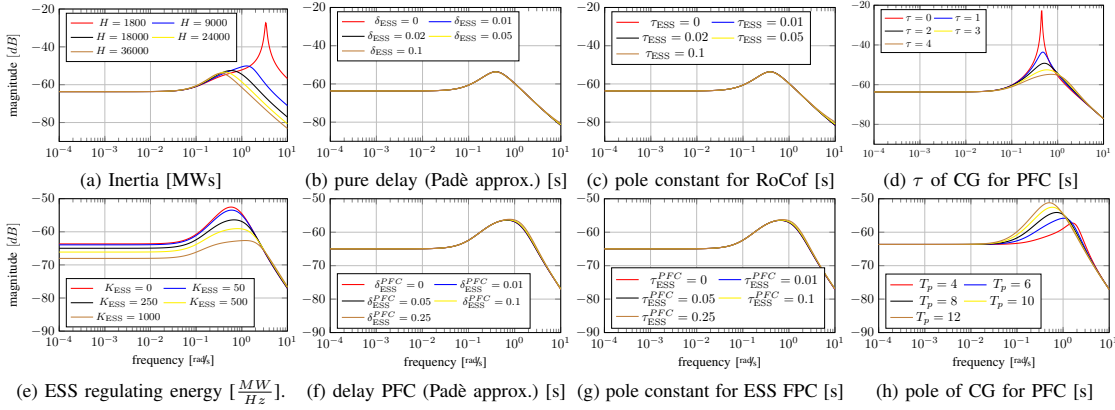
Figure 5.11: bode magnitude plots of the system transfer function changing various parameters. Parameters description and unit of measurements are located under the singles figures.

the last ones. The ΔP_{mis} is therefore a slow signal characterized by long period harmonics with high magnitude value.

Finally, by using equation 5.11 we have computed the $Var_{1,\text{pu}}$ related to PFC for each day and each N_x considered and $Var_{2,\text{pu}}$ as its complementary value. Figure 5.10 shows the results: the frequencies more subject to the intervention of RoCoF represent on average a very small part of the signal. In the case of $N_x = 0.1 rad/sec$ this is well under 10% and in the case $N_x = 1\ rad/sec$ even lower than 1% . This happens for two reasons: ΔP_{mis} is a slow signal and therefore interests slow frequencies which are more influenced by PFC. Moreover, the transfer function magnitude plots reveal that the system naturally (even for low inertia values) behaves like a low pass filter which damps high frequencies components.

From these results we expect that in normal operations fast PFC will have much bigger impact with respect to RoCoF control. This qualitatively analysis will be followed by time domain simulations to validate this concept.

Time domain results

BESSs clearly improves the frequency signal as depicted in figure 5.12. The results of h_BESS for day 3 and $c_{\text{f,CG}} = 0.25$ is shown in 5.13. The dotted line represents the simulations with both RoCoF and PFC control, while the green one represents the case with only RoCoF control by BESS. As clearly depicted, the RoCoF control action has very little impact on the frequency signal standard deviation. The index h_BESS has the same behaviour also for the others days and $c_{\text{f,CG}}$ values. In table 5.4 the average of h_BESS values considering all strategies (excluding the one with only RoCoF control) and the installed capacities are shown. Higher values of h_BESS are found in simulations with low $c_{\text{f,CG}}$, days with higher frequency standard deviation and when there is an important BESS capacity installed. This is due to the presence of the deadband in the PFC controllers which make BESSs work less when the frequency is in the neighborhood of the nominal value. The index K was computed for all $c_{\text{f,CG}}$ and days and for the best control strategy (the one with both full band used by PFC and rocof) in the case $c_{\text{f,BESS}} = 1$. The regulating energy offered by BESSs in these scenarios is equal to the one originally offered by CG, this can be verified by using equations (4.8) (5.13) (5.15) (5.15). Nevertheless, this index is near one (or in average 0.97), meaning that in normal operations BESSs keeps the frequency bounded similarly to CG. This result is apparently surprising due to the major velocity of BESSs PFC against to CG, but it can be explained by considering the slow dynamics of the frequency signal (the oscillations are substantially "very slow" concentrated on 30 minutes or higher period harmonics) and by the fact that CG and BESS impact slow harmonics in the same way.

Table 5.4: index h_BESS averaged values.

| | $c_{\text{f,CG}}$ | | |
Day	0.25	0.50	0.75
1	0.40	0.23	0.10
2	0.46	0.25	0.12
3	0.46	0.27	0.13

In figure 5.15, three frequency profiles of the same day are shown where regulating energy from BESS is the same of the CG lost. As can be seen, the difference

between blue (original signal with CG) and orange/yellow is very small. Moreover, the difference between orange and yellow (where we have RoCoF control in addition to PFC) is almost zero, except for a small difference in the deadband of the primary controller where PFC does not act. This difference is due to the dimensioning method used for RoCof control (see equations (4.10) (5.13)) which makes the inertia added to the grid by BESSs less than half of the one previously provided by CG.

For the same reasons, the almost zero value of h_{BESS} for RoCoF control is due to the slow nature of frequency oscillations in the grid. In fact, inertia has a low impact on these slow oscillations.

The low impact of inertia can also be seen in figure 5.14 where different level of inertia were simulated by keeping PFC reserves equal to the base case scenario. Only at inertia levels less than 10% with respect to the base case scenario, the frequency starts to overshoot with respect to the original case.
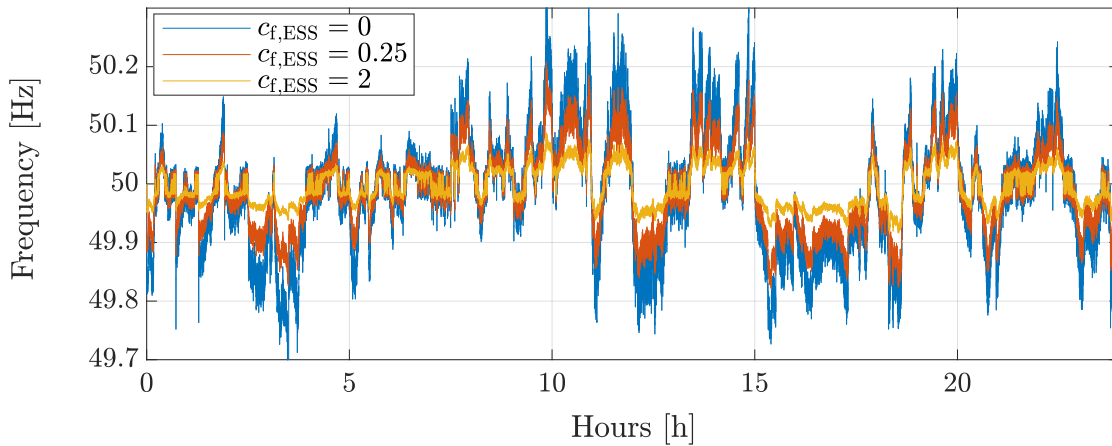
Figure 5.12: frequency profiles examples for day 3.

5.2.5 Further insights

From the above simulations, it is clear that inertia and RoCoF control have little value for frequency stability, except in very low inertia scenarios . On the contrary, inertia is fundamental during first moments after a contingency. As

---

[1]Note that this conclusion refers only to frequency stability. Inertia could also influence rotor-angle and voltage stability [182] so that higher level or particular distributions of inertia are needed in the grid during normal operations
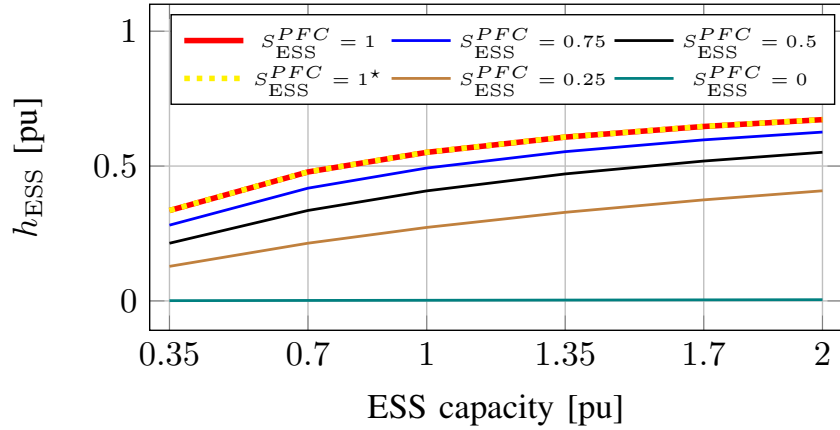
Figure 5.13: index h_{BESS} profiles for day 3 and $c_{\text{f,CG}} = 0.25$.
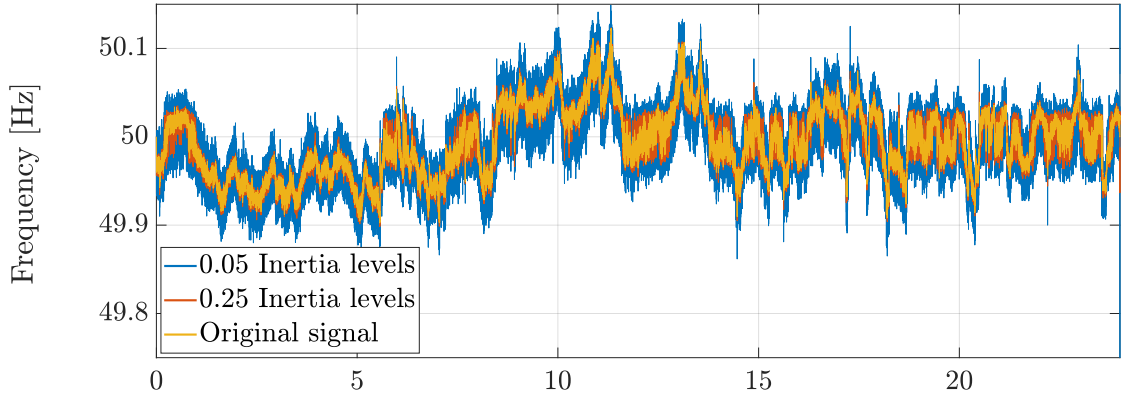
Figure 5.14: Frequency profiles examples by changing only inertia in the grid.

known, a contingency is modelled as a power step in time domain and characterized in the frequency domain by a wide range of harmonics: the fast ones are thus damped by the inertia of the grid which limits the RoCof at the initial moment.

Knowing that during normal operations the RoCoF control is under-used and PFC is instead important, one can think to keep both services always acting with the full band. In such a way RoCof control is ready to be used in the case of a contingency. However, making this choice it is possible to saturate both bands and consequently have a worse control impact. For this reason, we have performed a certain number of simulations to study the best strategy for the frequency control during a contingency.
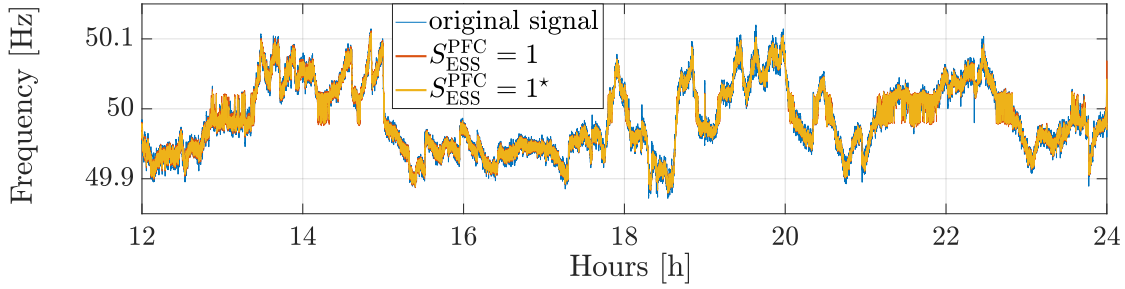
Figure 5.15: Frequency profiles examples for day 3 and $c_{\text{f,CG}} = 0.25$.

Contingency analysis

Without aim of completeness, we restrict ourselves to a unique example scenario which corresponds to day 1, $c_{\text{f,CG}} = 0.25$, $c_{\text{f,BESS}} = 1$. Four different strategies for BESS control are implemented: the first three have complementary bands with $S_{\text{BESS}}^{\text{PFC}} = [0, 0.5, 1]$ and the fourth has both bands equal to 1 (signed as $S_{\text{BESS}}^{\text{PFC}} = 1^\star$). A contingency is applied to the system and the frequency signal and BESS intervention is recorded and analyzed. The results show (see figure 5.16) that the best choice for BESS control is the use at the same time of full RoCoF and PFC band. In table 5.5 are reported the simulation output variables: $\overline{P_{\text{BESS}}}$ represents the average power provided by the BESS during the simulation. This value is higher in the case with $S_{\text{BESS}}^{\text{PFC}} = 1^\star$ therefore control in the grid has major impact even considering the potential presence of instabilities caused by bands saturation. In fact, as can be seen in figure 5.17, the two controls present different time ranges and characteristics during a contingency: on one hand RoCoF control acts in the first instants and goes very fast to zero, on the other hand PFC starts after the RoCoF control is already decreasing until reaching a stable point different from zero. The overlapping between the two services is still present but limited. In the simulated scenario, BESS output (shown in the figures below) does not reach saturation, but the same principle applies even in that case. Therefore, from the grid point of view, it turns out that applying full power bands to both control services is the best choice.

Notes on SOC profiles

In our simulations we have considered BESSs as a unique equivalent plant impacting the frequency signal. At the same time, the study of the SoC dynamics is important in order to identify possible energy requirements for BESSs. During the simulations we have recorded SOC profiles assuming a battery capacity $Q_c = 4 \cdot P_{BESS}$. Note that our analysis is restricted to the case with only PFC because RoCof control has negligible impact on the BESS SoC.
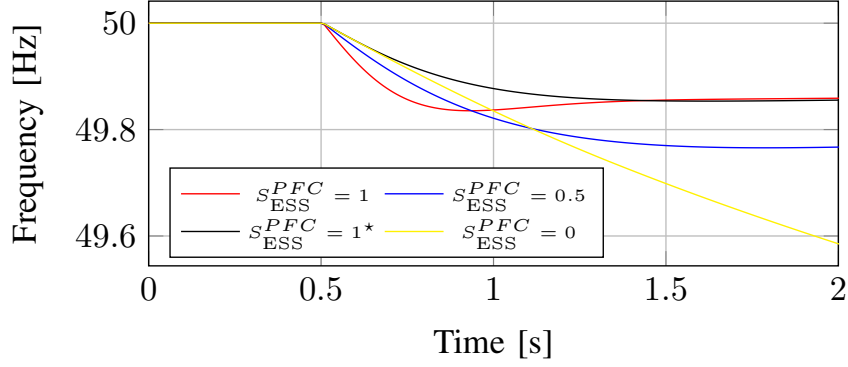
Figure 5.16: Example of frequency profiles after a contingency.
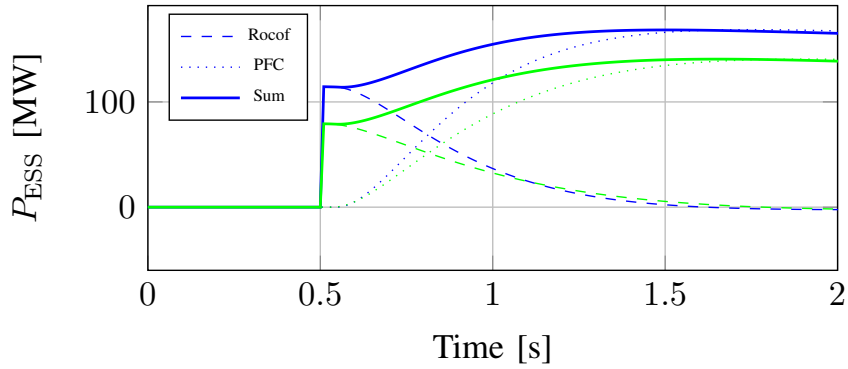
Figure 5.17: example of BESS requested power profiles in the case with $S_{\text{BESS}}^{\text{PFC}} = 1^{\star}$ (blue) and $S_{\text{BESS}}^{\text{PFC}} = 0.5$ (green).

State of Charge dynamics. Due to internal efficiencies we would expect the equivalent BESS SoC to decrease constantly in time but, by looking at the final SoC value we find out that in day 1 SOC tends to increase. As seen in table 5.3, the first day presents an average frequency signal over 50 Hz. This creates a bias effect in the primary frequency controller of the BESSs which, going against internal inefficiencies, makes the SOC increase. Another factor to take into account is the mentioned fact that the frequency is a slow oscillating signal. As a first hypothesis, we could state that the energy losses/gains of BESS PFC are composed by three terms with different time frames:

$$\Delta E_{\text{BESS}} = \Delta E_{\text{eta}}(\eta_{\text{cha}}, \eta_{\text{dis}}) + \Delta E_{\text{bias}}(\mu_f) + \Delta E_{\text{intraday}}(f(t) - \mu_f). \quad (5.16)$$

By normalizing the Delta energy with the battery capacity and introducing the BESS initial SOC, we have:

$$
\begin{aligned}
SOC(t) - SOC_{ini} &= \Delta SOC(t) \\
&= \Delta SOC_{eta}(t) + \Delta SOC_{bias}(t) + \Delta SOC_{intraday}(t).
\end{aligned}
\quad (5.17)
$$

98

Table 5.5: Frequency profile parameters results.

$S_{\text{BESS}}^{\text{PFC}}$ $[pu(MW)]$	RoCof $[Hz/s]$	f_{nadir} $[Hz]$	f_{reg} $[Hz]$	T_{nadir} $[s]$	T_{reg} $[s]$	$\overline{P_{\text{BESS}}}$
0	0.80	49.83	49.88		32.1	
0.5	0.49	49.76	49.84		35.3	
1	0.35	48.77	49.77		32.9	
$1^{\star}$	0.35	49.85	49.88		57.5	

In order to quantify these three parts we can simulate SOC dynamics with $\eta_{\text{cha}} = 1$ and $\eta_{\text{dis}} = 1$, so that $\Delta E_{eta} = 0$ obtaining the sum $DeltaSOC_{bias}(t) + \Delta SOC_{\text{intraday}}(t)$. Then, by subtracting this term to the original ΔE_{BESS} we can quantify the ΔE_{eta} component (equation 5.17). To separate the ΔSOC_{bias} and $\Delta SOC_{intraday}$ components we can simulate the BESS behaviour with $\eta_{cha} = 1$, $\eta_{dis} = 1$ and taking as input a new frequency error signal equal to $\Delta f_1 = f(t) - \mu_f$. In this way, we obtain the $\Delta SOC_{intraday}$ and in turn obtain ΔSOC_{bias} with a simple subtraction. Due to the presence of non-linearities (dead bands and saturation on the BESS control), this methodology is sufficiently precise, but not exact.

For this assessment on BESS SoC profiles, we repeat the simulations with $cf_{BESS}^{df} = 0$ and $cf_{BESS}^{fpc} = 1$ choosing just one simulation per day with $cf_{CG} = 0.25$ and $cf_{BESS} = 1$.

In the figure 5.19 we show the SOC time profiles of the three days decomposed into the different components. As expected, the efficiency component (figure 5.18a) decreases monotonically in time, while the bias factor is substantially linear (depending on the constant offset μ_f). Finally, the intra-day component includes all the different dynamics due to the oscillating cyclical nature of frequency reaching at the end the initial point. Let us note that the intra-day component does not return exactly to zero and that the bias factor is not exactly linear due to the the already mentioned presence of non linear effects. The efficiency component, while is not negligible, poses less danger for BESS SoC with respect to the intra-day and bias components, and depends on the standard deviation of the frequency signal: the more the BESS works, the more the internal efficiencies makes the SoC to decrease. As expected, the bias factor depends on the value of μ_f and the intra-day component profiles differ for each day considered.

The efficiency component causes SoC decrements from 1.5 to more than 3 %, while the bias factor can cause SoC change of more than 10 %. As written in table 5.3, we note that while the μ_f value is near 50 Hz, its effect is quite important due to the fact that it lasts for 24 hours.

99

(a)

(b)
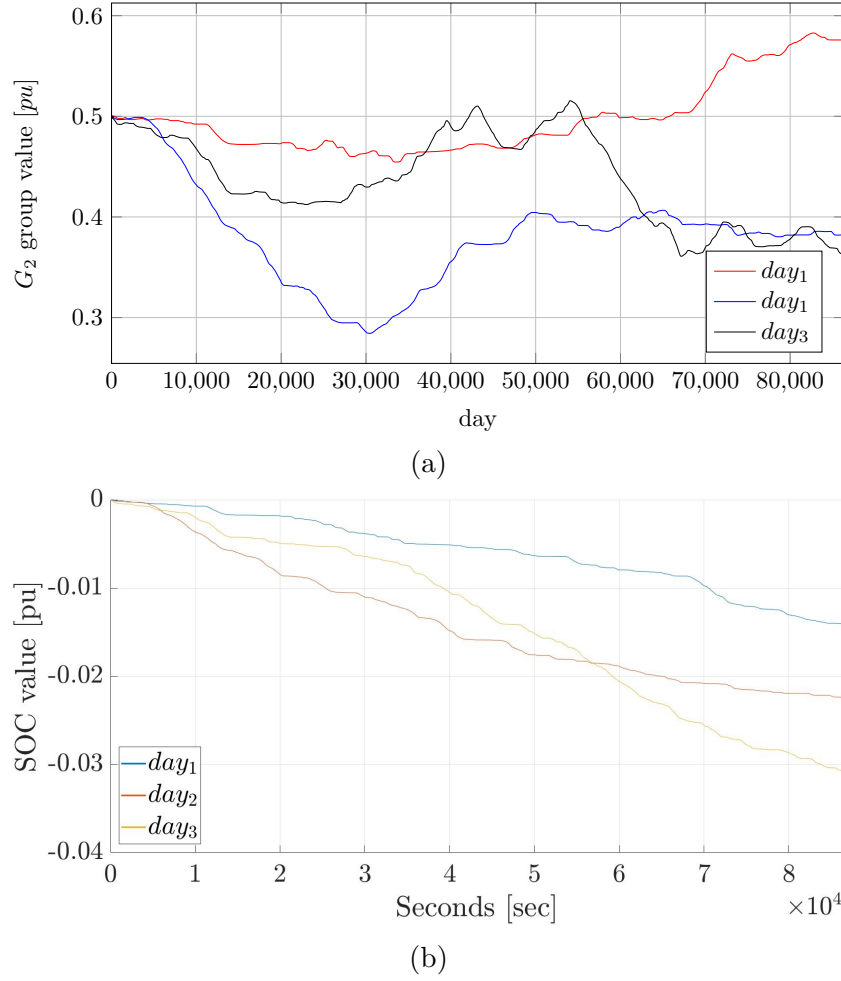
Figure 5.18: ΔSOC time profiles. (5.18a) represents the real SOC profile. (5.18b) represents the efficiency part.

The battery capacity is equal to $P_{BESS} \cdot 4$, which is a slightly higher energy-to-power ratio for today BESS installations: by using smaller ratios the problems, identified by this analysis, would be even more visible and dangerous for the continuous operation of the BESSs. For example, the efficiency losses could be as high as 12 % per day, while bias factor and intra-day components could reach ΔSOC as high as 40 %. Considering that a certain percentage of SoC should be always maintained for technology issues and contingency scenarios, this demands frequent intra-daily recharges/discharge.

(a)

(b)
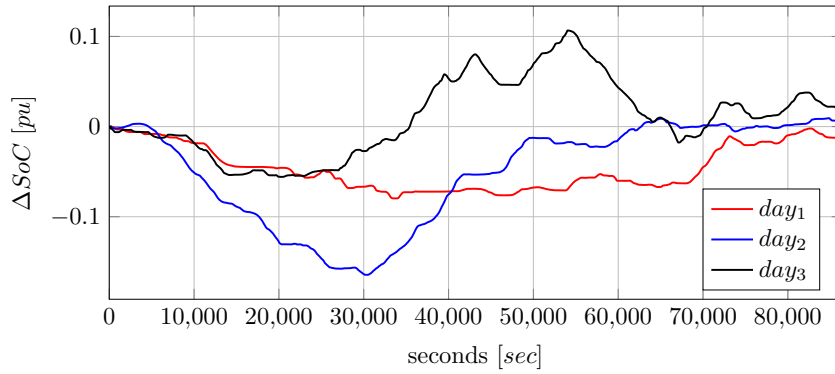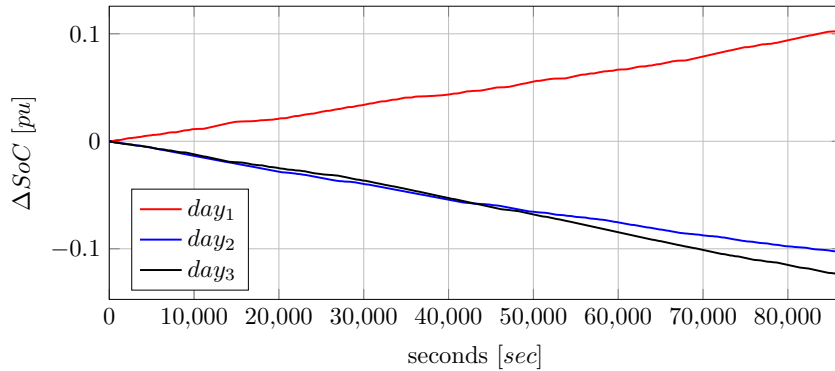
Figure 5.19: ΔSOC time profiles. figure (5.19a) represents the intra-day part. Finally, (5.19b) represents the bias component.

5.3 Notes on the Irish Frequency Jumps

Jumps characteristics. Irish frequency data used in this study are characterized by frequent and wide frequency jumps as shown in figure 5.20 for one day. Naively, these jumps could be linked to load abrupt changes, but a more accurate inspection leads to other considerations. In particular, in figure 5.21 we show four two hours periods of the same day presented above. In the first image, the frequency is slowing increasing, but it is stopped by two downwards jumps which re-unbalance the signal. It is probable that these jumps are caused by the activation of grid reserves by the TSO to stabilize the frequency value. In the second image, one can notice major stochastic swings around 50 Hz due to the presence of governor deadbands in PFC controllers. In image (c), more frequency swings are noticeable in the deadband area, but in this case some of the jumps move away from the 50 Hz value and could be potentially caused by the load fast deviation, while others are still probable connected to CG. In (d) two big jumps

101
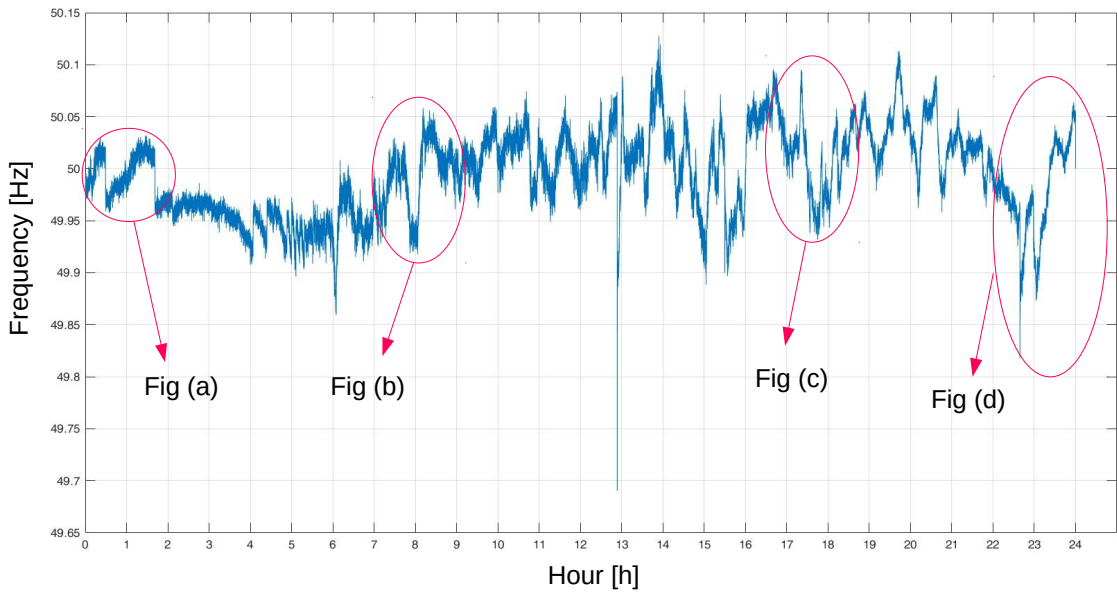
Figure 5.20: Ireland frequency on 23th of October.
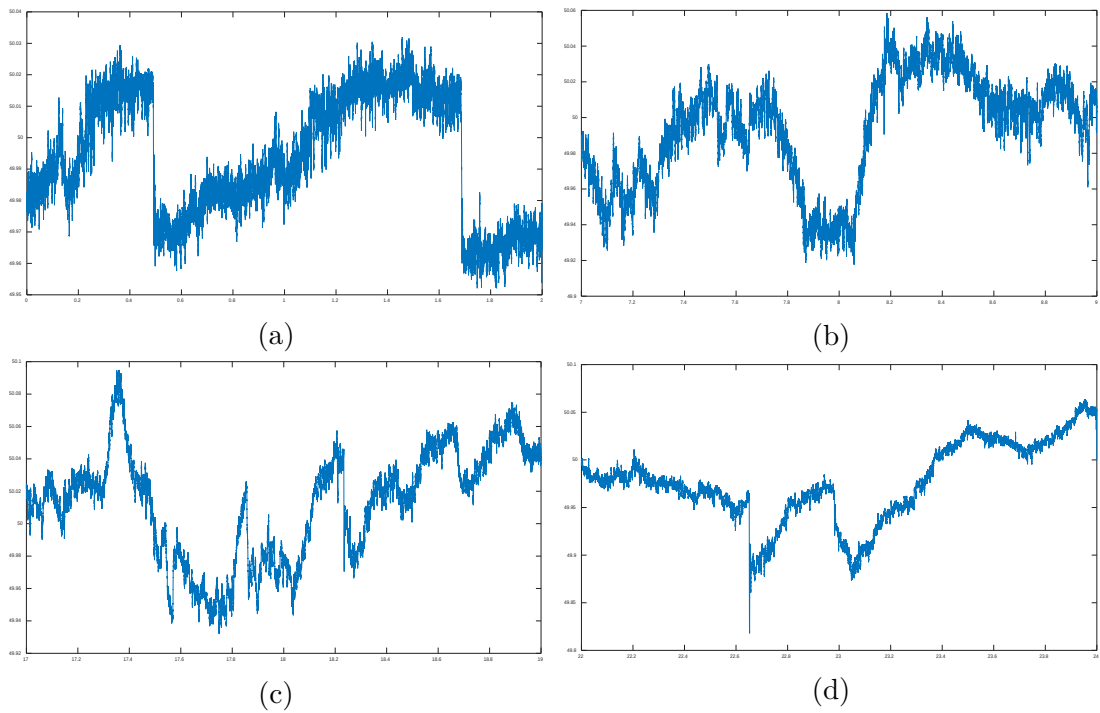
Figure 5.21: Different two hour periods.

decrease the already low frequency, and it is possible that they are caused by the

stochastic cascading generator disconnection.

In order to try and clarify the nature of these jumps, it is necessary to identify all their parameters: starting and ending frequency and time length. Additionally, by making a reasonable assumption on instantaneous regulating energy in the grid, it is also possible to guess the ΔP which cause the jumps. By studying the verse and the power unbalance we may characterize the jumps as being of deterministic or stochastic nature and construct different population characteristics.

Jump detection process. Different indicators can analyze the frequency signal and detect the jumps in an automatic way, in particular I designed two different techniques and the first tests are here reported.
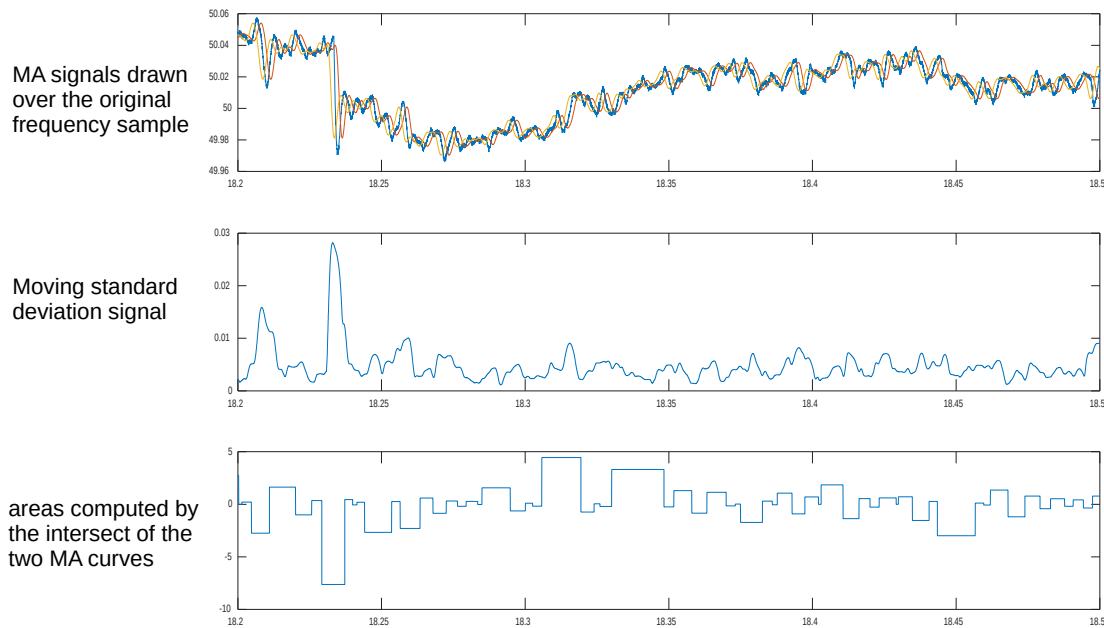
Figure 5.22: MAs and moving standard deviation computations.

First strategy is based on the use of the moving average. Given a generic discrete signal $x = [x_1, \ldots, x_i, \ldots, x_N]$ the forward moving average (MA) signal X with a computing window of m samples is computed as:

$$X_i = \frac{x_i + x_{i+1} + \cdots + x_{i+m}}{m}, \tag{5.18}$$

the backward MA goes from x_{i-m} to x_i and the centered MA from $x_{i-(m/2)}$ to $x_{i+(m/2)}$ with slightly adjustment for initial and final points of the signal in the case of odd or even m. To identify a frequency jump, a forward and a backward MA were used. As seen in figure 5.22 (a), the two MAs profiles are over-imposed to

103
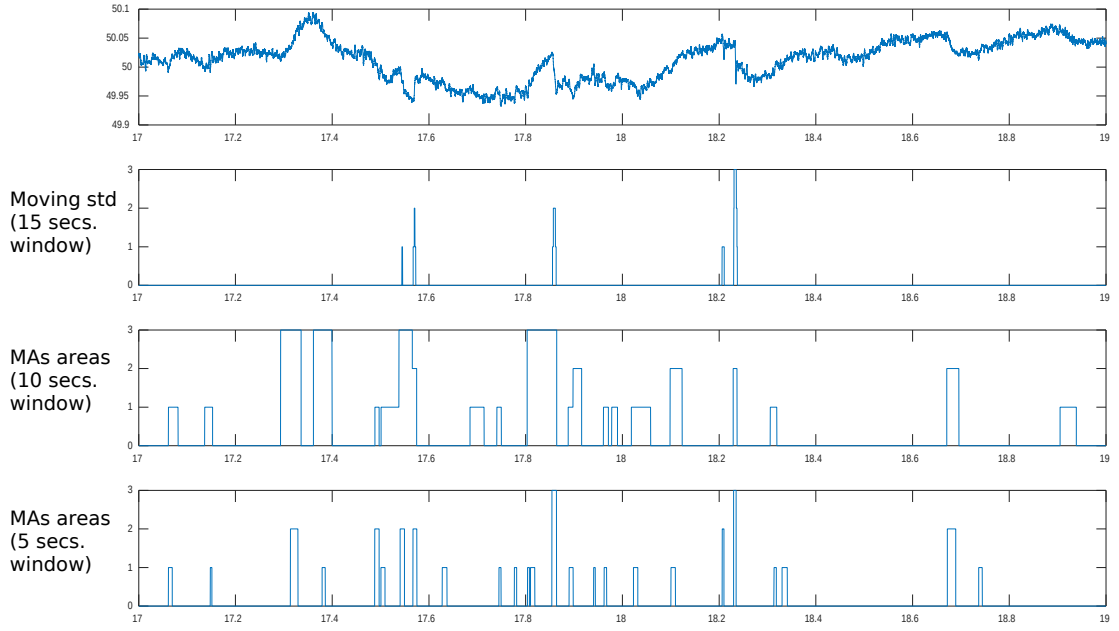
Figure 5.23: Index results.

the original signal and intersect each other every time there is a frequency change of verse. In the case of a jump, the area between two consecutive intersection is bigger (as seen in image (c)) and easily identifies a fast frequency dynamics. The second strategy is based on a moving standard deviation (MSTD). For a generic signal x, a forward MSTD with number of samples m can be computed as:

$$X_{\sigma,i} = \sigma(x_i + x_{i+1} + \cdots + x_{i+m}), \qquad (5.19)$$

where σ stands for standard deviation (STD). As seen in the figure 5.22 (b), the moving standard deviation is able to recognize jumps as high STD periods.

For both approaches, it is important to choose a suitable number m. The values of the presented indexes can be normalized computing the standard deviation of the whole X series and assigning to every sample X_i a level of jumps detection (JD). The JD is computed as follows:

$$JD = \begin{cases} 0, & \text{if } \sigma(X_i) \leq 1 \cdot \sigma(X), \\ 1, & \text{if } 1 \cdot \sigma(X) \leq \sigma(X_i) \leq 2 \cdot \sigma(X), \\ 2, & \text{if } 2 \cdot \sigma(X) \leq \sigma(X_i) \leq 3 \cdot \sigma(X), \\ 3, & \text{if } \sigma(X_i) > 3 \cdot \sigma(X). \end{cases} \qquad (5.20)$$

In 5.23 first results are obtained. Different time windows for choosing the m value are used and optimized with a trial & error approach. With respect to the

104

MAs, the MSTD method seems to better identify the jumps.

Frequency reconstruction with jumps. Once the stochastic jumps are detected, it would be possible to use a Poisson distribution to reproduce their occurrence as done in [119]. Then, we could enhance the formula presented in equation 5.4 to take into account the power jump components [2]:

$$\Delta P_{mis} = \Delta P_{Load} + \Delta P_{Load,jumps} - \Delta P_{CG} - \Delta P_{CG,jumps} - \Delta P_{Rene}, \qquad (5.21)$$

The Poisson distribution parameters of the load jumps can be varied in order to highlight the impact on frequency, rotor angle and voltage stability by making use of the appropriate grid dynamic simulator (for example, DOME, as presented in the next chapter).

5.4   Second case study: The Sardinian system

In the Irish case study, SFC was not considered as the system does not make use of an automatic reserve in order to bring the frequency back to 50 Hz. I developed a new case study in order to investigate the performances of the models when applying secondary and tertiary frequency control in normal operations.

For this case study the Sardinian power system was used as in the previous chapter. The FORWARD and REVERSE models are similar to the first case study, except that BESS can participate to SFC. For rocof and PFC the ESL is applied in order to properly share the power band used in these services, while an additional share P_{SEC}^{BESS} of P_{BESS} can be used for SFC. The instantaneous power to be produced by the BESS during secondary control ΔP_{Sec}^{BESS} is computed by using a specific participation factor $\rho_{SEC}^{BESS} = \frac{\Delta P_{Sec}^{BESS}}{\Delta P_{sec}}$, where ΔP_{sec} is the total Secondary activation requested (See Equ.(5.5)) . For all frequency services the total amount of reserves to be activated by each the single resource will depend on specific participation factors. The FORWARD model scheme is shown in figure 5.24. Parameters in bold in the figure vary during the simulation to reflect real changes in the system at different times. TFC is implemented assuming the first typology of implementation presented at the beginning of the chapter and summarized by equ.(5.6). We assume the TFC is called when the Secondary reserve reaches almost

---

[2]the stochastic part of the jumps can be associated to Load, while the deterministic part to the conventional generation. RES are not expected to produce notable frequency jumps due to their low density spatial concentration.

its maximum or minimum acceptable level l, which is equal respectively to TER_{up} and TER_{dw} as defined by the user. After the TFC is activated, it starts as a ramp and it restore the SFC level L_{Sec} back around 50. The ramp is formulated as follows:

$$\Delta P_{TER}(t) = Band_{SEC} \cdot \frac{t - t_0}{TER_{time} - t_0} \tag{5.22}$$

where $\Delta P_{TER}(t)$ is the TFC requested at time t, $Band_{SEC}$ is the total SFC, TER_{time} is the time by which the TFC needs to be fully activated and t_0 is the starting activation time. The TFC is stopped when the level is $0.48 < l < 0.53$.

Table 5.6 contains the parameters for SFC (proportional and integral gains) and TFC, set using values found in literature. For HVDC no dead band for PFC is considered, as dead band is imposed to traditional units for mechanical reasons which are not needed by power electronics devices without rotating masses. The other PFC parameters are similar to the previous chapter case.

Table 5.6: Frequency profile parameters results.

SFC		TFC		
K_p	K_T	TER_{up}	TER_{dw}	TER_{time}
0.05	300	0.85	0.15	10

5.4.1 Base scenarios setup and proposed simulations

The frequency and demand power data used for verification were obtained from the Italian TSO. The time step of the data is 15 minutes for generation and demand, and 1 second for frequency data. A base case scenario without BESS is constructed to reproduce a whole day of frequency signal. The signal was recorded on the Sardinian grid on the 18th January 2018 (winter peak) with average equal to 50.0021 and standard deviation equal to 0.0067. The actual dispatch of regulating generators is used and therefore inertia and frequency reserves quantities vary during the day (see figure 5.25). Sardinian system had a kinetic energy with a mean value of 9.6 GWs, ranging from a minimum of 9.3 GWs to a maximum of 10.3 GWs. The number of online synchronous units was changing from 18 to 22. Two reconstructions are proposed: (a) simulation with only FCP; (b) simulation with PFC, SFC and TFC to test the proposed model capabilities. In figure 5.26 the resulting ΔP_{mis} computed by the reverse model in the first case is shown together with the frequency signal. The power mismatch between generation and consumption is specular to the frequency signal as only PFC is present in the
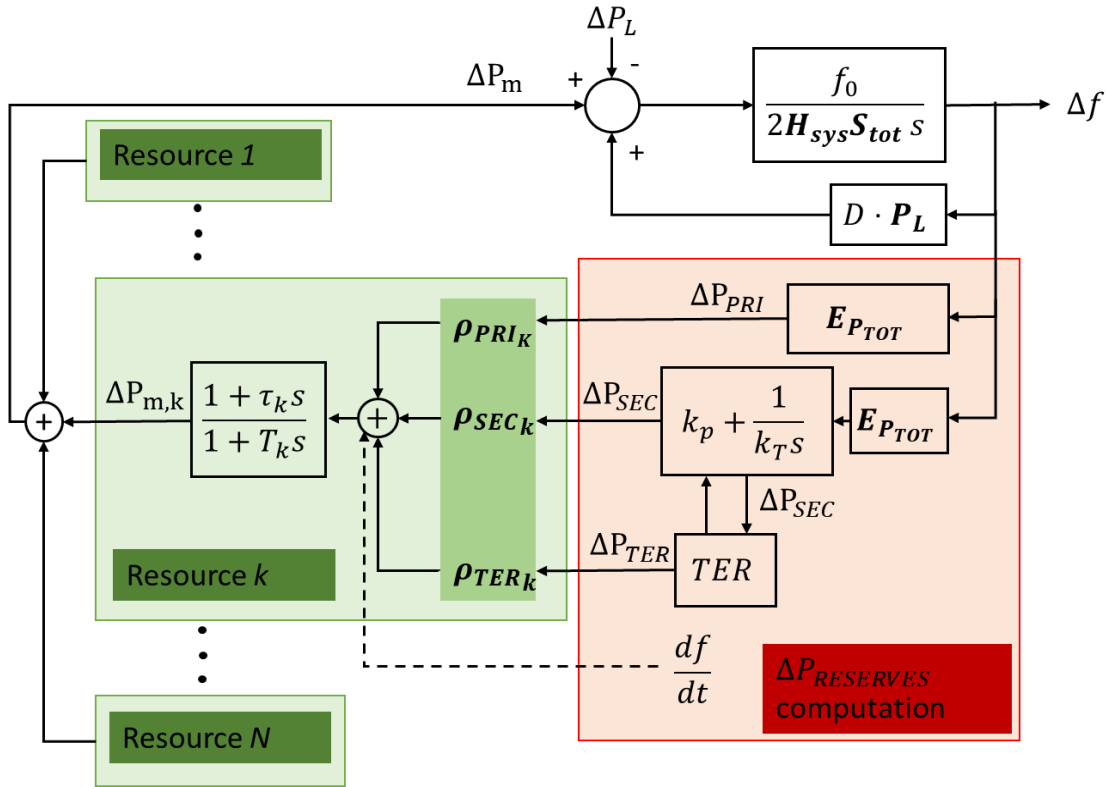
Figure 5.24: Main components of the forward model in the Sardinian case study

grid to oppose oscillations. The ΔP_{mis} is used to feed the forward model and to calculate the frequency signal. The standard deviation of the error between the simulated and the real frequency is $2.03 \cdot 10^{-4} Hz$ which is negligible being much smaller than the typical dead band value of the controller (0.01 Hz). This error is mainly due to the non-linearity present in the models such as dead bands and saturations and it can also be further reduced by decreasing the maximum allowed time step of the simulations.

In the second setup we show the results obtained if we consider the presence of PFC and TFC schemes by simulating an SFC with band of 120 MW. This is only an example to show the model capabilities, but it does not represent the reality of Sardinian frequency control, which actually present no automatic SFC. The frequency error is similar in magnitude to the previous case with a standard deviation slightly higher than before, equal to $2.4 \cdot 10^{-4} Hz$. In Fig. 7 the three frequency reserves profiles (PFC, SFC and TFC) are shown. The Tertiary reserve is continuously decreasing during the day since the frequency of the examined day is on average around 50.0021 Hz, higher than 50 Hz, and the SFC is therefore

107
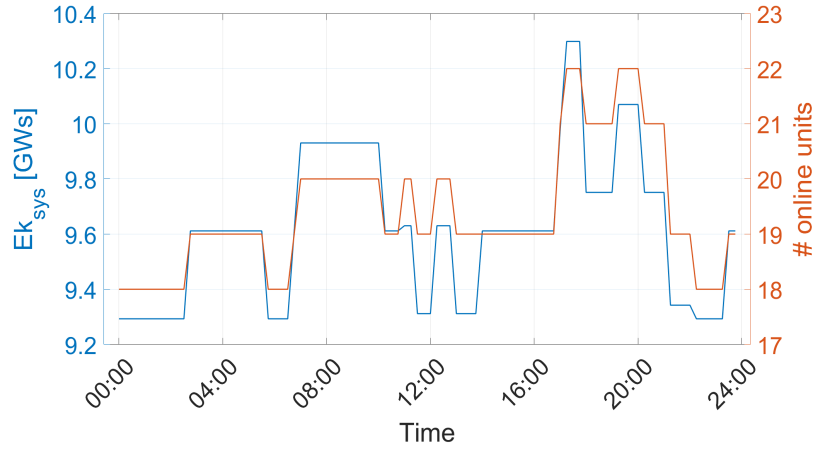
Figure 5.25: Kinetic energy and number of online synchronous units in Sardinia on the 18-th January 2018
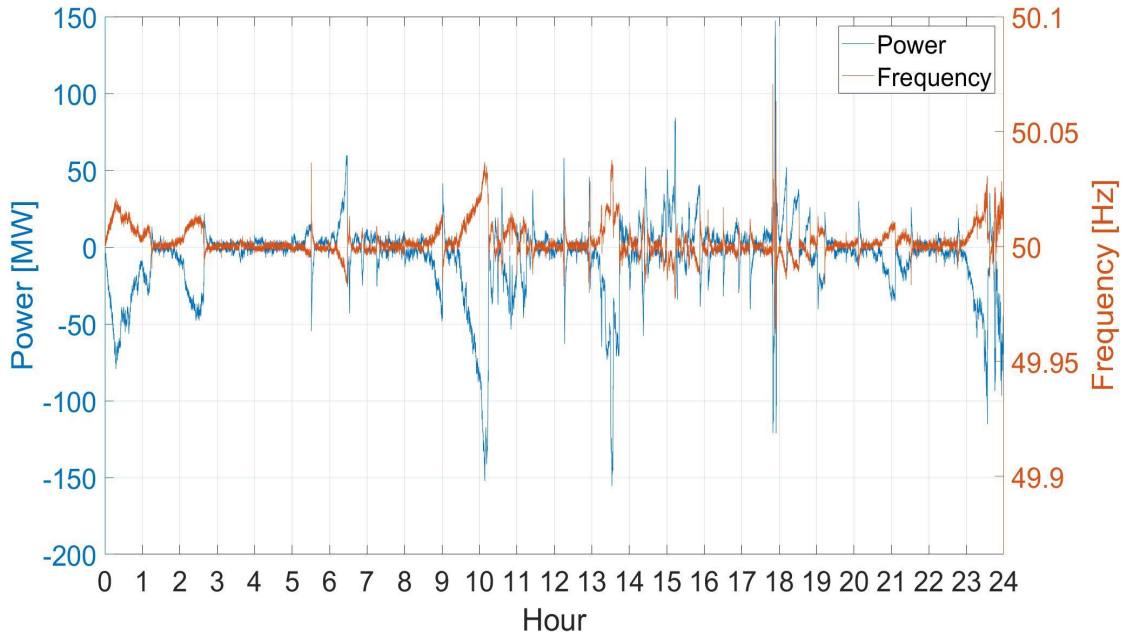
Figure 5.26: Comparison between the frequency signal and the reconstructed power imbalance with only PFC

continuously decreasing (by effect of equ.(5.6)). We can estimate analytically the sum of SFC and TFC activated by integrating the ACE during the day:

$$K_p \Delta f + \int_0^{24h} \frac{E_{P_{TOT}} \cdot \Delta f}{k_T} \cong \frac{\overline{E_{P_{TOT}}} \cdot \overline{\Delta f}}{k_T} \cdot 24h = 2736 MW \qquad (5.23)$$
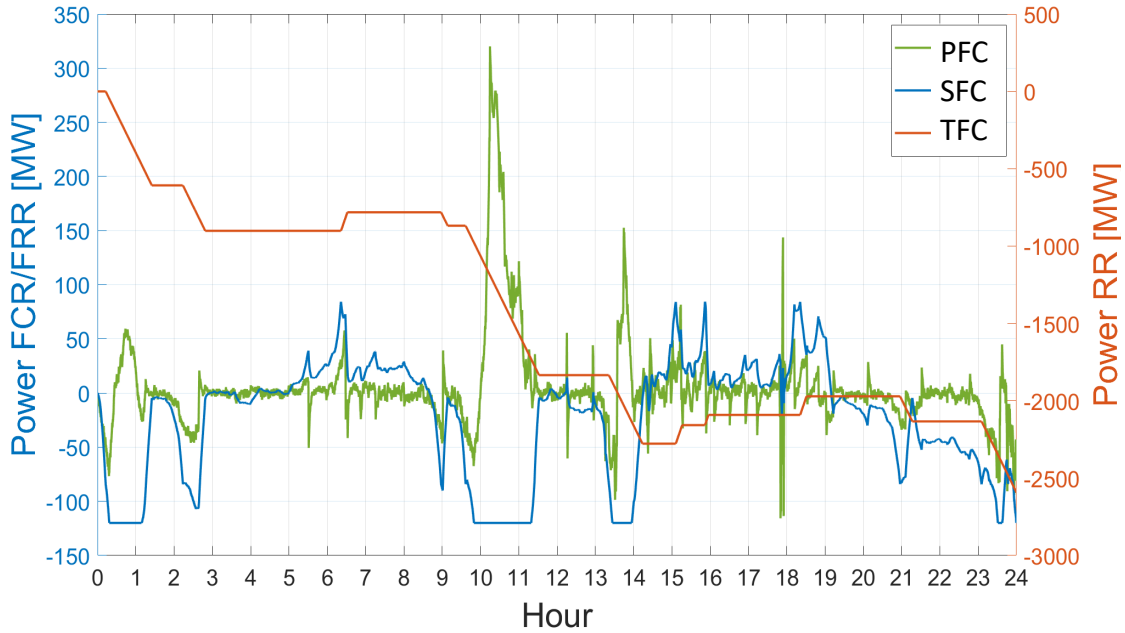
Figure 5.27: Frequency reserves simulated profiles based on the frequency signal of the 18-th January 2018

where $\overline{E_{P_{TOT}}}$ and $\overline{\Delta f}$ are the mean values during the day. $E_{P_{TOT}}$ is the total system regulating energy computed as the sum of all single resources regulating energies K_i The result is very close to the simulated sum of SFC and TFC (in absolute value), as we can see in figure 5.27, at the final time-step. It is possible to see the PFC, which follows the generation-demand mismatch due to the HVDC without dead band, while TFC is called during the day to restore the SFC reserve. The SFC is activated to bring the frequency value to the nominal value.

5.4.2   BESS results

The first setup proposed in previous section has been considered as reference case to test the BESS addition. The technical impact of BESS is evaluated when performing rocof, primary and secondary frequency control. RoCof and primary control are dimensioned using the ESL logic presented in the previous chapter.

PFC and Rocof results

A sensitivity analysis is performed on the capacity, droop and the share of inertial and primary response provided by the BESS. Two systems of 50 MW and 250 MW BESSs are analysed, with a pole time constant T_B =0.3 s. For the 250 MW case, two different droops of 0.005 and 0.004 [pu] are considered (In

109
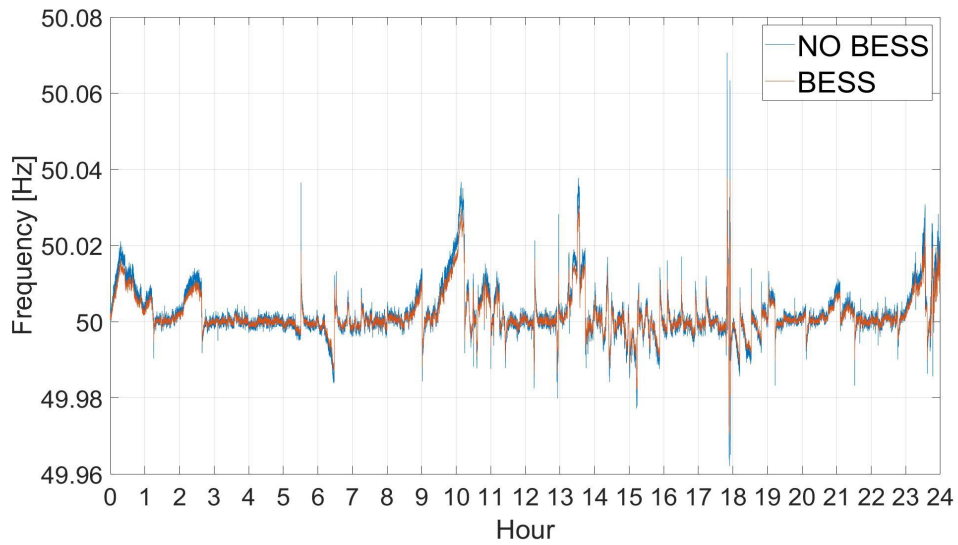
Figure 5.28: Comparison between the frequency signals with and without BESS with PFC control
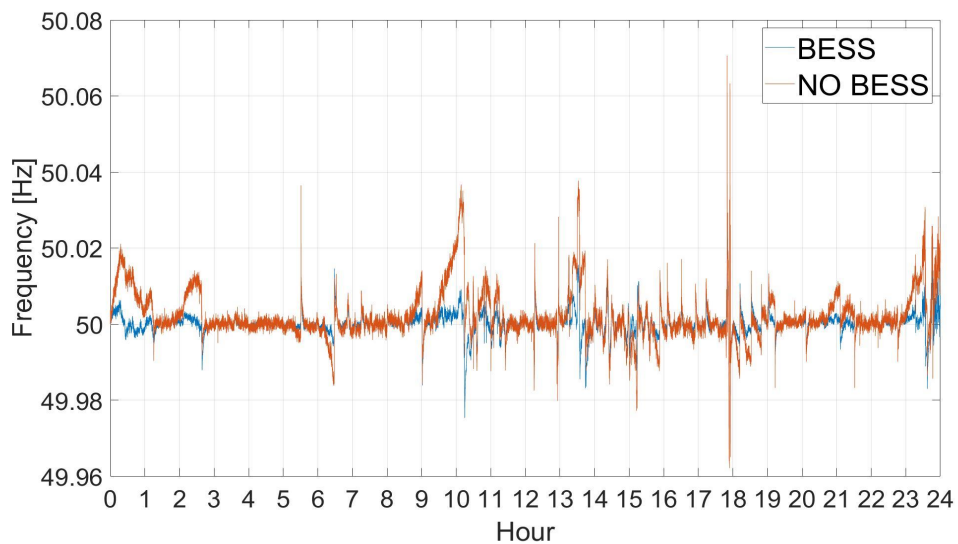
Figure 5.29: Comparison between the frequency signals with and without BESS with FR control.

previous chapter these values were computed in terms of BESS regulating energies E_{BESS} using the ESL approach. They corresponds to a droop of 5 and 4 % of a conventional SG unit). The frequency response of the BESS is compared using different shares of inertial and primary response, i.e., 50% of inertial and primary control, 100% inertial control and 100% of primary control. The two bands are

Table 5.7: Frequency profile parameters results.

BESS power [MW]	f_m [Hz]	$\sigma(f)$ [Hz]	droop (σ_p) [pu]	$RC_{\text{band}}^{\text{BESS}} = 0$ [pu]	ρ_{SEC}^{BESS} [pu]
-	50.0021	0.0067	-	-	-
50	50.0020	0.0064	0.005	0	-
50	50.0021	0.0067	0.005	1	-
50	50.0020	0.0065	0.005	0.5	-
50	50.0000	0.0037	0.005	-	1
250	50.0017	0.0054	0.005	0	-
250	50.0021	0.0067	0.005	1	-
250	50.0019	0.0059	0.005	0.5	-
250	50.0018	0.0058	0.004	0.5	-
250	50.0016	0.0051	0.004	0	-
250	50.0021	0.0067	0.004	1	-
250	50.0000	0.0029	0.005	-	1

proportional and the coefficient $RC_{\text{band}}^{\text{BESS}} = 0$ represent the power assigned to RoCof control. Figure 5.28 shows the frequency trend with the addition of 250 MW of BESS performing only PFC ($RC_{\text{band}}^{\text{BESS}} = 0$), compared with the case without BESS.

SFC results

In the second case, the BESS has been used only for the SFC. The impact in the case of normal operation is higher with respect to PFC regulation due to the integral part in the secondary controller. In fact, a purely proportional action, as in the PFC is higher when the frequency deviation is larger. The proportional action is fast and reduce the error, without compensating it. In the SFC the action is proportional to the integral of the frequency deviation and keep memory of the past deviation errors. It is higher in the case of a frequency signal unbalanced from the set-point, which is the case under examination. Table 5.7 reports the results of the simulations performed. The best performance in terms of mean frequency and standard deviation are with only SFC control (see figure 5.29), with a mean frequency reported to the nominal value from the initial 50.0021 Hz and a standard deviation improved of 45% in the case of 50 MW BESS (from the initial value of 0.0067 to 0.0037) and of 57% in the case of 250 MW BESS (from 0.0067 to 0.0029). In the case of only PFC control, the best improvements can be seen in the case with 250 MW BESS, lower droop equal to 0.004 and only primary control $RC_{\text{band}}^{\text{BESS}} = 0$, with a mean frequency equal to 50.0016 Hz and a standard deviation improved of 24% (from 0.0067 to 0.0051).

Conclusion

In this chapter we focus on the analysis of the frequency during normal operation and on the quantification of the impact of BESSs. In section 5.1 the two models presented are able to realistically reproduce the frequency in a framework which simulates the three main level of frequency hierarchical control. A SFRM model is used which guarantee proper dynamic behaviour and simulation velocity. In section 5.2 a case study is presented based on the Irish data: the time domain simulation are supplemented by an analysis in the frequency domain and both highlight the slow nature of frequency oscillations. BESS rocof control impact is negligible and PFC has an impact with the same performance of slower SG plants . As a matter of fact both channels of controls can be used at the same time with the full band in order to be always ready in the case a contingency will happen in the grid. SoC analysis highlights the importance of the frequency average on the SOC profile: also a slight deviation has a huge impact on BESS which have usually low energy–to–power ratio. In section 5.4 the study of the Sardinian grid, while different from the Irish case, confirms that slow frequency reserves such as Secondary Frequency Control have actually more impact with respect to faster ones. BESSs impact strictly depends on the characteristics of the services and of the frequency signal itself. In normal day oscillations, virtual inertia control is not effective in containing the frequency oscillations, PFC improves lightly the frequency signal while SFC is the most useful service. Typically frequency dynamics are characterized by cyclical slow components, therefore it is expected that slower services such as SFC are more effective in decreasing the oscillations, while in the case of fast changes, as sudden contingencies, virtual inertia and PFC are more important.

Chapter 6

Impact of BESSs on the Irish System: A Fourier Transform Approach

In this chapter a second study on impact of BESS during normal operations is performed. A Fourier transform procedure is developed to synthetize a realistic frequency signal depicting all the phenomena causing the Irish grid to deviate from nominal value of 50 Hz. the Irish grid model was used with more than 1000 buses and hundreds of power plants. Every load, RES and SG produces power oscillations such that the grid frequency changes as a whole in function of time. Finally BESS are added performing PFC control and their impact is compared with CG sources. Subsection 6.1.1 presents models of the resources present in the grid, 6.1.2 present the fourier transform based methodology to obtain an average frequency signal starting from real recorded data. Finally in section 6.2, case study and results are presented

6.1 Methodology

6.1.1 Resource models

The models of the various resources are as simple as possible, considering that we are not interested in the single load/power plant description, but on their overall contributions to grid frequency deviations.

Conventional generation

As already used in previous chapters, the conventional generation model is based on a zero-pole dynamic description and on the provision of PFC based on

a constant droop law and dead-band presence. The model is detailed enough for transient stability studies, where frequency variations remain well bounded and the focus is the overall response of the system. The power level set point can be user-defined. As explained later in subsection 6.1.2 the conventional generation is subject to user defined ramps ranging from few minutes up to one hour in order to mimic the power variations yielded by net load following dispatching. An example of such fluctuations is shown in figure 6.2.

Load

Load models are assumed to be voltage-dependent, i.e., exponential or ZIP models, and either static or dynamic voltage recovery [123]. The reference power consumption of a load, say p_{load}, is defined as the sum of two components:

$$p_{\text{load}} = p_{\text{det}} + p_{\text{sto}} \ , \tag{6.1}$$

p_{det} varies linearly between used defined values in a given period, e.g. 15 minutes, and represent the aggregated slow changes of power consumption; p_{sto} is a stochastic fluctuation thatm models volatility. p_{sto} is defined as a Gaussian distribution with a given standard deviation σ_{Load}in a given period Δt_i. figure 6.3 shows an example of load profiles.

Wind generation

Wind generators are modelled as doubly-fed induction generators (Type C). The turbine is fed by wind speed time series, which are defined as the sum of two components: wind speed stochastic component $w_{\text{s,sto}} \ [m/s]$ and $w_{\text{s,ramp}} \ [m/s]$ component modelled as linear wind speed ramps with a certain time period. The stochastic component is modelled as a set of Stochastic Differential Equations (SDEs) based on the Ornstein-Uhlenbeck Process [201], also known as mean-reverting process. The equations for the wind speed ω_s can be written as follows:

$$w_s = w_{\text{s,ramp}} + w_{\text{s,sto}} \ , \tag{6.2}$$

$$\dot{w}_{\text{s,sto}} = \alpha(\mu_w - w_{\text{s,sto}}) + b_w(\sigma_w)\xi_w \ , \tag{6.3}$$
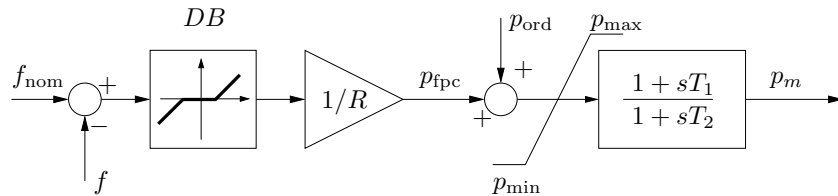
Figure 6.1: simplified model of the primary frequency control and turbine of conventional power plants. Note that all quantities in the figure are in pu.
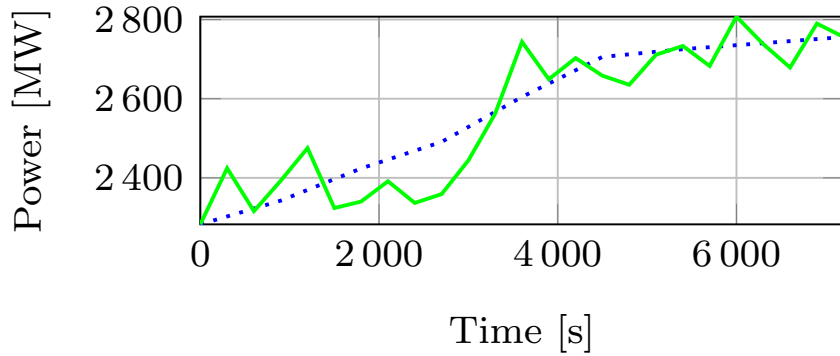
Figure 6.2: example of noise that reproduces slow fluctuations. The blue dotted line represents the net load, while the green solid line represents the net load plus CG fluctuations.
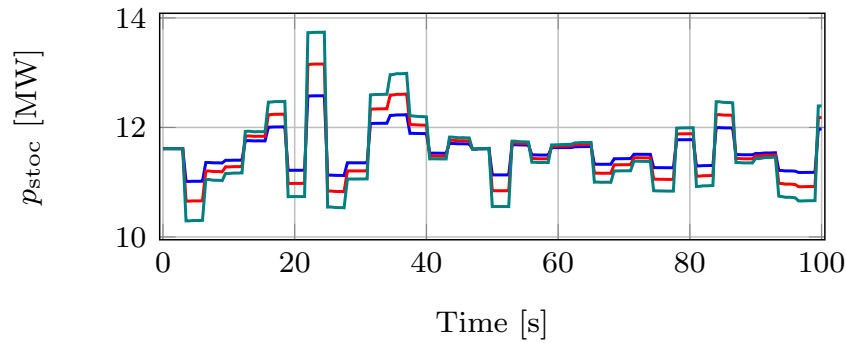
Figure 6.3: examples of p_{sto} profiles using $\Delta t_i = 3$ s and various standard deviations, namely 2.5, 4 and 5.5%.

α is the mean reversion speed that dictates how quickly the $w_{\text{s,sto}}$ tends to the given mean value μ_w (in our case 0). ξ_w is the white noise, formally defined as the time derivative of the Wiener process. This process is controlled by adjusting α and the standard deviation σ_w of the wind stochastic part which affects the b_w component. figure 6.4 shows three sample wind stochastic profiles obtained by changing the σ_w and α parameter.

BESS control strategy

The bess model in this study, is defined in [124] where the power produce by the BESS is transferred into the grid by a current source converter, opportunely controlled by a Proportional integral controller in order to set active and reactive power in less than one seconds in whatever initial BESS or grid condition. The BESS control strategies used are two: one is the usual fixed droop strategy (FDS),

115
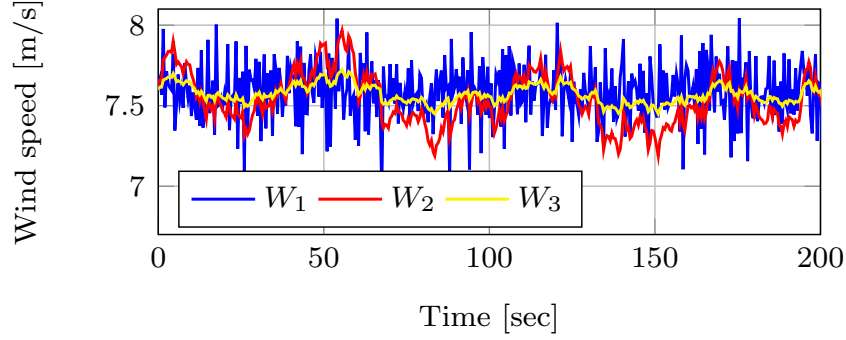
Figure 6.4: $w_{\text{s,sto}}$ profiles. W_1 ($\alpha = 10$, $\sigma_w = 0.17$); W_2 ($\alpha = 0.1$, $\sigma_w = 0.17$); W_3 ($\alpha = 0.1$, $\sigma_w = 0.06$).

while the second is based on a variable droop strategy (VDS), built in order to help SOC management along the provision of PFC.

FD is computed in the same way of the previous chapters. For every typical CG droop R_{CG} value we can compute an equivalent BESS droop R_{BESS} for which the BESS saturate its reserves at the same frequency error level. The formula used is:

$$R_{\text{BESS}} = R_{\text{CG}} \cdot \frac{PFC_{\text{band}}^{\text{CG}}}{PFC_{\text{band}}^{\text{BESS}}} = R_{\text{CG}} \cdot 0.1 \ . \tag{6.4}$$

where in this study in accordance to typical Irish parameters we set $PFC_{\text{band}}^{\text{CG}} = 0.1$ pu(MW) and $PFC_{\text{band}}^{\text{BESS}} = 1$ pu(MW).

During normal operations frequency will change around the nominal frequency value. As seen from previous chapter mean-day and intra-day deviations of frequency can lead the BESS to work over or underfrequency for long period endangering the SOC profile depending on the particular frequency signal. Finally even if frequency were to behave as fast stochastic noise, oscillating around f_{nom}, the internal inefficiencies of the BESS will lead the SOC to be gradually lead to 0. In the Variable Droop Strategy (VDS), the droop is left to vary in a certain range between two extreme values, namely R_{max} and R_{min}. These values are limited by system stability and resources technical considerations. Usually TSOs can request droop values between 2 and 8% [177] to attached resources, typical values are 4 and 5%. The droop can change in order for the BESS to avoid extreme SOC conditions. Depending on instantaneous SOC and frequency error, the droop will vary from the linear curve in order to discharge or charge the BESS accordingly to its needs.

The VD is implemented through the use of a two dimensional lookup table, where the droop value depends on the instantaneous frequency error $\Delta f_e = f_{\text{nom}} - f$

and the State of Charge (SOC). The droop values are divided in five different areas (see figure 6.6): (i) in the red areas the values are close to $R_{\max}$, (ii) in the blue areas the values are close to $R_{\min}$ and (iii) in the green area (which correspond to a column vector) the droop values are all equal to the average droop R_{ave}, at half distance between $R_{\max}$ and $R_{\min}$. The values of the table are therefore constructed symmetrically in such a way that the BESS is expected to avoid excess discharge or charge keeping its SOC close to SOC_{ave} level. As an example, if SOC is high and Δf_e is positive then the BESS discharges with a low droop to reach SOC_{ave}, whereas if Δf_e is negative it charges with a high droop to slow down the SOC increase.

Note that, in order to regulate the SOC the best choice would be to set the droop values equal to $R_{\max}$ in red areas and $R_{\min}$ in blue areas. However, to avoid sudden droop changes and less effective frequency regulation, droop values gradually approach $R_{\max}$ and $R_{\min}$.

A better SOC regulation is achieved by setting the SOC_i values close to SOC_{ave} and taking small values of $\Delta f_{e,j}$. Better SOC management is also expected if the distance between the maximum and minimum droop $R_{\max}$ and $R_{\min}$ is considerable.
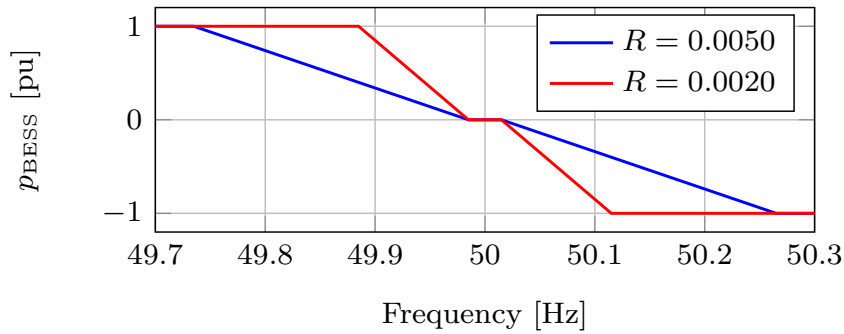
Figure 6.5: power limits example for the VD frequency control.

6.1.2 Fourier transform approach

basic idea

frequency signal can be regarded as a stochastic generic variable. To describe its behaviour classic parameters the mean, the standard deviation and the probability distribution function (PDF) of the signal. While these properties tell us a lot about a signal they cannot provide information on the "velocity" of the signal itself. A simple example to visualize this concept is shown in figure 6.7; the two simple signals have same mean, standard deviation and PDF. A tool to identify this time domain property of the signal is the Discrete Fourier Transform.

117

		Low SOC_i $\longrightarrow$ High SOC_i				
		SOC_1	$\cdots$	SOC_{ave}	$\cdots$	SOC_n
	$\Delta f_{e,1}$	$R_{1,1}$	$\cdots$	R_{ave}	$\cdots$	$R_{n,1}$
	$\vdots$	$\vdots$		$\vdots$		$\vdots$
$\Delta f_{e,j} > 0$	$\Delta f_{e,m}$					
$\Delta f_{e,j} < 0$	$\Delta f_{e,m+1}$	$\vdots$		$\vdots$		$\vdots$
	$\vdots$					
	$\Delta f_{e,2m}$	$R_{1,2m}$	$\cdots$	R_{ave}	$\cdots$	$R_{n,2m}$

Figure 6.6: VD lookup table scheme.
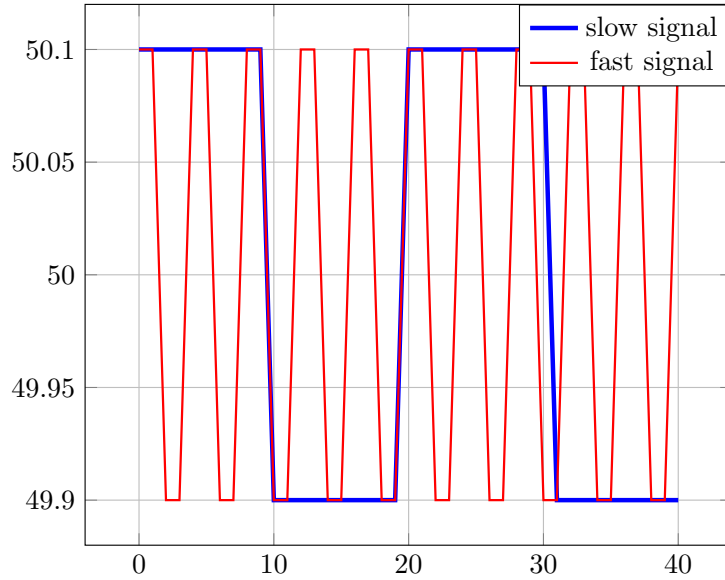
Figure 1: two signals examples

Figure 6.7: two signals with equal mean; σ and PDF.

The DFT converts a finite list of equally-spaced samples into a list of complex coefficients of a finite combination of sinusoids, ordered by their frequencies (also called harmonics). The sampled function from its original time domain is moved to the frequency domain. Given a generic input time series of the form $\chi = [x_1, x_2, \ldots, x_m]$, applying the DFT, after some manipulation we can write:

118

$$x_\nu = \frac{1}{N} \sum_{k=0}^{N-1} A_k \cos(\phi_k + k\omega_0 \nu), \qquad (6.5)$$

with ν that goes from 0 to m. $\omega_0 = {}^{2\pi}/_N$ is called the *fundamental frequency* and N is the number of observations in the equally-spaced input time series χ. if now we multiply and divide ω_0 by the sample frequency f_s in Hz of the data, we can write:

$$x(t) = \frac{1}{N} \sum_{k=0}^{N-1} A_k \cos(\phi_k + \frac{k\omega_0 t}{f_s}), \qquad (6.6)$$

and so at each harmonic k we can associate an angular frequency $\omega = \frac{k\omega_0}{f_s}$ and a corresponding period $T = \frac{2\pi}{\omega} = \frac{Nf_s}{k} = \frac{T_0}{k}$ with T_0 the length in seconds of our time series (see table 6.1 as an example. The phases of the harmonics gives frequency signal a specific time domain shape, but it is enough to reproduce the amplitudes of harmonics to reproduce the variability of the signal. So starting from our real frequency data of the Irish system, we want to reproduce the harmonic amplitudes of the real signal in order to obtain a realistic signal. In particular, the implemented procedure is valid to replicate the harmonic amplitudes of six hours of real frequency signal. Of all the thousands of harmonics computed through the DFT a for a six hour period, only the first 800 are considered, which represent more than the 98% of the variance of the signal for all the 300 days considered (as computed by applying Parseval's Theorem). This is because the irish frequency signal is quite a "slow" signal in which first harmonics with high periods hold much more weight than last harmonics. For example, in figure 6.8 we show the harmonic profiles related to the six hour period going from 6:00 to 12:00, the mean μ and the standard deviation σ of each harmonic for all days considered. All the profiles are similar. The grid frequency signal is therefore quite variable in time domain but much more similar in the harmonic content. Therefore, to reproduce similar harmonic amplitudes of the real data assures that the synthetic signal behaves realistically. Similar results hold for the other three time ranges (00:00-6:00, 12:00-18:00, 18:00-24:00).

Procedure

In order to reproduce real data harmonics, we make use of power stochastic profiles from generation and consumption. These processes are divided in two groups following the taxonomy presented in the literature review, as follows:

- *Fast Stochastic Processes (FSP)*. The stochastic processes of load consumption and wind speed discussed in Section 6.1.1 are used to replicate the events

119

Table 6.1: T_k values for the harmonics

k	T_k [s]
40	180
60	120
80	90
100	72
120	60
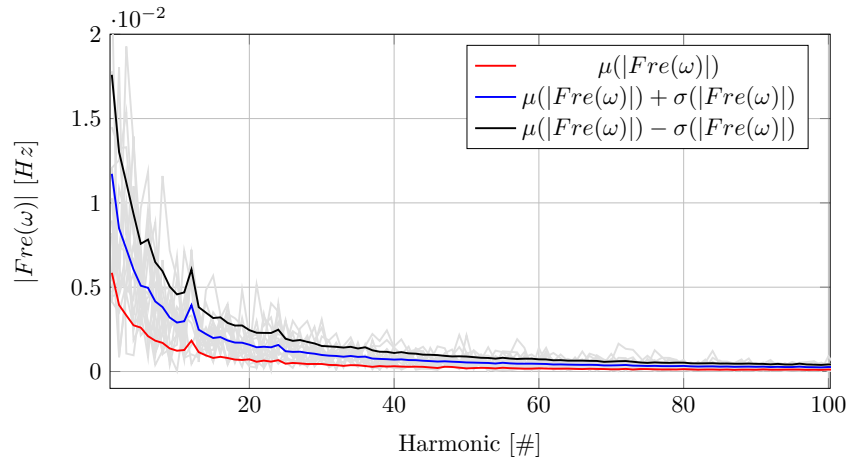
Figure 6.8: harmonics amplitudes related to the six hour period 6:00-12:00.

that cause stochastic frequency fluctuations in the grid (typically with period lower than 2 minutes).

- *Slow Stochastic Processes (SSP)*. Two noises are used to model deterministic frequency deviations: SSP1 which models wind and CG ramps and SSP2 which models the long term mismatch between net load and conventional generation due to the market structure of the system. SSP1 are noises up to 10 minutes, while SSP2 are up to one hour. We refer to these deviations as slow frequency variations.

To tune the parameters of each component of FSP and SSP, a precise mapping between stochastic processes and excited frequency harmonics is defined and stored in a database. This is obtained by varying the parameters values, simulating the grid and then computing and recording the resulting harmonic amplitude. To separate the effect of each stochastic process, one perturbation at a time is considered, being null all other stochastic processes. The parameters used to variate the stochastic processes are the ones described in Section 6.1.1 and are a

total of 7. The synoptic scheme that illustrates the procedure is shown in figure 6.9.
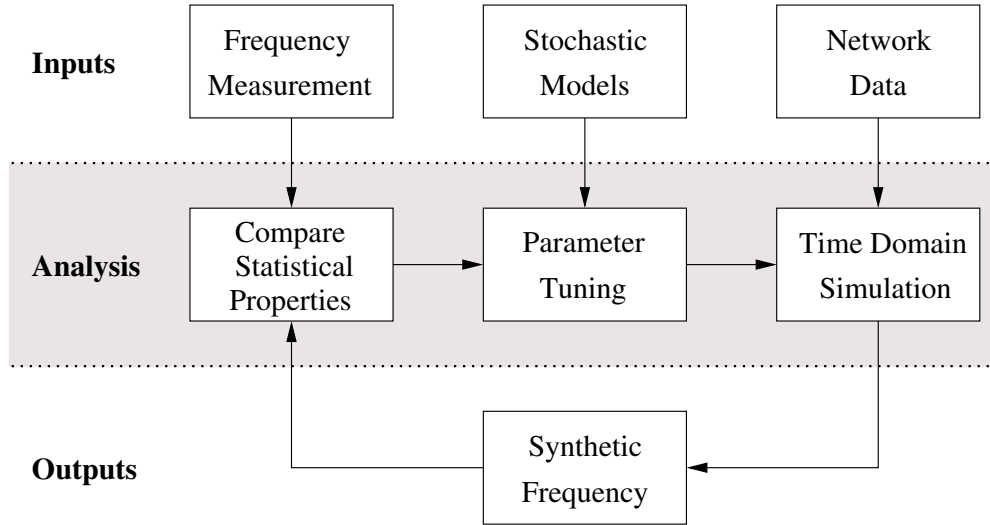
Figure 6.9: procedure to generate realistic scenarios.

In particular, for the load model, a variety of time periods Δt_i (going from 0.5 to 2 seconds) and standard deviations σ_{Load} (going from 2 to 15%) values are considered. σ_w is the only parameter to be changed to vary the stochasticity of the wind component with α fixed to 0.1. For the SSP, time steps and power ramps are chosen from uniform distributions with specified limit values. In the case of SSP1, time steps Δt_{CG} go from 2 to 10 minutes, while for SSP2 the period goes from 13 to 60 minutes. In the case of power variations, requested ramps are both negative or positive, with a maximum $|\Delta p_{\text{max}}|$ which goes from 10 MW up to 70 MW for both SSP noises.

Figures 6.10 and 6.11 show several harmonic profiles obtained from the simulation of FSP and SSP noises. As expected, The former noises excite short period harmonics, while the latter give rise exclusively to long period harmonics.

Finally, the stochastic processes of loads, wind speeds and CG power set points are summed together and the resulting profile, say p_{tot}, is thus identified by a given unique set of parameters that define the four stochastic processes.

From this point, if we could predict final global simulations harmonic values starting from single perturbations values, we could find analytically the combination which give us minimum difference with respect to the mean of real data.

As known DFT holds the important property of linearity. Given two time series $x_1[n]$ and $x_2[n]$ with Fourier complex coefficients $\chi_1[k]$ and $\chi_2[k]$ (where the generic $\chi = a + ib$), where k is the harmonic number. Linearity means that if we have a third temporal sequence $x_3[n] = x_1[n] + x_2[n]$ then $\chi_3[k] = \chi_1[k] + \chi_2[k] =$
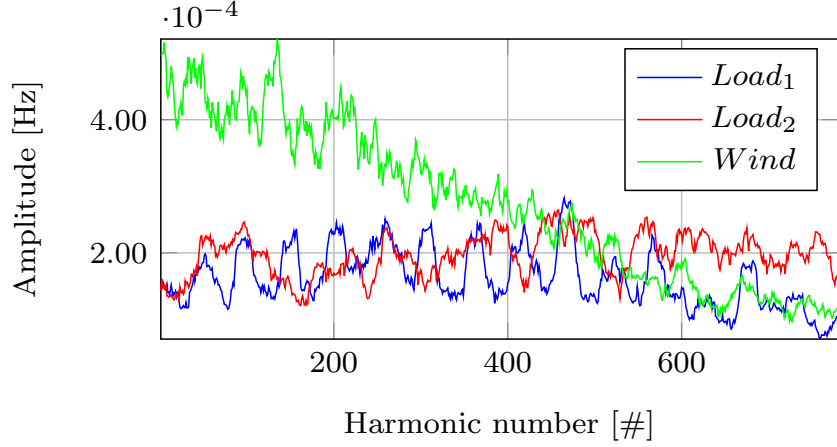
Figure 6.10: examples of harmonic obtained with load and wind stochastic processes. $Load_1$ ($\Delta t_i = 1s$, $\sigma_{\text{Load}} = 2\%$); $Load_2$ ($\Delta t_i = 0.5s$, $\sigma_{\text{Load}} = 2\%$); Wind ($\sigma_w = 3\%$).
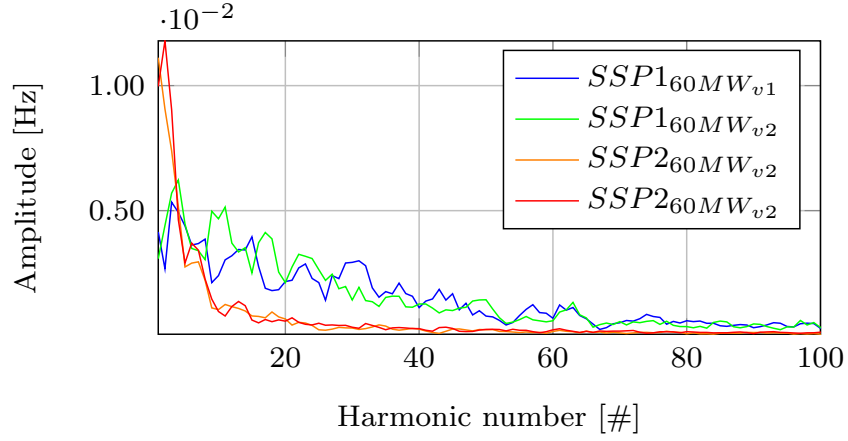
Figure 6.11: examples of harmonic groups obtained with the SSP1 and SSP2 noises. $v1$ and $v2$ refer to different noise profiles with equal $|\Delta p_{\text{max}}|$ value. Δt_{CG} is equal to 3-7 minutes for SSP1 and 13-50 minutes for SSP2.

$\Re(\chi_1) + \Re(\chi_2) + \Im(\chi_1) + \Im(\chi_2)$. In general, for a generic number of signals N we have:

$$|\chi_N[k]| = \sqrt{\left(\sum_{i=1}^{N}|\chi_i[k]|^2\right) + \left(\sum_{\substack{i,j=1 \\ i \neq j}}^{N} \Re(\chi_i)\Re(\chi_j) + \Im(\chi_i)\Im(\chi_j)\right)}, \tag{6.7}$$

In our case, linearity holds only if the frequency signal coming from combining the single simulations can be considered a linear sum of the 4 frequency signals

(generically called $f(t)_i$) coming from the 4 different used noises. This means:

$$\Delta freq_{mix} = \Delta freq_{Load} + \Delta freq_{Wind} + \Delta freq_{\text{SSP1}} + \Delta freq_{\text{SSP2}}, \qquad (6.8)$$

where the generic $\Delta f_i = f(t)_i - 50[Hz]$, in this case the global simulation harmonic groups are a linear combination of the single perturbation harmonics. This equality is strictly true only for the random stochastic variables of the 4 noises: wind velocity v, sun radiation G, load set point P_{Load} and $\Delta P_{OFFSET2}$. In our case, non linearities can arise in the global simulation, due to saturation and dead-bands inside the components control laws and differential equations. The main non linearity in the simulations is the presence of the dead-band in the primary controller, which affects the linearity. However it gives us an hand to predict the final results and how to adjust noises parameters values and presence.

an error ϵ_f is used to compare the frequency harmonics created by the simulated p_{tot} with the real data, which is defined as follows:

$$\epsilon_i = \begin{cases} |(Y\text{sim}_i - (Y\text{real}_i - \text{std}_i))|, & \text{if } Y\text{sim}_i < (Y\text{real}_i - \text{std}_i), \\ (Y\text{sim}_i - (Y\text{real}_i + \text{std}_i)), & \text{if } Y\text{sim}_i > (Y\text{real}_i + \text{std}_i), \\ 0, & \text{if } (Y\text{real}_i - \text{std}_i) < Y\text{sim}_i < (Y\text{real}_i + \text{std}_i) \end{cases} \qquad (6.9)$$

$$\epsilon_f = \frac{\sum_{i=1}^{N_{\text{harm}}} \epsilon_i}{\sum_{i=1}^{N_{\text{harm}}} Y\text{real}_i}, \qquad (6.10)$$

where ϵ_i is the error at the harmonic i; $Y\text{sim}_i$ is the value of the simulated frequency data at the harmonic i; $Y\text{real}_i$ is the mean of all real data at the harmonic i; std_i is the standard deviation of the real frequency data at the harmonic i; N_{harm} is the number of harmonic used.

If this error falls within the desired tolerance, the procedure ends, otherwise relevant noise parameters are increased or decreased according to their impact on the signal harmonics. In such a way the procedure creates a scenario in which frequency does not emulate a specific real day data, but it tries to recover the average variability of real measurements. The synoptic scheme that illustrates the procedure is shown in figure 6.9.

6.2 Case Study

6.2.1 Indexes and Software used

This section describes a variety of indexes that allow evaluating the impact of stochastic processes and the effectiveness of the PFC provided by BESSs and CG.

Impact of the stochastic processes on the system dynamic response

To quantify the contribution of each stochastic process to the overall frequency fluctuations, we consider the sum variance law of the frequency signal which defines the variance of a signal composed by N stochastic independent variables as:

$$\sigma^2_{\text{TOT}} = \sum_{i=1}^{N} \sigma_i^2 \ . \tag{6.11}$$

To compare the impact of each process, it is convenient to consider a normalized variance per process, namely:

$$\sigma^2_{i,\text{pu}} = \frac{\sigma_i^2}{\sigma^2_{\text{TOT}}} \ , \tag{6.12}$$

in such a way, from Equ. (6.11), we can write:

$$1 = \sum_{i=1}^{N} \sigma^2_{i,\text{pu}} \ . \tag{6.13}$$

Impact of BESSs on frequency fluctuations

This index provides a measure of the relative improvement to the dynamics response due to the BESSs. It is defined as:

$$h_{\text{B}} = 1 - \frac{\sigma_{\text{B}}}{\sigma_o} \ , \tag{6.14}$$

where σ_{B} is the standard deviation of the frequency of the system with inclusion of BESSs and σ_o is the standard deviation of the frequency for the same scenario but without BESSs.

Effectiveness of the PFC

This novel proposed index evaluates the effectiveness of the frequency control provided by any resource included in the system. Considering a resource k, the index is defined as:

$$e_k = \frac{E_k^+ + \left| E_k^- \right| - (E_{o,k}^+ + \left| E_{o,k}^- \right|)}{E_k^{\text{ref}}} \ , \tag{6.15}$$

where

$$E_k^{\text{ref}} = \int_o^T \frac{P_{\text{nom,k}}}{R_k(r)} \left| \Delta f(r) \right| dr \ . \tag{6.16}$$

R_k [pu] is the droop of the resource which, for the BESS regulated with VD, is a time-dependent quantity, $P_{\text{nom,k}}$ [MW] is the nominal power of the resource and

$|\Delta f(r)|$ [Hz] is the frequency error including the deadband. E_k^{ref} represents the integral of the exact real-time power profile requested by the PFC service in a given period T, E_k^{+} represents the actual energy produced by the resources for $\Delta f > 0$, whereas E_k^{-} is the energy produced for $\Delta f < 0$ in the same period T. The condition $E_k^{+} + E_k^{-} < E_k^{\text{ref}}$ generally holds as E_k^{+} and E_k^{-} account for the delays of the primary frequency control dynamics. $E_{o,k}^{+}$ and $\left|E_{o,k}^{-}\right|$ represent the energy produced for $|\Delta f| < db$ where db is the deadband of the controller. These energies work against the PFC requirements and thus reduce the effectiveness of the frequency control.

According to the above definition, $e_k = 0$ if the resource does not participate to PFC, $e_k \ll 1$ if the resource is slow and not able to follow the PFC reference signal and $e_k = 1$ for an ideal frequency control with instantaneous time response.

Table 6.2: Main elements of the transmission system used

Network	#	Loads and Power Plants	#
AC Power Lines	796	Loads	346
Bus	1479	Conventional Generators	22
Transformers	1055	Wind power plants	472

Table 6.3: Parameters of primary and secondary frequency control

Primary Control	Reserve Band [MW]	Reserved [%]	Droop [%]	Deadband [mHz]
S1	421	10	5	15
S2 & S3	302	10	5	15

Table 6.4: Parameters of the turbine governors of conventional generators

Time Constant	Steam	Hydro	Gas
T_1 [s]	10	2.5	0.5
T_2 [s]	3	0	0

This case study discusses the performance of the BESS PFC and its impact on various scenarios based on the procedure discussed before. With this aim, we make use of the Irish transmission system [51]. Table 6.2 in the appendix summarizes the main elements of the grid. The CG active installed capacity in S1 is 4347 MW

Table 6.5: Stochastic noises parameters values used to create the scenarios

Scenario #	Load		Wind	SSP1		SSP2	
	Δt_i [s]	σ_{Load} [%]	σ_w [%]	Δt_{CG} [min]	$\Delta p_{\max}$ [MW]	Δt_{CG} [min]	$\Delta p_{\max}$ [MW]
S1 (6:00-12:00)	0.5	2.75	2.5	3-6	33	13-50	50
S1 (12:00-18:00)	0.5	3	5	4-7	38	15-50	47.5
S2 (6:00-18:00)	0.5	8.5	12.5	3.5-6.5	39	14-50	22.5
S3 (6:00-18:00)	0.5	16	25	4-7	20	14-50	10

while wind active installed capacity is 2123 MW. In S2 and S3 CG capacity is decreased by 25%.

All simulations are solved using Dome [122, 96], a Python and C-software based tool which models a large scale power systems as a set of hybrid stochastic differential-algebraic equations (SDAEs) of the form:

$$
\begin{aligned}
\dot{\mathbf{x}} &= \mathbf{f}(\mathbf{x}, \mathbf{y}, \mathbf{u}, \mathbf{z}, \dot{\boldsymbol{\eta}}) \\
0 &= \mathbf{g}(\mathbf{x}, \mathbf{y}, \mathbf{u}, \mathbf{z}, \boldsymbol{\eta}) \\
\mathbf{j} &= \mathbf{a}(\mathbf{x}, \mathbf{y}, \eta) + \mathbf{b}(\mathbf{x}, \mathbf{y}, \boldsymbol{\eta})\boldsymbol{\xi}
\end{aligned}
\tag{6.17}
$$

where $\mathbf{f}$ are the differential equations; $\mathbf{x}$ are the state variables, e.g. generator rotor speeds; $\mathbf{y}$ are the algebraic variables, e.g. bus voltages; $\mathbf{u}$ are the inputs such as the power set points; $\mathbf{z}$ are discrete variables, e.g. protection or machine ON/OFF tags; $\boldsymbol{\eta}$ represent stochastic perturbations, e.g. wind speed variations and load stochasticity, which are modeled as shown in previous paragraphs ; $\mathbf{a}$ and $\mathbf{b}$ represent the drift and diffusion of the stochastic differential equations (SDEs), respectively; $\boldsymbol{\xi}$ represent the white noise vector. Different numerical integrations methods can be used to solve the system.

Besides the model represented in the previous sections, the SGs are modelled as a 6-th order machine model and posses automatic voltage regulators and power system stabilizers; wind power plants are modelled by aggregated models, which implement a 5-th order Doubly-Fed Induction Generator (DFIG) with voltage, pitch angle and MPPT controllers.

The grid topology consists of nodes, lines and transformers connecting the various elements of the grid (see table 6.2 for a brief recap on the main elements of the grid). For every node of the grid we can evaluate voltage and current values in the *dq* frame of reference. In this work we are interested in the grid frequency value which has been identified with the frequency of a stable node of the grid (negligible differences between different points of the grid can arise).

6.2.2 Scenarios construction results

Three scenarios, S1, S2 and S3, are considered and the report of the static and dynamic parameters of the CG PFC is presented in Table 6.2 6.3 6.4.
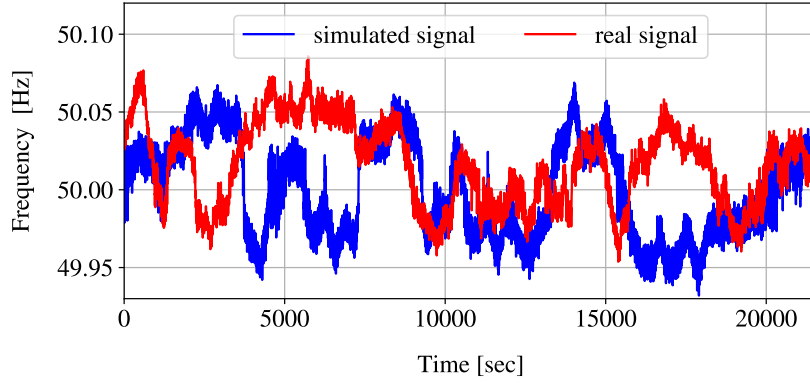
Figure 6.12: comparison between real and simulated (S1) frequency.
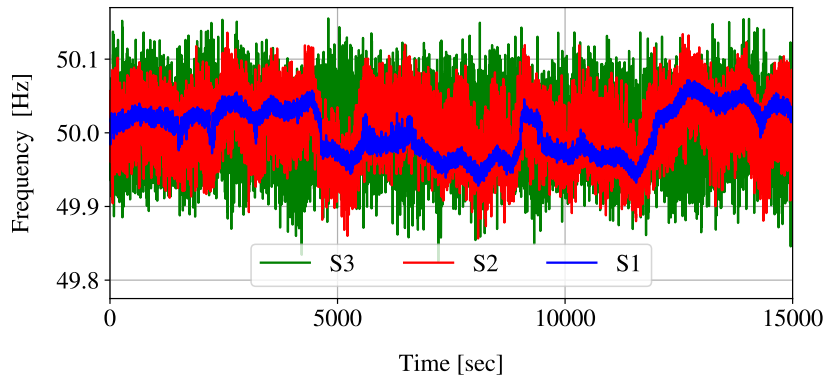
Figure 6.13: frequency profiles examples for the three considered scenarios.

The time horizon of the three scenarios is 12 hours, from 6:00 to 18:00. Load and wind linear slow power profiles are defined based on real-world data obtained by the Irish TSO Eirgrid, while the mismatch from the net load comes from the application of the 4 noises presented in section 6.1.2.

Each scenario is first simulated without the BESSs. S1 represents the scenario that reproduces the measurement data obtained in the lab. S2 and S3 include higher level of noises and decreasing inertia levels, which lead to greater and faster frequency fluctuations. In particular, in S2 we increase the FSP noises and decrease the SSP2 noise, while in S3 the SSP noises are reduced almost to zero and FSP noises are highly increased.

127
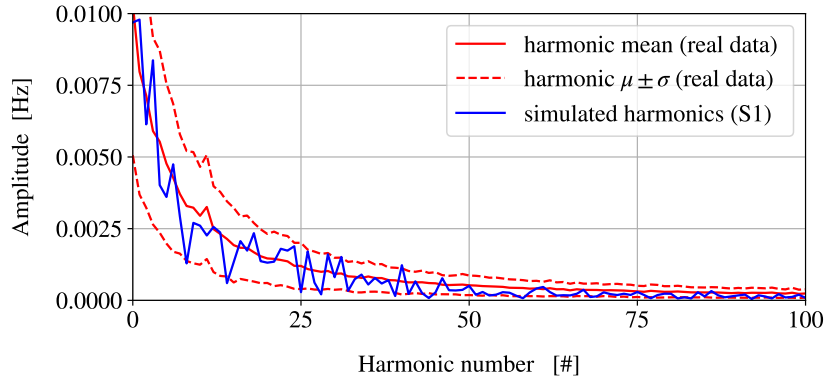
Figure 6.14: harmonic comparison between simulated and real data for the scenario S1, period 12:00 - 18:00.

One profile of scenario S1 and a real frequency time series are shown in figure 6.12. As expected, the synthetic frequency signal retains a similar variability with respect to the real data. Sample frequency fluctuations of the three scenarios are shown in figure 6.13. Table 6.6 summarizes the standard deviation of the frequency of the system σ_f, the normalized variances $\sigma_{i,\mathrm{pu}}^2$ of the four stochastic components and the two S1 errors ϵ_f evaluated by applying Equ. (6.10). In S1 (real-world scenario) the slow noises (SSP) represent almost 90% of the grid deviations with more than half coming from SSP2 noises. In S2 and S3, SSP2 noise goes towards zero. The noises parameters which were used to create the scenarios can be seen in Table 6.5. Note that in both this table and table 6.6 values of S2 ans S3 were computed as the average between the two six hours time periods.

In figure 6.8 the harmonics of real data and S1 scenario are compared and as expected from the definition of error ϵ_f, the simulated profile is well bounded by the real data harmonics standard deviation. Moreover the mean of the signal in the scenarios is set in accordance with the mean of the 330 real days. For this reason, frequency signal is slightly under 50 Hz for the first 6 hours and over 50 Hz for the period from 12:00 to 18:00. These frequency mean offsets are very important in order to capture day frequency dynamics which affect the BESS SOC profiles.

6.2.3   BESS frequency control

The simulations that include BESSs are divided in two groups: the first considers exclusively the dynamic behaviour of FD, the second compares FD and VD control strategies. For the first group, the three scenarios are simulated by considering four BESS capacities (100, 200, 300 and 400 MW) and three droop values ($R_{BESS} = 0.005, 0.004, 0.0035$). In the second group, S1 and S2 scenarios are

Table 6.6: normalized variances and frequency standard deviations for the three stochastic scenarios.

Scenario #	σ_f [Hz]	μ_f [Hz]	$\sigma_{i,\text{pu}}^2$				ϵ_f [pu]
			Load	$Wind_{\text{sto}}$	SSP_1	SSP_2	
S1 (6:00-12:00)	0.0308	49.9996	0.09	0.02	0.34	0.55	0.032
S1 (12:00-18:00)	0.0302	50.0038	0.075	0.07	0.34	0.515	0.021
S2 (6:00-18:00)	0.0359	50.0028	0.22	0.12	0.37	0.29	-
S3 (6:00-18:00)	0.0431	50.0021	0.55	0.24	0.16	0.05	-

simulated, with 100, 200 and 300 MW of BESSs characterized by two efficiencies ($\eta_{\text{BESS}} = 0.8, 0.9$) and by a power-energy ratio equal to 0.4.

With regard to the PFC, two FD droops (equal to 0.004 and 0.0035) are compared respectively to two VD strategies which are shown in Table 6.7: (i) "hard mode", for which the droop varies in the range $R \in [0.002, 0.005]$, and (ii) "soft mode", for which the droop varies in the range Rin$[0.003, 0.005]$. The tables have been built following the process described in subsection 6.1.1 considering 4 SOC_i and 4 $\Delta f_e, j$ points. For both modes $SOC_{\text{ave}} = 60\%$, while R_{ave} is equal to 0.004 in the hard mode and 0.0035 in the soft mode which are the values used by the FD strategy. Both setups, especially hard mode, make the droop to vary significantly during the simulations in order to regulate the SOC as well as possible.

Table 6.7: lookup tables for VD "hard" and "soft" control modes. Note that droop is here expressed in % and not in pu to improve readability of values.

Hard mode					**Soft mode**				
Δf_e	SOC range				Δf_e	SOC range			
[Hz]	50%	55%	60%	70%	[Hz]	45%	50%	60%	75%
0.03	0.20	0.20	0.35	0.50	0.040	0.3	0.35	0.40	0.50
0.0175	0.20	0.25	0.35	0.50	0.020	0.35	0.375	0.40	0.50
-0.0175	0.50	0.45	0.35	0.20	-0.020	0.45	0.425	0.40	0.30
-0.03	0.50	0.50	0.35	0.20	-0.040	0.50	0.45	0.40	0.30

FD control strategy

figure 6.15 shows the index h_{B} for the various scenarios. The improvement of the frequency signal is more relevant for both scenarios S2 and S3 (see figure 6.16 for an example) than for S1. This has to be expected as, in S1, frequency has

129
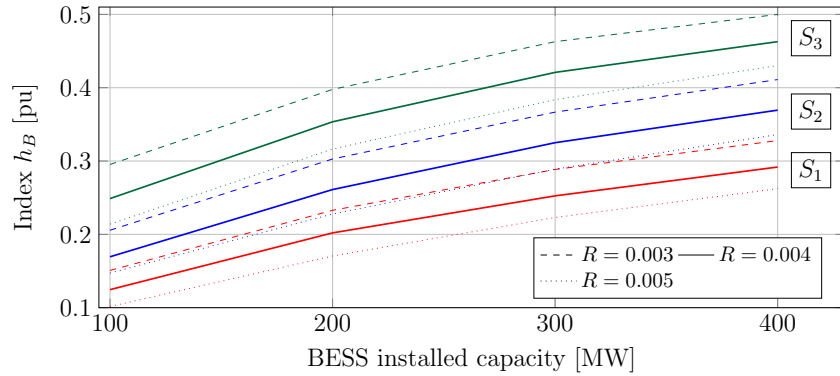
Figure 6.15: index h_{B} for the FD control strategy of the BESSs. The droop values is indicated by R. Different colors represents different scenarios.
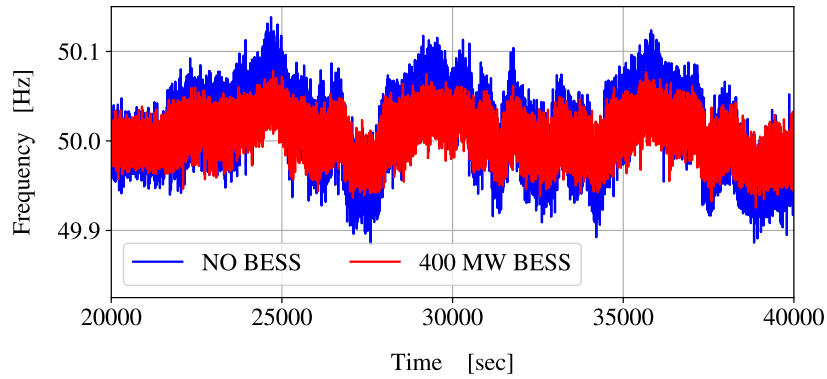
Figure 6.16: frequency profiles for scenario S2 without BESS and with BESS.

smaller standard deviation closer to the deadband value, which limits the impact of BESSs. For similar reasons, as shown figure 6.15, the h_{B} index increments tend to decrease as BESS capacity increases.

Table 6.8 shows the index e_k for the available resources that provide PFC. In the table, only one value for each scenario and each resource is shown, as e_k is not greatly affected by the BESS installed capacity and its droop value. Two parameters mostly influence the index e_k:

- *The time response of the resource.* A fast time response of the resource improves its frequency regulation. As an example figure 6.17 shows the active power outputs of the BESS and of a conventional steam power plant. The blu dotted line is the reference PFC signal to be followed by the two resources. The fast response of the BESS leads to an almost perfect tracking of the reference signal.

130

Table 6.8: index e_k for various scenarios and energy resources.

Device	S1	S2	S3
BESS	0.99	0.99	0.97
Steam	0.92	0.78	0.31
Hydro	0.94	0.84	0.44
Gas	0.99	0.98	0.89

- *The harmonic content of the frequency fluctuations.* The index e_k of the conventional power plants is higher in scenarios S1 and S2 than S3 in that the frequency signal is slower and easier to follow even for slower resources.
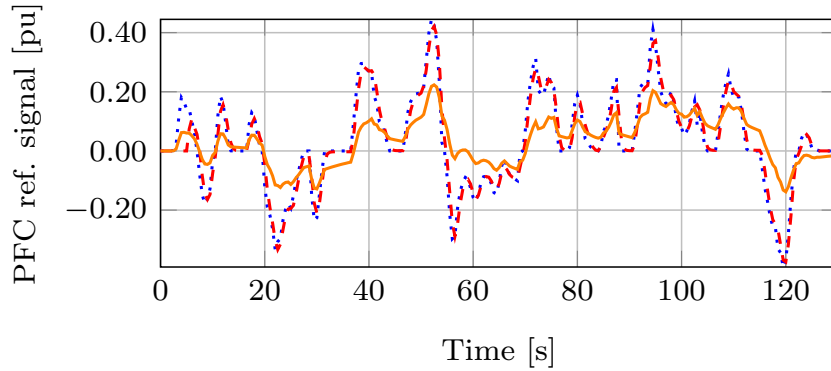
Figure 6.17: power production of the BESS (dashed red line) and of CG (solid orange line) following a PFC reference signal (dotted blue line).

The result of the simulations is that in scenario S1, which represents the current situation, the performance of the BESSs is comparable with that of conventional power plants. In S2 and S3, which are characterized by faster frequency fluctuations, the regulation provided by BESSs have much more value than CG PFC service.

VD control strategy

In order to asses the impact of VD strategies, several standard statistical properties of the frequency signal are used. Note that only the results with $\eta_{\text{BESS}} = 0.8$ are shown. The cases with $\eta_{\text{BESS}} = 0.9$ provide similar results and thus are here neglected. In the case of VD strategies, the standard deviation of the frequency signal has a negligible difference in the order of 10^{-4} Hz with respect to the FD strategies. In figure 6.18 we can visualize the frequency signal of selected simulations which show great similarity. As shown in Table 6.9, VD strategies generally
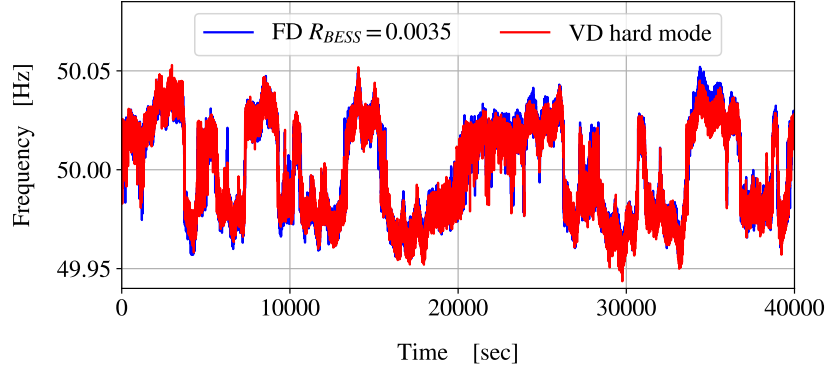
Figure 6.18: frequency profiles examples with FD and VD strategy ($\eta_{\mathrm{BESS}} = 0.8$) adopted and 200 MW BESS installed.

Table 6.9: relevant parameters of simulations related to the case $\eta_{\mathrm{BESS}} = 0.8$.

Sim.	Par.	VD_{hard}	$FD_{0.35}$	VD_{soft}	$FD_{0.4}$
$S1_{200\mathrm{MW}}$	$\sigma(fre)$	0.0239	0.02393	0.02444	0.02443
	Skew(fre)	-0.1004	-0.0662	-0.0821	-0.722
	$\mu(SOC)$	0.57	0.58	0.56	0.54
$S1_{300\mathrm{MW}}$	$\sigma(fre)$	0.0223	0.02235	0.02285	0.02286
	Skew	-0.143	-0.118	-0.122	-0.12
	$\mu(SOC)$	0.59	0.61	0.59	0.62
$S2_{200\mathrm{MW}}$	$\sigma(fre)$	0.02595	0.02581	0.02655	0.02648
	Skew	0.143	0.066	0.0938	0.0722
	$\mu(SOC)$	0.63	0.70	0.63	0.69
$S2_{300\mathrm{MW}}$	$\sigma(fre)$	0.02349	0.02342	0.02418	0.02416
	Skew	0.142	0.04	0.131	0.042
	$\mu(SOC)$	0.63	0.66	0.63	0.64

enlarge skewness, creating small asymmetries in the frequency signal. If the initial skewness is negative, the VD strategies will further lower this value, while the opposite is true in case the initial skewness is positive. The difference is bigger in the case of hard mode with respect to soft mode and when BESS installed capacity is higher, except for the case $S1_{300\mathrm{MW}}$. In general two compensating effects happen as BESS capacity increases: on one hand, as SOC diverges from the nominal SOC_{ave} value, the droop fluctuates around R_{ave}. This dynamic is responsible for creating the asymmetries in the frequency signal and increases its impact as more BESSs are used. On the other hand, the big BESS capacity makes the frequency

less variable and closer to the deadband limiting the impact of VD strategies.

For these reasons the differences in the frequency signal remain small in the order of 10^{-1} [pu] and the values of skewness are still quite close to 0 and therefore do not represent a big distortion. Finally, in both scenarios, the kurtosis slightly increase in the order of 10^{-3} [pu].

It is therefore clear that little difference exist between VD and FD strategies even if an important BESS capacity is installed. Both strategies are enough to guarantee stability in the grid during normal dynamic conditions.
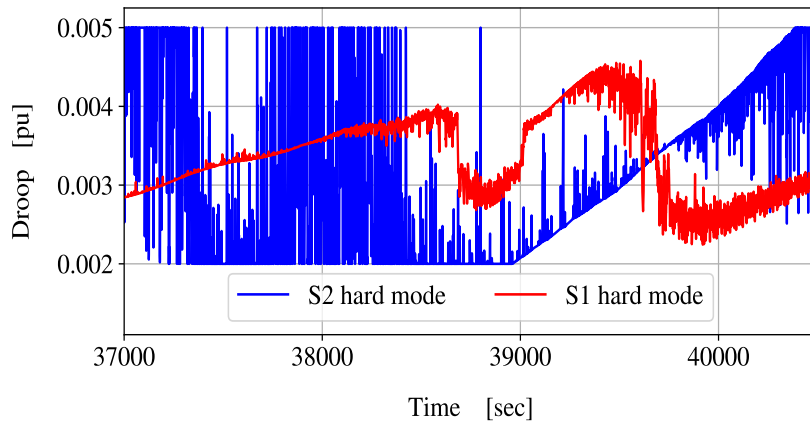
Figure 6.19: example of droop profiles in S2 with 100 MW of BESS installed and $\eta_{\text{BESS}} = 0.8$.
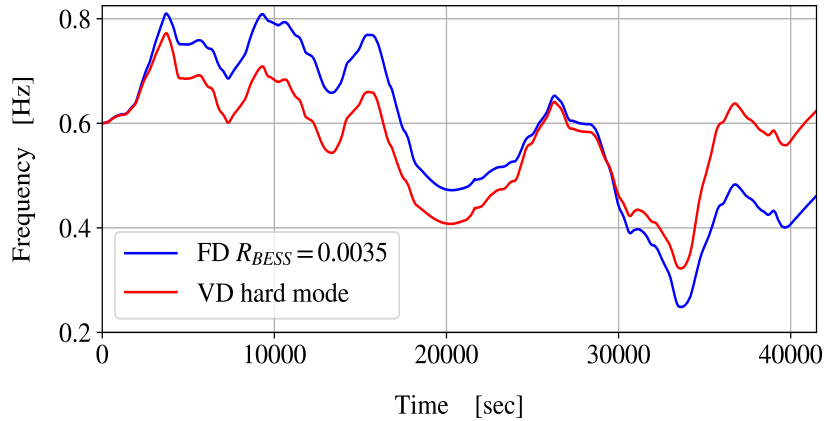
Figure 6.20: example of SOC profiles in the S1 scenario with 100 MW of BESS installed.
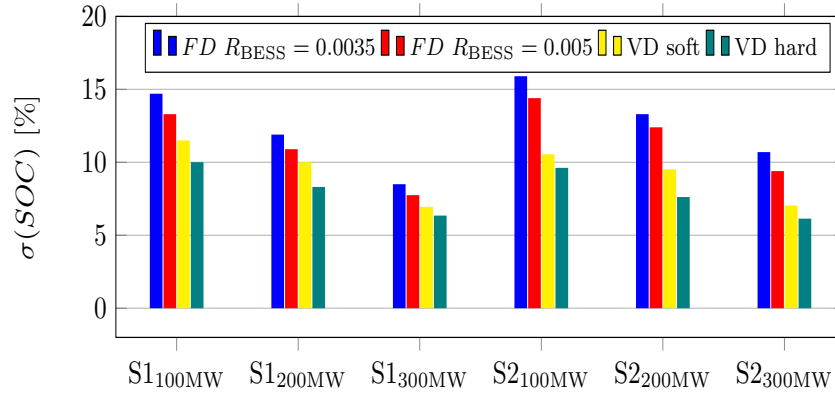
Figure 6.21: index $\sigma(SOC)$ for various BESS control strategies and capacities with $\eta_{\text{BESS}} = 0.8$.

For what concerns SOC, in Table 6.9 the mean SOC value $\mu(SOC)$ of several simulations is shown. VD strategies, especially for S2, are able to keep the SOC statistically closer to SOC_{ave} with respect to FD strategies. figure 6.20 shows as an example two profiles related to the different strategies. As can be seen, the VD strategy is not able to perfectly regulate the SOC, but manages to decrease its standard deviation with respect to the FD case avoiding too high or too low charge levels. figure 6.21 shows the SOC standard deviation for all the scenarios studied in the case $\eta_{BESS} = 0.8$. The decrease in standard deviation is slightly better in S2 where the alternation between over and under-frequency periods is faster, therefore the VD strategy changes values often (as shown in figure 6.19), reaching better performances. The possibility of using a bigger difference between $R_{\max}$ and $R_{\min}$ can further improve the SOC dynamics (e.g. $R_{\min} = 0.002$ and $R_{\max} = 0.008$), but its effect on the frequency must be carefully evaluated.

Conclusion

In this chapter the Irish grid is simulated in a electric grid dynamic simulator where the SFRM model approach of the previous chapter could not be used. In order to reproduce a realistic frequency signal, the various grid noises were designed in such a way that the harmonic content of the signal is similar to the one of the real data for each six hour period considered. Under normal slow noises their performance is just slightly better than SGs power plants, while they prove much more efficient in the case of fast frequency deviations. Finally the impact of Variable Droop strategy on the BESS SoC helps it retain its charge for a longer period of time while having a negligible impact on the frequency signal

Chapter 7

Electric Vehicles Studies

Electric vehicles numbers are steadily increasing in last years. EVs connect into the distribution grid in order to recharge after a road trip. Their presence in the grid is therefore not constant and can cause problems to the local networks. They need to be aggregated for market coordination and service provision. Evaluate their possible impact into the grid performing frequency control is therefore not straightforward: in section 7.1 we present all the elements which have to be taken into account in order to properly quantify the EVs potential presenting a scheme to gather frequency reserves. In section 7.2 and 7.3 we present two case studies developed to deal with two specific aspects of the presented EV framework. These steps can be used as a basis to build all the other elements of the problem.

7.1 Motivation and Framework

A great number of studies deals with the provision of frequency reserves from EVs considering several aspects: for example [202, 80, 90] focus on the EV frequency control strategy impact. Others [42, 79, 181] investigate the economics of EVs providing frequency services by considering at the same time recharge needs and availability of the vehicles. Some studies model the presence of distribution grid constraints due to the energy management of EVs [70, 165], however rarely consider the possibility of performing frequency control. The problem of evaluating EVs frequency reserves impact can be summarized in figure 7.1. The main stakeholders are:

Aggregator. It represents a solution to decrease the expected stocasticity in EV availability. In day ahead and intra-day market, aggregator buys the energy needed for recharging its fleet and then, in real time, it adjusts the power schedule by considering the real-behaviour of EVs. Moreover, it needs to

assure the dispatching of frequency reserves using some form of control (centralized, distributed etc.) in order to dispatch the available EVs from its fleet.

TSO. Depending on system needs, frequency reserves are typically set in advance by TSOs. Participation of resources can be compulsory or managed through the use of weekly or different time frame auctions. Reserves are required to be continuously operating and always available at the contracted nominal quantity.

DSO. It is responsible for the medium and low voltage levels of the grid. In the case of possible grid congestions, it needs to assure the resolution of the problems as fast as possible and for this reason it could impose some restrictions in specific points of the grid.

Not only EVs but also other new resources of the distribution grid (RES sources, smart buildings, water heaters, distributed storage, etc..) could offer new services to the grid being able to regulate their load. A stronger coordination between TSO and DSO should be designed to avoid that new resources destabilize the distribution grid itself. In [72], new TSO-DSO markets models are presented for various ancillary services and congestion management. Frequency control represents a great opportunity for new resources to increase profitability and for the grid regulators to compensate the loss of controllable power generation, increase efficiency of the market and decrease prices, thanks to the high number of additional competitors [166]. An example of such coordination is shown in figure 7.2 and describes a possible market design to offer frequency reserves from resources at the distribution level. In the figure, it is shown the process to qualify the resources over a certain specifiable time range: the lower it is (daily or hourly), the better it is for market efficiency. The new resources offer their power band for frequency control [1], each one possessing a certain level of price elasticity: for example, a smart home management system could decide to sacrifice some comfort or discharge the home battery in order to have economic benefits. Other resources, such as EV stations, have some level of flexibility as well. At the medium and high voltage level, the various bids coming from all the distribution grids are summed and the DSO, as a pre-qualification process, could already decide to decrease or discard some of the offered resources due to grid security issues. The market is cleared and the accepted bids are communicated back at the MV and LV level, before a new market period starts. In this period, the winning resources will provide frequency control.

---

[1]talking about primary or secondary does not create much differences in the market scheme, but in the offered prices.

As described in previous chapters, the worst situation happens when the whole power band is requested due to a big frequency deviation: in this case local problems to the distribution networks could emerge such as overvoltages, overcurrents, branch congestions, etc.. Therefore DSO, after having analyzed the current state of the grid, could deploy real time safety actions such as reactive compensation, re-dispatching or prohibit EVs performing PFC from certain positions.

To study the impact of EVs resources performing PFC, a series of intermediate steps are needed:

Electric vehicles spatio-temporal description. The starting point to evaluate EVs behaviour in large scale scenarios, is to give a realistic description of their energy requirements taking also into account the spatial spread of vehicles. Sizes of chargers are increasing in the course of the years (nowadays averaging around 22 KW) and therefore can represent a real threat for distribution systems. In section 7.2 an agent based modelling is constructed in order to simulate the behaviour of EVs making use of a simulated road and electric network and the impact on the grid using dumb charging is evaluated.

Smart charging algorithm. An aggregator of EVs have to optimize the cost of buying energy from the day ahead market considering the forecast of EVs needs and, in real time, respect the purchased profile in order to avoid any unbalance. Different optimization frameworks exist in literature, in section 7.3 a priority based approach is built. Moreover, a specific strategy to take into account the SOC losses and power band for frequency control needs to be designed.

DSO real time control. In order to keep the distribution grid stable and secure, the DSO should check the existence of bottlenecks in the grid in case the whole power band for frequency control is activated in up or down direction. If DSO does not have a complete estimation of its own grid, it could make use of probabilistic load flow to find out problematic points. Different control actions can be taken to assure the distribution grid stability: changing the networks layout, deploy reactive power and, in extreme cases, the internal re-dispatch or stop in the frequency control provision of EVs could be issued. In this last case, the aggregator should provide frequency reserves using different EVs.

The first and the second step of the previous list are implemented in the following sections. Next steps are described partly in the previous list and in the subsection 7.4.2

137
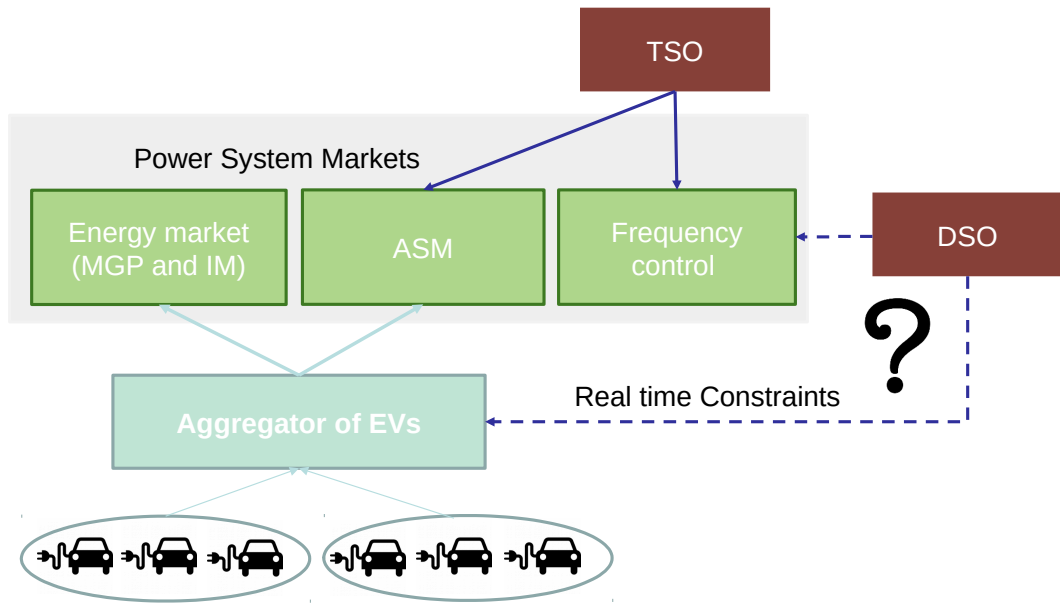
Figure 7.1: a scheme of the EVs interaction and stakeholders in the power systems.
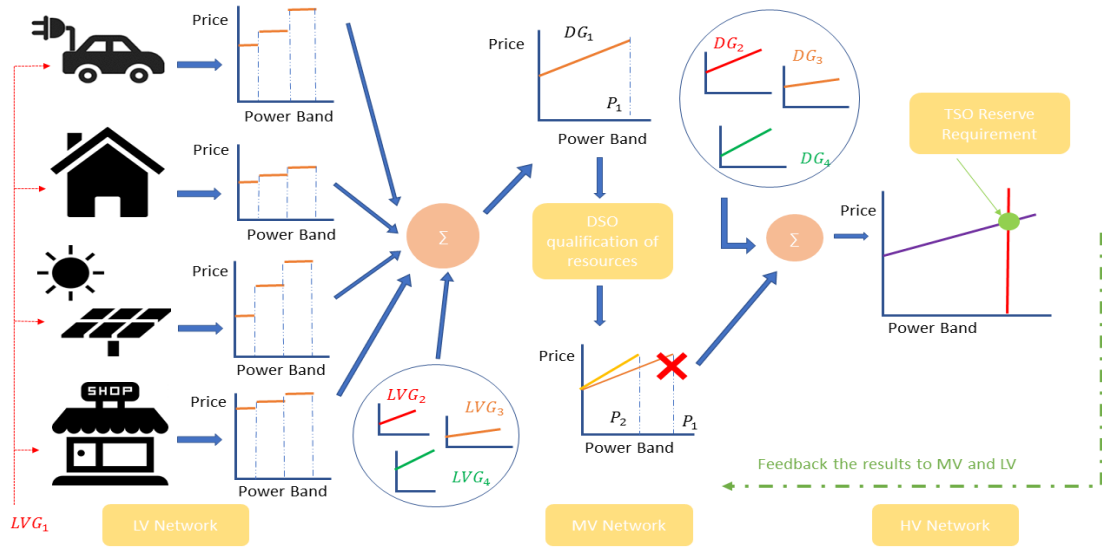
Figure 7.2: an example of DSO-TSO coordination for frequency control resources gathering.

7.2 First Application: Agent Based Model Approach

Typically real data data and/or probability distributions functions (for example, Gaussian and/or the Lognormal distribution or directly empirical PDF computed from travel diaries) to decide the travel characteristics are used in works such as [42, 6, 204]. This approach is the most common and it is able to reproduce consistent single trips for EV cars, but it cannot model consistent travel schedule for an EVs, neglecting the expected correlations between travels characteristics and day schedules. It is also possible to build several archetypal driving patterns [200] starting from on-field measurements or car diaries. However also in these cases the trips of EVs are fixed and strictly depend on the location and surveys used. In order to reach a better description activity based models are used where the EVs schedule is a consequence of the actions performed by people using cars. A certain schedule for every EV users is constructed, based on less or more complex set of rules and relations [108, 117]. In pure transport studies [77, 81] activities schedules creation is a complex task based on a socio-demographic description of the population and on a stepwise approach that determines activities based on different time decisions levels. In this way, every driver makes realistic decisions for his/her schedule.

In order to built a realistic activity based models, in which EVs users activities can change and potentially be influenced by other users, we decided to model both the electric and traffic model grid and use an agent based model framework [111]. Notably only in one paper a tool with such a philosophy was developed ([196]). However this tool was more concentrated in policy decision and medium-long term horizon (days to week) more than on daily distribution system operations. Road and recharge points also assimilated in few equivalent points. Typically an agent based model is characterized by 5 typologies of components:

Agents a self-contained program capable of controlling the decision making of each individual, and able to influence or be influenced by the environment.

Environment It represents the space and dimensions where agents move and interact.

Object populates the environment along with agents.

Relationship links agents and objects.

Operations allows agents to perceive and transform objects.
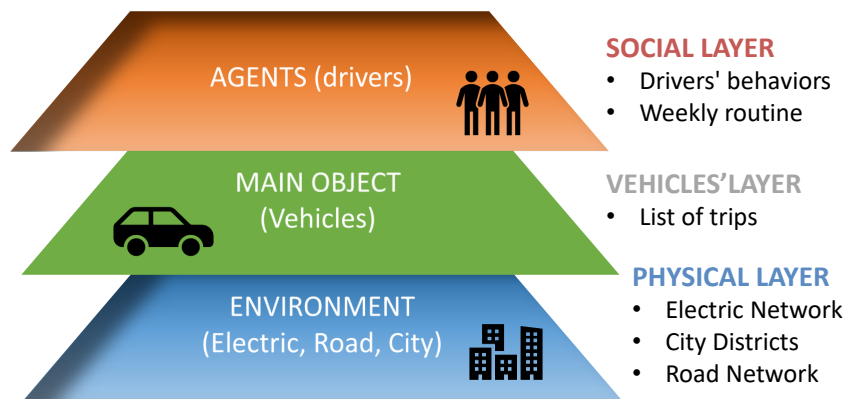
Figure 7.3: layer structure of the model.
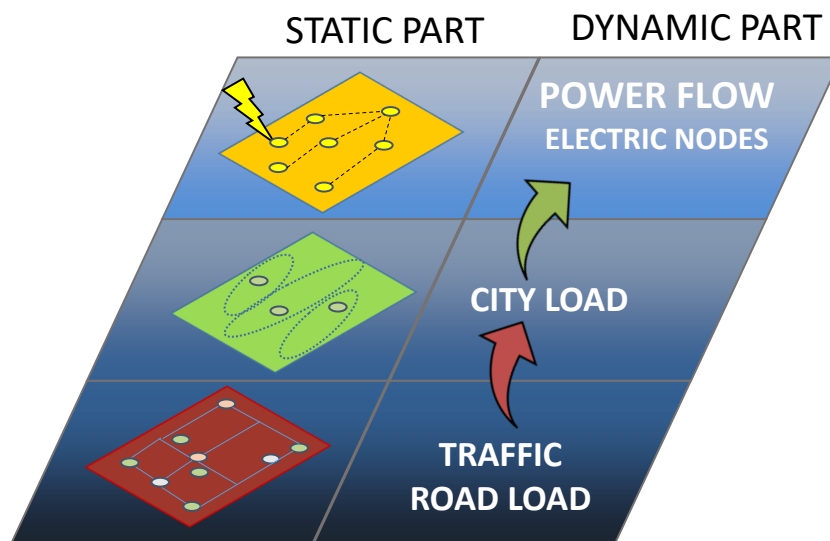
Figure 7.4: environment layers details.

7.2.1 Layers modelling

A three layers framework (see figure 7.3) was developed considering the presence of a time loop routine to keep consistency in the time line. The main agent is the drivers which makes use of a car, which can be electric or normal. The agent is characterized by a series of consistent set of parameters which defines its activity in space and in time. During travels, traffic is created when more agents need to reach the same destination influencing the time and energy spent in the travel itself. Finally EVs need to recharged as soon as they reach the destinations, influencing currents and voltages in the distribution network.

The Environments in which agent interact are actually 3: namely, the electrical

network, the road network, and the city structure (see figure 7.4). The networks have a static description in which the topology of the network is represented and a dynamic part which gathers the possible operations and methods agents and objects put in place during the day.

Static part
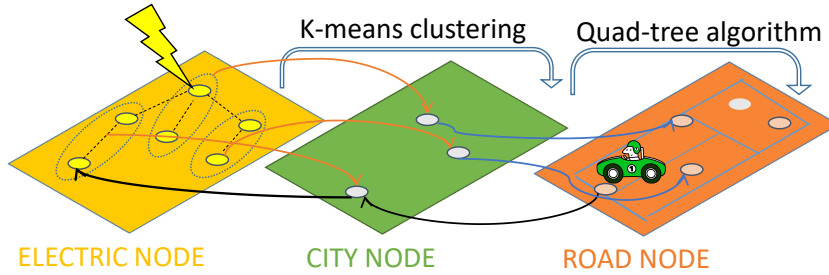
Figure 7.5: main step to create the System environment.
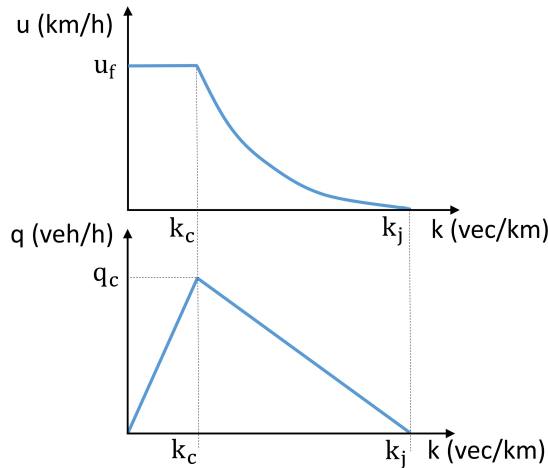
Figure 7.6: parameters referring to the traffic model.

The starting point of our study is the use of two reference distribution system networks as it is really difficult to obtain real electricity distribution grid models, it is quite common to use reference ideal network constructed to guarantee realistic results [66]. The electric grid is composed by electrical nodes and lines characterized by a certain resistance and inductance. Electrical loads are under the nodes of the grid. The nodes characterised by a certain nominal active power $P_{nom}^{(k)}$ and reactive power $Q_{nom}^{(k)}$ which are composed by a sum of residential, commercial, agriculture, industrial type of load. Starting from this description, the city layer is

141

built by using k-means (see figure 7.5) clustering to gather the electrical nodes into a certain number of groups. These new points represent city districts and define the possible interaction of agents. The city layer represents a mid-layer between road network and electric network is compulsory and opens the possibility of more precise sociological and urban descriptions. Finally the road network is obtained starting from the city districts by building a quadratic graph was around the city nodes. An algorithm is implemented such that areas with more city nodes will be surrounded by a bigger number of roads (bigger density of roads), as expected in a typical city area. Every branch is then described by three parameters referring to the traffic (see the top diagram in figure 7.6:

- u_f [km/h]: average travel speed of the vehicle withou traffic (called free mean velocity);

- K_c [veh/km]: minimum vehicle density to make the vehicles starting to decrease velocity due to traffic;

- K_j [veh/km]: road vehicle density that creates road congestion and stops the traffic.

The nodes represent the entry/exit points for the vehicles driven by the agents, and the branches represent the roads of the network.

Dynamic part

The electric grid is solved by means of the Backward-Forward Sweep method every minute for 1 week. The loads comes from typical power profiles of residential, industrial and commercial loads. Voltages and currents are computed and can be compared with permissible values. In fact should remain between 90 and 110 % of nominal value, while current is limited by temperature. In general, for every branch of the grid a maximum temperature can be tolerated by the conductor insulation. The maximum temperature imposes a limit on the maximum current a conductor can withstand, taking into account the ambient temperature, the joule losses, and the heat transfer processes. The city layer does not possess (in the present version) an independent dynamic. It basically serves to construct a consistent road network. The road network is indeed important, being where the interactions of agents (making use of the vehicles objects) work towards the creation of the traffic. The traffic dynamics are modelled following a microscopic traffic pattern method [112] able to trace the vehicle position at every time step. The goal is to compute the instantaneous vehicle density q in every road and subsequently the vector u_i for every vehicle i containing all the average speeds of cars (figure 7.6). With these parameters it is possible to compute the energy consumption of the EV based on

142

an aerodynamic model of the vehicle itself taken from [117]. The traffic method starts from a list of vehicles that enter the road network graph and update the vehicles position and velocity in every road based on the lines defined in figure 7.6. The possibility of vehicles finishing their journey entering a new road before the one-minute time step is also taken into account.

for one week, every agent is characterized by a series of activities. possible ones are: (i) HOME: agent are at home (ii) WORK: agent is at work (iii) LEISURE: the agent is outside home to perform some social or spare time activity. (iv) ER-RAND: the agent is not home for mandatory activity (buying food, pharmacy, bureaucracy, doctor, etc.) (v) OUT: the agent is outside the city/simulated environment (for work, holidays, etc.). (vi) ILL: the agent is ill at home (while in normal conditions should be outside home). The when of these activities depends on the characteristics of each agent. Manifold characteristics define a unique agent:

NODE HOME. It is the city node/district where the agent lives. The assignment of this node is not random, but is obtained by an extraction from the Cumulative Distribution Function (CDF) of residential power P_{res}. So nodes with higher installed residential power have bigger probability to be chosen as HOME of the agent.

NODE WORK. This is composed of a principal node, which is the primary working environment, extracted in the same way as NODE HOME considering the sum of industrial, commercial, tertiary and agricultural powers of city nodes (through a sum on electrical nodes). A second node is extracted to represent a secondary working place which could be used by some agents in some special days.

WORK TYPE. depending on the node where the driver works, the work sector is extracted from the cumulative work power installed. Then, by using real or reasonable statistics, the type of employment is chosen between full time worker, part time worker, and freelance.

SEDENTARINESS. The nodes where agents go to perform non-working actions are actually not fixed, and are extracted trip by trip according to a CDF influenced by three parameters: (a) the distance of the agent from the surrounding nodes; (b) the level of installed commercial power (for ER-RANDS), and the tertiary installed power (for LEISURE activities); (c) the sedentary level of the agent, which is the tendency of performing LEISURE and ERRANDS activities far outside home. A high level of SEDENTARI-NESS means that the agent tends to use the car even to reach near places (from 500 meter to 1.5 km, for shorter paths the agent always goes on foot:

143

for longer paths the agent always uses the car) and it will anyway try to perform activities near home. The sedentary parameter introduces an exponential condition on the previously computed CDF. FAMILY: this binary flag [0, 1] indicates if a person has a family or is single, since this greatly influences agent activities like ERRAND and LEISURE. The activities at this level, using the first 5 parameters, are divided on an hourly basis. To obtain sub-hourly and minute division the parameter ACCURACY and DELAY are used.

EV USER. Every agent is assigned a vehicle object to perform its activities inside the city. The possibilities are two: private non-electric car, or car-sharing EV. In the latter case, this means that the driver does not own an EV, but makes use of whatever electric vehicle is available. The EV car makes uses of an aerodynamic model to convert the average speed velocity of the power into energy consumed by the EV.

Normally the agent will start its journey considering the hour at which it should arrive at destination, subtracting the ideal time of travel (computed without considering the traffic). The true starting time is computed considering other two time steps: (a) a first extraction (ACCURACY) from a normal distribution with expected value of zero and variance 30 minutes to take into account the possible delay/advance of the agent due to the activity starting time differing from an hourly schedule, (b) a second component (DELAY) which add a stochastic delay (positive or negative) due to driver faults.

EVENTS override all the other activities and could last a DAY or a WEEK. In particular ILL or OUT could be extracted and last one day or one week or a weekend (in case of OUT for short holidays).

In order to create an agent's routine, the actions are divided in three categories: fixed actions, semi-aleatory actions and aleatory actions. Depending mainly on the type of WORK and FAMILY status, every driver has a certain type of fixed actions (for example WORK) in predetermined days and hours of the week. Semi-aleatory actions are instead usually LEISURE or ERRAND activities, for each of which there is a fixed number of hours for the agents to fulfil, but the choice of the specific days and time when it is fulfilled depends on random extractions. A typical example could be the agent with family which two or more times a week will take the children to school before going to work. Finally, aleatory actions have to respect some basic constraints (as maximum number of times and hours) and depend on agent characteristics, but are quite random in nature and give the agent a more realistic routine. An example to explain the semi-aleatory activities is shown in table 7.1. These activities provide a list of vehicle trips to perform with
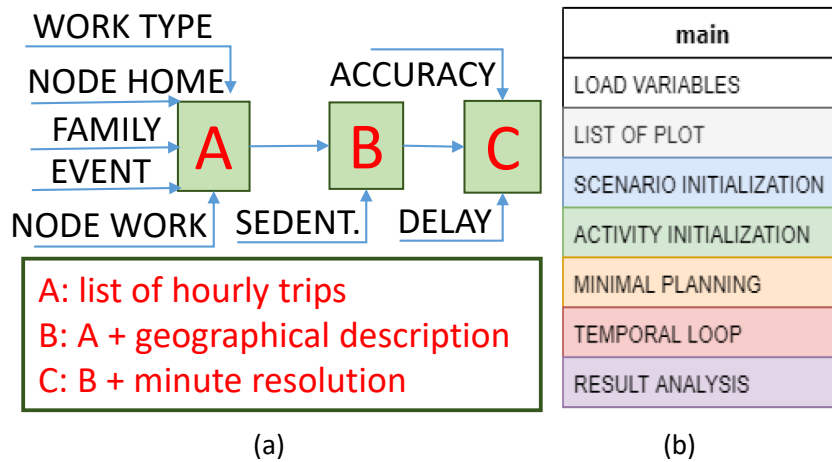
Figure 7.7: a scheme summarizing the driver trip creation procedure. (b) Main temporal loop steps of the simulation.

starting times and trip details (see figure 7.7a for a scheme that summarises the approach). Finally the system dynamics are simulated. Figure 7.7b shows the main steps of the tool. In "load variable" the databases and the parameters to define the simulations are loaded. "Scenario initialisation" deals with initialisation" with the creation of the vehicle trip lists. "Minimal planning" is a particular initialisation procedure to choose the number and initial position of EV such that the number is neither too small nor too big with respect to EV users, and positions are consistent with the request of the EV users. Finally in "Temporal loop" the dynamics of the networks are solved.

Table 7.1: acronyms and actions for the agents.

Acronym	Meaning	Start	End	Prob.	Action
NFWD	No Family-Working days	18	20	0.5	ERRANDS
NFWE	No Family-Week End	20	23	0.6	LEISURE
WFWD	With Family-Working days	18	19	0.4	ERRANDS
WFWE	With Family-Week End	10	13	0.45	LEISURE

7.2.2   Case study and results

The electric grid used is the reference network developed by JRC [151]. The parameters for each road segment were extracted by Gaussian extractions considering four different typologies of roads (for example backbone roads are bigger

145
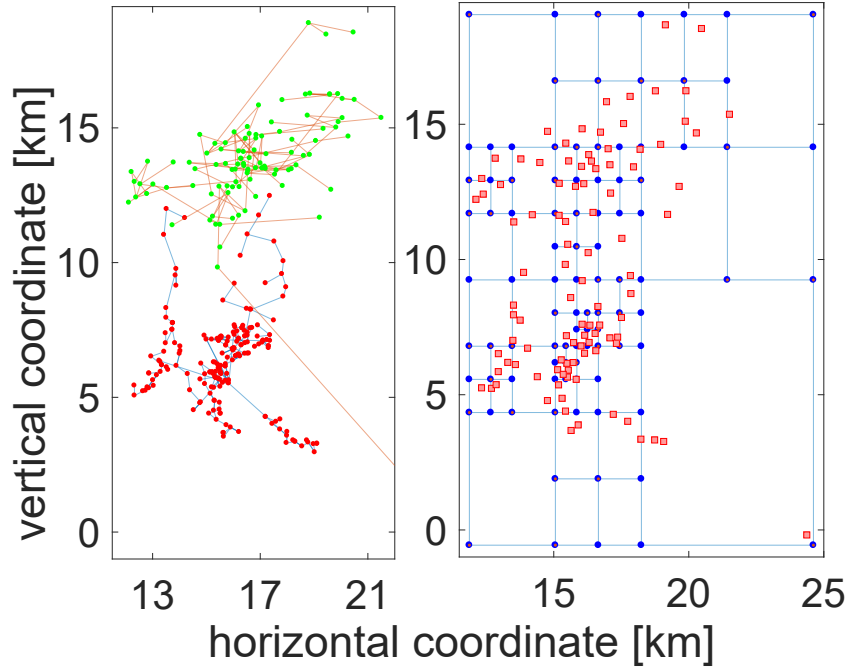
Figure 7.8: case study road construction.

Table 7.2: acronyms and actions for the agents.

Num. drivers	EV users %	Road type	Power [kW]
1000	10	GOOD	3
5000	30	BAD	6
10000	60		11
20000			13

road with high free mean velocity; on the contrary rural roads are characterized by low free mean velocities and low quality parameters). The three networks (electrical, city and road) are shown in figure 7.8. To define the type of work of the agents and their family conditions, and make other reasonable assumptions, data from the Italian institute of statistics and city municipalities were used [106] [2]. A considerable number of simulations were performed by changing the most meaningful parameters. In these scenarios, the EVs recharge with a dumb strategy, which means that they are recharged at a fixed power as soon as they connect to the grid. The parametric analysis is summarised in Table 7.2. GOOD road mean

---

[2]Statistiche veicoli (in Italian), http://www.comuni-italiani.it

higher free mean velocities and better parameters with respect to bad roads. EV users % represents the percentage of drivers making use of the EV car sharing. Power refers to the power rate at which EVs are recharged once they reach the EV car parking (by hypothesis there is always the possibility to park). All the possible combinations of the parameters were simulated, for a total of 72 simulations (every simulations consists of 7 simulated days). All the simulations were performed in Matlab® in commercial available Desktop computers. A sample of the results that can be obtained from the proposed framework is shown below. In general, the agents tend to live in the city, while particular rural nodes with very high industrial power attract many workers. Figure 7.9 shows the nodes where people live and work for the case of 15000 people. Figure 8 shows the cumulative presence of vehicles in the case of 20000 drivers.
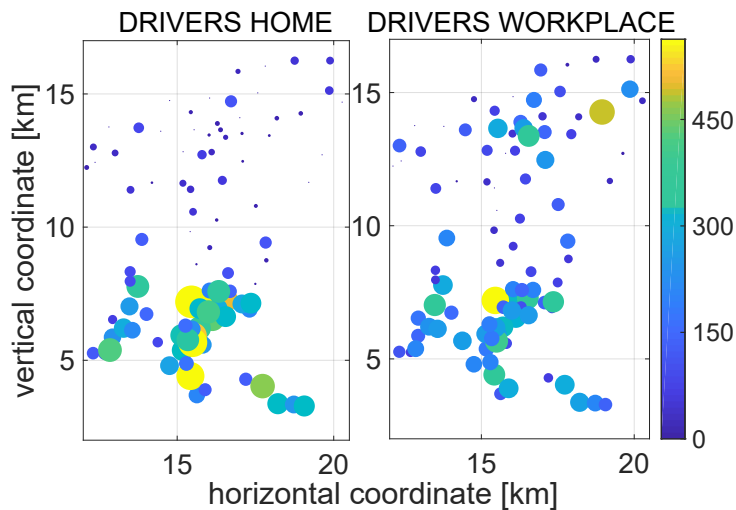
Figure 7.9: nodes where drivers live and work.

Figure 7.10: vehicles presence for one working day.

147
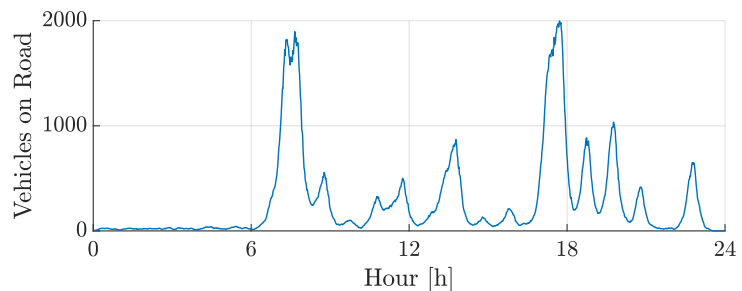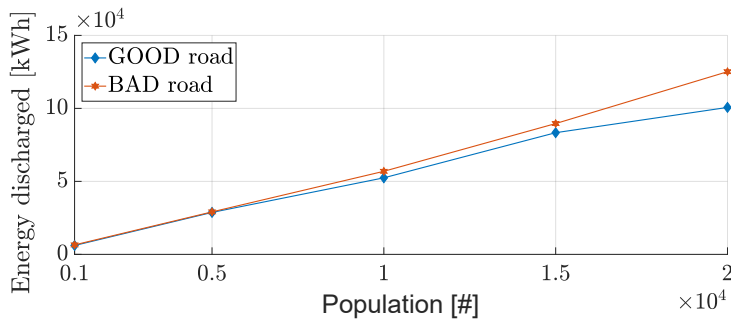
Figure 7.11: total energy spent by EVs considering different populations.

Figure 7.12: spatio-temporal distribution of voltages in the rural network.
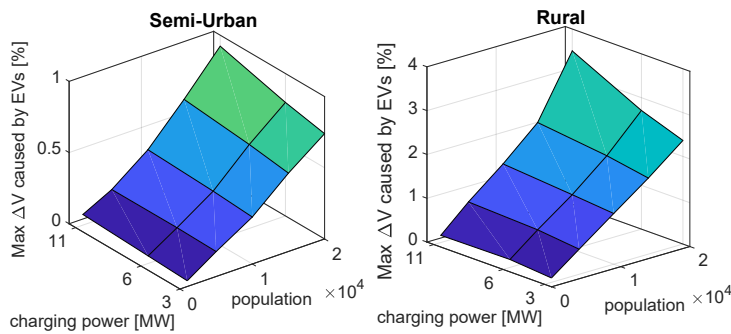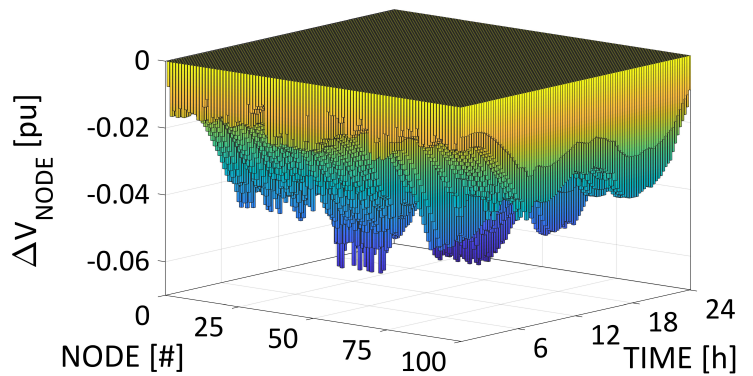
Figure 7.13: $\Delta V_{\max}$ caused by EVs in the grid.

Figure 7.14: spatio-temporal distribution of voltages in the rural network.
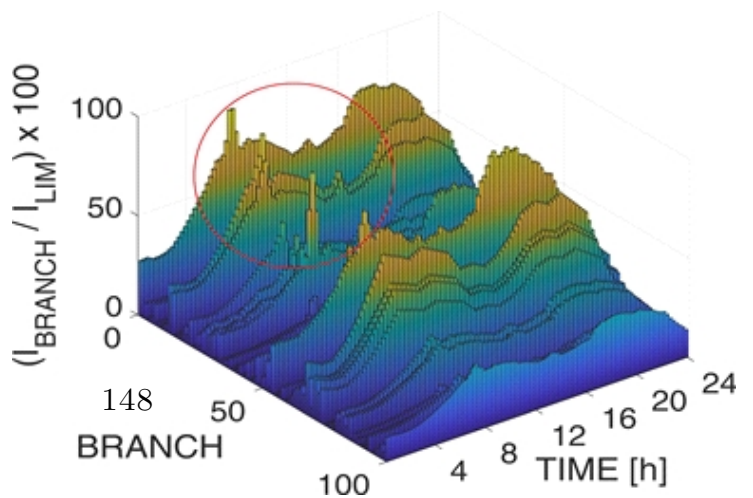
The model is able to grasp the morning and night peak of working days, while the travels along the day are rather variable, less smooth than expected from typical traffic curves [3]. This suggest that new kind of work types could populate the model, such as retired or unemployed people, people who uses the car to work and perform multiple trips a day in not standard hours, and so forth. Moreover a better use of ACCURACY and DELAY parameters can help smoothing the traffic curve. The road characteristics influence the time spent by drivers in the grid and the energy spent by EVs. Figure 7.11 shows the energy discharged by all the EVs in the whole week. The energy discharged is higher when BAD road characteristics are used due to bigger traffic problems and more time spent by the drivers on the road. For what concerns the electric network, Figure 7.12 shows the time-spatial distribution of voltages (computed as $\Delta V_{i,t} = V_{i,t} - V_{\mathrm{nom}}$ for every node i and time step t) for the rural network for one of the days in the case of 20000 people with a recharge power for EVs of 11 kW. The ΔV is caused both by the loads and the EVs recharging. By analysing all the time-spatial series coming from the simulations, it is possible to evaluate that:

- the rural network, due to the resistive nature of the line impedance and less nominal power, tends to be more affected by EV introduction, both in terms of voltages and currents even if the presence of EVs is smaller. The semi-urban network is already characterised by a bigger installed load capacity, which makes more difficult for EVs to affect the grid. Figure 7.13 shows the maximum ΔV caused by EVs. With 20000 people and 11 kW used for recharging, the voltage changes more than 3.5% in the rural network and slightly less than 1% in the semi- urban network.

- The current in the branches almost reaches the thermal limits in the case with 20000 drivers, 60% EV adoption in the rural network (figure 7.14) due to the EV recharging in the morning. In general, EVs could increase the $\frac{I_{\mathrm{BRANCH}}}{I_{\mathrm{lim}}}$ ratio more than 20% in both grids. Adding more EV users will lead to violations of the line thermal limits and, in the case of rural networks, can produce excessively low voltages.

7.3 Second Application: Day Ahead-Real Time Market Optimization

In this second study a day ahead-real time management system for an aggregator of EVs was deleopped. The aggregator has the possibility to control all the

---

[3]Open Mobility data of Turin, http://www.5t.torino.it/open-data.

chargers where the EVs are connected. EVs are always connected when parked, thus vehicles are always connected if not traveling. The algorithm will participate in the Day ahead market making use of EVs use forecasts and optimizing the costs solving an optimization problem. (the problem will be formulated in order to actually perform Energy Arbutrage: Evs could also discharge to the grid if this is convenient). Then in real time a priority based logic will guarantee the respect of the power profile purchased in the day-ahead to avoid unblance which is fined in typical power system markets design. This algorithm is used without the need of formulating an optimization problem. In this way it is possible to manage big EVs system without the need of heavy computational power and communication channels. Schematic of the aggregator operation are shown in figure 7.15.
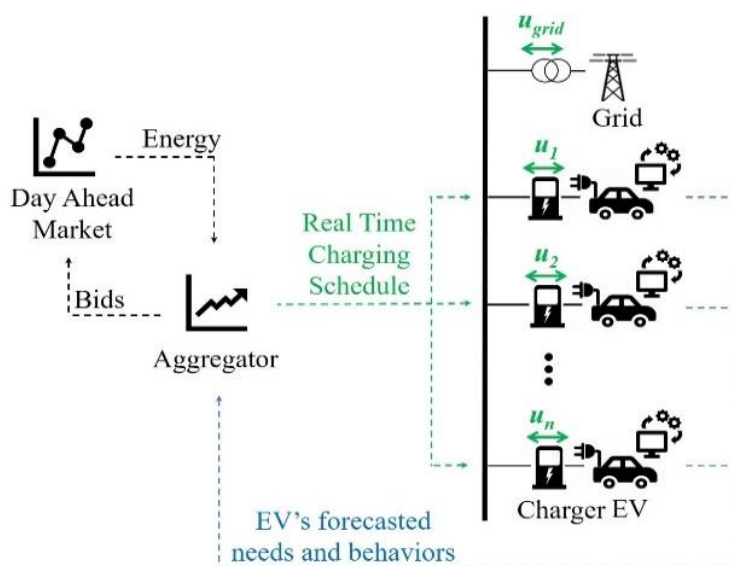
Figure 7.15: schematic of EVs and aggregator Operation. The quantities $u_1, u_2, \ldots, u_n$ represent the power exchanged by the EVs.

For this demonstrative example actually , only 3 EVs are used and are always controllable in whatever chargers they end up stopping their car. Moreover their travel history and actual travles in simulations comes from car diaries field measurement. Figure 7.16 shows a flowchart containing the subroutine used to estimate the future use of a single EV. Without entering in too much detail, the algorithm order the past travels and for each day of the week identify the statistical mean and the more ordinary days and then applies k-medois clusterizzation in order to predict the typical number of trips, time needed and the energy cost of each travel. The most probable departure times are indicated with $\hat{d}_{j,z}$, with j
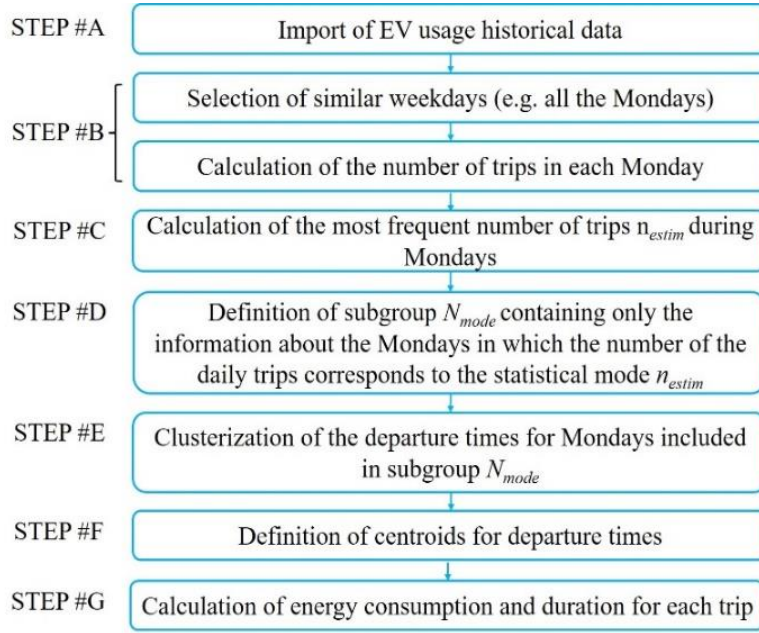
Figure 7.16: EV forecast subroutine algorithm.
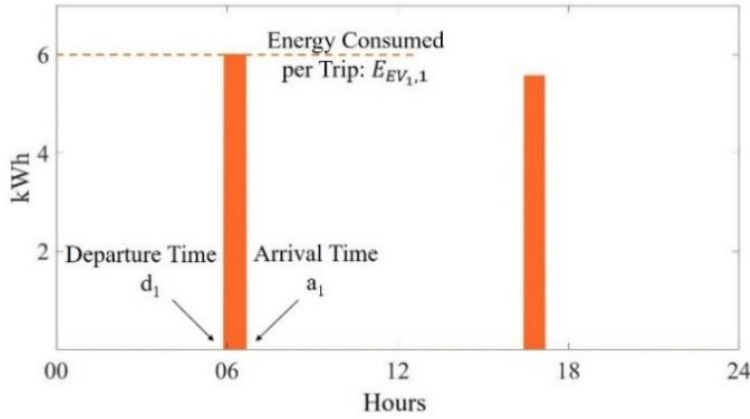
Figure 7.17: output of the forecasting subroutine of the EV_1 usage profiles.

$= 1, \dots , l$ where l represents the number of vehicles and z=1, ..., $Num_{\mathrm{EV_j}}$ where $Num_{\mathrm{EV_j}}$ is the number of the trips of the EV_j in the day andˆis used in order to identify the variables related to the forecasts. arrival time is indicated by $\hat{a}_{\mathrm{j,z}}$ and energy consumption by $\hat{E}_{\mathrm{EV_{j,z}}}$. An example of a prediction is shown in figure 7.17.

7.3.1 Problem formulation

Charger scheduling

Once the next day forecasted behaviors of the EVs are known, it is necessary to allocate the EVs in the respective chargers. The charger schedule algorithm provides, basing on the forecasts, a binary state signal $\hat{s}_{i,k}$ which is sent to the aggregator and indicates if at time slot k, an EV is connected to the charger i, as defined in below.

$$\hat{s}_{i,k} = \begin{cases} 1, & \text{if charger } i \text{ has an EV connected} \\ 0, & \text{if charger } i \text{ has not an EV connected} \end{cases} \tag{7.1}$$

The charger i in which the EVs are allocated during the day is chosen according to the forecasted behaviors in such a way that the charger changes at every departure time while at the end of the day the single EV returns at the charger from which it was parked at the beginning of the day. Fig. 7.18 shows an example of EVs allocation in the chargers. Given that, over the course of the day the single charger i can charge several EVs, thus a dynamic SoC $x_{i,k}$ associated with the i-th charger needs to be defined. Firstly, the evolution of the energy stored in the EV battery is described by the following model:
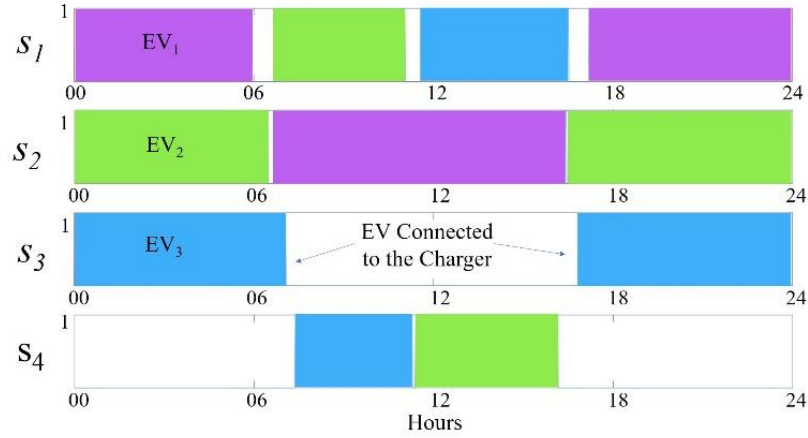
Figure 7.18: forecasted EVs allocation in the chargers during a day. Different colors correspond to different electric vehicles.

$$\hat{SOC}_{j,k+1} = \begin{cases} \hat{SOC}_{j,k} + \Delta t \cdot u_{i,k}, & \text{if } EV_j \text{ is connected in i} \\ \hat{SOC}_{j,k} - \hat{E}_{EVj,k}, & \text{if } k = \hat{d}_{j,z} \text{ h} \\ \hat{SOC}_{j,k}, & else \end{cases} \tag{7.2}$$

In Equation 7.2, Δt is the sampling time; $\hat{SOC}_{j,k}$ is the accumulated energy in the EV_j battery through integration of the power $u_{i,k}$ delivered from the charger i where the vehicle j is connected; $E_{EV_{j,z}}$ is the forecasted consumed energy per trip and subtracted when the EV_j leaves the charger i; Therefore, the forecasted charger State of charge $\hat{x}_{i,k}$ assumes the SoC of the relative connected EV during the charging/discharging operations ($\hat{s}_{i,k} = 1$) while 0 if no car is plugged. The forecasted $\hat{x}_{i,k}$ is mathematically defined as in equation below:

$$\hat{x}_{i,k+1} = \begin{cases} \hat{x}_{i,k} + \Delta t \cdot u_{i,k}, & if\ \hat{s}_{i,k} = 1 \lor \hat{a}_{j,z} < k < \hat{d}_{j,z} \\ \hat{SOC}_{j,k}, & if\ \hat{s}_{i,k} = 1, \lor k = \hat{a}_{j,z} \\ \hat{0}, & if\ \hat{s}_{i,k} = 0, \lor k = \hat{d}_{j,z} \end{cases} \tag{7.3}$$

Finally, in order to guarantee that each vehicle will leave the charging station with a sufficiently high SoC to allow the performance of the next forecasted travel, the minimum departure $\hat{SOC}_{j,d_{j,z}}$ is defined in equation below, where $SoC_{\min}$ represents a minimum security level, and a tolerance SoC percentage ΔSoC.

$$\hat{SOC}_{j,d_{j,z}} = SoC_{\min} + E_{EV_{j,z}} + \Delta SoC. \tag{7.4}$$

Day ahead optimization based on the forecasts

The day ahead strategy evaluates the injected power ui, k at any time k for each charger i based on the forecasted EVs behaviors. Hence, optimality here refers to minimize the station operation costs guaranteeing at least the minimum SoC defined by the forecast of the next trip in equation 7.4. Then, the aggregator solves the following energy arbitrage optimal problem to obtain the charging profile:

$$\min_{u^*} \Delta t \sum_{k=1}^{N} (C_k \cdot \sum_{i=1}^{n} u_{i,k} \tag{7.5a}$$

$$s.t.\ \textbf{Equ.7.3}, \tag{7.5b}$$

$$0 \le u_{i,k} \le \hat{s_{i,k}} \cdot u_{i,max}\ if\ So\hat{C}_{j,k} \le SoC_{\min}, \tag{7.5c}$$

$$-\hat{s_{i,k}} \cdot u_{i,max} \le u_{i,k} \le hats_{i,k} \cdot u_{i,max}\ if\ So\hat{C}_{j,k} \ge SoC_{\min}, \tag{7.5d}$$

$$0 \le x_{i,k} \le x_{i,max}, \tag{7.5e}$$

$$So\hat{C}_{i,d_{j,i}} \le x_{i,d_{j,z}} \le x_{i,max}, \tag{7.5f}$$

$$\forall k = 1, ..., N; \forall i = 1, ..., n; \forall j = 1, ..., l; \forall z = 1, ..., Num_{EV_j}, \tag{7.5g}$$

where, $x_{i,k}$ are the state variables corresponding to the charger SoC and $u_{i,k}$ are the manipulated variables corresponding to delivered power profile. Finally, C_k are the energy prices per time step k and are assumed known. Moreover, $u_{i,max}$

depends on the maximum power that the charger can deliver and the EV can accept. The output of the optimization are the optimized powers $u_{i,k}$ over the day from each charger i. However, in order to participate at the day-ahead market the aggregator needs to provide its total power profile. Therefore, the optimized day ahead profile $P_{da,k}$, is defined as follow:

$$P_{da,k} = \sum_{i=1}^{n} u_{i,k}^{\star}. \tag{7.6}$$

Real time Logic

The real time functioning is operated by a priority-based logic which finally applies the effective charging/ discharging profile to each charger. This logic aims to apply the optimized day-ahead profile by splitting the $P_{da,k}$ among the different chargers on the base of a defined Priority Index ($PI_{i,k}$). The Priority Index, is a value, between 0 and 1, which represent the portion of the $P_{da,k}$ that must be charged by the charger i according to the forecasted charging urgency of the connected vehicle j. It follows that the inverse of $PI_{i,k}$ represents the discharging availability of each vehicle j as explicated in (7.7) Equation below and it is used in order to define EVs discharging status when aggregators is selling energy to the grid. The $PI_{i,k}$, in (7.8), is obtained as the mean between other two indexes: the SoC Priority Index $SPI_{i,k}$ and the Departure Priority Index $DPI_{i,k}$. The $SPI_{i,k}$ represents the charging urgency of the vehicle j with respect to its departure energy needs. It is defined in (7.9), as the ratio between the forecasted departure SoC of the vehicle j connected in i at the time step $k(SoC_{j,d})$, and the sum in j of the forecasted departure state of charge of the other vehicles. In a similar way $DPI_{i,k}$ is defined in (7.10). This index aims to identify the charging urgency on the base of the next departure time of the vehicle j.

$$u_{i,k} = \begin{cases} P_{da,k} \cdot PI_{i,k}, & \text{if } P_{da,k} > 0 \\ P_{da,k} \cdot \frac{1}{PI_{i,k}}, & \text{if } P_{da,k} \leq 0 \end{cases} \tag{7.7}$$

$$PI_{i,k} = mean(DPI_{i,k}; SPI_{i,k}), \tag{7.8}$$

$$SPI_{i,k} = \begin{cases} \frac{\hat{SoC_{j,d_{j,z}}}}{\sum_{j=1}^{n} \hat{SoC_{j,d_{j,z}}}}, & \text{if } EV_j \text{ in } i \text{ at } k \\ 0, & \text{else} \end{cases} \tag{7.9}$$

$$DPI_{i,k} = \begin{cases} \frac{1/\hat{d}_{j,z}}{1/\sum_{j=1}^{n} \hat{d_{j,z}}}, & \text{if } EV_j \text{ in } i \text{ at } k \\ 0, & \text{else} \end{cases} \tag{7.10}$$

$$\forall k = 1,...,N; \forall i = 1,...,n; \forall j = 1,...,l; \forall z = 1,...,Num_{EV_j}. \tag{7.11}$$

This strategy only divides the available power bought at the day ahead between the cars present in real time. However, if the forecasts are close to the actual EVs behavior, this control will be able to recharge the cars at the right point in order to reach the needed actual SoC for the next trip ($SoC_{\mathrm{j,d_j,z}}$).

7.3.2   Case study and results
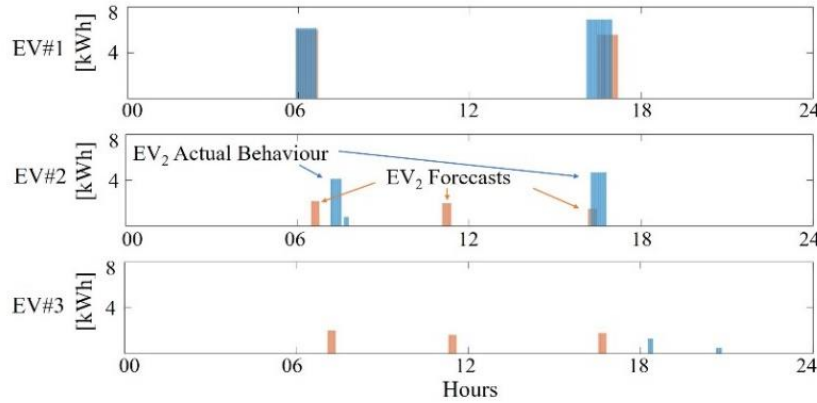
Figure 7.19: EVs usage scenarios: actual (blue) and forecasts (red).
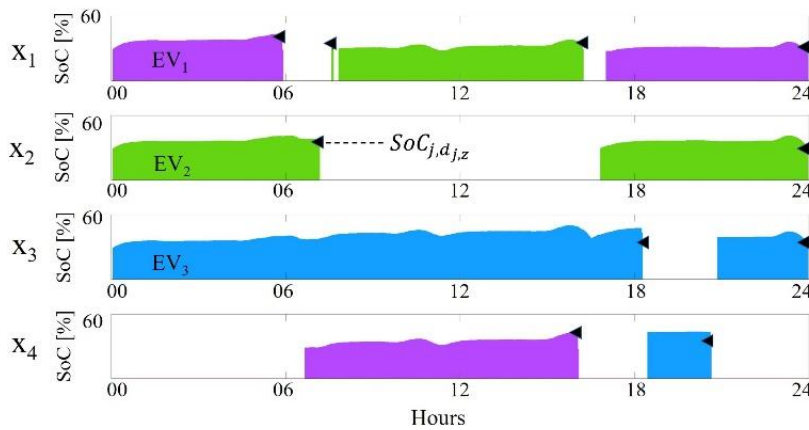
Figure 7.20: EVs allocation and chargers SoC evolution during the day
.

The proposed methodology is tested on a simple case study with three EVs. The EV historical data have been selected through a clusterization analysis among
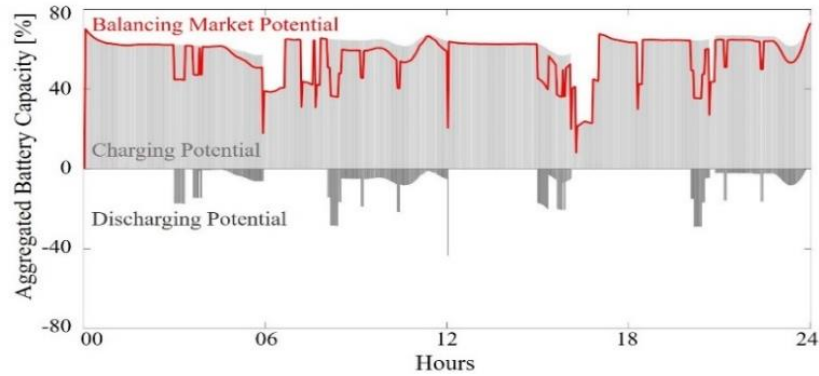
Figure 7.21: Charging, Discharging and Balancing market potential over the day of the simulation for the three EVs.

a database composed of 215 EV real usage behaviors available in [4] and covering three years of recording (2013-2015). As a result, EV1, EV2 and EV3 are different and well represent three typical electric vehicle usage profiles. In particular, EV1 represent the highest energy consuming and contemporarily the most systematic usage profile. On the other hand, EV3 represents the lowest energy consumption and contemporarily the most variable usage profile. EV2, represents a medium behavior. Figure 7.19, shows EV1, EV2 and EV3 usage profiles and the respective forecasts. According to the analysis conducted in [74], the chosen battery capacity of each vehicle is 40 kWh, and the considered initial state of charge is assumed to be 30%. The energy prices refer to the December 13th, 2017 Italian market, chosen because it registers the highest prices mean value and contemporarily the highest standard deviation compared to the other days of the year [5].

Since the energy requested from each EV during a day is a marginal part of its installed battery capacity, the power profile that minimizes the cost function (7.5a, makes use of only a small part of the total available battery capacity for the aggregator. Furthermore, under the assumption that the cars are connected to the same aggregator when not traveling, there is no time period where no car is connected. From the above, it follows that the optimized power profile bought at day-ahead market $P_{da,k}$, results perfectly respected in the real-time operation, thus avoiding any liability to the network. Moreover, in the examined case study, the proposed methodology was always able to guarantee the mobility needs of each EV users. Fig. 7.20, provide an entire overview of the system operation of

---

[4]My Electric Avenue Data, 2015. [Online]. Available: http://myelectriavenue.info/

[5]GME (Gestore Mercati energetici), Italian Market Operator: https://www.mercatoelettrico-.org/En/Default.aspx

the elapsed day operated by the real time logic. In particular, is shown the SoC evolution of the three EVs while it is highlighted the departure State of Charge $\hat{SoC}_{j,d_{j,z}}$, that guarantee the actual EVs trips. For sake of clarity, $SoC_{j,d_{j,z}}$, is calculated similarly to equation 7.4 by using the actual consumed energy per trip $E_{EV_{j,z}}$. From figure 7.20, it can be seen that the state of charge of the EVs at the departure times is always higher than the $SoC_{j,d_{j,z}}$. Table I lists the cost due to the total energy bought from the aggregator to satisfy the mobility needs of its clients and the revenues due to the V2G operations. Moreover, in order to provide the effect of the forecasts and investigate the full potential of the methodology, Table I, shows the costs obtained in the case of exact predictions. The results highlight a cost saving for the aggregator close to 60%. Note that, the deviations in savings between solutions with exact and forecasted EVs information, is just 3%. This suggests that the single EV forecasts errors can be easily mitigated thanks to the EVs aggregated behavior.

7.4 Next steps of the framework

7.4.1 From an Agent based model to a frequency impact evaluation

The models presented in section 7.2 can be further improved in order to increase their realism. In particular:

- New agents and actions can be introduced considering detailed socio-demographic descriptions based on activity based models [99].

- The models parameters can be set with the goal of obtaining a traffic load curve which is similar to real data from different cities in order to represent a variety of realistic situations and scenarios. Model setting can be lengthy as the number of parameters increase with the number of agents in the network, for this reason an optimization approach could be built based on heuristic optimization techniques. Different typologies of cities could be modelled also considering different distribution network parameters.

- A smart charging algorithm can be implemented in order to replace the dumb charging proposed before. Rigorously we could apply the techniques developed in previous section to our case (see also next section for further details). While this is surely the most correct approach, it can be computational heavy in the case of simulations with thousands or dozens of thousands of agents. A real time smart charging algorithm based on the concept of laxity [130] and energy price levels can be considered a realistic approach [194, 204].

Laxity is defined as "a measure for the flexibility (or urgency) in charging of an EV". the laxity of EV i is computed as:

$$LX_i(t) = \overline{T_f} - \frac{E_{nom_i} \cdot (\overline{SOC_i(t_f)} - SOC_i(t))}{P_{max_i}} \qquad (7.12)$$

where $\overline{T_f}$ is the forecasted time of departure and $\overline{SOC_i(t_f)}$ is desired SOC at departure. Laxity is equivalent to the remaining time minus the minimum remaining time needed to fully charge an EV at the maximum rate. An EVs aggregator charging algorithm based on this index will share the available power (as optimized by considering day ahead prices) prioritizing the lowest laxity vehicles. Uncertainty in forecasting could be dealt by using stochastic optimization approaches. Over this charging strategy the possible distribution network bottlenecks can be evaluated.

- Finally based on the simulations results, equivalent model of EVs can be build considering the time profiles of EV availability and maximum power that can be used for frequency control (as limited by distribution grid capacity and recharging considerations). These equivalent EVs can be integrated in the SFRM model developed in previous chapters for explicit time domain computations or in order to study how much capacity in time can be provided by EVs for frequency control and what's their impact on the power system frequency.

7.4.2 Integrating frequency control into Priority based logic

As seen in previous chapters, especially in the fifth and sixth, typical SOC profiles of BESSs during PFC vary according to the day considered and they are composed by three parts: inefficiency, intraday oscillations and mean part. This information needs to be integrated in the EVs control logic. Here I list some initial hints on how this can happen and how the control algorithm can still be improved:

- Use a ΔSoC tolerance. In order to assure participation in frequency control, a certain amount of SoC margin both in charge and in discharge could be kept. This ΔSoC could be set to a mid point between $SoC_{\min}$ and $SoC_{\max}$, while, as for now, to minimize costs, the aggregator makes EVs work at the lowest possible SoC, leaving space to charge but not enough to discharge (see figure 7.21). A better study of the three SOC components based on their forecastability can generate even additional ways to cope with the SoC dynamics.

- Integrate intraday market. Participation in this market is useful in order to adjust the SoC of EVs during the day. The current status of EVs average SoC, DPI and SPI indexes can be used to predict how much energy should be purchased or sold. The more the forecast are good the more is possible to better optimize. The three indexes could be unified exploiting the concept of laxity introduced before. The laxity of single EVs, of charging stations and even of the total Evs populations give a strong index of how much flexibility is possible for the Aggregator to use.

- Distributed control. With a high number of EVs, more robusteness in the control can be gained by passing from a total centralized control in which forecasts, day ahead and real time control signals are sent from a central unit to each EVs, to a distributed framework [62]. In such a case, the central unit sends orders to charging stations (composed by n chargers i) which in turn, depending on real time conditions, dispatch EVs. Forecasts and relevant indexes (average SOC, SPI, DPI, Laxity) can be reformulated at the charging stations level and exchanged between the local and central control unit. This control retains less communications and computational requirements and it is preferable in the case of high numbers and geographical spread of EVs.

Conclusion

In this chapter a framework to study the electric vehicles in the grid is presented. In section 7.2 the stochastic spatio-temporal presence of electrical vehicles is simulated starting from the behaviour of single agents. This framework is able to capture the mains dynamics of vehicles presence in the road-electric network and correctly assess the impact in the grid. On the other hand in 7.3 a strategy for an EVs aggregator is developed to minimize its cost of recharging the vehicles. The strategy works by dividing the available power between the EVs during the day. Finally in section 7.4 a detailed view on the methodologies and the simulations still needed to evaluate EVs potential is provided.

Conclusion

Following the chapters order, we may recap the following key points:

- Europe is the most ambitious continent for what concern de-carbonizzation, aiming to reach substantial zero GHG emissions within 2050. Although many efforts are being done, there is still a significant mismatch between our goal and our current direction.

- Converters are going to replace Synchronous Generators due to the increase of RESs and new resources into the grid. System stability can be jeopardized by this change. In particular, Frequency stability depends on the inertia and reserves provided by conventional generation plants. BESS are already being used in order to fulfill fast frequency services in addition to other uses.

- Three categories of studies about BESS performance performing fast frequency control can be conceptualized after a critical review of the literature. Open loop studies are concerned with BESS economics and SoC management. Researchers try to optimize SoC by exploiting variable droop strategies or activating slower resources. More complex attempts make use of multi-units aggregation or BESS participation to multiple services in order to maximize BESS profits. Every solution must be designed taking into account the country specific market rules. The battery model and the degradation process have a great influence on the results. An interesting opportunity for further research could be to devise experimental methodologies in order to recreate empirical models which are able to describe accurately BESS dynamics and degradation maintaining at the same time maintain low computational complexity. The second group is about the impact of BESS after a contingency. The current researches substantially agree in the fact that Rocof control from BESSs can actually work as a substitute for physical inertia, even considering the presence delays and the Phase Locked Loop measurements systems. Hardware in the loop experiments and field tests could add more insights on this issue and in the possible problems arising in

digital controllers performing Rocof control. Voltage Source Converter set-up should also be considered essential for a future converter dominated grid. Distributed control with converter sharing frequency or other control signals is an interesting opportunity which still needs a better focus to evaluate the possibility of gaining more stability for the grid. Finally the last group deals with the impact of BESS during normal operations. A substantial absence of clear and systematic methodologies to reproduce typical frequency variations in the grid was identified. The develop of such a method could help us to evaluate the performance of BESSs and the impact of Variable Droop Strategy or more complex frequency controls on the frequency signal itself.

- In chapter 4 the impact of Rocof and fast PFC by BESSs were assessed. The simulation of the Sardinian Island and the parametric analysis on the two area system showed us how RoCof is useful in smoothing the frequency signal after a contingency, even in the presence of small delays. The performed simulations help us to understand the minimal levels of inertia and reserves to assure that frequency dynamics to be acceptable (especially for what concerns initial RoCof and f_{nadir}). The BESS intervention was dimensioned according to the saturation point of typical Synchronous generators in order to design comparable services. In the Sardian system a 40-50 % decrease in inertia can cause frequency problems, besides 100 MW of BESSs are more than enough to guarantee good frequency dynamics. Best strategy is to reserve half of the band for RoCof and half for PFC.

- From the simulations in chapter 5, many hints and results can be extracted. By reproducing a real frequency signal in a SFRM it is in fact possible to appreciate that Rocof control has a very small impact under normal grid conditions and that PFC of BESSs is almost comparable to CGs impact. This is due to the slow nature of deterministic frequency deviations which represent the most part of the frequency signal. In the case of Sardinian power system Secondary frequency control has even much more impact than primary itself for the same reasons. Moreover, during a contingency Rocof control and PFC are almost complementary with RoCof control being requested within the first 1-2 seconds and PFC being requested slightly after. This suggests that instead of dividing the power bands between the two control channels, the best approach would be to use at the same time the two services with the full bands: during a contingency a double full band will guarantee the best frequency control, while during normal operations RoCof band will be almost no used and it will leave space for PFC.

The SoC profile of BESSs was investigated during the provision of PFC. This

leads to discover that inefficiencies account much less with respect to intra-day swings and SoC decrease or increase, due to the average of the frequency signal. This analysis gives important hints to the best strategy to be devised for better SoC management. By simplifying the converter dynamics with a power balance over the DC link and using a fast pole to account for converter delays, we can make use of a BESS complete electrical equivalent model together with a computational light SFRM model. Finally few indexes are introduced in order to detect jumps in the Irish frequency signal used for the simulations. Jumps will be then analyzed in order to compute and record their frequency range, duration and estimated load mismatch. The starting hypothesis is that jumps are created by TSOs activated reserves and their objective is to re-establish frequency under a certain range. This process is part of the frequency deterministic deviations phenomena.

- In chapter 6, another methodology to create a realistic frequency signal is used in which the goal is to reproduce the average harmonic content of real data. These data are characterized by similar harmonic content in the different days, so that their average behaviour is realistic and can function as a standardized test case. It was also possible to estimate the deterministic and stochastic frequency deviations proportions in the simulated frequency signal. As expected they are about 85 % to 15 % for deterministic slow deviations. BESS PFC efficacy was compared with conventional generation and results just slightly better than fast conventional resources, due to the slow nature of frequency oscillations. In the case of faster frequency dynamics scenarios, BESSs would have much more efficacy. Finally it was possible to simulate the impact of Variable Droop Strategy on the frequency signal. While SoC standard deviation has an appreciable standard deviation decrease (around 6-8 %), the frequency signal remains substantially equal.

- In chapter 7 a complete framework is presented in order to correctly model the impact of EVs in frequency control. An agent based model was developed to create vast scale scenarios simulations with thousand of EVs interacting in road and electric networks. A dumb charging was used to asses the impact of EVs. The impact is not negligible and depends on the R-X ratio of the lines. Voltage changes are up to 3.5% and current in the branches can increase even up to 20 %. This example justify the need for an explicit Distribution System description when evaluating the potential of EVs for frequency control. Bottlenecks at the distribution level can effectively prevent PFC from EVs. A smart strategy for EVs control was presented in the second part considering day ahead energy optimization with real time balancing from the EVs Aggregators. This strategy can be enhanced considering frequency

control.

Many possibilities are left as future works. For electric vehicles main steps and ideas to continue the research have been already presented in Chapter 7. For the sake of brevity I add just a single idea for what concerns BESSs frequency control. By using the frequency recorded data from European Continental system and the frequency reserves data published by ENTSO-E, it could be possible to enhance the model built in Chapter 5 as a Two Area system (Italy and the rest of Europe) similarly to the one proposed in Chapter 4. European system, contrarily to the Irish one, posses secondary and tertiary frequency control. It could be interesting to quantify the BESSs distortion effects in a real electric system due to Variable droop strategy considering also the presence of secondary frequency control and the effects on a Two Area system. With respect to Chapter 6 more than one initial SoC for the various BESSs systems can be considered in the same simulation. For example 10 different values could be chosen to consider all the possible situations that can happen during real operations of the power systems. Rainflow counting can be also used to better evaluate battery degradation.

Bibliography

[1]   50Hertz et al. *TSO proposal for the establishment of common and harmonised rules and processes forthe exchange and procurement of balancing capacity for frequency containment reserves (fcr) in accordance with article 33 of commission regulation (eu) 2017/ 2195 establishing a guideline on electricity balancing.* 2018. URL: https://docstore.entsoe.eu/Documents/Network%5C%20codes%5C%20documents/NC%5C%20EB/FCR_%20Proposal-Article%5C%2033_1_EBGL_20180426_FV.PDF (visited on 10/01/2020).

[2]   Atinuke Ademola-Idowu and Baosen Zhang. "Optimal Design of Virtual Inertia and Damping Coefficients for Virtual Synchronous Machines". In: *2018 IEEE Power & Energy Society General Meeting (PESGM).* IEEE. 2018, pp. 1–5.

[3]   International Energy Agency. "World energy Outlook". In: *Paris, France* (2018).

[4]   Samir M Alhejaj and Francisco M Gonzalez-Longatt. "Impact of inertia emulation control of grid-scale BESS on power system frequency response". In: *2016 International Conference for Students on Applied Engineering (ICSAE).* IEEE. 2016, pp. 254–258.

[5]   PM Rocha Almeida, Filipe Joel Soares, and JA Peças Lopes. "Electric vehicles contribution for frequency control with inertial emulation". In: *Electric Power Systems Research* 127 (2015), pp. 141–150.

[6]   M Hadi Amini, Mohsen Parsa Moghaddam, and Orkun Karabasoglu. "Simultaneous allocation of electric vehicles' parking lots and distributed renewable resources in smart power distribution networks". In: *Sustainable Cities and Society* 28 (2017), pp. 332–342.

[7]   Paul M Anderson and Aziz A Fouad. *Power system control and stability.* John Wiley & Sons, 2008.

[8]   Philip M Anderson and Mahmood Mirheydar. "A low-order system frequency response model". In: *IEEE Transactions on Power Systems* 5.3 (1990), pp. 720–729.

[9]   Göran Andersson. "Modelling and analysis of electric power systems". In: *ETH Zurich* (2008), pp. 5–6.

[10] A Anisie and Boshell F. "Utility Scale Batteries: Innovation Landscape Brief". In: *International Renewable Energy Agency: Abu Dhabi, UAE* (2019).

[11] *Annual Energy Outlook 2019 with projections to 2050*. Tech. rep. US Energy Information Administration, 2019.

[12] Francesco Arrigo, Marco Merlo, and Ferdinando Parma. "Fourier transform based procedure for investigations on the grid frequency signal". In: *2017 IEEE PES Innovative Smart Grid Technologies Conference Europe (ISGT-Europe)*. IEEE. 2017, pp. 1–6.

[13] F Arrigo et al. "Assessment of primary frequency control through battery energy storage systems". In: *International Journal of Electrical Power & Energy Systems* 115 (2020), p. 105428.

[14] Simone Barcellona and Luigi Piegari. "Lithium ion battery models and parameter identification techniques". In: *Energies* 10.12 (2017), p. 2007.

[15] Roberto Benato et al. "Large-scale electrochemical energy storage in high voltage grids: Overview of the Italian experience". In: *energies* 10.1 (2017), p. 108.

[16] Hassan Bevrani. *Robust power system frequency control*. Springer, 2014.

[17] Yuankai Bian et al. "Demand side contributions for system inertia in the GB power system". In: *IEEE Transactions on Power Systems* 33.4 (2017), pp. 3521–3530.

[18] Fabio Bignucolo et al. "Integration of lithium-ion battery storage systems in hydroelectric plants for supplying primary control reserve". In: *Energies* 10.1 (2017), p. 98.

[19] E Bompard et al. *Report on opportunities and options for PtG in power systems*.

[20] Theodor S Borsche, Juan de Santiago, and Göran Andersson. "Stochastic control of cooling appliances under disturbances for primary frequency reserves". In: *Sustainable Energy, Grids and Networks* 7 (2016), pp. 70–79.

[21] Theodor S Borsche, Andreas Ulbig, and Göran Andersson. "Impact of frequency control reserve provision by storage systems on power system operation". In: *IFAC Proceedings Volumes* 47.3 (2014), pp. 4038–4043.

166

[22] Theodor Borsche, Andreas Ulbig, and Goran Andersson. "A new frequency control reserve framework based on energy-constrained units". In: *2014 Power Systems Computation Conference*. IEEE. 2014, pp. 1–7.

[23] Theodor Borsche et al. "Power and energy capacity requirements of storages providing frequency control reserves". In: *2013 IEEE Power & Energy Society General Meeting*. IEEE. 2013, pp. 1–5.

[24] Claudio Brivio, Stefano Mandelli, and Marco Merlo. "Battery energy storage system for primary control reserve and energy arbitrage". In: *Sustainable Energy, Grids and Networks* 6 (2016), pp. 152–165.

[25] Claudio Brivio et al. "A physically-based electrical model for lithium-ion cells". In: *IEEE Transactions on Energy Conversion* 34.2 (2018), pp. 594–603.

[26] Paul Vincent Brogan et al. "Effect of BESS Response on Frequency and RoCoF During Underfrequency Transients". In: *IEEE Transactions on Power Systems* 34.1 (2018), pp. 575–583.

[27] Ye Cai et al. "Self-sustainable community of electricity prosumers in the emerging distribution system". In: *IEEE Transactions on Smart Grid* 8.5 (2016), pp. 2207–2216.

[28] Silvia Canevese, Adriano Iaria, and Marco Rapizza. "Impact of fast primary regulation and synthetic inertia on grid frequency control". In: *2017 IEEE PES Innovative Smart Grid Technologies Conference Europe (ISGT-Europe)*. IEEE. 2017, pp. 1–6.

[29] S Canevese et al. "Battery Energy Storage Systems for frequency regulation: Simplified aging evaluation". In: *2017 6th International Conference on Clean Electrical Power (ICCEP)*. IEEE. 2017, pp. 291–297.

[30] Jun Cao et al. "Optimal sizing and control strategies for hybrid storage system as limited by grid frequency deviations". In: *IEEE Transactions on Power Systems* 33.5 (2018), pp. 5486–5495.

[31] Pantelis Capros et al. "EU Reference Scenario 2016-Energy, transport and GHG emissions Trends to 2050." In: (2016).

[32] Pantelis Capros et al. "Outlook of the EU energy system up to 2050: The case of scenarios prepared for European Commission's "clean energy for all Europeans" package using the PRIMES model". In: *Energy strategy reviews* 22 (2018), pp. 255–263.

[33] Smart Grid Coordination CEN-CENELEC-ETSI. "Group.(2012)". In: *Smart Grid Reference Architecture* (2012), pp. 1–107.

167

[34] Shuaixun Chen et al. "Penetration rate and effectiveness studies of aggregated BESS for frequency regulation". In: *IEEE Transactions on Smart Grid* 7.1 (2015), pp. 167–177.

[35] Bolong Cheng and Warren B Powell. "Co-optimizing battery storage for the frequency regulation and energy arbitrage using multi-scale dynamic programming". In: *IEEE Transactions on Smart Grid* 9.3 (2016), pp. 1997–2005.

[36] Yunzhi Cheng et al. "Dynamic available AGC based approach for enhancing utility scale energy storage performance". In: *IEEE Transactions on Smart Grid* 5.2 (2014), pp. 1070–1078.

[37] *China Renewable Energy Outlook*. Tech. rep. Energy Research Institute of Academy of Macroeconomic Research and China National Renewable Energy Centre, 2018.

[38] Woo Yeong Choi and Kyung Kook. "Impact Analysis of BESS for Providing Frequency Response in Korean Power System". In: Oct. 2017.

[39] European Commission. *Commission Regulation (EU) 2017/1485 of establishing a guideline on electricity transmission system operation.* 2017.

[40] M Coppo et al. "The Italian smart grid pilot projects: Selection and assessment of the test beds for the regulation of smart electricity distribution". In: *Electric Power Systems Research* 120 (2015), pp. 136–149.

[41] Dennis W Dees, Vincent S Battaglia, and André Bélanger. "Electrochemical modeling of lithium polymer batteries". In: *Journal of power sources* 110.2 (2002), pp. 310–320.

[42] Nicholas DeForest, Jason S MacDonald, and Douglas R Black. "Day ahead optimization of an electric vehicle fleet providing ancillary services in the Los Angeles Air Force Base vehicle-to-grid demonstration". In: *Applied energy* 210 (2018), pp. 987–1001.

[43] Maurizio Delfanti, Davide Falabretti, and Marco Merlo. "Energy storage for PV power plant dispatching". In: *Renewable Energy* 80 (2015), pp. 61–72.

[44] Gauthier Delille, Bruno Francois, and Gilles Malarange. "Dynamic frequency control support by energy storage to reduce the impact of wind and solar generation on isolated power system's inertia". In: *IEEE Transactions on sustainable energy* 3.4 (2012), pp. 931–939.

[45] *Deliverable 5.5 V2. Report on trial for frequency control in Laboratory and validation of initial network codes and ancillary service definitions.* Tech. rep. RESERVE European project, 2019.

[46] Florian Dörfler, John W Simpson-Porco, and Francesco Bullo. "Breaking the hierarchy: Distributed control and economic optimality in microgrids". In: *IEEE Transactions on Control of Network Systems* 3.3 (2015), pp. 241–253.

[47] Mohammad Dreidy, H Mokhlis, and Saad Mekhilef. "Inertia response and frequency control techniques for renewable energy sources: A review". In: *Renewable and Sustainable Energy Reviews* 69 (2017), pp. 144–155.

[48] Adam Dyśko et al. "Assessment of Risks Resulting from the Adjustment of ROCOF Based Loss of Mains Protection Settings Phase II". In: *University of Strathclyde, ref: NGC/LOM/TR/2013-001b* (2013).

[49] EirGrid/SONI. *DS3 Joint Grid Code Working Group Position Paper on RoCoF*. Tech. rep. 2012.

[50] EirGrid/SONI. *RoCoF Modification Proposal - TSOs' Recommendations*. Tech. rep. 2012.

[51] Eirgrid and SONI. *All-island ten year transmission forecast statement*. 2017.

[52] P Energy. "Rate of change of frequency (ROCOF)-review of TSO and generator submissions final report". In: (2013).

[53] Jonas Engels, Bert Claessens, and Geert Deconinck. "Techno-economic analysis and optimal control of battery storage for frequency control services, applied to the German market". In: *Applied energy* 242 (2019), pp. 1036–1049.

[54] ENTSO-E. "Continental Europe significant frequency deviations". In: (2019).

[55] ENTSO-E. *Frequency Stability Evaluation Criteria for The Synchronous Zone of Continental Europe*. 2016.

[56] ENTSO-E. *Network Code on Emergency and Restoration*. 2017. URL: http://www.entsoe.eu/network_codes/load/ (visited on 10/07/2019).

[57] ENTSO-E. *Network Code on Load-Frequency Control and Reserves*. 2013. URL: http://www.entsoe.eu/network_codes/load/ (visited on 10/07/2019).

[58] ENTSO-E. *Network Code on System Operations*. 2017. URL: http://www.entsoe.eu/network_codes/load/ (visited on 10/07/2019).

[59] ENTSO-E. *Supporting Document for the Network Code on Load-Frequency Control and Reserves*. 2013. URL: https://www.acer.europa.eu/Official_documents/Acts_of_the_Agency/Annexes/ (visited on 10/07/2019).

[60] Mircea Eremia and Mohammad Shahidehpour. *Handbook of electrical power system dynamics: modeling, stability, and control*. Vol. 92. John Wiley & Sons, 2013.

[61] Joint Investigation Team EURELECTRIC—ENTSO-E. "Deterministic Frequency Deviations—Root Causes and Proposals for Potential Solutions". In: *EURELECTRIC: Brussels, Belgium* (2011).

[62] Samy Faddel, Ali T Al-Awami, and Osama A Mohammed. "Charge control and operation of electric vehicles in power grids: A review". In: *Energies* 11.4 (2018), p. 701.

[63] Michele Falco et al. "Agent-based Modelling to Evaluate the Impact of Plug-in Electric Vehicles on Distribution Systems". In: *2019 International Conference on Smart Energy Systems and Technologies (SEST)*. IEEE. 2019, pp. 1–6.

[64] Ricardo Fernandes. "Simulation of a Subcritical Power Plant using a Boiler Following Control sequence". In: (2012).

[65] Masoud Hajiakbari Fini and Mohamad Esmail Hamedani Golshan. "Determining optimal virtual inertia and frequency control parameters to preserve the frequency stability in islanded microgrids with high penetration of renewables". In: *Electric Power Systems Research* 154 (2018), pp. 13–22.

[66] Marco Giacomo Flammini et al. "Interaction of consumers, photovoltaic systems and electric vehicle energy demand in a Reference Network Model". In: *2017 International Conference of Electrical and Electronic Technologies for Automotive*. IEEE. 2017, pp. 1–5.

[67] Johannes Fleer and Peter Stenzel. "Impact analysis of different operation strategies for battery energy storage systems providing primary control reserve". In: *Journal of Energy Storage* 8 (2016), pp. 320–338.

[68] Johannes Fleer et al. "Techno-economic evaluation of battery energy storage systems on the primary control reserve market under consideration of price trends and bidding strategies". In: *Journal of Energy Storage* 17 (2018), pp. 345–356.

[69] *Frequency Stability Evaluation Criteria for The Synchronous Zone of Continental Europe*. Tech. rep. ENTSO-E, 2016.

[70] Ana Gadea, Mattia Marinelli, and Antonio Zecchino. "A market framework for enabling electric vehicles flexibility procurement at the distribution level considering grid constraints". In: *2018 Power Systems Computation Conference (PSCC)*. IEEE. 2018, pp. 1–7.

[71] Lijun Gao, Shengyi Liu, and Roger A Dougal. "Dynamic lithium-ion battery model for system simulation". In: *IEEE transactions on components and packaging technologies* 25.3 (2002), pp. 495–505.

[72] Helena Gerard, Enrique Rivero, and Daan Six. "Basic schemes for TSO-DSO coordination and ancillary services provision". In: *SmartNet Deliv. D 1* (2016), p. 3.

[73] Francesco Giordano et al. "Forecast-Based V2G Aggregation Model for Day-Ahead and Real-Time Operations". In: *2020 IEEE Power & Energy Society Innovative Smart Grid Technologies Conference (ISGT)*. IEEE. 2020, pp. 1–5.

[74] Francesco Giordano et al. "Self-consumption improvement for a nanogrid with photovoltaic and vehicle-to-home technologies". In: *2018 IEEE International Conference on Environment and Electrical Engineering and 2018 IEEE Industrial and Commercial Power Systems Europe (EEEIC/I&CPS Europe)*. IEEE. 2018, pp. 1–6.

[75] Francisco M Gonzalez-Longatt. "Effects of fast acting power controller of BESS in the system frequency response of a multi-machine system: probabilistic approach". In: *2018 IEEE Innovative Smart Grid Technologies-Asia (ISGT Asia)*. IEEE. 2018, pp. 798–803.

[76] Josep M Guerrero et al. "Hierarchical control of droop-controlled AC and DC microgrids—A general approach toward standardization". In: *IEEE Transactions on industrial electronics* 58.1 (2010), pp. 158–172.

[77] Mohammad Hesam Hafezi, Lei Liu, and Hugh Millward. *Modeling Activity Scheduling Behavior of Travelers for Activity-Based Travel Demand Models*. Tech. rep. 2018.

[78] Hua Han et al. "Review of power sharing control strategies for islanding operation of AC microgrids". In: *IEEE Transactions on Smart Grid* 7.1 (2015), pp. 200–215.

[79] Sekyung Han, Soohee Han, and Kaoru Sezaki. "Optimal control of the plug-in electric vehicles for V2G frequency regulation using quadratic programming". In: *ISGT 2011*. IEEE. 2011, pp. 1–6.

[80] Jesus C Hernández et al. "Primary frequency control and dynamic grid support for vehicle-to-grid in transmission systems". In: *International Journal of Electrical Power & Energy Systems* 100 (2018), pp. 152–166.

[81] Tim Hilgert et al. "Modeling week activity schedules for travel demand models". In: *Transportation Research Record* 2666.1 (2017), pp. 69–77.

[82] Linbin Huang et al. "A virtual synchronous control for voltage-source converters utilizing dynamics of DC-link capacitor to realize self-synchronization". In: *IEEE Journal of Emerging and Selected Topics in Power Electronics* 5.4 (2017), pp. 1565–1577.

[83] Tarun Huria et al. "High fidelity electrical model with thermal dependence for characterization and simulation of high power lithium battery cells". In: *2012 IEEE International Electric Vehicle Conference*. IEEE. 2012, pp. 1–8.

[84] IEEE. "IEEE standard for synchrophasors for power systems". In: *IEEE Standard* 37 (2005), pp. 118–2005.

[85] Wardah Inam et al. "Stability, control, and power flow in ad hoc dc microgrids". In: *2016 IEEE 17th Workshop on Control and Modeling for Power Electronics (COMPEL)*. IEEE. 2016, pp. 1–8.

[86] IRENA. *Battery Storage for Renewables: Market Status and technology outlook*. 2016.

[87] C ISO. "What the duck curve tells us about managing a green grid". In: *Calif. ISO, Shap. a Renewed Futur* (2012), pp. 1–4.

[88] Pietro Iurilli, Claudio Brivio, and Marco Merlo. "SoC management strategies in Battery Energy Storage System providing Primary Control Reserve". In: *Sustainable Energy, Grids and Networks* 19 (2019), p. 100230.

[89] Seyedmahdi Izadkhast, Pablo Garcia-Gonzalez, and Pablo Frı************************ "An aggregate model of plug-in electric vehicles for primary frequency control". In: *IEEE Transactions on Power Systems* 30.3 (2014), pp. 1475–1482.

[90] Seyedmahdi Izadkhast et al. "Design of plug-in electric vehicle's frequency-droop controller for primary frequency control and performance assessment". In: *IEEE Transactions on Power Systems* 32.6 (2017), pp. 4241–4254.

[91] Hyeondeok Jo et al. "Development of frequency control performance evaluation criteria of BESS for ancillary service: A case study of frequency regulation by KEPCO". In: *2017 IEEE Innovative Smart Grid Technologies-Asia (ISGT-Asia)*. IEEE. 2017, pp. 1–5.

[92] Ali Jokar et al. "Review of simplified Pseudo-two-Dimensional models of lithium-ion batteries". In: *Journal of Power Sources* 327 (2016), pp. 44–55.

[93] Mostafa Kazemi and Hamidreza Zareipour. "Long-term scheduling of battery storage systems in energy and regulation markets considering battery's lifespan". In: *IEEE Transactions on Smart Grid* 9.6 (2017), pp. 6840–6849.

[94] Mostafa Kazemi et al. "Operation scheduling of battery storage systems in joint energy and ancillary services markets". In: *IEEE Transactions on Sustainable Energy* 8.4 (2017), pp. 1726–1735.

[95] Ruud Kempener and Eric Borden. "Battery storage for renewables: Market status and technology outlook". In: *International Renewable Energy Agency, Abu Dhabi* (2015), p. 32.

[96] Taulant Kërçi, J Giraldo, and Federico Milano. "Analysis of the impact of sub-hourly unit commitment on power system dynamics". In: *International Journal of Electrical Power & Energy Systems* 119 (2020), p. 105819.

[97] Thongchart Kerdphol et al. "Robust virtual inertia control of an islanded microgrid considering high penetration of renewable energy". In: *IEEE Access* 6 (2017), pp. 625–636.

[98] M Khalid and AV Savkin. "An optimal operation of wind energy system for frequency control based on model predictive control". In: *Renewable energy* 48 (2012), pp. 127–132.

[99] Nazmul Arefin Khan. "Modelling and Microsimulation of Activity Generation, Activity Scheduling and Mobility Assignment". In: (2020).

[100] Vaclav Knap et al. "Sizing of an energy storage system for grid inertial response and primary frequency reserve". In: *IEEE Transactions on Power Systems* 31.5 (2015), pp. 3447–3456.

[101] Michael Koller et al. "Review of grid applications with the Zurich 1 MW battery energy storage system". In: *Electric Power Systems Research* 120 (2015), pp. 128–135.

[102] Benjamin Kroposki et al. "Achieving a 100% renewable grid: Operating electric power systems with extremely high levels of variable renewable energy". In: *IEEE Power and Energy Magazine* 15.2 (2017), pp. 61–73.

[103] Prabha Kundur et al. "Definition and classification of power system stability". In: *IEEE transactions on Power Systems* 19.2 (2004), pp. 1387–1401.

[104] Prabha Kundur, Neal J Balu, and Mark G Lauby. *Power system stability and control.* Vol. 7. McGraw-hill New York, 1994.

[105] H-J Kunisch, KG Kramer, and H Dominik. "Battery energy storage another option for load-frequency-control and instantaneous reserve". In: *IEEE Transactions on Energy Conversion* 3 (1986), pp. 41–46.

[106] *Lavoro e Retribuzioni, occupazioni dipendenti e retribuzioni.* Tech. rep. Italian Institute of Statistichs, 2017.

[107] Rachel Lee et al. "A closed-loop analysis of grid scale battery systems providing frequency response and reserve services in a variable inertia grid". In: *Applied Energy* 236 (2019), pp. 961–972.

[108] Bei Li et al. "Coordinated scheduling of a gas/electricity/heat supply network considering temporal-spatial electric vehicle demands". In: *Electric Power Systems Research* 163 (2018), pp. 382–395.

[109] Tao Liu, David J Hill, and Congchong Zhang. "Non-disruptive load-side control for frequency regulation in power systems". In: *IEEE transactions on smart grid* 7.4 (2016), pp. 2142–2153.

[110] Mihai Sănduleac Lucian Toma and Stefan Andrei Baltac. *Deliverable 2.1. Review of relevance of current techniques to advanced frequency control.* Tech. rep. RESERVE European project, 2017.

[111] Charles M Macal and Michael J North. "Agent-based modeling and simulation". In: *Proceedings of the 2009 Winter Simulation Conference (WSC)*. IEEE. 2009, pp. 86–98.

[112] Sven Maerivoet and Bart De Moor. "Cellular automata models of road traffic". In: *Physics reports* 419.1 (2005), pp. 1–64.

[113] Yuri V Makarov et al. "Sizing energy storage to accommodate high penetration of variable energy resources". In: *IEEE Transactions on sustainable Energy* 3.1 (2011), pp. 34–40.

[114] Jürgen Marchgraber, Wolfgang Gawlik, and Günter Wailzer. "Reducing SoC-Management and losses of battery energy storage systems during provision of frequency containment reserve". In: *Journal of Energy Storage* 27 (2020), p. 101107.

[115] Uros Markovic et al. "Lqr-based adaptive virtual synchronous machine for power systems with high inverter penetration". In: *IEEE Transactions on Sustainable Energy* (2018).

[116] Uros Markovic et al. "Optimal Sizing and Tuning of Storage Capacity for Fast Frequency Control in Low-Inertia Systems". In: *2019 International Conference on Smart Energy Systems and Technologies (SEST)*. IEEE. 2019, pp. 1–6.

[117] Charalampos Marmaras, Erotokritos Xydas, and Liana Cipcigan. "Simulation of electric vehicle driver behaviour in road transport and electric power networks". In: *Transportation Research Part C: Emerging Technologies* 80 (2017), pp. 239–256.

[118] Olivier Mégel, Johanna L Mathieu, and Göran Andersson. "Maximizing the potential of energy storage to provide fast frequency control". In: *IEEE PES ISGT Europe 2013*. IEEE. 2013, pp. 1–5.

[119] Francesca Madia Mele, Rafael Zárate-Miñano, and Federico Milano. "Modeling Load Stochastic Jumps for Power Systems Dynamic Analysis". In: *IEEE Transactions on Power Systems* 34.6 (2019), pp. 5087–5090.

[120] Francesca Madia Mele et al. "Impact of variability, uncertainty and frequency regulation on power system frequency distribution". In: *2016 Power Systems Computation Conference (PSCC)*. IEEE. 2016, pp. 1–8.

[121] Pascal Mercier, Rachid Cherkaoui, and Alexandre Oudalov. "Optimizing a battery energy storage system for frequency control application in an isolated power system". In: *IEEE Transactions on Power Systems* 24.3 (2009), pp. 1469–1477.

[122] Federico Milano. "A python-based software tool for power system analysis". In: *2013 IEEE Power & Energy Society General Meeting*. IEEE. 2013, pp. 1–5.

[123] Federico Milano. *Power system modelling and scripting*. Springer Science & Business Media, 2010.

[124] Federico Milano and Álvaro Ortega Manjavacas. *Converter-based Energy Storage Systems: Context, Modelling and Dynamic Analysis*. Cambridge University Press, 2019.

[125] Federico Milano et al. "Foundations and challenges of low-inertia systems". In: *2018 Power Systems Computation Conference (PSCC)*. IEEE. 2018, pp. 1–25.

[126] Markus Mirz et al. "Dynamic phasors to enable distributed real-time simulation". In: *2017 6th International Conference on Clean Electrical Power (ICCEP)*. IEEE. 2017, pp. 139–144.

[127] Iman Naziri Moghaddam and Badrul Chowdhury. "Optimal sizing of hybrid energy storage systems to mitigate wind power fluctuations". In: *2016 IEEE Power and Energy Society General Meeting (PESGM)*. IEEE. 2016, pp. 1–5.

[128] Carmelo Mosca et al. "Mitigation of frequency stability issues in low inertia power systems using synchronous compensators and battery energy storage systems". In: *IET Generation, Transmission & Distribution* 13.17 (2019), pp. 3951–3959.

[129] Yunfei Mu et al. "Primary frequency response from electric vehicles in the Great Britain power system". In: *IEEE Transactions on Smart Grid* 4.2 (2012), pp. 1142–1150.

[130] Yorie Nakahira et al. "Smoothed least-laxity-first algorithm for ev charging". In: *Proceedings of the Eighth International Conference on Future Energy Systems*. 2017, pp. 242–251.

[131] Nebojsa Nakicenovic et al. "Energy scenarios". In: *World Energy Assessment of the United Nations* (2000).

175

[132] Emil Namor et al. "Control of battery storage systems for the simultaneous provision of multiple services". In: *IEEE Transactions on Smart Grid* 10.3 (2018), pp. 2799–2808.

[133] Daniel E Olivares et al. "Trends in microgrid control". In: *IEEE Transactions on smart grid* 5.4 (2014), pp. 1905–1919.

[134] Australian Energy Market Operator. *International review of frequency control adaptation.* Tech. rep. 2016.

[135] Australian Energy Market Operator. *Quaterly Energy Dynamics - Q1 2019.* 2019.

[136] Alvaro Ortega and Federico Milano. "Combined Frequency and RoCoF Control of Converter-Interfaced Energy Storage Systems". In: *IFAC-PapersOnLine* 52.4 (2019), pp. 240–245.

[137] Alvaro Ortega and Federico Milano. "Frequency control of distributed energy resources in distribution networks". In: *IFAC-PapersOnLine* 51.28 (2018), pp. 37–42.

[138] Alvaro Ortega and Federico Milano. "Modeling, simulation, and comparison of control techniques for energy storage systems". In: *IEEE transactions on Power Systems* 32.3 (2016), pp. 2445–2454.

[139] Alvaro Ortega and Federico Milano. "Stochastic transient stability analysis of transmission systems with inclusion of energy storage devices". In: *IEEE Transactions on Power Systems* 33.1 (2017), pp. 1077–1079.

[140] Álvaro Ortega and Federico Milano. "Comparison of different PLL implementations for frequency estimation and control". In: *2018 18th International Conference on Harmonics and Quality of Power (ICHQP)*. IEEE. 2018, pp. 1–6.

[141] Álvaro Ortega and Federico Milano. "Impact of frequency estimation for VSC-based devices with primary frequency control". In: *2017 IEEE PES Innovative Smart Grid Technologies Conference Europe (ISGT-Europe)*. IEEE. 2017, pp. 1–6.

[142] Álvaro Ortega et al. "Hardware-in-the-Loop Validation of the Frequency Divider Formula". In: *2018 IEEE Power & Energy Society General Meeting (PESGM)*. IEEE. 2018, pp. 1–5.

[143] Erik Ørum et al. "Future system inertia". In: *ENTSOE, Brussels, Tech. Rep* (2015).

[144] Alexandre Oudalov, Daniel Chartouni, and Christian Ohler. "Optimizing a battery energy storage system for primary frequency control". In: *IEEE Transactions on Power Systems* 22.3 (2007), pp. 1259–1266.

[145] J Palermo. "International review of frequency control adaptation". In: *Australian Energy Market Operator* (2016).

[146] Georgios Papaefthymiou and Ken Dragoon. "Towards 100% renewable energy systems: Uncapping power system flexibility". In: *Energy Policy* 92 (2016), pp. 69–82.

[147] European Parliament and Council. *Directive (EU) 2019/944 of the European Parliament and of the Council of 5 June 2019 on common rules for the internal market for electricity and amending Directive 2012/27/EU*. 2019.

[148] F Parma et al. "A tool to investigate the PV and storage plants effective integration in the European interconnected transmission network". In: *2013 International Conference on Clean Electrical Power (ICCEP)*. IEEE. 2013, pp. 254–261.

[149] Bala Kameshwar Poolla, Saverio Bolognani, and Florian Dörfler. "Optimal placement of virtual inertia in power grids". In: *IEEE Transactions on Automatic Control* 62.12 (2017), pp. 6209–6220.

[150] Vasileios Poulios et al. "Optimal placement and sizing of battery storage to increase the PV hosting capacity of low voltage grids". In: *International ETG Congress 2015; Die Energiewende-Blueprints for the new energy age*. VDE. 2015, pp. 1–8.

[151] Giuseppe Prettico et al. "Distribution system operators observatory: From european electricity distribution systems to representative distribution networks". In: *JRC report EUR 27927 EN* (2016).

[152] P Ralon et al. "Electricity storage and renewables: costs and markets to 2030". In: *International Renewable Energy Agency: Abu Dhabi, UAE* (2019).

[153] Miguel Ramirez et al. "Placement and sizing of battery energy storage for primary frequency control in an isolated section of the Mexican power system". In: *Electric Power Systems Research* 160 (2018), pp. 142–150.

[154] Giuliano Rancilio et al. "Modeling a Large-Scale Battery Energy Storage System for Power Grid Application Analysis". In: *Energies* 12.17 (2019), p. 3312.

[155] Simon Remppis et al. "Influence of 15-minute contracts on frequency deviations and on the demand for balancing energy". In: *International ETG Congress 2015; Die Energiewende-Blueprints for the new energy age*. VDE. 2015, pp. 1–7.

[156] *Results of the EUCO3232.5 scenario on Member States*. Tech. rep. European Commission, 2019.

[157]   Michel Rezkalla, Michael Pertl, and Mattia Marinelli. "Electric power system inertia: requirements, challenges and solutions". In: *Electrical Engineering* 100.4 (2018), pp. 2677–2693.

[158]   Michel Rezkalla et al. "Trade-off analysis of virtual inertia and fast primary frequency control during frequency transients in a converter dominated network". In: *2016 IEEE Innovative Smart Grid Technologies-Asia (ISGT-Asia)*. IEEE. 2016, pp. 890–895.

[159]   David Rosewater and Summer Ferreira. "Development of a frequency regulation duty-cycle for standardized energy storage performance testing". In: *Journal of Energy Storage* 7 (2016), pp. 286–294.

[160]   David Rosewater, Paul Scott, and Surya Santoso. "Application of a uniform testing protocol for energy storage systems". In: *2017 IEEE Power & Energy Society General Meeting*. IEEE. 2017, pp. 1–5.

[161]   Sandro Rubino et al. "Advanced control of inverter-interfaced generation behaving as a virtual synchronous generator". In: *2015 IEEE Eindhoven PowerTech*. IEEE. 2015, pp. 1–6.

[162]   Ehsan Samadani et al. "Empirical modeling of lithium-ion batteries based on electrochemical impedance spectroscopy tests". In: *Electrochimica Acta* 160 (2015), pp. 169–177.

[163]   Benjamin Schafer, Marc Timme, and Dirk Witthaut. "Isolating the impact of trading on grid frequency fluctuations". In: *2018 IEEE PES Innovative Smart Grid Technologies Conference Europe (ISGT-Europe)*. IEEE. 2018, pp. 1–5.

[164]   Marc Scherer. "Frequency control in the European power system considering the organisational structure and division of responsibilities". PhD thesis. ETH Zurich, 2016.

[165]   Robert Schmidt et al. "Revenue-optimized Marketing of electric Vehicles' Flexibility Options". In: *International ETG-Congress 2019; ETG Symposium*. VDE. 2019, pp. 1–6.

[166]   R Schwerdfeger et al. "Approach for load frequency control participation by decentralized energy devices". In: *2015 IEEE Power & Energy Society General Meeting*. IEEE. 2015, pp. 1–5.

[167]   Ioan Serban, Remus Teodorescu, and Corneliu Marinescu. "Energy storage systems impact on the short-term frequency stability of distributed autonomous microgrids, an analysis using aggregate models". In: *IET Renewable Power Generation* 7.5 (2013), pp. 531–539.

[168] AA Shaltout and KA Abu Al-Feilat. "Damping and synchronizing torque computation in multimachine power systems". In: *IEEE transactions on power systems* 7.1 (1992), pp. 280–286.

[169] Qingxin Shi, Fangxing Li, and Hantao Cui. "Analytical method to aggregate multi-machine SFR model with applications in power system dynamic studies". In: *IEEE Transactions on Power Systems* 33.6 (2018), pp. 6355–6367.

[170] B Shoeiby et al. "Dynamics of droop-controlled microgrids with unequal droop response times". In: *2013 Australasian Universities Power Engineering Conference (AUPEC)*. IEEE. 2013, pp. 1–6.

[171] Lakshmi Srinivasan et al. "Provision of frequency control by a BESS in combination with flexible units". In: *2018 IEEE International Energy Conference (ENERGYCON)*. IEEE. 2018, pp. 1–6.

[172] Karl Stein et al. "Characterization of a Fast Battery Energy Storage System for Primary Frequency Response". In: *Energies* 11.12 (2018), p. 3358.

[173] Daniel-Ioan Stroe et al. "Operation of a grid-connected lithium-ion battery energy storage system for primary frequency regulation: A battery lifetime perspective". In: *IEEE transactions on industry applications* 53.1 (2016), pp. 430–438.

[174] Insight_E energy think tank. *How Can batteries Support Eu electricity System.* 2016.

[175] Ali Tayyebi et al. "Gridforming converters–inevitability, control strategies and challenges in future grid applications". In: *International Conference on Electricity Distribution (CIRED)*. 2018.

[176] *Technical report on Member State results of the EUCO policy scenarios.* Tech. rep. E3MLAB and IIASA, 2016.

[177] Terna. *Allegato A15 al Codice di Rete; Regolazione Frequenza Potenza.* 2008.

[178] Terna. *Progetto pilota riserva ultra-rapida di frequenza.* 2019.

[179] Terna. *Terna pilot projects. [Online].* URL: http://www.terna.it/en-gb/sistemaelettrico/progettipilotadiaccumulo.aspx (visited on 10/01/2020).

[180] Terna. *Terna UVAM pilot project. [Online].* URL: https://www.terna.it/it/sistema-elettrico/progetti-pilota-delibera-arera-300-2017-reel/progetto-pilota-uvam (visited on 10/01/2020).

[181] Andreas Thingvad, Charalampos Ziras, and Mattia Marinelli. "Economic value of electric vehicle reserve provision in the Nordic countries under driving requirements and charger losses". In: *Journal of Energy Storage* 21 (2019), pp. 826–834.

[182] Pieter Tielens and Dirk Van Hertem. "The relevance of inertia in power systems". In: *Renewable and Sustainable Energy Reviews* 55 (2016), pp. 999–1009.

[183] Lucian Toma et al. "On the virtual inertia provision by BESS in low inertia power systems". In: *2018 IEEE International Energy Conference (ENER-GYCON)*. IEEE. 2018, pp. 1–6.

[184] Politecnico di Torino. *Deliverable 1.4. Use Case Definition for Research in Frequency and Voltage Control*. Tech. rep. RESERVE European project, 2017.

[185] Politecnico di Torino and RESERVE partners. *Deliverable 1.1. Scenarios & architectures for 100% RES and roles of sector actors*. Tech. rep. RESERVE European project, 2016.

[186] Christoph Trabert, Andreas Ulbig, and Göran Andersson. "Model predictive frequency control employing stability constraints". In: *2015 American Control Conference (ACC)*. IEEE. 2015, pp. 5678–5685.

[187] Operation Handbook UCTE. *Appendix 1, Load-frequency Control and Performance*. 2009.

[188] Willem Uijlings, DNV KEMA Ltd Cathedral Street, and SE London. *An independent analysis on the ability of Generators to ride through Rate of Change of Frequency values up to 2Hz/s*. Tech. rep. s. Technical report, Uijlings, 2013.

[189] Andreas Ulbig et al. "General frequency control with aggregated control reserve capacity from time-varying sources: The case of PHEVs". In: *2010 IREP Symposium Bulk Power System Dynamics and Control-VIII (IREP)*. IEEE. 2010, pp. 1–14.

[190] Andreas Ulbig et al. "Predictive control for real-time frequency regulation and rotational inertia provision in power systems". In: *52nd IEEE Conference on Decision and Control*. IEEE. 2013, pp. 2946–2953.

[191] Ivan Vera and Lucille Langlois. "Energy indicators for sustainable development". In: *Energy* 32.6 (2007), pp. 875–882.

[192] Petr Vorobev et al. "Deadbands, Droop and Inertia Impact on Power System Frequency Distribution". In: *IEEE Transactions on Power Systems* (2019).

180

[193]   Evangelos Vrettos, Frauke Oldewurtel, and Göran Andersson. "Robust energy-constrained frequency reserves from aggregations of commercial buildings". In: *IEEE Transactions on Power Systems* 31.6 (2016), pp. 4272–4285.

[194]   Qinglong Wang et al. "Smart charging for electric vehicles: A survey from the algorithmic perspective". In: *IEEE Communications Surveys & Tutorials* 18.2 (2016), pp. 1500–1517.

[195]   Xiongfei Wang et al. "A review of power electronics based microgrids". In: *Journal of Power Electronics* 12.1 (2012), pp. 181–192.

[196]   Rashid A Waraich et al. "Plug-in hybrid electric vehicles and smart grids: Investigations based on a microsimulation". In: *Transportation Research Part C: Emerging Technologies* 28 (2013), pp. 74–86.

[197]   Tobias Weißbach, Simon Remppis, and Hendrik Lens. "Impact of current market developments in Europe on deterministic grid frequency deviations and frequency restauration reserve demand". In: *2018 15th International Conference on the European Energy Market (EEM)*. IEEE. 2018, pp. 1–6.

[198]   Bolun Xu et al. "Modeling of lithium-ion battery degradation for cell life assessment". In: *IEEE Transactions on Smart Grid* 9.2 (2016), pp. 1131–1140.

[199]   Weijia Yang et al. "Wear reduction for hydropower turbines considering frequency quality of power systems: a study on controller filters". In: *IEEE Transactions on Power Systems* 32.2 (2016), pp. 1191–1201.

[200]   Alireza Zakariazadeh, Shahram Jadid, and Pierluigi Siano. "Multi-objective scheduling of electric vehicles in smart distribution system". In: *Energy Conversion and Management* 79 (2014), pp. 43–53.

[201]   Rafael Zárate-Miñano, Marian Anghel, and Federico Milano. "Continuous wind speed models based on stochastic differential equations". In: *Applied Energy* 104 (2013), pp. 42–49.

[202]   Antonio Zecchino et al. "Enhanced primary frequency control from EVs: a fleet management strategy to mitigate effects of response discreteness". In: *IET Smart Grid* 2.3 (2019), pp. 436–444.

[203]   Fang Zhang et al. "Assessment of the effectiveness of energy storage resources in the frequency regulation of a single-area power system". In: *IEEE Transactions on Power Systems* 32.5 (2017), pp. 3373–3380.

[204]   Hongcai Zhang et al. "Evaluation of achievable vehicle-to-grid capacity using aggregate PEV model". In: *IEEE Transactions on Power Systems* 32.1 (2016), pp. 784–794.

181

[205]   Qing-Chang Zhong et al. "Self-synchronized synchronverters: Inverters without a dedicated synchronization unit". In: *IEEE Transactions on power electronics* 29.2 (2013), pp. 617–630.

[206]   Yue Zhou, Meng Cheng, and Jianzhong Wu. "Enhanced frequency response from industrial heating loads for electric power systems". In: *IEEE Transactions on Industrial Informatics* 15.6 (2018), pp. 3388–3399.